Petroleum-derived dissolved organic matter from natural seepage in deep sea environments

Dissertation

zur Erlangung des Doktorgrades

der Naturwissenschaften

- Dr. rer. nat. -

Am Fachbereich Geowissenschaften

der Universität Bremen

vorgelegt von

Jonas Brünjes

Bremen

Januar 2023

This thesis was prepared in the time from April 2019 to January 2023 in the Organic Geochemistry group at MARUM - Center for Marine Environmental Sciences, University of Bremen in collaboration with the Marine Geochemistry group at the Institute for Chemistry and Biology of the Marine Environment (ICBM), Carl von Ossietzky University of Oldenburg. This project was funded by the German Science Foundation (DFG) within the Cluster of Excellence EXC 2077 “The Ocean Floor – Earth’s Uncharted Interface”.

Gutachter/Reviewers:

Prof. Dr. Kai-Uwe Hinrichs

Dr. Elizabeth Kujawinski

Datum des Kolloquiums: 14.02.2023

Table of Contents

Abstract

Natural petroleum seepage discharges approximately 600,000 tons of oil every year into the marine environment. A fraction of the released petroleum is water-soluble and becomes part of oceanic dissolved organic matter (DOM), one of the largest and most complex pools of organic matter on Earth's surface. Despite the constant discharge of petroleum by natural seepage, the environmental implications and persistence of petroleum-derived DOM are vastly unknown. This thesis investigates molecular transformations of DOM in natural petroleum seepages and assesses the potential release of petroleum-compounds to oceanic deep-sea DOM.

In a first step, the release of oil-derived DOM from natural deep sea asphalt seeps was studied using controlled laboratory incubation experiments. Fresh asphalt samples collected at the Chapopote asphalt volcano in the Southern Gulf of Mexico were incubated aerobically in artificial seawater over four weeks. The compositional changes in the water-soluble fraction of asphalt-derived DOM were determined with ultrahigh-resolution mass spectrometry (Fourier-transform ion cyclotron resonance mass spectrometry, FT-ICR-MS) and by excitation-emission matrix spectroscopy to characterize fluorescent DOM (FDOM) applying parallel factor (PARAFAC) analysis. Result showed that highly reduced aliphatic asphalt-derived DOM was readily biodegraded, while aromatic and sulfur-containing DOM (DOS) appeared to be less bioavailable and accumulated in the aqueous phase. This indicates that natural asphalt and potentially other petroleum seepages can be marine sources of recalcitrant dissolved black carbon (DBC) which has apparent radiocarbon ages older than 20,000 years in the deep sea.

In order to evaluate this laboratory finding in the natural environment, petroleum-derived DOM was investigated in the Guaymas Basin. The Guaymas Basin in the Gulf of California is a young rift system where hot basaltic sill intrusions into organic-rich sediments lead to the generation of large amounts of complex petroleum compounds. The effect of hydrothermal heating and the resulting presence of petroleum compounds on the porewater DOM composition were investigated. Sediment samples were retrieved from sites with *in situ* temperatures ranging from 4 to >106 °C that exhibited a strong petroleum smell and partially contained oil droplets. A strong correlation of sediment temperature to both composition and quantity of porewater DOM was observed, driven by enhanced microbial transformation of organic matter at temperatures below ~60 °C and increasingly sulfurized DOM at high-temperature sites. DOM associated with hydrothermal heating had elevated contributions of highly unsaturated, reduced, sulfur-containing DOM and petroleum-associated PARAFAC components. A considerable DOM fraction of hydrothermal origin was present both in overlying

bottom waters and in recalcitrant deep-sea DOM, suggesting hydrothermal sediments as a source of recalcitrant DOM to the water column.

To assess elemental fluxes in DOM of hydrothermal porewaters, composition and quantities of DOM from sedimentary porewaters and from the hot-water soluble fraction by Soxhlet extraction of the same sediments were evaluated. Results showed highly elevated concentrations of DBC and potentially recalcitrant DOS in porewater, suggesting the release of both DOM fractions from hydrothermal sediments. DBC in porewaters and hot-water extracts originated from two distinct sources: hydrothermal petroleum and re-dissolved presumably terrestrial-derived, pre-aged DBC. This study further assessed quantities of DBC and dissolved organic nitrogen, sulfur and phosphorus that could be discharged into the water column in case of basin-wide hydrothermal heating. Results indicate that hydrothermal alteration and subsequent petroleum impregnation of sediments can be sources of recalcitrant DOS and DBC to deep sea environments.

This thesis provides important novel information about the transformation and release of water-soluble petroleum compounds from natural deep-sea seepage into the marine environment. By introducing radiocarbon-depleted DOM to the marine environment, natural petroleum seepages and hydrothermal alteration of sediments with subsequent petroleum impregnation may be an explanation for observed old radiocarbon ages of recalcitrant DOM in the deep ocean.

Zusammenfassung

Durch die natürliche Freisetzung von Erdöl gelangen jährlich etwa 600.000 Tonnen Öl in die Meeresumwelt. Ein Teil des freigesetzten Erdöls ist wasserlöslich und wird Teil des gelösten organischen Materials (engl. „dissolved organic matter“, DOM) im Ozean, einem der größten und komplexesten Reservoire für organisches Material auf der Erdoberfläche. Trotz der ständigen Freisetzung von Erdöl durch natürliche Austritte sind die Auswirkungen auf die Umwelt und die Persistenz des aus Erdöl stammenden DOM weitgehend unbekannt. In dieser Arbeit werden die molekularen Umwandlungen von aus natürlichen Erdölaustritten stammendem DOM untersucht und die mögliche Freisetzung von wasserlöslichen Ölkomponenten in die Tiefsee bewertet.

In einem ersten Schritt wurde die Freisetzung von aus Öl stammendem DOM aus natürlichen Asphaltablagerungen in der Tiefsee mit Hilfe von kontrollierten Inkubationsexperimenten im Labor untersucht. Frische Asphaltproben, die am Asphaltvulkan Chapopote im südlichen Golf von Mexiko entnommen wurden, wurden vier Wochen lang in künstlichem Meerwasser aerob inkubier.t Die Veränderungen in der Zusammensetzung der wasserlöslichen Fraktion des aus dem Asphalt stammenden DOM wurden mit ultrahochauflösender Massenspektrometrie (Fourier Transformations Ionen Zyklotron Resonanz Massenspektrometrie, FT-ICR-MS) und durch Anregungs-Emissions-Matrixspektroskopie zur Charakterisierung von fluoreszierendem DOM (FDOM) unter Anwendung der parallelen Faktoranalyse (PARAFAC) bestimmt. Die Ergebnisse zeigten, dass stark reduzierte aliphatische DOM aus Asphalt leicht biologisch abgebaut wurden, während aromatisches und schwefelhaltiges DOM (engl. „dissolved organic sulfur, „DOS“) weniger bioverfügbar war und sich in der wässrigen Phase anreicherte. Dies deutet darauf hin, dass natürliche Asphalt- und möglicherweise auch andere Erdölaustritte marine Quellen für rekalzitranten gelösten schwarzen Kohlenstoff (engl. „dissolved black carbon“, DBC) sein können, welcher in der Tiefsee Radiokohlenstoffalter von mehr als 20,000 Jahren aufweist.

Um diese Laborergebnisse in der natürlichen Umgebung zu verifizieren, wurde das aus Erdöl stammendes DOM im Guaymas-Becken untersucht. Das Guaymas-Becken im Golf von Kalifornien ist ein junges Riftsystem in welchem heiße basaltische Intrusionen in organisch reiche Sedimente zur Bildung großer Mengen komplexer Erdölverbindungen führen. Es wurden die Auswirkungen der hydrothermalen Erhitzung und der daraus resultierenden Vorkommen von Erdölverbindungen auf die DOM-Zusammensetzung des Porenwassers untersucht. Es wurden Sedimentproben von Standorten mit *in situ* Temperaturen zwischen 4 und >106 °C untersucht, die einen starken Erdölgeruch aufwiesen und Öl enthielten. Es wurde

eine deutliche Korrelation zwischen der Sedimenttemperatur und der Zusammensetzung und Menge des DOM festgestellt, die auf eine verstärkte mikrobielle Umwandlung organischer Stoffe bei Temperaturen unter ~60 °C und eine zunehmende Verschwefelung des DOM unter hohen Temperaturen zurückzuführen ist. Porenwasser-DOM, das mit hydrothermaler Erwärmung in Verbindung gebracht wurde, wies einen erhöhten Anteil an hochgradig ungesättigtem, reduziertem, schwefelhaltigem DOM und erdölassoziierten PARAFAC-Komponenten auf. Eine beträchtliche DOM-Fraktion hydrothermalen Ursprungs war sowohl im darüber liegenden Bodenwasser als auch in rekalzitrantem Tiefsee-DOM vorhanden, was auf hydrothermale Sedimente als Quelle von rekalzitrantem DOM in der Wassersäule hindeutet.

Um die Stoffflüsse im DOM von hydrothermalen Porenwässern zu evaluieren, wurden die Zusammensetzung und die Menge des DOM aus Porenwässern und aus der heißwasserlöslichen Fraktion durch Soxhlet-Extraktion derselben Sedimente untersucht. Die Ergebnisse zeigten stark erhöhte Konzentrationen von DBC und potenziell rekalzitrantem DOS im Porenwasser, was auf die Freisetzung beider DOM-Fraktionen in hydrothermalen Sedimenten hindeutet. Das DBC im Porenwasser und in den Heißwasserextrakten stammte aus zwei verschiedenen Quellen: hydrothermales Erdöl und wieder aufgelöstes, vorgealtertes DBC vermutlich terrestrischen Ursprungs. In dieser Studie wurden außerdem die Mengen an DBC und gelöstem organischem Stickstoff, Schwefel und Phosphor ermittelt, die im Falle einer beckenweiten hydrothermalen Erhitzung in die Wassersäule gelangen könnten. Die Ergebnisse deuten darauf hin, dass die hydrothermale Erhitzung von Sedimenten eine Quelle für rekalzitrantes DOS und DBC in der Tiefsee sein kann.

Diese Arbeit liefert wichtige neue Informationen über die Umwandlung und Freisetzung von wasserlöslichen Erdölverbindungen aus natürlichen Erdölaustritten in die Meeresumwelt. Durch den Austritt von an Radiokarbon abgereichertem DOM in die Meeresumwelt könnten natürliche Erdölaustritte und hydrothermale Erhitzung von Sedimenten mit anschließender Imprägnierung von hydrothermalem Erdöl eine Erklärung für das beobachtete hohe Radiokohlenstoffalter von rekalzitrantem DOM in der Tiefsee sein.

Acknowledgements

First of all, I want to thank you, Florence, for your supervision and confidence in me, giving me the opportunity to pursue such an interesting topic for my PhD and the numerous encouraging meetings across two continents. I highly appreciate that you opened up the opportunity to join an Alvin cruise, allowing me to observe hydrothermal vents on the seafloor with my own eyes. A special thanks to Micha for your excellent scientific advice, supervision and support over coffee/video chats that always lift my mood. You managed to shift my initial interest in petroleomics to the mysterious and fascinating area of environmental dissolved organic matter.

Thank you, Kai, for your scientific and career advice and reviewing this thesis. In this regard, I would like to thank Elizabeth Kujawinski for agreeing to review this thesis and hope you find it worthwhile to read. Thanks to Chris Reddy and Bernd Engelen for joining my thesis committee and guidance in the initial phase of this PhD and Andreas Teske for sharing your knowledge about the mysteries of the Guaymas Basin. A special thank you to everyone from the working group Organic Geochemistry at Marum for providing technical and administrative support and perhaps most importantly, a welcoming and inspiring working environment. Thank you Xavi, Jenny, Yvonne, Heidi, Evert, Julius, Qing-Zeng, Igor, Susanne, Weimin, Janina, Lars, Verena, Marcus, Jan, Tiffany and all other present and former group members! I acknowledge the excellent work of my Hiwis Chris and Palash. Your laboratory work helped me a lot!

I want to acknowledge my second “home”, the working group Marine Geochemistry at the ICBM. Thank you, Melina, Ina, Matze, Heike and Jana for your technical assistance and accepting me as one amongst your own. I thank Thorsten and Jutta for scientific advice and valuable discussions. I further want to acknowledge Urban Wünsch and Kate Murphy, whose workshop on PARAFAC analysis initiated to go down a deep and interesting rabbit hole about algorithms and programming.

Many thanks to my family and friends, continuously supporting me even 6000 km away from home. Last but not least a very special thank you to Min - not only for your scientific expertise but more importantly for your love, patience and emotional support during all these years.

I. Introduction

I.1 Dissolved organic matter in the marine environment

All living organisms release polar organic molecules to their environment which dissolve in water and become part of the dissolved organic matter (DOM) pool. Each Liter of seawater contains about 35 g of inorganic salts but only 0.001 g or 1 ppm dissolved organic carbon (DOC). Although DOC is present at such low concentrations in seawater, the marine DOM pool contains more carbon than all living biomass on our planet, comparable to the amount of carbon in atmospheric carbon dioxide: 662 Pg of DOC. (Dittmar and Stubbins, 2014; Hansell, 2013).

DOM is generally referred to as the organic compounds in water that pass through a filter, usually of a pore size below 0.2 to 0.7 μM. The highest concentrations of DOC are usually found in the productive surface ocean (60 to 90 μM) and decreases with water depth to ~40 μM DOC in deep sea waters (Dittmar and Stubbins, 2014). Most DOM is released by phytoplankton in the surface ocean, serves as a nutritional basis for heterotrophic microorganisms and is turned over within hours to days, and is hence defined as labile. The accumulated fractions in the DOM pool can be grouped after their turnover times and include semi-labile, semi-refractory, refractory and ultra-refractory DOM (Hansell, 2013). Labile (hours to days), semi-labile (~1.5 yrs) and semi-refractory (~20 yrs) DOM fractions contain combined about 20 Pg DOC (Figure 1). The majority of DOC in global oceans is composed of refractory DOM with modeled lifetimes of ~16,000 yrs and mean radiocarbon ages on the timescales of millennia (Hansell, 2013). Oceanic DOM consists to ~95% of refractory DOM which may have implications on climate cycles by sequestering the enormous amount of 630 Pg of carbon (Dittmar *et al.*, 2021; Shen and Benner, 2020). The reasons behind the apparent longevity of oceanic DOM are not completely understood, and are still being discussed (Dittmar, 2015; Dittmar *et al.*, 2021; Lennartz and Dittmar, 2022; Shen and Benner, 2020). Freshly produced organic matter can be transformed during microbial degradation into a complex mixture of compounds that potentially contributes to refractory DOM (Jiao *et al.*, 2010; Kujawinski, 2011; Noriega-Ortega *et al.*, 2019). Much of global oceanic DOM is composed of a multitude of relatively small components, whose very low individual concentrations may impede microbial degradation. Estimates about the complexity of DOM assume more than 600,000 and possibly >1,000,000 different compounds (Dittmar *et al.*, 2021; Hertkorn *et al.*, 2007; Riedel and Dittmar, 2014; Zark *et al.*, 2017). Another explanation may be stable molecular structures resistant to microbial degradation, where recalcitrant compounds are eventually removed on

timescales of ocean circulation by abiotic processes such as photooxidation or hydrothermal heating (Dittmar and Paeng, 2009; Dittmar *et al.*, 2021; Shen and Benner, 2020).

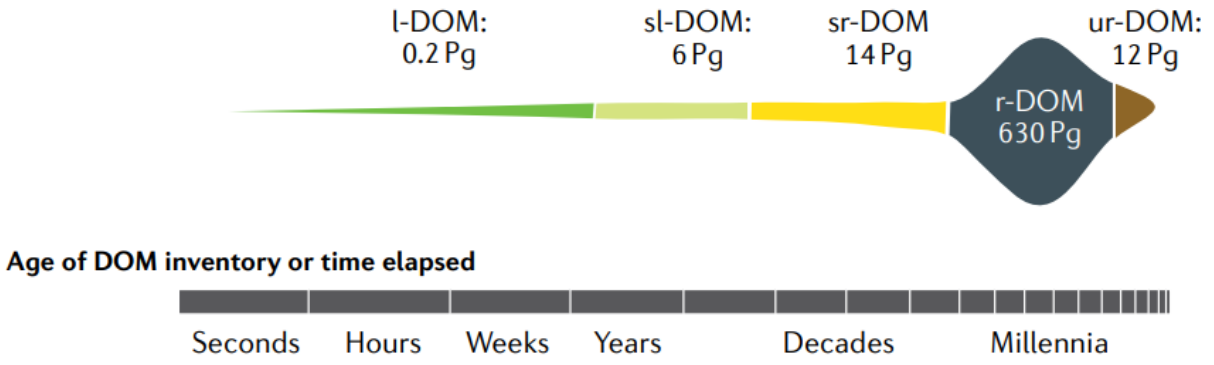

Figure 1: Global inventory of marine DOM, grouped after their modeled turnover times according to (Hansell, 2013): labile (l-DOM, semilabile (sl-DOM), semirefractory (sr-DOM), refractory (r-DOM) and ultrarefractory (ur-DOM). Figure from Dittmar et al. (2021)

A fraction of the deep-oceanic DOM consists of about 12 Pg ultra-refractory DOC (Figure 1)(Hansell, 2013). This fraction contains dissolved black carbon (DBC) which has proposed core structures of fused rings with carboxylic functional groups, comparable to compounds detected in petroleum asphaltenes (Figure 2) (Dittmar and Paeng, 2009; Ruiz-Morales and Mullins, 2007; Schuler *et al.*, 2015; Zhang *et al.*, 2020; Ziolkowski *et al.*, 2011). The highly condensed aromatic core structures are resistant to microbial decomposition and hence persistence of this compound class is observed in the natural environment (Goldberg, 1985; Schmidt *et al.*, 2011). DBC is the oldest molecularly characterized component of the present carbon cycle with radiocarbon ages of more than 23,000 years in the deep sea (Coppola and Druffel, 2016). DBC containing 5 or more fused rings is assumed to be produced by the incomplete combustion of terrestrial organic matter on land, transported to marine environments by rivers or wind (Kappenberg *et al.*, 2016; Wagner *et al.*, 2018). Particularly rivers are a main source of DBC to marine environments and contain ca. 10% of their DOC as DBC (Jaffé *et al.*, 2013). However, cycling of DBC is poorly constrained: the stable isotopic carbon composition of riverine DBC reflects terrestrial organic matter, while deep-sea DBC has a marine isotopic composition (Wagner *et al.*, 2019). In addition, radiocarbon dating of riverine DBC shows modern radiocarbon signatures of DBC, contrasting observations of old oceanic DBC (Coppola *et al.*, 2019). Known DBC flux rates from rivers ($18 \pm 4\ 10^{12}$g C yr^{-1} (Jaffé *et al.*, 2013)) would be sufficient to sustain the turnover of the marine DBC pool in 500 years, yet marine DBC has radiocarbon ages on timescales of millennia (Coppola and Druffel,

2016). Moreover, photooxidation on the sea surface, a major sink for condensed aromatic carbon, could remove the global marine DBC pool in theory within 30-800 years (Stubbins *et al.*, 2012; Stubbins *et al.*, 2010). This mismatch between sources and sinks is a conundrum in the modern marine carbon cycle: global models of DBC cycling point to additional, unknown marine sources (Coppola *et al.*, 2022; Wagner *et al.*, 2018).

The first study describing DBC distribution in the open ocean by Dittmar and Koch (2006) suggested a widespread source at the seafloor of deep-sea basins, for instance hydrothermal vents. However, laboratory experiments and environmental hydrothermal vent samples could not confirm them as a DBC source but rather suggested hydrothermal cycling as an efficient sink for recalcitrant marine DOM via thermal degradation at temperatures exceeding 200°C (Hawkes *et al.*, 2015a; Hawkes *et al.*, 2015b). Dissolution of old, petrogenic carbon was further hypothesized as a potential source which would match radiocarbon-depleted DBC in the deep ocean (Wagner *et al.*, 2019). If this petrogenic DBC source was water-soluble petroleum, the stable isotopic carbon composition would reflect a marine signal, similar to deep ocean DBC. A recent study by Podgorski *et al.* (2020) observed enhanced DBC concentrations in groundwater after an oil spill on land. Petroleum as a DBC source in marine environments, however, has not yet been confirmed. Petroleum-derived ultra-refractory DOM could be a potential source for radiocarbon-depleted, old DBC with marine isotopic carbon composition in ocean environments.

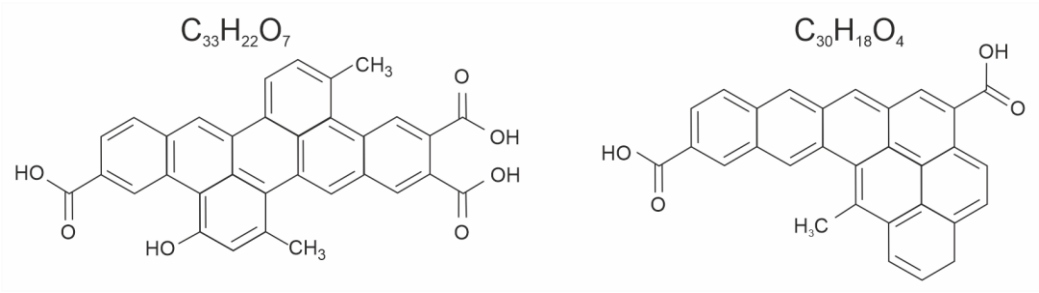

Figure 2: Two proposed structures of dissolved black carbon in deep ocean waters. The carboxylic functional groups likely render these highly condensed molecules water-soluble. In petroleum asphaltenes, aliphatic side changes are present instead of carboxylic functional groups. Figure recreated after Dittmar and Paeng (2009).

I.1.1 Water-soluble petroleum compounds

Water-soluble petroleum that passes through a 0.7 μm filter becomes part of the DOM pool by definition. Classical assessment of water-soluble petroleum focuses on aromatic compounds like benzene, toluene, ethylbenzene, xylene or small polycyclic aromatic hydrocarbons (PAH) like naphthalene, which can impar marine life even at very low concentrations of 1 to 10 μg per liter (Brussaard *et al.*, 2016; Incardona *et al.*, 2014). Since the 1990s, a framework has been

developed to quantify the total petroleum hydrocarbons (TPH) of contaminated sites using gas chromatography coupled with flame ionization detection (ITRC). Analyzing TPH dissolved in water involves the extraction with a liquid solvent like dichloromethane or hexane which does not fully retain dissolved petroleum compounds or its degradation products (Bekins *et al.*, 2020; Zito *et al.*, 2019a). For instance, microbial degradation of petroleum releases intermediates containing oxygen which increases its polarity (Islam *et al.*, 2016; Liu *et al.*, 2020; Podgorski *et al.*, 2018). Most polar petroleum compounds containing heteroatoms such as oxygen, nitrogen or sulfur are outside of the analytical window of gas chromatography (Liu and Kujawinski, 2015). Polar petroleum compounds can make up approximately 70-80% of the water-soluble petroleum fraction (Melbye *et al.*, 2009; Siron *et al.*, 1987). They appear to be relatively resistant to degradation (Corilo *et al.*, 2013; McKenna *et al.*, 2013; Seidel *et al.*, 2016) and can have mutagenic effects to benthic microbial communities (Lübcke-von Varel *et al.*, 2011). As a consequence, recent research has increasingly focused on determining polar, water-soluble petroleum outside the TPH assessment framework using the same methodological approaches used to characterize DOM, i.e. the isolation of DOM from seawater and subsequent characterization by ultrahigh-resolution mass spectrometry (Corilo *et al.*, 2013; Harriman *et al.*, 2017; Islam *et al.*, 2016; Podgorski *et al.*, 2018) (see section 1.3).

Most laboratory (Kleindienst *et al.*, 2015; Seidel *et al.*, 2016; Tomco *et al.*, 2021; Zito *et al.*, 2019b) and environmental studies (Corilo *et al.*, 2013; McKenna *et al.*, 2013; Podgorski *et al.*, 2018) on petroleum-derived DOM focused on anthropogenic oil input, while water-soluble oil from natural seepage has not been investigated so far. Petroleum from natural seepages likely contains more polar and larger compounds than refined oil, though compositional differences in spilled crude oil compared to natural seepage are not predictable. More importantly, the majority of anthropogenically spilled oil in the marine environment takes place on the surface ocean, where sunlight oxidizes dissolved petroleum compounds, including PAHs (Dong *et al.*, 2022; Stubbins *et al.*, 2012; Zito *et al.*, 2020; Zito *et al.*, 2019b). Natural seepage on the other hand can introduce petroleum to deep-sea waters devoid of light, where hydrocarbons further have different solubility compared to the surface ocean. For instance, low temperatures and low concentrations of DOC in the surrounding water likely decrease the solubility, while high ambient pressure and high concentrations of dissolved gases often present at petroleum seeps can increase solubility (Boehm and Quinn, 1973; Price, 1976). Since photo-oxidation as a main removal mechanism for highly condensed aromatics does not occur in the deep sea, assessing the contribution of natural seepage on pools of refractory DOM in the deep ocean is crucial for constraining the oceanic carbon cycle. Petroleum hydrocarbons not only contain stable compounds resistant to microbial degradation, they further introduce radiocarbon-depleted

organic matter (Wang *et al.*, 2001). Relatively small but constant contributions of fully radiocarbon depleted organic matter to deep sea pools of refractory or ultra-refractory DOM could shape observed radiocarbon ages of these DOM fractions. The contribution of natural seepage-derived dissolved petroleum on cycling of oceanic DOC is currently unknown.

I.1.2 Dissolved organic nitrogen, sulfur and phosphorus

Although DOM is mainly composed of carbon, oxygen, and hydrogen, subfractions contain nitrogen (dissolved organic nitrogen, DON), sulfur (dissolved organic sulfur, DOS) and phosphorus (dissolved organic phosphorus, DOP). Global pools and cycling of marine DON, DOS and DOP are not well constrained. Dittmar and Stubbins (2014) estimated global inventories of DON to approximately 53 Pg nitrogen and DOP of roughly 4.3 Pg phosphorus. Ratios of DOC:DON, and DOC:DOP in marine DOM are much higher than in the average elemental composition of marine organisms, about a factor of 2 for DOC:DON and 4 for DOC:DOP. Nitrogen and phosphorus are often limiting nutrients for phytoplankton growth, but unlike dissolved inorganic nitrogen (e.g. NH_3, NO_3, NO_2) and phosphorus (PO_4), DON and DOP are not necessarily directly available to marine organisms (Dittmar and Stubbins, 2014). Nonetheless, a subset of DON compound groups such as peptides and amino acids are considered to be highly labile, whereas other DON compound groups like deaminated peptides are considered recalcitrant (Abdulla *et al.*, 2018). Even less is known about DOP, but similar to DON, DOP contains both labile and recalcitrant subfractions (Karl and Björkman, 2015; Ni *et al.*, 2022; Worsfold *et al.*, 2008). Along with DON and DOP, DOS in the ocean is mainly derived from phytoplankton. The marine DOS inventory consists of approximately 3.8 to 6.7 Pg sulfur (Ksionzek *et al.*, 2016; Longnecker *et al.*, 2020). A recent study investigating the stable sulfur isotopic composition in DOS revealed that ca. 8% of marine DOS is not derived by primary production and instead presumably from sulfidic sediment porewater (Phillips *et al.*, 2022). Abiotic sulfurization increases the content of sedimentary organic sulfur by incorporating inorganic sulfide into organic matter including DOM (Pohlabeln *et al.*, 2017). This process is not limited to sediments and can take place in anoxic (sulfidic) ocean waters, potentially sequestering carbon (Gomez-Saez *et al.*, 2021).

Heteroatoms such as sulfur in petroleum can increase the polarity and hence water-solubility of petroleum compounds (Liu and Kujawinski, 2015). Previous laboratory (Hegazi *et al.*, 2012) and field studies at terrestrial oil spills (Dvorski *et al.*, 2016; Islam *et al.*, 2016) reported an enrichment of sulfur-containing DOM derived from the petroleum which was apparently resistant to microbial degradation. Known water-soluble sulfur-containing petroleum hydrocarbons such as thiophenes or condensed thiophenes are considered to be

bio-refractory (Kropp and Fedorak, 1998). It is currently unknown whether recalcitrant petroleum-derived DOS contributes to the 8% of non-phytoplankton derived marine DOS pool.

I.1.3 Porewater dissolved organic matter

Degradation of sedimentary particulate organic matter can produce large amounts of DOM in marine porewater. Porewater often contains elevated DOC concentrations compared to the overlying bottom water and diffusive transport is considered a source of microbially-processed porewater DOM to the adjacent water column (Burdige and Komada, 2015). Porewater diffusion and outwelling can, for example, contribute DON (Abdulla *et al.*, 2018; Zhou *et al.*, 2022), DOP (Worsfold *et al.*, 2008) and potentially recalcitrant DOS to the water column (Abdulla *et al.*, 2019; Pohlabeln *et al.*, 2017; Schmidt *et al.*, 2009; Seidel *et al.*, 2014). While porewater DON and DOP are derived from remineralization of organic matter and hence ultimately primary production, porewater DOS can additionally be produced by abiotic sulfurization of particulate and dissolved organic matter (Abdulla *et al.*, 2019; Pohlabeln *et al.*, 2017; Seidel *et al.*, 2014).

Sediments are efficiently retaining DOM and DOM fluxes account for <10% of the sedimentary carbon oxidation rate (Burdige and Komada, 2015). Two models are commonly used for explaining carbon preservation in sediments. In the geopolymerization model, condensation reactions convert low-molecular weight DOM to larger molecules (Hedges, 1988). In the mesopore protection model, DOM adsorbed onto small mesopores on mineral surfaces is assumed to be protected from microbial enzymes and hence preserved (Hedges *et al.*, 1999; Mayer, 1994). In addition, marine sediments contain up to 30% of their organic carbon as particulate black carbon, even in the abyssal ocean (Masiello and Druffel, 1998; Middelburg *et al.*, 1999). In deep-sea sediments, this fraction is presumed to be derived from terrestrial DBC in the water column, adsorbed onto sinking particles. Black carbon in sediments can be several thousands of radiocarbon years older than the surrounding organic matter (Coppola *et al.*, 2014). It was previously hypothesized that resuspension of these sediments may be a source of pre-aged, re-dissolved DBC to the deep ocean (Wagner *et al.*, 2018). Measurements of DBC in marine porewaters are scarce. One study reported DBC in porewaters from a sulfidic intertidal creek of the southern North Sea (Wadden Sea). There, porewater DOC contained 7-14% of the ultra-refractory DBC fraction (Seidel *et al.*, 2014). Due to the proximity to the coast, these sediments were presumably heavily influenced by terrestrial and anthropogenic BC input. So far, sufficient quantitative measurements of porewater DBC in deep-sea sediments are lacking and this should be addressed to close the knowledge gaps in our understanding of the global BC cycle.

I.2 Natural petroleum seepage in marine systems

Catastrophic anthropogenic accidents such as the Deepwater Horizon or the Exxon Valdez oil spills can release enormous amounts of crude oil into the environment, polluting thousands of kilometers of coastal areas for years and poisoning marine life (Beyer *et al.*, 2016; Peterson *et al.*, 2003). Yet, even the largest anthropogenic oil spills release less oil into the marine environment than the overall annual contribution by natural seepage (Beyer *et al.*, 2016; Kvenvolden and Cooper, 2003). About 600,000 tons of oil are released every year by natural seepage (Kvenvolden and Cooper, 2003; NRC, 2003). This is a best estimate with a lower limit of 200,000 t and an upper limit of 2,000,000 t per year, quantified by satellite remote sensing of oil slicks on the ocean surface using synthetic aperture radar. However, not all petroleum released at the seafloor eventually reaches the sea surface and forms quantifiable oil slicks. For instance, about a quarter of the petroleum released at the seafloor during the Deepwater Horizon oil spill formed a stable deep-water intrusion and 2 to 20% were deposited on the seafloor (Gros *et al.*, 2017; Passow and Stout, 2020). Similar observations have been made at natural deep sea seepage sites, where, for example, seafloor deposits or oil bubbles of neutral buoyance occur (MacDonald *et al.*, 2004; Sahling *et al.*, 2016). Consequently, amounts of released petroleum from deep sea seepages quantified by satellite sea surface images may underestimate the real input to the marine environment. The actual contribution of natural seepage to the total annual input of petroleum is ambiguous, and estimates range from 6 to 47% (Dong *et al.*, 2022; Kvenvolden and Cooper, 2003). In contrast to anthropogenic oil spills which often rapidly release large quantities, natural seepages can be a constant source of regularly discharged oil of smaller quantities, providing carbon and energy to adapted ecosystems in the deep sea (MacDonald *et al.*, 2004; Teske, 2018; Wegener *et al.*, 2020). Natural seepage is a global phenomenon, observed for example in the Gulf of Mexico, the Coast of California, the Persian Gulf, the Black Sea, Caspian Sea, Gulf of Guinea, the coast of Ecuador and Peru and the coast of Alaska. (Dong *et al.*, 2022). In this thesis, two sites with natural petroleum seepages were investigated: Deep-sea heavy oil seepage in the Southern Gulf of Mexico (GOM) and deep-sea sediments impregnated by hydrothermal petroleum in the Guaymas Basin, Gulf of California (Figure 3).

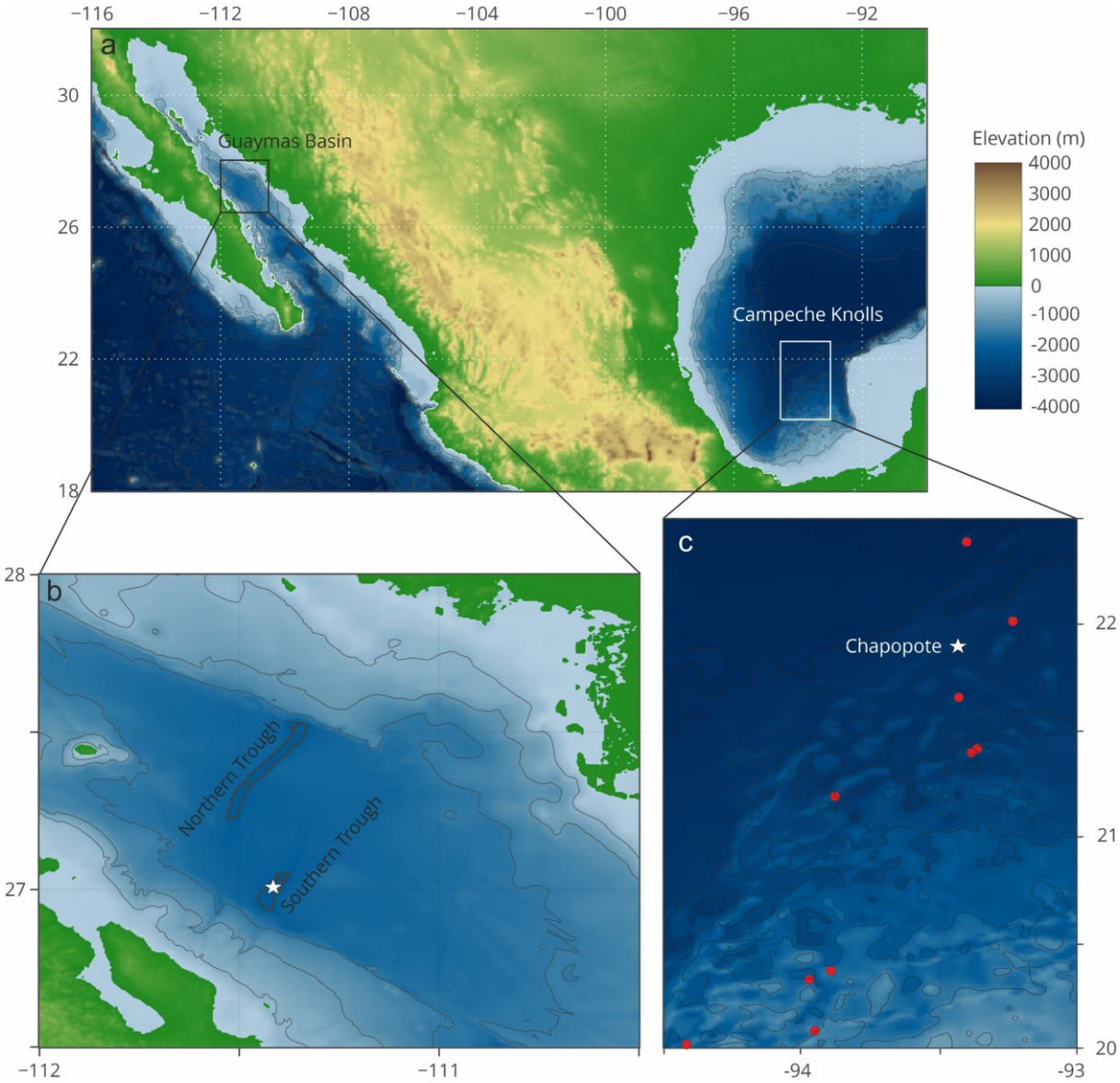

Figure 3: Map showing the location of the study areas of this thesis (a), and a detailed Map of the Guaymas Basin in the Gulf of California (b) and the Campeche Knolls in the Southern Gulf of Mexico (c). In map (b) of the Guaymas Basin, isobars at 2000 m water depth are highlighting the Northern and Southern rift zones. Samples examined in this study were retrieved from the Southern Trough, denoted with a star. In the close-up of the Campeche Knolls map (c), red dots highlight knolls and asphalt seeps examined during cruises SO 174/2, M67/2 and M114/2 described in detail in Sahling et al. (2016). Samples examined in Chapter II were retrieved from the Chapopote Asphalt volcano at 2900 m water depth. Maps were drawn in R using marmap (Pante and Simon-Bouhet, 2013) and based on bathymetric data hosted by the US National Ocean and Atmospheric Administration. High-resolution bathymetry retrieved during Cruise M114 was overlain on top of this basemap in the bottom right plot using data available in the Pangaea database (Wintersteller, 2019).

I.2.1.1 Study site 1: Chapopote asphalt volcano

Figure 4: Seafloor image of asphalt-deposits of the Chapopote Asphalt volcano. The seafloor image is available in the Pangaea database, GeoB19340-1,Sahling and Bohrmann (2016). The horizontal extent of this seafloor image is approximately 5 meters.

The GOM region is influenced by salt tectonism, which controls the development of reservoirs and faults, allowing hydrocarbons to escape at the sea floor (Macgregor, 1993).The GOM is an important contributor to global petroleum emissions where natural seepage contributes 43% of the visible oil slicks on the sea surface. About a quarter of the natural petroleum seepage occurs in the Southwestern GOM (MacDonald *et al.*, 2015). The Campeche Knolls located in this part of the GOM show a distinct form of natural petroleum seepage, called asphalt volcanism (MacDonald *et al.*, 2004). Here, satellite images of oil slicks on the sea surface suggest annual rates of 9,600 to 30,500 tons of oil seepage towards the sea surface (Suresh, 2015). Several asphalt fields have been identified to date at the Campeche Knolls (Sahling *et al.*, 2016). At one type locality, Chapopote, high-density oil forms 10,000 m³ of lava-like flow structures on the seafloor in 2900 m water depth (Marcon *et al.*, 2018; Schubotz *et al.*, 2011).

The Chapopote site was a target for several research cruises, where a rich and unique cold seep chemosynthetic ecosystem containing tubeworms, clams and white microbial mats

was observed (Figure 4) (Bohrmann *et al.*, 2008; MacDonald *et al.*, 2004; Sahling *et al.*, 2017). Other notable observations of this deep-water asphalt seep system include free gas and gas hydrate deposits, petroleum laden anoxic sediments and authigenic carbonates (MacDonald *et al.*, 2004; Naehr *et al.*, 2009; Schubotz *et al.*, 2011). In brittle asphalt exposed over a long period of time to seawater, almost all petroleum hydrocarbons detectable via gas chromatographic techniques are lost, suggesting biodegradation or dissolution in ambient seawater (Schubotz *et al.*, 2011; Wegener *et al.*, 2020). However, degradation of asphalt appears to be a slow process since almost no visual changes to asphalt deposits were observed between expeditions in 2006 and 2015, indicating that these asphalts may be exposed to seawater for decades to centuries (Sahling *et al.*, 2016). Asphalt seafloor deposits are not a unique phenomenon and were observed offshore Algeria (Jones *et al.*, 2014), Brazil (Fujikura *et al.*, 2017), the northern GOM (Weiland *et al.*, 2008), and the Santa Barbara Basin (Valentine *et al.*, 2010). Asphalts contain a large fraction of asphaltenes with > 40% in fresh Chapopote asphalt (Schubotz *et al.*, 2011). Since ultra-refractory DBC has proposed core structures comparable to compounds detected in petroleum asphaltenes (Dittmar and Paeng, 2009; Ruiz-Morales and Mullins, 2007; Ziolkowski *et al.*, 2011), investigating asphalt-derived DOM will provide insights on the extent to which natural (asphalt) seepage contributes to the pool of ultra-refractory oceanic DOM.

I.2.1.2 Study site 2: Guaymas Basin

The Guaymas Basin located in the Gulf of California is a young rift basin with active seafloor spreading in about 2000 m water depth. The Northern and Southern rift zones annotated in Figure 3 are accompanied by extensive axial-parallel fault lines (Lonsdale and Becker, 1985). The highly productive overlying waters deposit sediments rich in organic material that cover the spreading centers of the Guaymas Basin (Calvert, 1966). These layers alternate with shallow intrusions of basaltic sills into the loose sediments (Einsele *et al.*, 1980). On unsedimented mid-ocean ridges, magma is usually emplaced directly at the spreading center, but in the Guaymas Basin, the overlying sediments of up to 540 m thickness allow for the emplacement of magma into the flanking regions further away from the center (Lizarralde *et al.*, 2011; Teske *et al.*, 2020).

Sedimentary organic matter of 3-4% total organic carbon content is heated up at 200-300 °C and converted into hydrothermal petroleum under high pressure on short geological timescales (Simoneit, 1985): the resulting hydrothermal petroleum has radiocarbon ages of 4240-5705 years (Peter *et al.*, 1991), is rich in sulfur and has a high content of aromatic hydrocarbons, including PAHs and polycondensed aromatic heterocycles (PASH) (Didyk and Simoneit, 1989; Simoneit, 1985, 1988). At localized hotspots, thermal maturation of organic

matter can also generate hydrothermal petroleum in the shallow subsurface (Mara *et al.*, 2022; Ondréas *et al.*, 2018). Besides petroleum, gaseous hydrocarbons (Simoneit *et al.*, 1988; Song *et al.*, 2021), low-molecular weight organic acids (Martens, 1990), alcohols (Zhuang *et al.*, 2019) and ammonia (Von Damm *et al.*, 1985) are released and fuel highly active benthic microbial communities (Ramírez *et al.*, 2021; Teske *et al.*, 2002; Teske *et al.*, 2016). Active venting sites are usually characterized by bacterial mats of sulfur-oxidizing, nitrate-reducing filamentous *Beggiatoaceae* covering hot, sulfidic, often oil-impregnated sediments (Figure 5)(Jannasch *et al.*, 1989).

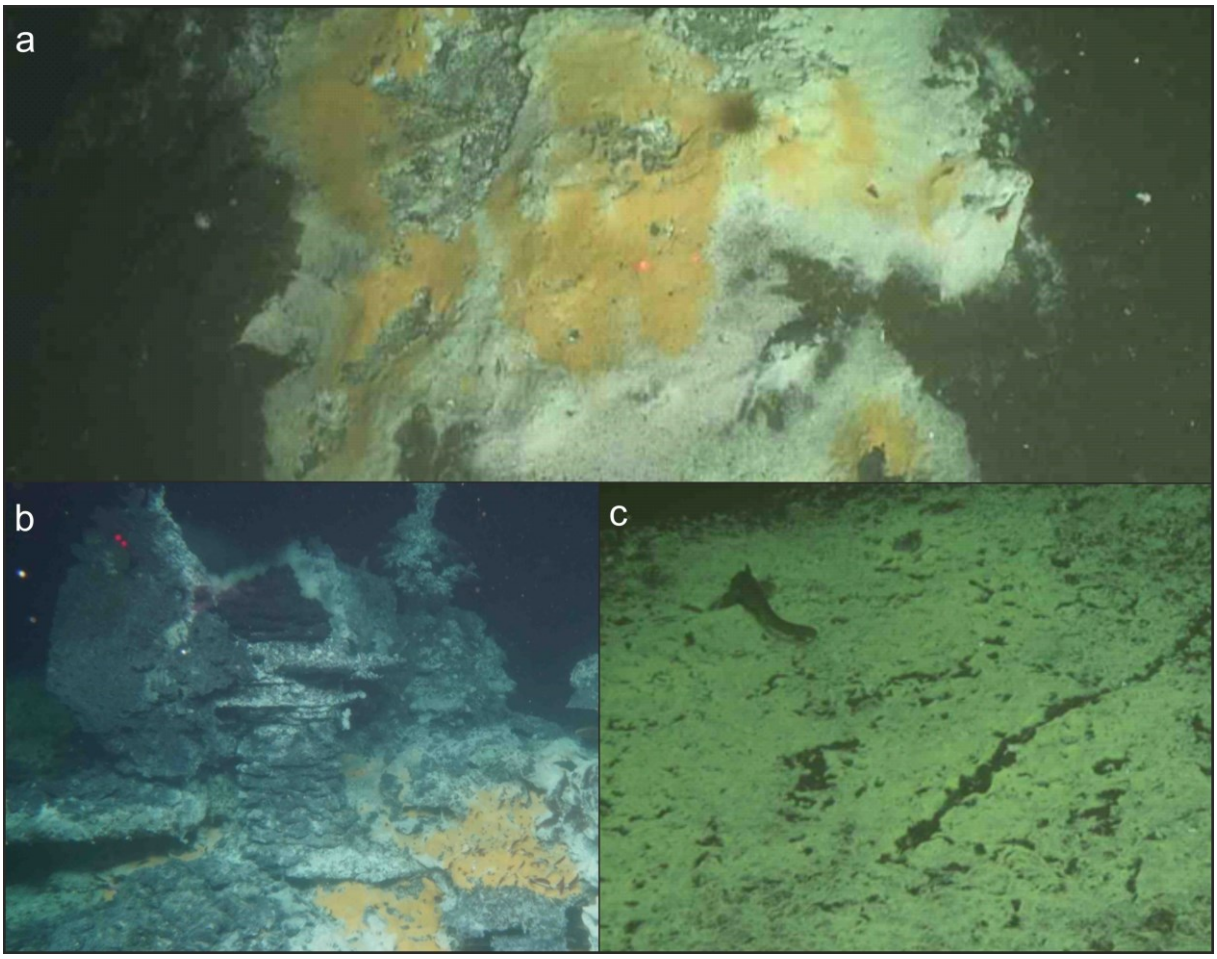

Figure 5: Seafloor images of the Guaymas Basin, taken by HOV Alvin during expedition AT42-05. A: Orange and white Beggiatoaceae mats covering a local hotspot at the type locality Cathedral Hill with oil-laden sediments and steep temperature gradients (>105 °C in 30 cm sediment depth). B: Massive hydrothermal mound structures at type locality Rebecca´s Roost. C: Large white microbial mat covering sediment-impregnated sediments at type locality Aceto Balsamico with moderate temperature gradients (21 °C in 45 cm). Pictures were taken during dives 5001 (a) and 4992 (b,c) and are available under Alvin Framegrabber (2023). All features shown are several meters in extent.

Steep temperature gradients usually limit benthic microbial activity towards surficial sediments. Depending on the locally highly variable heat flow, culturable cells can be below the detection limit already at 20 cm sediment depth, reaching 105 °C (Teske *et al.*, 2009).

Microbial carbon degradation is likely limited to temperatures below 100 °C in Guaymas Basin sediments (McKay *et al.*, 2016), suggesting that DOM in porewaters above this temperature is derived by heat mobilization or hydrothermal cracking of sedimentary organic matter. DOC concentrations in bottom waters are highly elevated of up to a factor of 50 compared to non-hydrothermal deep-sea environments, indicating that advective porewater fluxes transport hydrothermally-derived DOM into the adjacent water column (Lin *et al.*, 2017; Ziervogel and Arnosti, 2020). Lin *et al.* (2017) simulated hot-water discharge events of Guaymas Basin sediments and observed the rapid discharge of large amounts of mainly labile DOM being released from non-altered sediments. Hydrothermally altered sediments on the other hand contain petroleum adsorbed onto mineral particles and dissolved in porewater. Dissolved PAH and PASH compounds are present in porewaters and probably migrate rapidly out of the sediment (Mara *et al.*, 2022). Since both previously hypothesized sources of marine DBC (hydrothermal heating and petroleum generation) occur in the Guaymas Basin, studying dynamics of DOM at this location provide an excellent opportunity to test these hypotheses.

I.3 Methodological approach

DOM is one of the most complex mixtures known. Estimates about the complexity of DOM assume more than 600,000 and possibly >1,000,000 different compounds (Dittmar *et al.*, 2021; Hertkorn *et al.*, 2007; Riedel and Dittmar, 2014; Zark *et al.*, 2017). The complexity of DOM along with very low concentrations of individual compounds presumably in the pico- and femtomolar range makes it resistant to typical preparative procedures like chromatographic separation. Instead, DOM is commonly characterized by untargeted analysis of its optical properties or molecular-level analysis by ultrahigh-resolution mass spectrometry. Nuclear magnetic resonance spectroscopy (NMR) provides the best approach to gain structural information on DOM. However, overlapping signals prevent DOM compounds from being fully resolved, though recent developments in multi-dimensional NMR provided promising results (Mitschke, 2022; Seidel *et al.*, 2022). In this thesis, DOM was mainly analyzed by using its optical properties and by ultrahigh-resolution mass spectrometry.

I.3.1 Quantitative analysis of dissolved organic matter

Only few small biomolecules such as monomeric carbohydrates, amino acids or fatty acids can be isolated and analytically determined from DOM. Individual quantifiable compounds account for only about 1% of marine DOM (Dittmar and Stubbins, 2014). Bulk chemical properties, for instance the concentration of DOC, can be determined by high temperature

catalytic oxidation after removing inorganic carbon by acidification. DON concentrations cannot be measured directly: instead, the total dissolved nitrogen is determined by high temperature catalytic oxidation and separately measured inorganic nitrogen species are subtracted (Sipler and Bronk, 2015). Even more problematic is the determination of DOS because seawater sulfate concentration is generally orders of magnitude higher than DOS. This requires an isolation of DOM, commonly performed by ultrafiltration or solid-phase extraction (SPE). Extraction yields are generally higher for SPE, i.e. ~50-80% of DOC vs. ~30% by ultrafiltration, respectively (Amon and Benner, 1996; Dittmar *et al.*, 2008)). During SPE, DOM adsorbs onto a sorbent (e.g., styrene divinyl benzene polymer, PPL), while the inorganic phase is removed with acidified ultrapure water. Adsorbed DOM is then eluted with a solvent, which also allows to concentrate the sample for further investigation. Although some discrimination between bulk waters and eluted DOM is observed, for instance higher N:C ratios in DOM_{SPE}, SPE provides a representative method for isolation of both bulk water and petroleum-derived DOM (Dittmar *et al.*, 2008; Zito *et al.*, 2019a). Solid-phase extracted DOS (DOS_{SPE}) can subsequently be quantified, for example by inductively coupled plasma optical emission spectrometry (Pohlabeln and Dittmar, 2015), although discrimination between bulk water S:C and SPE S:C remains unknown. Concentrated DOM_{SPE} further allows to determine the ultra-refractory DOM fraction, DBC. For this, the SPE extract is oxidized with nitric acid, which converts polycondensed aromatics like DBC to benzenepolycarboxylic acids (BPCA) (Dittmar, 2008). The number of carboxylic substitutions in converted BPCA provides information about the number of fused rings in DBC. BPCA can then be quantified using absorbance spectra after separation by liquid chromatography and original DBC concentrations are determined using conversion factors (Stubbins *et al.*, 2015).

I.3.2 Qualitative untargeted analysis of dissolved organic matter

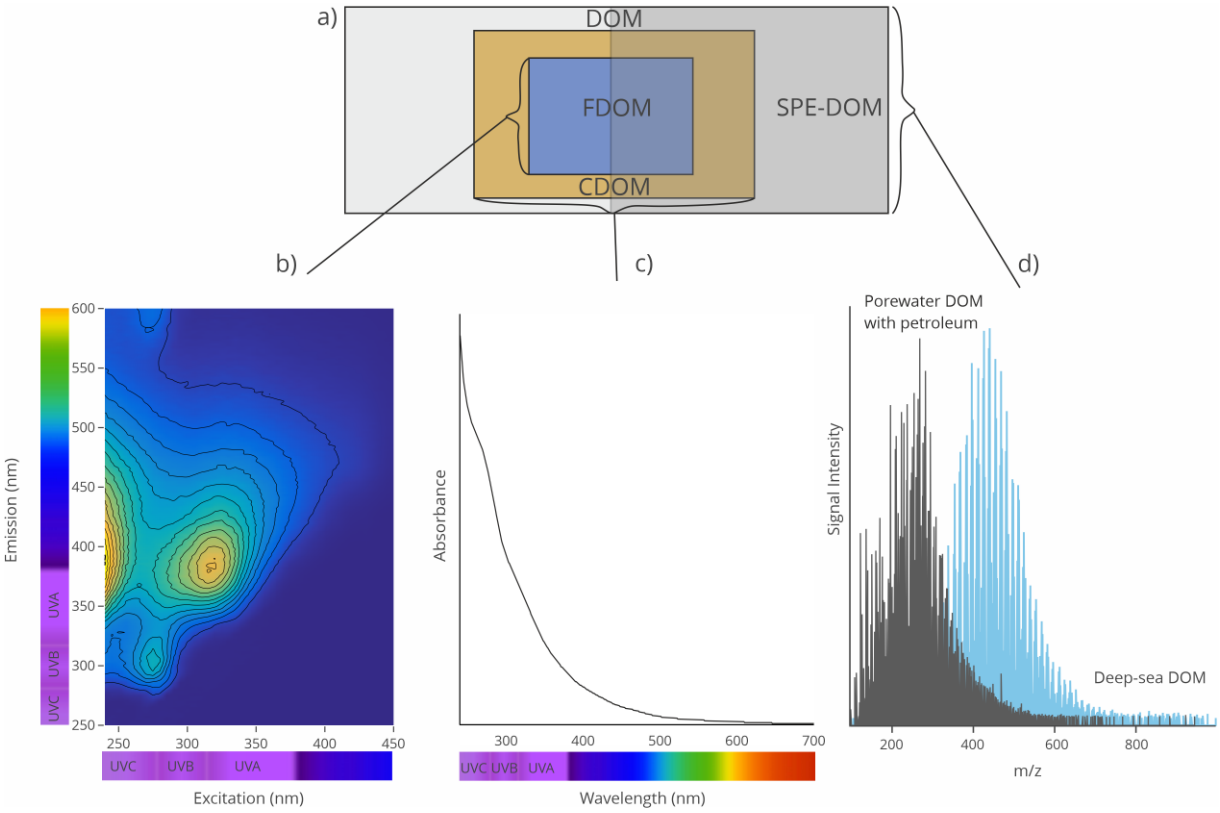

Figure 6: Schematic presentation of the different main DOM fractions targeted (a), the subfraction of fluorescent DOM (FDOM) represented by an excitation-emission matrix (EEM), semi-quantified by its fluorescence intensity (b), the subfraction of chromophoric DOM (CDOM), semi-quantified by its light absorption (c) and a mass spectrum from ultra-high resolution mass spectrometry (FT-ICR-MS) analysis of solid-phase extracted (SPE) DOM, showing the molecular composition of a porewater sample containing petroleum and typical deep-sea DOM. Color scales in b), absorbance in c) and signal intensities in d) are on arbitrary scales for schematic representation.

I.3.2.1 Molecular characterization by ultra-high resolution mass spectrometry

Originally developed in the context of petroleomics, ultrahigh-resolution mass spectrometry by Fourier-transform ion cyclotron resonance mass spectrometry (FT-ICR-MS) allows to characterize DOM on the molecular level (Comisarow and Marshall, 1974; Kujawinski, 2002; Marshall and Rodgers, 2008). FT-ICR-MS requires the pre-concentration of DOM and ionization techniques such as electrospray ionization (ESI) of salt-free samples. Hence, isolated DOM by ultrafiltration or SPE is usually analyzed. A typical mass spectrum of marine DOM contains thousands of peaks of which most are in the range of 250-500 Da, whereas water-soluble petroleum-derived DOM usually has lower average masses (Figure 6 a, d)(Seidel *et al.*, 2016). Peak intensities are detected semi-quantitatively and are controlled by the ionization efficiency of a given molecule, not necessarily reflecting its actual concentration.

High mass accuracy of detected ionized intact DOM molecules allows to calculate molecular formulae utilizing the mass defect of a given molecule. So far, this allowed the identification of more than 20,000 individual molecular formulae in DOM, each representing multiple structural isomers (Dittmar *et al.*, 2021; Riedel and Dittmar, 2014; Zark *et al.*, 2017). Multiple indices were developed to infer structural information from molecular formulae such as the double bond equivalent (DBE) (Korsten, 1997)), aromaticity index (AI_{mod}) (Koch and Dittmar, 2006, 2016) and nominal oxidation state of carbon (NOSC) (LaRowe and Van Cappellen, 2011). A typical graphical representation for the thousands of molecular formulae are van Krevelen plots, where each molecular formula is plotted according to its O:C and H:C ratios (Figure 7) (Kim *et al.*, 2003). Based on the location in the van Krevelen diagram and molar ratios, molecular formulae can be assigned into the following compound groups: (1) polycondensed aromatics ($AI_{mod} > 0.66$ and DBC if $C \geq 15$; (2) aromatics ($0.5 < AI_{mod} \leq 0.66$); (3) unsaturated aliphatics ($1.5 < H/C \leq 2$, $O/C < 0.9$, $N = 0$);(4) unsaturated aliphatics with nitrogen ($1.5 < H/C \leq 2$, $O/C < 0.9$, $N > 0$); (5) highly unsaturated ($AI_{mod} \leq 0.5$, $H/C < 1.5$, $O/C < 0.9$) and (6) saturated ($H/C > 2$ or $O/C \leq 0.9$) (Osterholz *et al.*, 2016; Šantl-Temkiv *et al.*, 2013; Seidel *et al.*, 2014). It is important, however, to emphasize that the molecular formulae in these compound groups describe a mixture of isomers and hence do not necessarily indicate the presence of a structural entity or functional group in the DOM samples. Based on NMR and FT-ICR-MS analysis, carboxyl-rich alicyclic molecules (CRAM) (Hertkorn *et al.*, 2006) were identified as a major component of refractory oceanic DOM. In terrestrial-derived DOM, saturated compounds are further divided into lipids, amines, amino sugars/carbohydrates and highly unsaturated compounds into lignins/tannins (Sleighter and Hatcher, 2008). However, these compound classes are generally not present in marine DOM in case of lignin/tannin or highly labile (saturated compounds).

Another simplified approach to infer lability from molecular formulae was presented by D'Andrilli *et al.* (2015), where molecular formulae with $H/C \geq 1.5$ are considered labile and $H/C < 1.5$ recalcitrant. Most detected molecular formulae in oceanic DOM have a medium saturation with an average H/C ratio slightly above 1 and an O/C ratio of ~0.5 (Dittmar and Stubbins, 2014). Water-soluble, petroleum-derived DOM on the other hand can have a large abundance of highly reduced molecular formulae with low O/C ratios (Figure 7 b)(Seidel *et al.*, 2016). However, microbial transformations generally oxidize these compounds causing similar H/C and O/C ratios compared to marine DOM, which makes an identification of highly degraded petroleum-derived DOM difficult (Bekins *et al.*, 2020; Kleindienst *et al.*, 2015; Liu *et al.*, 2020; Seidel *et al.*, 2016). Nonetheless, petroleum-derived DOM seems to be enriched in heteroatoms (N, S) compared to background DOM (Dvorski *et al.*, 2016; Islam *et al.*, 2016; Liu

and Kujawinski, 2015; Seidel *et al.*, 2016). For petroleum-derived DOM, Liu and Kujawinski (2015) introduced the ratio of NSO:C in a given molecular formula to assess the potential hydrophobicity. Based on an enhanced solubility of slightly more polar, heteroatom-containing molecules, molecular formulae with low NSO:C ratios or high molecular masses are considered more hydrophobic and conversely, formulae with high NSO:C ratios are considered to be more hydrophilic.

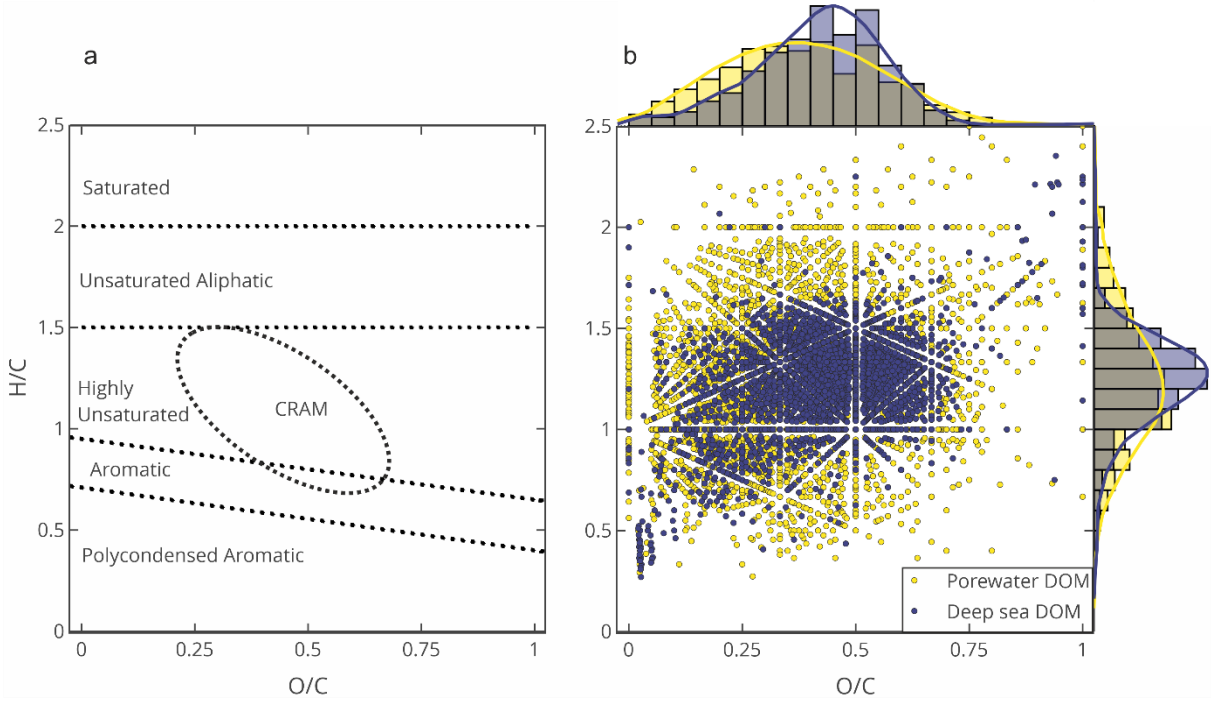

Figure 7: Van Krevelen plot for visualization of molecular formulae of DOM resolved by FT-ICR-MS analysis. Typically inferred compound groups are shown in (a) and molecular formulae assigned to a deep sea DOM_{SPE} sample (blue) compared to oil-impregnated porewater DOM_{SPE} (yellow). Van Krevelen plots further display densities and the relative abundance of molecular formulae grouped after H/C (binsize = 0.1) and O/C (binsize = 0.05) ratios. (b). CRAM = carboxyl-rich alicyclic molecules.

I.3.2.2 Optical spectroscopy

While determining the optical properties of DOM provides less detailed information than ultrahigh-resolution mass spectrometry, general structural information of bulk DOM can be inferred. Measuring the light absorbance or fluorescence of DOM does not require sample preparation or isolation of the DOM. Hence, results reflect the actual bulk DOM not fractionated in an isolation procedure. At the same time, optical properties can also be determined on re-dissolved DOM extracts or the permeate during SPE, proving valuable information about DOM discrimination by SPE (Figure 6 a-c) (Wünsch and Murphy, 2020; Wünsch *et al.*, 2018).

About 20-70% of DOC is made up of chromophoric DOM (CDOM), a subfraction of bulk DOM semi-quantified by its light absorption (Figure 2 c) (Laane and Koole, 1982). Aromatic

molecules usually absorb UV-light, hence higher light absorption in the UV-range is associated with a higher content of aromatic carbon in DOM (Weishaar *et al.*, 2003). In riverine DOM, specific CDOM absorbance can be applied to estimate the content of DBC in DOM (Stubbins *et al.*, 2015). Assessing the slope of the absorbance spectrum further provides information about molecular weight and source of DOM (Helms *et al.*, 2008). However, these observations were developed in a different context than petroleum-derived DOM and are based on typical marine or terrestrial DOM. Nonetheless, quantifying the specific absorption intensity at a given wavelength in the UV range (typically 254 nm) in oil-derived DOM has shown promising results as a tracer, possibly due to the high content of aromatic carbon in oil-derived DOM (Harriman *et al.*, 2017; Podgorski *et al.*, 2018).

I.3.2.3 Fluorescence spectroscopy

A subfraction of CDOM also fluoresces (fluorescent DOM, FDOM). For its analysis, FDOM is excited with light of certain wavelengths (~240-450 nm) and the emitted fluorescent light intensities at a given wavelength (~300-600 nm) is recorded, producing excitation-emission matrices (EEMs, Figure 7a). EEMs are comprised of fluorophore peaks, generally divided into humic-like and protein-like peaks (Coble, 1996). Several typical peak locations of fluorophore groups have been reported in the literature and they have been extensively studied in terrestrial and marine environments (Coble, 1996; Korak *et al.*, 2014; Ziegelgruber *et al.*, 2013). Ratios of certain wavelengths such as the fluorescence index, biological index or freshness index can provide information about the sources and lability of FDOM (Huguet *et al.*, 2009; McKnight *et al.*, 2001; Parlanti *et al.*, 2000). However, similar to CDOM slope ratios, these observations apply to typical terrestrial or marine FDOM and may be misleading in petroleum-derived DOM. For instance, petroleum-derived FDOM contained humic-like fluorescence in a laboratory experiment even though petroleum does not contain humic acids (Zito *et al.*, 2019b). Moreover, petroleum-derived DOM particularly emits protein-like fluorescence, while the protein content in petroleum should be negligible (Podgorski *et al.*, 2018; Zito *et al.*, 2019b). A more detailed insight into underlying fluorophores is possible by parallel-factor analysis (PARAFAC), a mathematical tensor decomposition of the EEM spectra.

$$X_{ijk} = \sum_{f=1}^{F} a_{if} b_{jf} c_{kf} + \varepsilon_{ijk} \quad (1)$$

Spectral fluorescence is multi-way (3-way) as it varies as a function of excitation and emission, described in equation 1. Measurements are stacked to form a box of data X, where i represent samples, j emission wavelengths and k excitation wavelengths (Figure 8). The PARAFAC algorithm fits an alternating least squares approach to minimize unexplained data (ε_{ijk}) and calculates the sum of the concentrations of each component (a_i), the emission properties (b_j)

and the excitation properties (c_k) for a given factor f. (Bro, 1997; Murphy *et al.*, 2013; Stedmon *et al.*, 2003). Each PARAFAC component represents an underlying mathematical fluorophore which usually represents >98% of the detected signal in the original EEM. In environmental samples, these PARAFAC components are not pure, isolated fluorophores but rather represent a group of dissolved compounds exhibiting similar spectral properties (Murphy *et al.*, 2013). Individual PARAFAC components can be compared with a database using their specific excitation and emission wavelengths and the degree of factor similarity assessed using Tuckers congruence coefficient (Lorenzo-Seva and Ten Berge, 2006; Murphy *et al.*, 2014). Several petroleum-derived PARAFAC components have been identified, showing similar optical and hence underlying structural properties comparable to typical natural FDOM (Podgorski *et al.*, 2018; Zhou *et al.*, 2013; Zito *et al.*, 2019b).

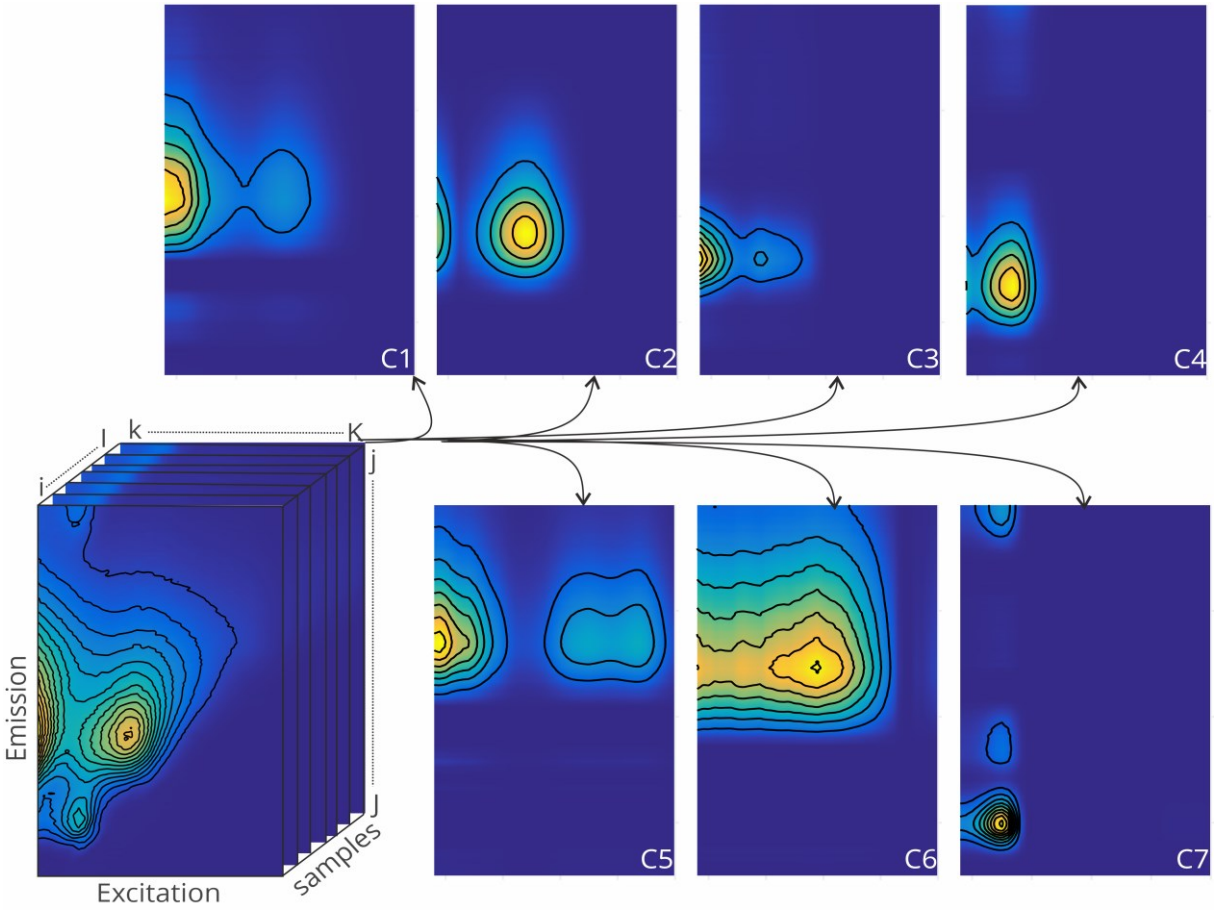

Figure 8: Schematic explanation of the PARAFAC algorithm, adapted after Murphy et al. (2013). Measured data (i to I samples, j to J emission wavelengths, k to K excitation wavelengths) is decomposed by the PARAFAC algorithm into underlying factors, here represented as PARAFAC components C1-C7. The model shown here is presented in Chapter 3; excitation and emission range displayed is 240 to 450 nm and 250 to 600 nm, respectively.

I.4 Thesis Objectives

The overarching goal of this thesis was to assess molecular transformations of DOM in natural petroleum seepages and the potential release of petroleum-compounds to oceanic deep sea DOM. Chapter II examines the molecular composition of water-soluble petroleum compounds from a natural asphalt seep in a controlled laboratory experiment. The bio-availability of petroleum-derived DOM is assessed by conducting incubation experiments. Quantification of asphalt-derived DOC, DBC, and DOS allows conclusions to be drawn about their release to the environment as part of the oceanic DOM. The research questions of this study were: (1) what is the quantity of asphalt-derived dissolved organic carbon (DOC) that is released by fresh asphalts, (2) what are the optical properties and the molecular composition of the released DOM, (3) how do microbial transformations affect the DOM composition, (4) are natural asphalt seeps a potential source of ultra-refractory DOM and DOS to the ocean?

Chapter III explores hydrothermal petroleum-derived DOM in porewaters and bottom waters of hydrothermal, oil-laden sediments of the Guaymas Basin. By applying a combined approach of optical analysis of bulk porewater FDOM and molecular-level analysis of DOM_{SPE}, (1) the composition of DOM in hydrothermal porewaters was assessed, (2) the effects of high temperatures on changes in the DOM composition were investigated, and (3) fractions of hydrothermal petroleum-derived porewater DOM reaching bottom waters were determined.

Chapter IV extends the molecular and optical DOM analyses of Chapter III using a quantitative approach targeting petroleum-derived DOM. In this study, different DOM fractions in hydrothermal porewaters and overlying bottom waters were quantified: ultra-refractory DBC, as well as potentially recalcitrant DOS and potentially bio-available DON and DOP. To assess the release of these DOM fractions into the porewater and adjacent water column, hydrothermal hot-water mobilization of sedimentary organic matter was simulated by Soxhlet extraction. By using this comprehensive approach, the impact and contribution of hydrothermal sediment alteration on the deep-sea DOM cycle was evaluated.

II. Manuscript 1

Natural asphalt seeps are potential sources for recalcitrant dissolved organic sulfur and dissolved black carbon

Jonas Brünjes,[†] Michael Seidel,[‡] Thorsten Dittmar,[‡,¶] Jutta Niggemann,[‡] and Florence Schubotz[†]

[†]MARUM Center for Marine Environmental Sciences, University of Bremen, Bremen, 28359, Germany

[‡]Institute for Chemistry and Biology of the Marine Environment (ICBM), Carl von Ossietzky University of Oldenburg, 26129, Oldenburg, Germany

[¶]Helmholtz Institute for Functional Marine Biodiversity at the University of Oldenburg, Oldenburg, 26129, Germany

Published in *Environmental Science & Technology* (2022), Vol 56, pages 9092-9102, doi: 10.1021/acs.est.2c01123

Author-directed link:

http://pubs.acs.org/articlesonrequest/AOR-6FNARR2DG7BGQF8UHKUG

Abstract

Natural oil seepages contribute about half of the annual petroleum input to marine systems. Yet, environmental implications and persistence of water-soluble hydrocarbons from these seeps are vastly unknown. We investigated the release of oil-derived dissolved organic matter (DOM) from natural deep sea asphalt seeps using laboratory incubation experiments. Fresh asphalt samples collected at the Chapopote asphalt volcano in the Southern Gulf of Mexico were incubated aerobically in artificial seawater over four weeks. The compositional changes in the water-soluble fraction of asphalt-derived DOM were determined with ultrahigh-resolution mass spectrometry (Fourier-transform ion cyclotron resonance mass spectrometry, FT-ICR-MS) and by excitation-emission matrix spectroscopy to characterize fluorescent DOM (FDOM) applying parallel factor (PARAFAC) analysis. Highly reduced aliphatic asphalt-derived DOM was readily biodegraded, while aromatic and sulfur-enriched DOM appeared to be less bioavailable and accumulated in the aqueous phase. A quantitative molecular tracer approach revealed the abundance of highly condensed aromatic molecules of thermogenic origin. Our results indicate that natural asphalt and potentially other petroleum seepages can be sources of recalcitrant dissolved organic sulfur and dissolved black carbon to the ocean.

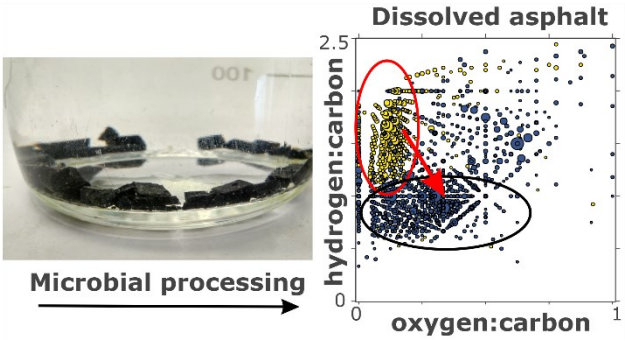

Graphical Abstract.

Synopsys statement for environmental significance

Natural asphalt seepage can release water-soluble hydrocarbons such as recalcitrant organic sulfur and black carbon to the deep ocean.

II.1 Introduction

About half of the annual input of petroleum to the ocean is released by natural oil seepage, which is estimated to contribute 600,000 tons per year (Kvenvolden and Cooper, 2003). A fraction of the oil enriched in polar molecules of low molecular mass can dissolve in seawater and enter the dissolved organic matter (DOM) pool. The environmental implications and persistence of this water-soluble oil fraction from natural seeps are vastly unknown.

Several studies investigated the molecular composition of DOM associated with terrestrial and marine oil spills (Dvorski *et al.*, 2016; Islam *et al.*, 2016; Podgorski *et al.*, 2018; Podgorski *et al.*, 2020), tracked oil sources and weathering products such as oxygenated hydrocarbons with ultrahigh- resolution mass spectrometry (Fourier-transform ion cyclotron resonance mass spectrometry, FT-ICR-MS) (Corilo *et al.*, 2013; Lemkau *et al.*, 2014). FT-ICR-MS resolves thousands of molecules in complex organic matter mixtures such as oil and DOM in aquatic samples (Kujawinski, 2002; Marshall and Rodgers, 2008). Several laboratory experiments were conducted after the Deepwater Horizon oil spill investigating oil-derived DOM from Macondo oil surrogate on the molecular level: Liu and Kujawinski (2015) found an enrichment of heteroatom-containing DOM compared to the parent oil and explained this with higher polarity and consequently higher solubility in seawater. Microbial incubation experiments were conducted by Kleindienst *et al.* (2015) and Seidel *et al.* (2016). In their oil-only incubations, oil-derived DOM exhibited a characteristic fingerprint of compounds with a low molecular oxygen to carbon (O/C) ratio and low molecular masses compared to the natural marine DOM background. A further laboratory incubation study by Liu *et al.* (2020) found an increase in the chemical diversity and oxygen content of oil-derived DOM following microbial transformations. Besides FT-ICR-MS, excitation-emission matrix fluorescence spectroscopy (EEM) and subsequent parallel factor analysis (PARAFAC) are commonly used to characterize the fluorescent part of DOM (FDOM) and were previously applied to track oil-related DOM after oil spills (Bianchi *et al.*, 2014; Podgorski *et al.*, 2018; Zhou *et al.*, 2013). In field studies (Dvorski *et al.*, 2016; Podgorski *et al.*, 2020) and laboratory experiments (Zito *et al.*, 2020; Zito *et al.*, 2019b), EEM-PARAFAC and FT-ICR-MS can be used as complementary techniques to trace changes in oil-derived DOM. However, our understanding of the fate of DOM released by natural oil seepages is still limited.

Oceanic DOM contains 662 Pg dissolved organic carbon (DOC) (Hansell *et al.*, 2009), of which a fraction of 12 Pg is considered ultra-refractory with 14C ages older than 20,000 years in the deep sea (Coppola and Druffel, 2016; Dittmar and Paeng, 2009). This fraction contains dissolved black carbon (DBC), which has proposed core structures of fused rings with

carboxylic functional groups, comparable to compounds detected in petroleum asphaltenes (Dittmar and Paeng, 2009; Ruiz-Morales and Mullins, 2007). While DBC is assumed to be mainly produced by the incomplete combustion of terrestrial organic matter on land, recent studies have pointed out mismatches between ^{13}C and ^{14}C isotopic signatures of terrestrial DBC sources and oceanic DBC, suggesting additional marine sources of DBC (Coppola and Druffel, 2016; Wagner *et al.*, 2018; Wagner *et al.*, 2019). In addition, sulfur-containing DOM, dissolved organic sulfur (DOS) is a petagram inventory of oceanic DOM, and known DOS sources such as phytoplankton and sulfidic environments (Pohlabeln *et al.*, 2017; Seidel *et al.*, 2014) do not balance out sinks of non-labile DOS in a global inventory (Ksionzek *et al.*, 2016). In this study we hypothesize that petroleum seeps are a source of DBC and water-soluble petroleum-derived DOS to the deep ocean.

Asphalt volcanism is a special type of deep-sea heavy oil seepage first described in the southern Gulf of Mexico (GOM) (MacDonald *et al.*, 2004; Sahling *et al.*, 2016). Several asphalt fields have been identified to date at the Campeche Knolls, of which one, the Chapopote asphalt volcano, exhibits 10,000 m³ of lava-like asphalt flows on the seafloor in 2,900 m water depth (Marcon *et al.*, 2018). By conducting a laboratory incubation experiment of Chapopote-derived asphalt in artificial seawater, we studied the composition of oil-derived DOM and assessed the lability to microbial degradation to provide an estimate on the potential impact of oil- seepage on the deep-oceanic carbon cycle. Unlike previous laboratory incubation studies (Kleindienst *et al.*, 2015; Liu and Kujawinski, 2015; Seidel *et al.*, 2016; Zito *et al.*, 2019b), we chose artificial seawater instead of filter-sterilized seawater as the incubation medium, because seawater contains DOM that may conceal the oil-derived DOM imprint or metabolites of oil degradation. We targeted the following research questions: (1) what is the quantity of asphalt-derived dissolved organic carbon (DOC) that is released by fresh asphalts, (2) what are the optical properties and the molecular composition of the released DOM, (3) how do microbial transformations affect the DOM composition, and (4) are natural asphalt seeps a potential source of ultra-refractory DOM and DOS to the ocean? Our study shows that natural asphalt and potentially other petroleum seeps can be sources of recalcitrant DOS and DBC to the ocean.

II.2 Materials and Methods

II.2.1 Material and incubation setup

Visually non-biodegraded asphalt samples were collected during *RV* Meteor leg 114 in March 2015 by a gravity corer (GeoB 19339-1) at the Chapopote asphalt volcano in a water depth of 2905 m from oxic bottom waters (Sahling *et al.*, 2017; Wegener *et al.*, 2020). The asphalt samples are similar to fresh asphalt described in Wegener *et al.* (2020) and contain a high proportion of asphaltenes (>45% asphaltenes, ca. 40% aliphatic and aromatic hydrocarbons and ca. 15% resins). The location was assigned to the most recent asphalt flow of the main asphalt field and was not covered by microbial mats or metazoans (Marcon *et al.*, 2018) (Figure S1). Samples were kept at 4°C in the dark and aerated in filtered (0.2 μm) bottom seawater from Chapopote for three years before this experiment. This filtration was performed to remove microbes and particles from the seawater. We did not monitor the integrity of sterility of the added seawater, but instead expect microbial communities living on the surface of the asphalts (Wegener *et al.*, 2020) to be primarily active during these several months to 10-year incubations.

Artificial seawater was prepared using an adapted version described by Widdel and Bak (1992) with high nutrient concentrations to avoid nutrient limitation for microbial activity during the incubations (Table S1). Asphalt samples were cut into small cubes of approximately 3-5 mm side lengths after the exterior and potentially weathered part of the asphalt was removed. Microorganisms are present in asphalt samples from the main asphalt field that are affiliated to known hydrocarbon degrading organisms (Wegener *et al.*, 2020). To stimulate microbial growth and distribute microorganisms homogenously on the asphalt, asphalt cubes were mixed with 150 mL of artificial seawater and pre-incubated for 10 days in the dark at room temperature. Between 3.6 and 3.8 g of asphalt and 10 mL of the inoculum were then transferred into combusted and autoclaved 500 mL glass bottles (Schott) together with 490 mL of artificial seawater. The incubation was set up in triplicates on a roller table (45 rpm) at room temperature in the dark and performed over 28 days. A control was established by pasteurizing one incubation bottle after the initial experimental setup and again after 20 and 24 days (2 hours at 65°C in a water bath, as previously described in Kleindienst *et al.* (2015)). Pasteurization was chosen, because common techniques such as the addition of ZnCl, autoclaving and gamma-radiation could interfere with electrospray ionization (ESI) in mass spectrometry or alter the asphalts composition and DOC concentrations, respectively (Otte *et al.*, 2018). The incubation bottles were loosely screwed with lids to minimize the loss of volatile compounds and left open for a few minutes and gently shaken on sampling days to prevent

anoxic conditions. In a preliminary study in closed bottles, 55% of initial dissolved oxygen remained after 28 days. Sample aliquots for optical and dissolved inorganic carbon (DIC) analysis were taken out of the incubation bottles with precleaned (pH2 rinsed) polystyrene pipettes (Sarstedt) after 0, 2, 6, 10, 20, and 28 days (2 mL) and after 0, 10, and 28 days for DOM analysis (100 - 150 mL). Asphalt samples for long-term incubation experiments were collected on *RV* Meteor expedition M67/2b and M114. Approximately 20 to 40 g of asphalt was incubated in 200 mL filtered (0.2 μm) Chapopote bottom seawater at 4°C in the dark over a period of 6 months to 10 years in glass bottles loosely screwed with lids (Table S2).

II.2.2 Dissolved inorganic carbon analysis

For determination of the isotopic carbon composition of dissolved inorganic carbon (DIC), water samples were filtered through 0.2 μm RC cellulose syringe filter (Sartorius) and stored frozen without headspace until analysis. Measurements were conducted on a Delta Ray Isotope Ratio Infrared Spectrometer (IRIS) with URI Connect and autosampler (Thermo Fisher Scientific, Germany). 1 mL of water sample was acidified with 45% phosphoric acid and after an equilibration time of 10 hours released CO_2 was analyzed in the Delta Ray IRIS with URI connect for stable carbon isotope ratio of CO_2 against CO_2 reference gas, using synthetic air as a carrier. Results are given as $\delta^{13}C$ DIC (‰ VPDB).

II.2.3 Dissolved organic matter analysis

Water samples were vacuum-filtered through pre-combusted (5 hours at 450 °C) 0.3 μm glass fiber filters (GF/F, Sterlitech). Samples were acidified to pH 2 with HCl (25%, p.a.) and stored at 4°C in amber glass bottles. Following acidification and temperature change precipitation occurred, which was removed by filtration using pre-rinsed 0.45 μm hydrophilic polypropylene membrane filters (GHP, Acrodisc) for 10-day and 28-day incubated samples. Precipitations probably occurred because mesocosm experiments were performed at 20°C, which means that the water-solubility of hydrocarbons was likely slightly higher relative to the natural deep-sea environment (4°C). This precipitation likely affected only water- insoluble unpolar compounds which would not end up in the DOM pool. DOC concentration was measured by high temperature catalytic oxidation on a Shimadzu TOC-VCPH instrument with an analytical precision better than 5%. Trueness was tested in each run against deep Atlantic seawater reference material provided by the consensus reference materials program (D.A. Hansell, University of Miami, Coral Gables, FL, USA). DOM was extracted and concentrated from filtered and acidified (pH 2, HCl) water samples by solid phase extraction (SPE) using 0.5 g PPL sorbent cartridges (Agilent Bond Elut) and eluted with 3 mL of methanol (MS-grade) after

Dittmar *et al.* (2008). DOC concentration in SPE extracts was determined by evaporating an aliquot of the methanol extract at 40 °C and re-dissolving the dried extract in ultrapure water. The isotopic carbon composition (‰ VPDB) of DOCSPE was measured on an elemental analyzer by evaporating an aliquot of the methanol extract in tin caps and analyzed with continuous-flow elemental analyzer isotope ratio mass spectrometer. Molecular DOM analysis was performed on a solariX XR FT-ICR-MS (Bruker Daltonik GmbH, Bremen, Germany) connected to a 15 Tesla superconducting magnet (Bruker Biospin, Wissembourg, France) (Seidel *et al.*, 2015). Details on measuring conditions and subsequent molecular formula and compound group assignment are provided in the supplementary information. The molecular parameters for the aromaticity index (A_{Imod} (Koch and Dittmar, 2006, 2016)), double bond equivalents (DBE (Korsten, 1997)), average nominal oxidation state of carbon (NOSC (LaRowe and Van Cappellen, 2011)) and the ratio of nitrogen, sulfur and oxygen to carbon (NSO:C (Liu and Kujawinski, 2015)) were calculated for each detected molecular formula.

To distinguish between biotically or abiotically released compounds, we defined the DOM pools as follows: (i) molecular formulae which were present in the triplicate setups after 28 days of incubation but not detected in the control experiment were considered as biologically released and produced, and (ii) formulae present in the control but in none of the three biotic replicates as exclusively abiotic. Differences in detected molecular formulae were visualized based on their molar oxygen-to-carbon (O/C) and hydrogen-to-carbon (H/C) ratios in van-Krevelen plots (Kim *et al.*, 2003).

DOM_{SPE} extracts equivalent to approximately 70 μg TOC were evaporated under N2 stream and re-dissolved in 2100 μL 2% nitric acid (Suprapur). DOS_{SPE} concentrations were determined on an Inductively Coupled Plasma Optical Emission Spectrometer (ICP-OES, iCAP 6000, Thermo Fisher Scientific GmbH, Bremen, Germany), as described previously (Pohlabeln and Dittmar, 2015). DBC concentrations were determined via the benzenepolycarboxylic acids (BPCAs) method according to Dittmar (2008), by oxidizing a dried aliquot of SPE extract with nitric acid and subsequent separation and quantification by liquid chromatography and diode-array detection (Waters Acquity UPLC) (Stubbins *et al.*, 2012). BPCAs were identified according to retention time and absorbance spectra (220 to 380 nm). Individual samples were spiked with BPCA (benzene-penta - and benzene-hexa-carboxylic acid, B5CA and B6CA) standard mixtures to confirm retention times in this specific sample matrix and hence verify the presence of BPCAs. Individual BPCA concentrations were then converted to the sum of DBC concentration according to Stubbins *et al.* (2015). Standard deviation of repetitive measurements was ± 3.0% (B5CA) and ± 2.0% (B6CA).

II.2.4 Optical analysis

Water samples for optical analysis were filtered through acetate cellulose filters (Sartorius, 0.2 μm) and kept frozen until analysis. Fluorescence measurements were conducted using a fluorescence spectrophotometer (Agilent Cary Eclipse, USA) at room temperature in a 10 mm quartz fluorescence cell. A range of emission spectra spanning 300 – 530 nm in 2-nm steps was recorded while exciting at wavelengths in the range of 230 – 410 nm in 5 - nm steps. Inner filter effects were eluded by diluting the samples with 3.5% NaCl solution (combusted NaCl, ultrapure water 18 Ω), receiving a maximum absorption coefficient $a_{254} < 10\ m^{-1}$. The fluorescence spectrum of ultrapure water was subtracted from the raw data set of each measurement day. The integral area of the Raman peak was calculated using ultrapure water as a reference and measured fluorescence signals normalized to the peak area (Lawaetz and Stedmon, 2009). The humification index (HIX) and freshness index (FrI) were calculated after Ohno (2002) and Parlanti *et al.* (2000), respectively. The toxicity index was calculated as the ratio of peak T/A (Coble, 1996; Podgorski *et al.*, 2018). Absorbance measurements were conducted on an UV-VIS absorption spectrophotometer (UV-1280, Shimadzu) in 10 mm quartz cell in a 1:2 (*v/v*) dilution at room temperature. Specific absorption at 254 nm ($SUVA_{254}$) was calculated by dividing the absorption coefficient at 254 nm by the DOC concentration (mg CL^{-1}) (Weishaar *et al.*, 2003).

II.2.5 Statistical analysis

Differences in the distribution of molecular formulae at different sampling timepoints was assessed with a Wilcoxon test, because differences were not normal distributed (test for normal distribution with Shapiro-Wilk's test). PARAFAC analysis of 24 samples was performed using the dr.EEM toolbox in MATLAB (Murphy *et al.*, 2013). Each EEM was normalized to the 3/2 root of the standard deviation of all EEM total fluorescence to improve fitting (Wünsch and Murphy, 2020). Raman and Rayleigh scatter were thoroughly removed and not interpolated because of fluorescence peaks located close to the scatter area. Non-negativity constraints were applied to calculate a 4-component model with a R^2 fit of 0.995. The number of components was determined by checking excitation and emission loadings of each component to their chemical plausibility and residual analysis. The samples were allocated to one of four splits and recombined to form 6 splits with 12 samples each to be validated by split half validation, after emission and excitation loadings split combinations showed Tuckers congruence coefficients (TCC) ≥ 0.95 (Lorenzo-Seva and Ten Berge, 2006). Sample loadings of the calculated model were then dilution corrected to receive fluorescent intensities of each

PARAFAC component. Relative fluorescent intensities were calculated by dividing the intensity of one component by the sum of intensities.

II.3 Results and Discussion

II.3.1 Microbial activity enhances DOM release

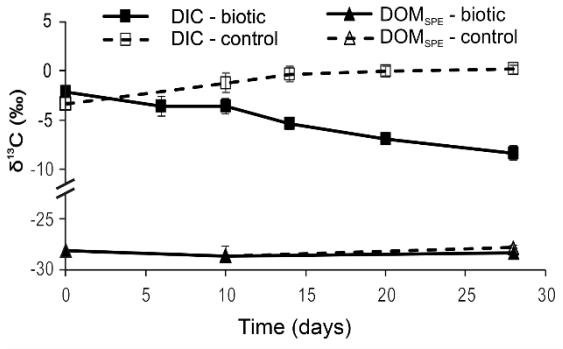

Figure II. 1: Changes in isotopic composition of DIC and DOM_{SPE} in incubated water samples. Shown are mean values and the standard deviation of the triplicate setups. $\delta^{13}C$ of solid Chapopote asphalt: - 27 ‰ (Schubotz et al., 2011). The initial source of DIC is a mixture of bicarbonate from the artificial seawater setup (Table S1) and laboratory air.

The incubation medium turned turbid and white microbial aggregates appeared on the asphalt pieces after 4 days. In addition, elongated, approximately 1 cm long white filaments appeared in the water (Figure S2) similar to marine snow deposits observed after the Deepwater-horizon oil spill (Passow, 2016). Asphalt exposed to the artificial seawater released large amounts of DOC within hours after the start of the experiment (Figure 2 A, Table S5). During this leaching process, water-soluble asphalt compounds are released from the asphalt and accumulate as DOM. In addition, microbial reworking of both solid asphalt and asphalt DOM can mobilize further DOM compounds. DOC concentrations increased from 853 ± 58 μM to 2401 ± 489 μM after 28 days, which was equivalent to a total release of 180 ± 25 μM DOC per gram asphalt. This accounted for about 0.22 ± 0.03% of the initial asphalt weight being released as DOC, ignoring microbial assimilation and respiration of DOC and loss of volatile compounds. A previous study in a controlled laboratory incubation of heavy oil simulating photooxidation with a similar oil to water ratio (Zito *et al.*, 2019b) observed DOC concentrations in a dark control setup after 10 days in the same range as concentrations in our study. DOM_{SPE} had $\delta^{13}C$ values of around –28 ‰ at all timepoints (Figure 1, Table S5), identical to that of particulate Chapopote asphalt organic carbon (Schubotz *et al.*, 2011). This indicates that the sole source of DOC is solubilized asphalt and its degradation products. No fractionation of stable carbon isotopes between DOM_{SPE} and Chapopote asphalt was observed.

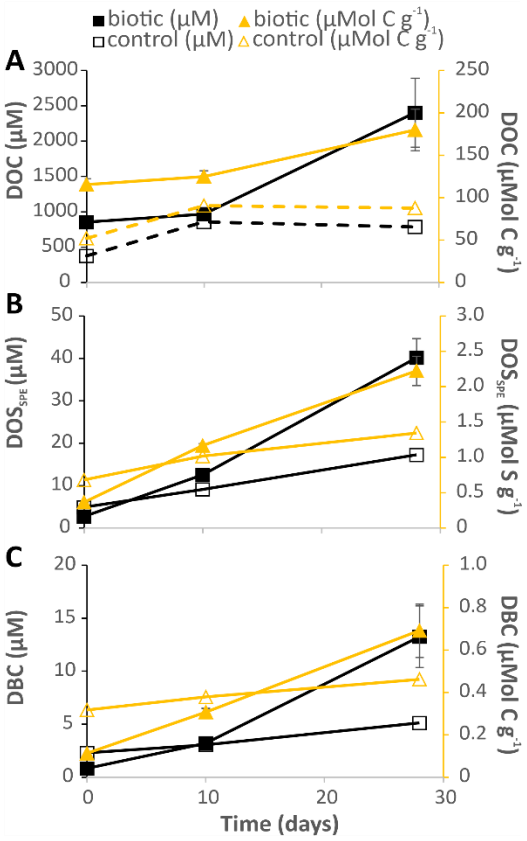

Figure II. 2: Dissolved organic carbon concentrations (A), SPE dissolved organic sulfur concentrations (B), dissolved black carbon concentrations (C) throughout the time of the incubations. While the primary y axis displays concentrations in the incubated water samples (black), cumulative amounts normalized to initial asphalt mass are presented on the secondary y axis (yellow). Shown are mean values and the standard deviation of the triplicate setups.

Our microcosm experiments were performed under oxic conditions with regular ventilation intervals. This did not allow for tracing microbial activity by monitoring, for example, oxygen consumption. Instead, we determined the isotopic composition of DIC as a qualitative indicator for remineralization of asphalt, which we expect to only be minimally affected by the ventilation of the bottles. $\delta^{13}C$ DIC values became more negative with ongoing incubation time (Figure 1, Table S5), which showed that parts of the asphalt organic carbon were remineralized to carbon dioxide. The pasteurized control setup did not show negative isotopic excursions, indicating that pasteurization was suitable to suppress microbial organic carbon remineralization in the timeframe of this experiment. Moreover, DOC concentrations were lower in the control compared to the biotic incubations (Figure 2 A, Table S5). We attribute the enhanced DOC release in the biotic experiment to asphalt dissolution largely initiated by the release of biosurfactants and enzymatically mediated partial breakdown or functionalization of unsoluble asphalt by oil-degrading microorganisms (Das and Chandran, 2011).

II.3.2 Optical properties of released DOM

A four-component model was validated with PARAFAC modeling of the 24 EEM spectra (Figure 3A; Table S3). Components 1 - 3 were identified as protein-like components (Coble, 1996), whereas C4 was identified as microbial humic-like fluorescence (Ziegelgruber *et al.*, 2013). The PARAFAC components were compared with previous studies by using the OpenFluor database and applying a threshold of TCC > 0.97 (excitation) and TCC > 0.98 (emission) for similarity (Murphy *et al.*, 2014)(Table S3). Most of our PARAFAC components matched with similar components from a previous study from a groundwater oil spill (Podgorski *et al.*, 2018) and a laboratory-based oil photodegradation experiment (Zito *et al.*, 2019b). C1 is similar to C2 in Podgorski *et al.* (2018) and was described as low molecular weight aromatic FDOM. Further matches include C4 in Derrien *et al.* (2019), which described this component as soil-related in an endmember incubation experiment. Although not present in the database, similarities were further found in C3 described by Zhou *et al.* (2013) and C1 in Dvorski *et al.* (2016), where this component was associated with polycyclic aromatic hydrocarbons (PAHs) and its degradation products. C2 is similar to C5 in Zito *et al.* (2019b) and C1 in Podgorski *et al.* (2018) in which this protein- like compound was interpreted to be related to (alkyl-substituted) benzene-derivates and considered semi-biolabile. Hence, we interpret this PARAFAC component to be derived from the petroleum. This component was also found in porewaters from a mud volcano in the Beaufort Sea (C4 in Retelletti Brogi *et al.* (2019)). No matches above the threshold were found for our C3, which we attribute to its presence in a region with high noise due to physical scat- tering. Comparable components are C2 in Zito *et al.* (2019b) (TCC Ex/Em: 0.92/0.93) and C5 in Podgorski *et al.* (2018)(TCC Ex/Em: 0.93/0.93), where these components were correlated to petroleum toxicity. C4 matches well with 16 studies describing it as humic-like, it was found in many different ecozones e.g. porewaters (Retelletti Brogi *et al.*, 2019), Arctic Ocean (Walker *et al.*, 2009) and Northern Pacific Ocean (Murphy *et al.*, 2013). Only one of the matches is associated with oil degradation and is probably related to molecular-level structural properties comparable to humic and fulvic acids (C1 in Zito *et al.* (2019b)).

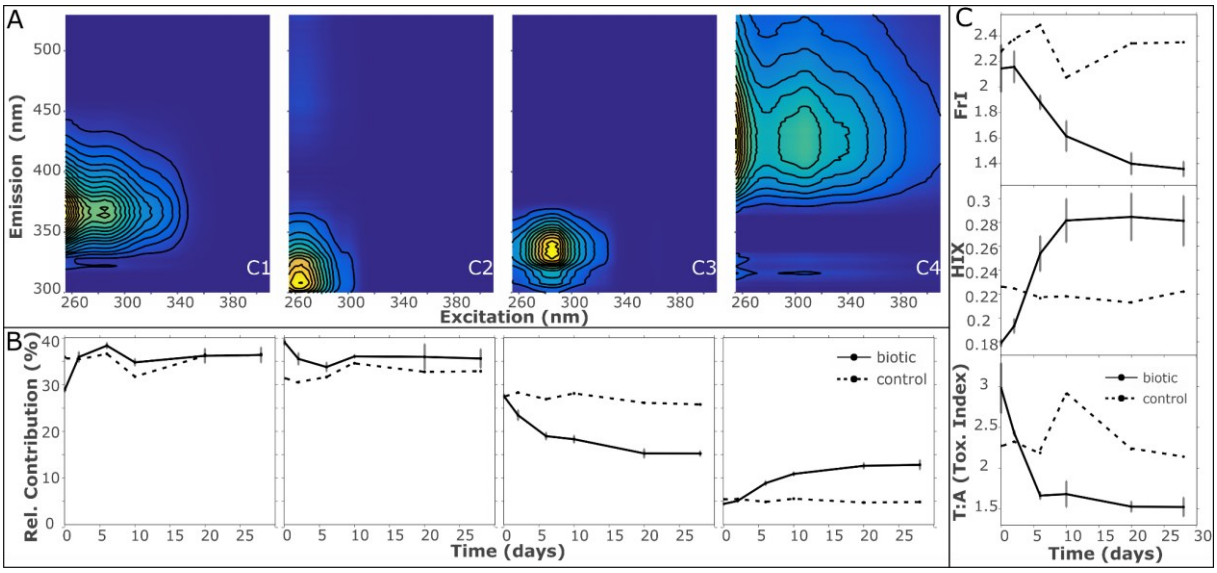

Figure II. 3: PARAFAC Model showing the location of the 4 compounds (A), the relative contribution of each compound shown in A over time (B) and change of 2-D indices (C). Shown are mean values of the triplicate setup, error bars represent the standard deviation.

At the beginning of the experiment, the PARAFAC components C1, C2 and C3 emitting in the UVA and UVB range made up most of the fluorescent signal (combined 96% of total fluorescence), whereas emission at longer wavelengths had only minor relative contributions (Figure 3B). From 0 to 28 days, C2 relative abundances stayed constant, while the relative contribution of C1 slightly increased and then stayed constant. Changes were observed for C3 and C4: the relative contribution of petroleum-"humic"-like C4 increased, whereas the potentially toxic petroleum-protein-like C3 decreased. This potential decrease in toxicity is in accordance with lower values of the toxicity index (Podgorski *et al.*, 2018) (Figure 2C), suggesting that microbial processing removed potentially toxic FDOM.

Liu and Kujawinski (2015) discussed a solubilization effect of humic and fulvic acids on the enhanced solubilization of oil compounds in seawater, which can increase the solubility of semi soluble and insoluble hydrocarbons (Boehm and Quinn, 1973; Tanaka *et al.*, 1997). Assuming that the petroleum-humic-like C4 has the same underlying molecular properties as environmental humic-like FDOM (Zito *et al.*, 2019b) such as conjugated aromatic structures (Wünsch *et al.*, 2017), the observed increase of DOC concentrations in the biological incubations could also be attributed to an increase of asphalt solubility due to the extended release of this compound class. This assumption is supported by a positive linear correlation between C4 and aromatic molecular formulae (R^2 adj. = 0.94, $p < 1 * 10^{-6}$, df = 10; Figure S6). These results demonstrate that similar to photooxidation (Zito *et al.*, 2019b), microbial processing can release FDOM emitting at longer wavelengths in the UVV range from petroleum.

II.3.3 Microbial transformation of DOM on a molecular level

We observed drastic changes in carbon-based extraction efficiencies (EE) of DOM_{SPE} by PPL: while EEs were low after the start of the incubation (6.2 ± 0.8%), an efficiency of 50.9 ± 4.6% was determined after 28 days (Table S5), indicating noticeable changes in the DOM composition. The low EE at the beginning of our incubations suggest either a DOM pool that was not well retained by the PPL resin (Flerus *et al.*, 2012; Hawkes *et al.*, 2015b) and/or irreversible adsorption of a part of the DOM to the PPL resin, although a method comparison study generally recommended using SPE for extracting oil-related DOM (Zito *et al.*, 2019a). Following the mesocosm setup at t_0, we observed a loss of DOC after the pasteurization of the control setup (Figure 2 A). This can best be explained by a loss of volatile compounds – a compound class that is not well retained by SPE (Hawkes *et al.*, 2015b), thus resulting in low EEs at t_0 for biological samples. With ongoing incubation time, the increase in EEs very likely reflected the decreasing relative abundances of volatile and increasing relative abundances of non-volatile DOM as volatile compounds evaporated and/or were microbially processed while more water-soluble asphalt-derived DOM was released due to the microbial functionalization of previously water-insoluble asphalt compounds. Moreover, isotopic fractionation of petroleum has been shown previously, e.g., lower $\delta^{13}C$ values of polycondensed aromatic 5- and 6-ring asphaltenes compared to the parent oil (Goranov *et al.*, 2021). Even though EEs changed considerably, $\delta^{13}C$ of DOM_{SPE} was at around -28 ‰ at all timepoints (Table S5). Hence, we expect the fraction of DOM retained by PPL to be similar, allowing a comparison of DOM_{SPE} within the same analytical window (Hawkes *et al.*, 2015b).

We detected 6813 different molecular formulae with ESI-FT-ICR-MS analysis of DOM_{SPE} in our incubation setups. FT-ICR-MS signal intensity weighted-averages of DOM molecular masses were low compared to natural marine DOM in the deep GOM (ca. 400 Da (Seidel *et al.*, 2016)) at the beginning of the experiment and significantly ($p < 0.001$) decreased over time from 299 ± 20 Da at t_0 to 251 ± 9 Da after 28 days (Table S6). This is consistent with previous studies investigating oil degradation in the water phase (Kleindienst *et al.*, 2015; Seidel *et al.*, 2016). Furthermore, the weighted-average molar H/C ratios decreased significantly ($p < 0.001$) from 1.49 ± 0.03 to 1.32 ± 0.02, which was further represented in higher AI_{mod} values, while molar O/C ratios stayed constant between 0.28-0.29. Consequently, aromatic and polycondensed aromatic molecular formulae became relatively more enriched from 0 to 28 days, whereas the relative abundance of DOM aliphatic molecular formulae decreased (Figure S3). This is in accordance with a general preference of microbial degradation of aliphatic over aromatic hydrocarbons (Peters *et al.*, 2007) and was also

observed at a groundwater oil spill site (Podgorski *et al.*, 2020) and for DOM in general (D'Andrilli *et al.*, 2015).

General changes in FDOM composition were monitored by using the 2D indices FrI (Parlanti *et al.*, 2000) and HIX (Ohno, 2002)(Figure 3C; Figure S6): although these indices were developed in very different contexts, they have been applied previously in petroleum mesocosm studies (Harriman *et al.*, 2017; Zito *et al.*, 2019b) under the assumption that compounds resembling similar underlying molecular properties are accounted for by these indices, e.g. the ratio of aliphatic to aromatic DOM by FrI (Harriman *et al.*, 2017) and extended, conjugated aromatic structures by HIX (Zito *et al.*, 2019b). Values for the FrI decreased from 2.1 ± 0.2 to 1.3 ± 0.1 after 28 days, while the HIX slightly increased from 0.18 ± 0.0 to 0.28 ± 0.02 (Figure 3 C), suggesting an enrichment of aromatic and removal of aliphatic FDOM on the timescales of our experiment. A positive linear correlation between FrI and aliphatic molecular formulae (R^2 adj. = 0.46, $p < 0.01$, df = 10) and a negative correlation between FrI and aromatic molecular formulae (R^2 adj. = 0.78, $p < 1 * 10\text{-}4$, df = 10) suggests that although this index is used out of context, changes in the underlying molecular properties can be approximated. The same applies to the HIX, which was positively correlated with aromatic molecular formulae (R^2 adj. = 0.75, $p < 0.001$, df = 10). An increase of aromatic DOM content is further supported by increasing $SUVA_{254}$ (Table S5), an indicator for the abundance of dissolved aromatic carbon (Weishaar *et al.*, 2003). This exemplifies that general changes in asphalt-derived DOM compounds can be observed with little effort using optical analysis compared to SPE followed by FT- ICR-MS analysis. It further supports our observations from molecular DOM_{SPE} analysis by FT-ICR-MS, reflecting changes in the overall DOM composition.

To examine the potential of microbial degradation of asphalt-derived DOM, we compared the distribution of molecular formulae exclusively present in the biologically active incubations with the pasteurized control (Figure 4). After 28 Days, 497 molecular formulae were found exclusively in the abiotic control but not in the biotic incubations suggesting that they were biodegraded. These molecular formulae had relatively high molar H/C and very low O/C ratios, corresponding to reduced, highly unsaturated and aliphatic DOM (Table S6). On the other hand, 1102 more aromatic and less reduced molecular formulae were exclusively present in the biologically active incubations, indicating either a release of DOM by microorganisms or the release from (microbially altered) asphalt due to enhanced DOM solubilization. The fact that DOM can increase the solubility of petroleum hydrocarbons in water has been shown previously (Boehm and Quinn, 1973). To assess the potential solubility, we calculated the molar ratios of NSO:C in molecular formulae, which were (along with molecular masses) related to modeled octanol-water partition coefficients of water-soluble petroleum

compounds in a study by Liu and Kujawinski (2015). Higher NSO:C ratios correspond to more hydrophilic DOM, whereas lower NSO:C ratios and higher molecular masses correspond to more hydrophobic DOM. Weighted-average NSO:C ratios of 0.39 ± 0 and their low molecular masses indicated that the majority of these exclusive molecular formulae were likely not hydrophobic and instead potentially more water-soluble than the bulk DOM after 28 days (Table S6). This implies that these exclusive molecular formulae were released as metabolites of microbial processing of asphalt organic matter and not leached out of the asphalt due to an enhanced DOM solubilization effect. Therefore, we expect most qualitative changes in the DOM pool observed by FT-ICR-MS to be related to microbial processing of particulate and dissolved asphalt.

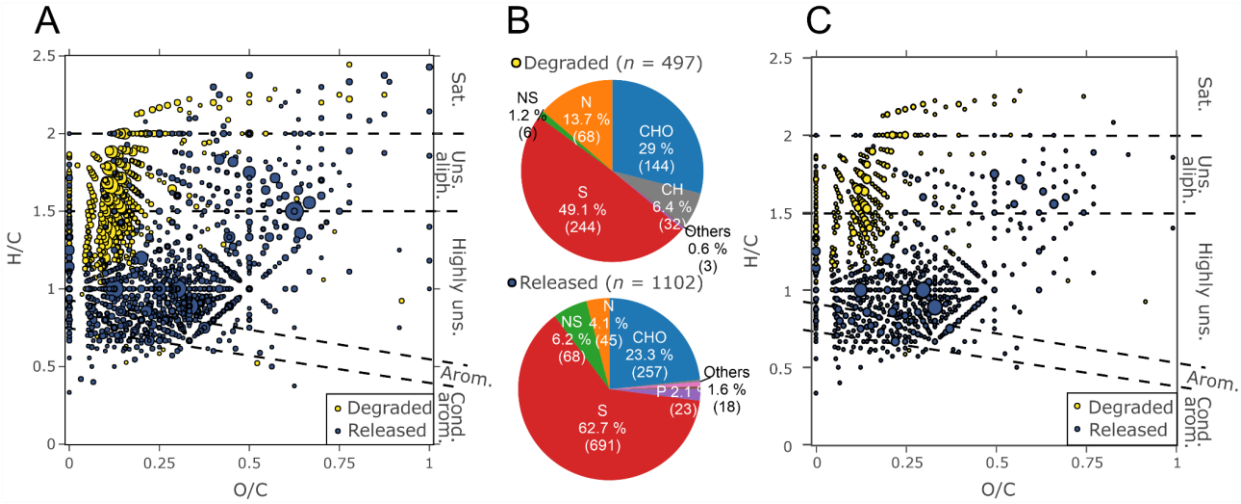

Figure II. 4: Van Krevelen plot showing 497 molecular formulae exclusively present in the pasteurized control after 28 days (yellow) and 1102 molecular formulae present in all three biological incubations, but not in the control (blue) (A), Pie chart illustrating the relative contribution of molecular formulae shown in A according to the presence of heteroatoms in the respective molecular formula (B), Van Krevelen plot showing molecular formulae from A containing at least one S in the molecular formula. Displayed are 244 molecular formulae exclusively present in the pasteurized control (yellow) and 691 molecular formulae present in all three biological incubations, but not in the control (blue) (C).

II.3.4 Release of dissolved organic sulfur species

More than half of all molecular formulae detected in DOM_{SPE} contained sulfur, which increased from 45.2 ± 5.6% to 62.1 ± 0.1% after 28 days (Figure S3). To confirm the abundance of S-containing DOM as detected by ultrahigh-resolution mass spectrometry, we quantified DOS in the SPE extracts. Concentrations of DOS_{SPE} reached 40.1 ± 4.5 μM after 28 days (Table S5, Figure 2 B), which was about 500 times higher than deep sea DOS_{SPE} concentrations in the deep Atlantic Ocean (Ksionzek *et al.*, 2016). Moreover, S/C_{SPE} ratios between 0.052 ± 0.003% and 0.034 ± 0.005% exceeded reported values in deep atlantic water by a factor of 10 - 15 and even sulfidic porewater by a factor of 2-5 (Gomez-Saez *et al.*, 2017; Ksionzek *et al.*, 2016;

Pohlabeln *et al.*, 2017). Molar S/C ratios in the original asphalt were lower than these values (0.024), indicating a selective dissolution of sulfur-containing asphalt- derived DOM compounds.

Hundreds of highly unsaturated or aliphatic DOS molecular formulae were only present in the control and not in the biologically active incubations (Figure 4 C), illustrating that this fraction can be microbially degraded. However, more S-containing molecular formulae were released, of which about half (45%) is expected to have an aromatic or polycondensed aromatic structure based on $AI_{mod} > 0.5$ and $AI_{mod} > 0.67$, respectively (Figure 4 C). S-containing marine DOM is likely composed of sulfonic acids and thiophenes (Pohlabeln and Dittmar, 2015). In petroleum, aromatic organic sulfur compounds such as thiophenes and condensed thiophenes can make up a substantial fraction of all sulfur compounds (Kropp and Fedorak, 1998) and several methylated benzo – and dibenzothiophenes are present in solid Chapopote asphalt (Smit, 2016). Liu *et al.* (2018) analyzed sulfur-rich immature crude oils from China and showed that sulfur-containing compounds polar enough to be ionized by ESI in mass spectrometry applications mainly contained thiophene rings in their molecular structures. It is therefore conceivable that the aromatic and polycondensed aromatic DOS formulae released by asphalt seepage contain thiophene or condensed thiophene (benzothiophene) rings, which are abundantly present in the Chapopote asphalts (Smit, 2016) and are relatively resistant to biodegradation (Hegazi *et al.*, 2012; Kropp and Fedorak, 1998). A potential recalcitrance is illustrated by the high abundance of aromatic DOS molecular formulae after 28 days of incubation (Figure 4 C). An elevated abundance of DOS compounds from petroleum was reported in several studies using FT-ICR-MS, e.g. in a laboratory experiment (Liu and Kujawinski, 2015), groundwater oil spills (Dvorski *et al.*, 2016; Islam *et al.*, 2016), oil-entrapped water droplets (Meckenstock *et al.*, 2014) and above an oil seep in the GOM (D'Andrilli *et al.*, 2015). We hypothesize that DOS species released by petroleum seepage may be a consistent source of non-labile DOS to the global marine DOS inventory. The global marine DOS inventory is currently unbalanced since known marine DOS sources from phytoplankton (Ksionzek *et al.*, 2016) and sulfidic environments (Pohlabeln *et al.*, 2017; Seidel *et al.*, 2014) are not enough to balance out sinks of non-labile DOS (Ksionzek *et al.*, 2016).

II.3.5 Asphalt leaching releases dissolved polycondensed aromatic compounds

Optical analysis by fluorescence spectroscopy and UV-VIS absorbance indicated an increased release of aromatic DOM (Figure 3: C4, HIX; Table S5: $SUVA_{254}$). Furthermore, we detected an increase of aromatic and polycondensed aromatic formulae by FT-ICR-MS in our incubations, including dissolved black sulfur (DBS) (Hertkorn *et al.*, 2016) and dissolved black

nitrogen (DBN) (Wagner *et al.*, 2015) (Table S4). Environmental implications of DBS and DBN are unknown and their sources were previously associated with biomass burning. (Roebuck *et al.*, 2018) speculated that spilled diesel fuel may be a source for DBS. While DBS and DBN currently can only be identified qualitatively by FT-ICR-MS, concentrations of DBC without N or S heteroatoms can be determined by converting them to BPCAs. We quantified DBC as B5CA and B6CA, which indicate the presence of DBC with at least 5 fused rings (Ziolkowski *et al.*, 2011), presumed to be of thermogenic origin (Kappenberg *et al.*, 2016). Here, we observed an increase of DBC concentrations of 0.83 μM to 13.3 ± 2.9 μM after 28 days (Figure 2 C, Table S5). These compounds accumulated in the DOM pool: their relative contribution to DOC concentrations increased within 28 days to 0.55 ± 0.03%. For the deep ocean, DBC contribution to DOC is estimated to be 2% (e.g. (Dittmar and Paeng, 2009)), but DOC concentrations are much higher in our 28 day incubation, still including more labile fractions than deep-sea DOM. To get a better understanding of long-term leaching of DBC from these asphalt samples, we investigated additional asphalts from the same location that were incubated for 6 months to 10 years and observed that this trend was continuing: between 0.5 - 0.9% of DBC in DOC were observed after 6 months and 2.9 – 12.6% after 10 years, confirming its relative resistance to microbial degradation (Table S2). DBC in biotic incubations after 28 days showed high B6CA/B5CA ratios (0.6-0.7) compared to natural deep sea DBC (ca. 0.3 (Wagner *et al.*, 2019)), an indication for highly condensed DBC (Stubbins *et al.*, 2012; Wagner *et al.*, 2018).

A recent study detected a mismatch between the isotopic carbon composition of known terrestrial DBC sources and DBC in the open ocean, indicating a so far unidentified DBC source with a marine isotopic signature (Wagner *et al.*, 2019). In this study, Wagner *et al.* (2019) hypothesized that the dissolution of particulate petrogenic BC is a potential DBC source which would match the isotopic composition of open ocean DBC. The first study describing DBC distribution in the open ocean by Dittmar and Koch (2006) suggested a widespread source at the seafloor of deep-sea basins. Here, we provide experimental evidence that this compound class can also be released by natural asphalt seepage into deep sea waters. A DBC release in the deep sea would not be affected by photooxidation, which is a major removal mechanism of terrestrial DBC transported by rivers (Stubbins *et al.*, 2010; Wagner *et al.*, 2018).

The $\delta^{13}C$ composition of DOM_{SPE} has been reported to be similar to that of isolated DBC (Wagner *et al.*, 2019), which was on average -28 ‰ in our experiment (-27 ‰ in particulate asphalt from Chapopote (Schubotz *et al.*, 2011), Table S5). The stable carbon isotopic composition of B5CA and B6CA in petroleum asphaltenes were reported to be similar (B5CA) or slightly ^{13}C-depleted (B6CA) compared to the parent crude oil in a recent study by

Goranov *et al.* (2021). The stable carbon isotopic composition of crude oils varies over geologic times but mean $\delta^{13}C$ were reported around -26 ‰ (Degens, 1969). Natural asphalt and petroleum seepage with fossil ^{14}C values could therefore be an overlooked source of ^{14}C-depleted DBC with a slightly more positive ^{13}C signature compared to riverine DBC (Wagner *et al.*, 2019) in the deep ocean. Contribution of asphalt DBC may be an explanation for the observed very old ^{14}C ages of deep-sea DBC (Coppola and Druffel, 2016) and is consistent with reports of distinct young and very old marine DBC pools (Coppola *et al.*, 2019; Wang *et al.*, 2016).

II.3.6 Implications for natural environments

Although asphalt seepage is a localized phenomenon, it is not limited to the southern GOM and has been reported from offshore Algeria (Jones *et al.*, 2014), Brazil (Fujikura *et al.*, 2017), the northern GOM (Weiland *et al.*, 2008), and the Santa Barbara Basin(Valentine *et al.*, 2010). We have shown that fresh asphalt exposed to water can release large amounts of DOC, of which a considerable fraction of aliphatic DOM can readily be transformed by microbial degraders. Hydrocarbon seepage can stimulate microbial life at seeps and in the water column above and has been observed to increase the abundance of primary producers as indicated by chlorophyll concentrations in euphotic zones above seep sites (D'souza *et al.*, 2016). Studies by Wang *et al.* (2001) and Pohlman *et al.* (2010) proposed hydrocarbon seeps as potential major contributors of old DOC to the deep sea in the GOM. However, the fate of DOC from seepage is poorly understood: (Chanton *et al.*, 2020) observed relatively young ^{14}C ages of DOC in the water column of the abyssal GOM, concluding that seep DOC has a local effect only. Our results suggest that asphalt seepages release ultra-refractory DOM with a fossil ^{14}C signature, contributing to the DBC pool that makes up ~2% of the DOC pool in the deep sea (Dittmar and Paeng, 2009). We hypothesize that while the general DOC release may only have a local effect, the released fraction of refractory fossil ^{14}C compounds could be a larger contributor to ultra-refractory DOC cycles that is not visible in bulk $\Delta^{14}C$ analysis of DOC. Dittmar and Paeng (2009) proposed a possible molecular structure of deep-sea DBC containing fused ring structures similar to that of petroleum asphaltenes. Therefore, we hypothesize that an additional source of deep-sea DBC might be asphaltenes from natural petroleum seepage, which are rendered water-soluble by microbial degradation and functionalization. This could mean that particularly asphaltene-rich petroleum seeps may release DBC into the water column. However, this cannot be the only explanation, since DBC concentrations also increased in the pasteurized (abiotic) control setup (Figure 2, Table S5). Podgorski *et al.* (2020) detected enhanced DBC concentrations via the BPCA method in

groundwater of an oil spill site of light crude oil, suggesting that DBC can also be released by petroleum with a lower asphaltene content.

Oil seepage is estimated to release about 600,000 tons of crude oil annually into the oceans, with an equal contribution of petroleum from anthropogenic sources (Kvenvolden and Cooper, 2003). We applied the results from our 28-day incubation to get a rough, first-order estimate of global DBC and DOC release (Figure 2, Table S7). We estimate between 6.3 * 108 - 1.1 * 10^9 g as DOC, 1.0 * 10^7 - 4.3 * 10^7 g as likely non-labile DOS_{SPE} as well as 3.3 * 10^6 - 5.0 * 10^6 g as DBC could be released by natural seepage annually to the oceanic DOM pool without considering contribution from anthropogenic sources. This is 4-5 orders of magnitude lower than the estimated annual removal of refractory DOS (Dittmar *et al.*, 2017; Ksionzek *et al.*, 2016) and 6-7 orders of magnitude lower than annual riverine DBC input (Jaffé *et al.*, 2013) to the ocean and may therefore be significant only on local scales. However, if natural seepage releases fossil ^{14}C DBC into the deep-sea DOM pool, the apparent very old bulk ^{14}C ages of deep-sea DBC (Coppola and Druffel, 2016) could be shaped by fossil DBC contribution. In a two-component ^{14}C mixing model of recent terrestrial DBC and fossil petroleum DBC, reported deep-sea $\Delta^{14}C$ DBC values of -945 ‰ (Coppola and Druffel, 2016) could in theory be explained by a contribution of up to 94.2% of fossil DBC (Figure S5). A relatively small proportion of recent and reactive DBC from land could therefore constrain apparent DBC ages dynamically. Nevertheless, the stable carbon isotopic composition of asphalt- DOM in this study and DBC from the asphaltene fraction of petroleum (Goranov *et al.*, 2021) are lighter than observed ^{13}C values of deep-sea DBC (Wagner *et al.*, 2019), suggesting a rather minor contribution of petroleum-derived DBC, which is in agreement with estimated rates of DBC release in this study. Future work is needed to clarify if contribution of natural seepage is significant to deep-sea cycles.

II.4 Acknowledgement

We appreciate the efforts conducted by the crew and scientists of RV Meteor expedition M114. We thank Matthias Friebe, Ina Ulber, Heike Simon, Melina Knoke, Heidi Taubner, Jenny Wendt, Xavier Prieto and Min Song for help in the laboratory and Gunter Wegener and Frank Wenzhöfer for laboratory equipment. We thank Shuchai Gan for initial help with the PARAFAC model, Helena Osterholz for assistance with FT-ICR-MS measurements, Bernhard Schnetger and Eleonore Gründken for ICP-OES measurements and Kai-Uwe Hinrichs for helpful discussions and providing access to laboratory infrastructure. The authors thank four anonymous reviewers for their helpful comments. We acknowledge funding by the German

Science Foundation (DFG) within the Cluster of Excellence EXC 2077 “The Ocean Floor – Earth’s Uncharted Interface” (Project number 390741603).

II.5 Supplementary Information

Six additional figures (sample location, picture of asphalt after 4 days, heteroatom and compound groups composition of DOM, PCoA of DOM molecular formulae, DBC $\Delta^{14}C$ mixing model, FDOM linear correlation), seven additional tables (artificial seawater composition, DBC in long-term incubations, PARAFAC OpenFluor matches, DBC >C15 molecular formulae, Compound group concentrations and isotopic composition, FT-ICR-MS intensity-weighted parameters, calculation for asphalt DOC, DOS and DBC release) and in-detail method description on FT-ICR-MS analysis. Data files are available in the Pangaea repository.

II.5.1 Molecular formulae assignment

The DOM_{SPE} extracts were diluted 1:1 (*v/v*) with ultra-pure water and methanol to a DOC concentration of 2.5 ppm for analysis with FT-ICR-MS. Samples were infused by an autosampler at a flowrate of 360 μL hr^{-1} into the electrospray source (ESI; Apollo II ion source, Bruker Daltonik GmbH, Bremen, Germany) with the capillary voltage set to 4 kV in negative mode. Ions were accumulated in the hexapole for 0.2 s prior to transfer into the ICR cell. Data acquisition was done in broadband mode using 8 megaword data sets and a scanning range of 92 – 2000 Da. The instrument was internally calibrated with a list of > 100 known $C_xH_yO_z$ molecular formulae, with a minimum presence of 10 known formulae in one sample. With this calibration procedure, a mass error of < 0.1 ppm was achieved. For each mass spectrum, 200 scans were accumulated. Before each sample set, blank checks with methanol/ultrapure water 1:1 (v/v) were measured, as well as the internal NEqPIW (North Equatorial Pacific Intermediate Water) DOM_{SPE} standard to account for instrument variations (Osterholz *et al.*, 2014). In addition to this, each sample was measured twice on different days. Molecular formulae were calculated in the mass range between 92 and 1500 Da with the formula template $C_{1\text{-}60}H_{0\text{-}150}O_{0\text{-}60}N_{0\text{-}4}S_{0\text{-}2}P_{0\text{-}1}$, $H/C_{min} = 0.3$, $O/C_{max} = 1.0$ (Merder *et al.*, 2020). A method detection limit (MDL) of 0.98 after Riedel and Dittmar (2014) was used to filter the data. Molecular formulae present in only one of the replicate measurements were removed. The dataset was processed by removing known contaminants and compounds with a signal to noise ratio >20 in a blank extraction. Additionally, compounds with masses >1000 Da were removed, as well as compounds in the whole dataset, including replicate measurements, present less than 4 times. The peak intensity of each identified molecular formula was normalized to the sum of peak intensities in each sample and multiplied by 10.000.

Molecular formulae were assigned as described in (Osterholz *et al.*, 2016; Šantl-Temkiv *et al.*, 2013; Seidel *et al.*, 2014) to the following compound groups: (1) polycondensed aromatics ($AI_{mod} > 0.66$; (2) aromatics ($0.5 < AI_{mod} \leq 0.66$); (3) unsaturated aliphatics ($1.5 < H/C \leq 2$, $O/C < 0.9$, $N = 0$);(4) unsaturated aliphatics with nitrogen ($1.5 < H/C \leq 2$, $O/C < 0.9$, $N > 0$); (5) highly unsaturated ($AI_{mod} \leq 0.5$, $H/C < 1.5$, $O/C < 0.9$).

II.5.2 Supplementary Figures

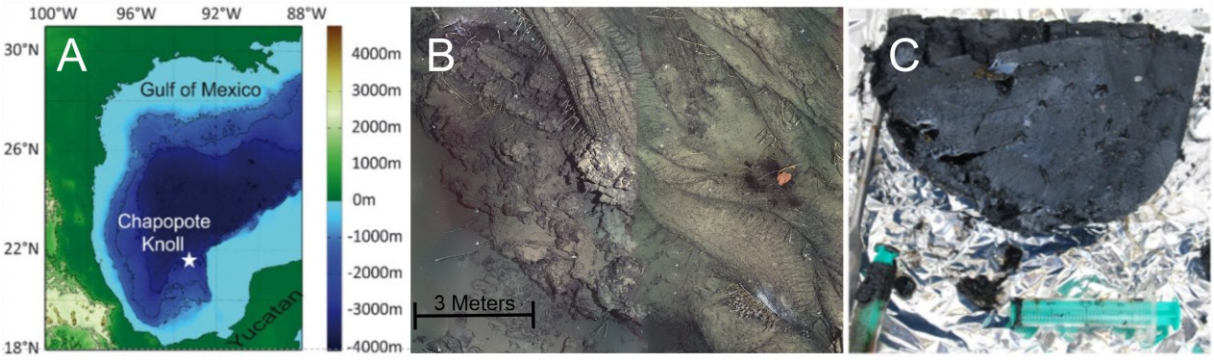

Supplementary Figure 1: Map showing the location of the Chapopote knoll in the GOM (A), seafloor image of sample location GeoB 19339-1 (red flag, 2905 m below sea surface; 21° 53' 57.0600" N, 93° 26' 12.6000" W) taken from a photomosaic of the asphalt flows at Chapopote (Marcon et al., 2018) (B), retrieved asphalt sample GeoB 19339-18 (Sahling et al., 2017) (C).

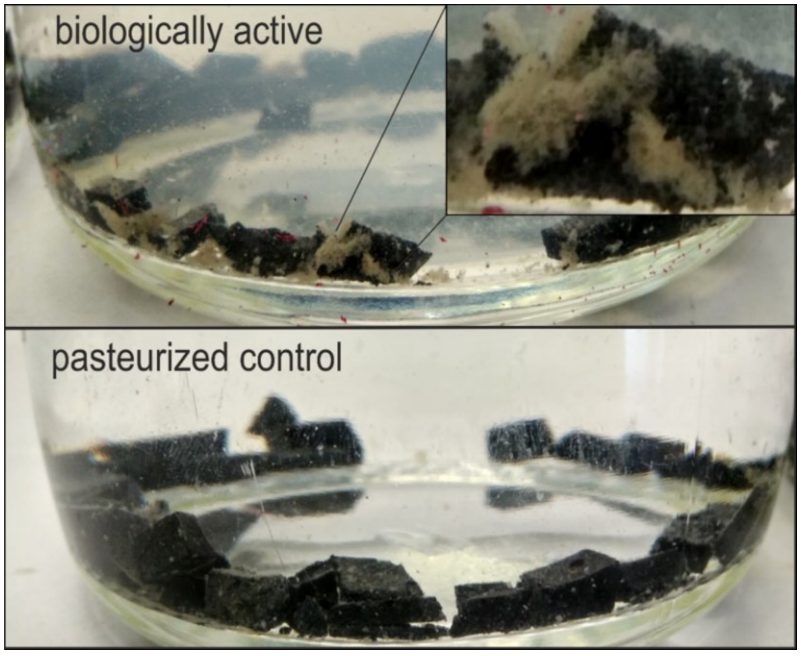

Supplementary Figure 2: Picture of the incubated asphalt after 4 Days, showing white microbial aggregates (top), while none were seen in the control setup (bottom).

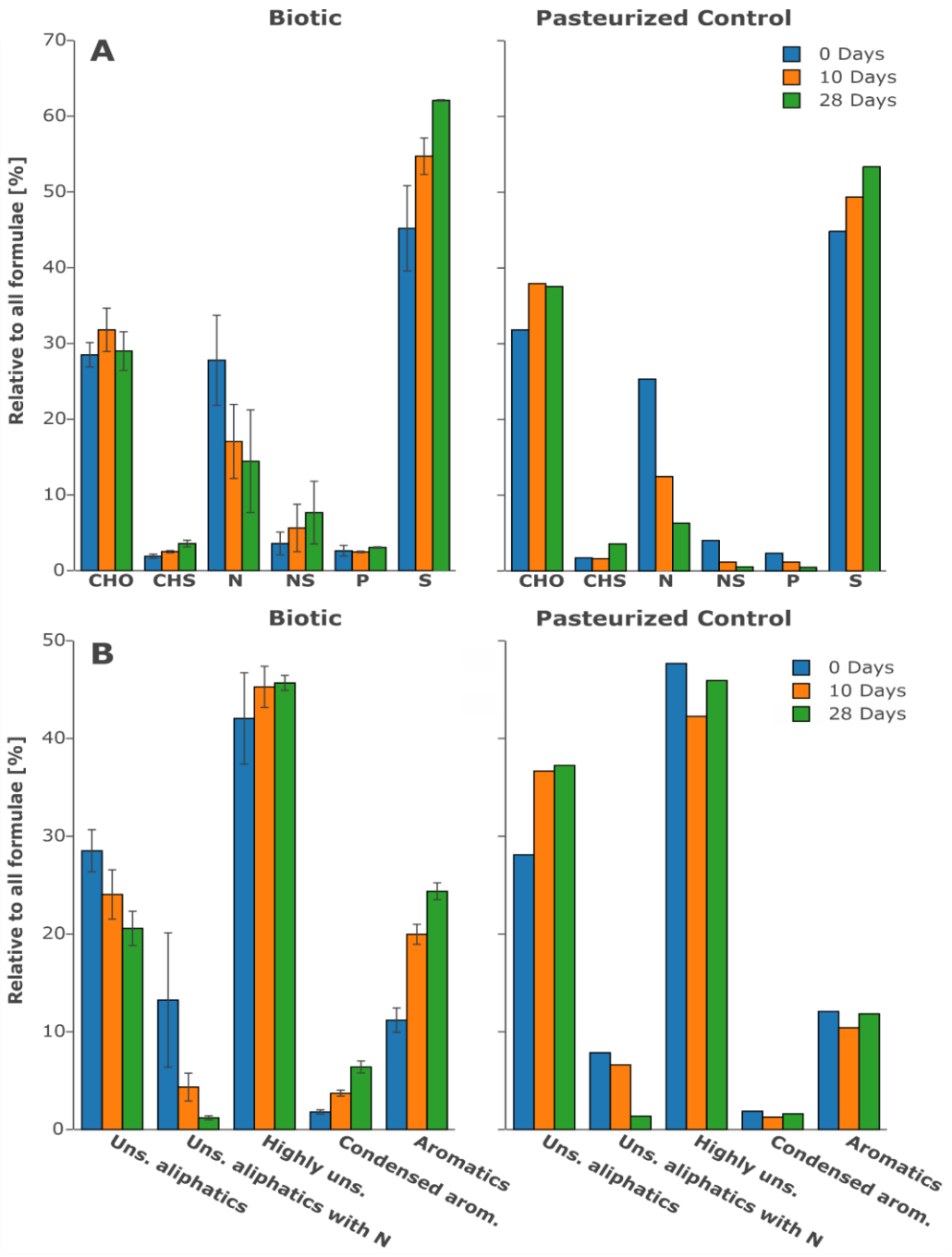

Supplementary Figure 3: Bar chart showing the relative contribution of molecular formulae containing heteroatoms (A) and assignment to compound groups (B) at three different timepoints during the course of asphalt incubations. Shown are mean values and standard deviation for the triplicate setup.

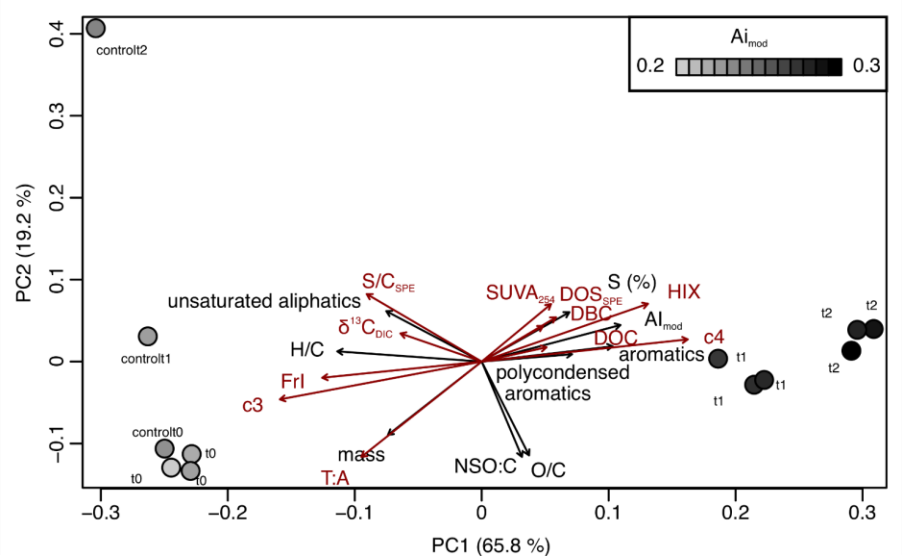

Supplementary Figure 4: Principle coordinate analysis (PCoA) based on a Bray-Curtis dissimilarity matrix of all detected molecular formulae and post-fit of environmental parameters (red) and molecular parameters (black), p < 0.01.

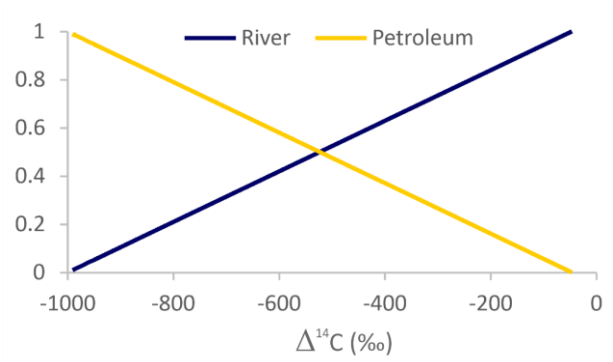

Supplementary Figure 5: Two-component ^{14}C mixing model of terrestrial DBC and petroleum DBC, where $\Delta^{14}C$DBC river = -46 ‰ (Coppola et al., 2019) and $\Delta^{14}C$DBC petroleum= -1000 ‰. Reported deep-sea $\Delta^{14}C$ DBC values of -945 ‰ (Coppola and Druffel, 2016) could be explained by a contribution of up to 94.2% of fossil DBC.

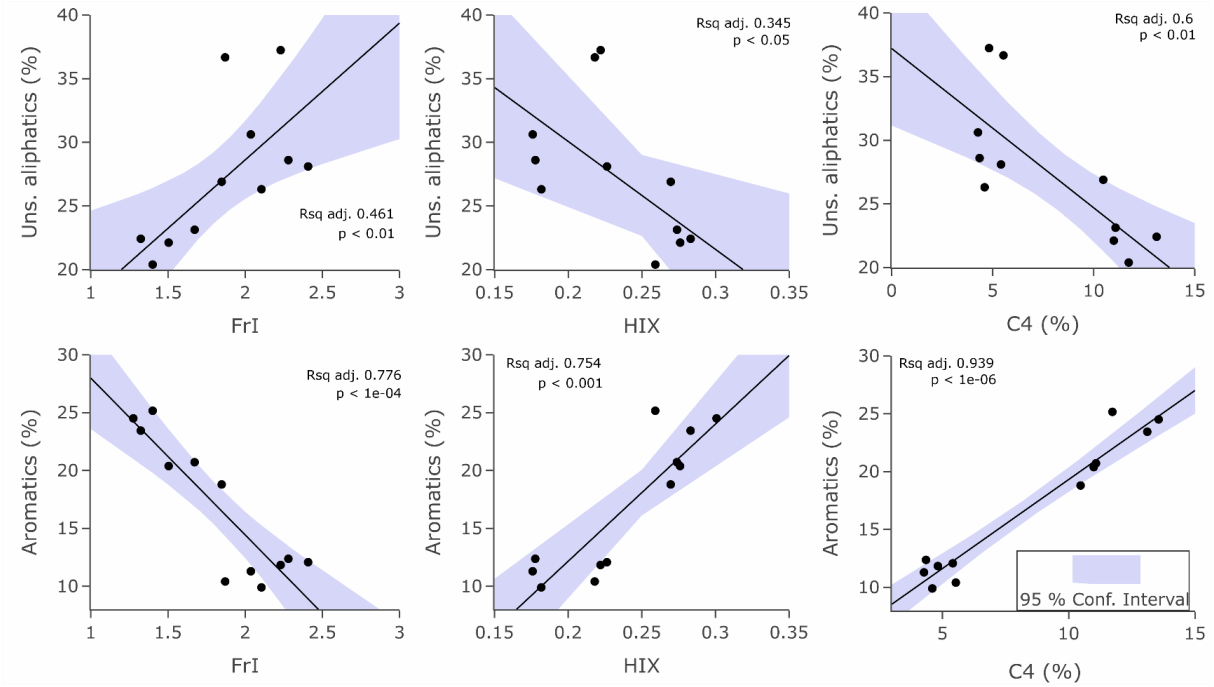

Supplementary Figure 6: Linear correlation between FDOM indices and relative abundance of molecular formulae assigned to unsaturated aliphatics and aromatics. Shown are 95% confidence intervals in blue, displayed are adjusted R^2 and p-values.

II.5.3 Supplementary Tables

Supplementary Table 1: Composition of artificial seawater used in the incubation media, adapted after Widdel and Bak (1992).

Ingredient	Amount
Ultrapure water	1 L
NaCl	26 g
$MgCl_2 * 6H_2O$	3 g
$CaCl_2 * 2H_2O$	0.15 g
Na_2SO_4	4 g
NH_4Cl	0.25 g
KH_2PO_4	0.2 g
KCl	0.5 g
KBr	0.1 g
Nonchelated trace element mixture (Widdel et al., 1983)	1 mL
$FeClFeCl_2$	1 mL
Selenite-tungstate solution	1 mL
$NaHCO_3$ solution (1 M)	30 mL

Supplementary Table 2: Long-term leaching experiment of asphalts from the main asphalt field in sterile bottom water. 10 year incubated samples were taken during cruise M67 in 2006 (Bohrmann et al., 2008).

Sample	Duration	DOC (μM)	DBC (μM)	B6CA/B5CA	DBC:DOC (%)
GeoB19345-1 (surface)	6 months	1504	13.8	0.18	0.9
GeoB19345-1 (12-18 cm)	6 months	4113	22.6	0.07	0.5
GeoB19339-1 (surface)	6 months	3977	30.1	0.17	0.8
GeoB10617-6 (surface)	10 years	314	39.7	0.59	12.6
GeoB10618 (50 cm)	10 years	614	17.9	0.24	2.9
Sterile Bottom Water-1	-	52	1.2	0.27	2.3
Sterile Bottom Water -2	-	82	1.2	0.26	1.4

Supplementary Table 3: Location of the PARAFAC components modeled in this study, the number of matches above the threshold criteria of TCC Ex/Em > 0.97/0.98 in the OpenFluor database (Murphy et al., 2014) and compound interpretation.

Compound	Ex/Em max (nm)	OpenFluor matches	Synonyms	TCC Ex/Em	Description
C1	280/364	3	C2 in Podgorski *et al.* (2018)	1.00/0.99	Low m/z aromatic, likely PAH related
C2	265/308	4	C5 in Zito *et al.* (2019b)	0.97/0.99	Protein-like
C3	285/332	-	C5 in Podgorski *et al.* (2018)	0.93/0.93	Protein-like toxic petroleum
C4	305/420	16	C1 in Zito *et al.* (2019b)	0.98/0.99	Microbial-humic-like

Supplementary Table 4: Polycondensed aromatic molecular formulae (C>15; AI_{mod} > 0.66) detected in incubated water samples. Shown are normalized relative intensities (per 10,000) in biotic and control samples (ctrl) at t_0, t_1 (10 days) and t_2 (28 days).

	Formula	mass	H/C	O/C	AI_{mod}	DBE	t0	t0	t0	t1	t1	t1	t2	t2	t2	ctr0	ctr1	ctr2
CH(O)	C16H10O	217.06589	0.6	0.1	0.74	12	-	0.8	1	-	-	-	-	-	-	0.58	-	0.96
	C17H12O	231.08154	0.7	0.1	0.7	12	-	0.5	0.6	-	-	-	-	-	-	0.5	-	-
	C16H12O2	235.07645	0.8	0.1	0.67	11	1.8	1.9	2	1.1	-	0.9	-	0.7	0.5	2.13	2.29	3.05
	C19H14O	257.09719	0.7	0.1	0.68	13	-	-	-	-	-	-	-	-	-	0.5	-	-
	C18H12O2	259.07645	0.7	0.1	0.71	13	-	-	-	-	-	-	0.5	-	-	-	-	-
	C17H12O3	263.07137	0.7	0.2	0.68	12	-	-	0.6	1.4	-	1.1	-	0.6	-	0.5	-	-
	C16H10O4	265.05063	0.6	0.3	0.71	12	-	-	0.4	-	-	-	0.5	-	-	-	-	-
	C19H14O2	273.0921	0.7	0.1	0.67	13	-	-	-	-	-	-	-	-	-	0.41	-	-
	C17H12O4	279.06628	0.7	0.2	0.67	12	-	-	0.4	-	-	0.8	0.6	0.5	0.6	0.49	-	-
	C16H10O5	281.04555	0.6	0.3	0.7	12	-	-	-	-	-	-	-	-	-	0.43	-	-
	C16H10O6	297.04046	0.6	0.4	0.69	12	-	-	-	-	-	-	-	-	-	0.46	-	-
	C24H8O3	343.04007	0.3	0.1	0.87	21	-	-	0.8	-	-	-	-	-	-	-	-	-
	C30H10	369.07097	0.3	0	0.87	26	-	-	-	-	-	-	-	-	-	-	-	0.9
	C22H8O7	383.01973	0.4	0.3	0.84	19	0.4	-	-	-	-	-	-	-	-	-	-	-
	C25H12O6	407.05611	0.5	0.2	0.77	20	-	-	0.5	-	-	-	-	-	-	-	-	-
	C28H18O6	449.10306	0.6	0.2	0.68	20	-	-	0.5	-	-	-	-	-	-	-	-	-
	C37H24O2	499.17035	0.7	0.1	0.69	26	-	-	-	-	-	-	-	-	-	0.65	-	-
	C48H20O14	819.07803	0.4	0.3	0.78	39	-	-	0.7	-	-	-	-	-	-	-	-	-
	C44H16O23	911.00097	0.4	0.5	0.78	37	-	-	-	-	-	-	-	-	0.5	-	-	-
CHS	C16H8S	231.0274	0.5	0	0.8	13	-	-	-	-	-	-	0.8	-	0.4	-	-	-
	C16H12S	235.0587	0.8	0	0.67	11	-	-	-	-	0.8	0.72	1.3	1.6	1.9	-	-	-
	C16H10OS	249.03796	0.6	0.1	0.72	12	-	-	-	-	1.4	1.05	1.8	1.6	1.3	-	-	-
	C18H10S	257.04305	0.6	0	0.76	14	-	-	-	-	-	-	1.1	0.6	0.9	-	-	-
	C18H12S	259.0587	0.7	0	0.71	13	-	-	-	1	0.9	0.92	2.3	1.2	1.5	-	-	-
	C16H8S2	262.99947	0.5	0	0.79	13	-	-	-	-	-	-	-	1.1	0.5	-	-	-
	C16H8O2S	263.01723	0.5	0.1	0.79	13	-	-	-	-	-	-	1	1	1	-	-	-
	C17H12OS	263.05361	0.7	0.1	0.68	12	-	-	-	-	-	-	1	1.2	1.1	-	-	-
	C16H10S2	265.01512	0.6	0	0.71	12	0.7	0.9	0.6	-	-	-	0.5	0.5	-	0.55	-	-
	C16H10O2S	265.03288	0.6	0.1	0.71	12	-	-	-	-	-	0.67	0.6	0.9	0.6	-	-	-
	C18H8OS	271.02231	0.4	0.1	0.82	15	-	-	-	-	-	-	-	-	0.5	-	-	-
	C18H10OS	273.03796	0.6	0.1	0.76	14	-	-	-	-	-	-	0.7	0.5	0.6	-	-	-
	C17H10O2S	277.03288	0.6	0.1	0.73	13	-	-	-	-	-	-	-	0.4	-	-	-	-
	C16H8OS2	278.99438	0.5	0.1	0.78	13	-	-	-	-	-	-	0.5	1.4	0.5	-	-	-
	C17H12S2	279.03077	0.7	0	0.67	12	1.2	0.7	0.9	-	0.7	-	-	-	-	0.65	-	-
	C17H12O2S	279.04853	0.7	0.1	0.67	12	-	-	-	1.1	1.5	1.63	1.5	1.9	1.5	-	-	-
	C16H10OS2	281.01003	0.6	0.1	0.7	12	-	-	-	-	-	-	0.6	2.8	1.3	-	-	-
	C16H10O3S	281.02779	0.6	0.2	0.7	12	-	-	-	-	-	0.83	1.1	1.1	1	-	-	-
	C18H6S2	284.98382	0.3	0	0.88	16	-	-	-	-	-	-	0.5	1	0.8	-	-	-
	C19H10OS	285.03796	0.5	0.1	0.77	15	-	-	-	-	-	-	-	-	0.5	-	-	-
	C19H12OS	287.05361	0.6	0.1	0.71	14	-	-	-	-	-	-	0.9	0.6	0.8	-	-	-
	C18H12O2S	291.04853	0.7	0.1	0.69	13	-	-	-	-	-	0.64	0.7	0.9	0.7	-	-	-
	C17H10O3S	293.02779	0.6	0.2	0.72	13	-	-	-	-	-	-	-	-	0.5	-	-	-
	C16H10O4S	297.02271	0.6	0.3	0.69	12	-	-	-	0.9	-	0.85	0.6	1	0.7	-	-	-
	C18H12OS2	307.02568	0.7	0.1	0.68	13	-	-	-	-	-	-	-	0.6	-	-	-	-
	C18H12O3S	307.04344	0.7	0.2	0.68	13	-	0.6	0.5	1	-	0.82	0.9	0.8	0.7	0.49	-	-
	C22H16S	311.09	0.7	0	0.67	15	-	-	-	-	-	-	-	-	0.6	-	-	-
	C16H10O3S2	312.99986	0.6	0.2	0.68	12	-	-	-	3	1.6	0.9	1.1	0.6	-	-	-	-
	C16H10O5S	313.01762	0.6	0.3	0.68	12	-	-	-	-	-	-	-	0.5	0.7	-	-	-
	C19H10OS2	317.01003	0.5	0.1	0.76	15	-	-	-	-	-	-	-	0.5	-	-	-	-
	C20H14O2S	317.06418	0.7	0.1	0.67	14	-	-	-	-	-	-	0.6	0.6	0.6	-	-	-
	C19H12OS2	319.02568	0.6	0.1	0.7	14	-	-	-	-	-	-	-	0.5	-	-	-	-
	C18H12O2S2	323.0206	0.7	0.1	0.67	13	-	-	-	-	-	-	0.7	0.7	0.7	-	-	-
	C18H12O4S	323.03836	0.7	0.2	0.67	13	-	-	-	-	0.9	0.72	0.7	1.1	0.9	-	-	-
	C17H10O3S2	324.99986	0.6	0.2	0.7	13	-	-	-	-	-	-	0.7	-	-	-	-	-
	C16H10O6S	329.01254	0.6	0.4	0.67	12	-	-	-	-	-	-	-	0.5	0.6	-	-	-
	C19H12O2S2	335.0206	0.6	0.1	0.69	14	-	-	-	-	-	-	0.8	0.9	0.7	-	-	-
	C21H14O3S	345.05909	0.7	0.1	0.68	15	-	-	-	-	-	-	-	0.5	0.6	-	-	-
	C20H12O2S2	347.0206	0.6	0.1	0.71	15	-	-	-	-	-	-	0.9	0.6	0.6	-	-	-
	C19H12O3S2	351.01551	0.6	0.2	0.68	14	-	-	0.6	-	-	-	0.7	-	-	-	-	-
	C19H12O5S	351.03327	0.6	0.3	0.68	14	-	-	-	-	-	-	-	0.5	-	-	-	-
	C21H14O4S	361.05401	0.7	0.2	0.67	15	-	-	-	-	-	-	0.7	0.5	0.5	-	-	-
	C20H12O3S2	363.01551	0.6	0.2	0.7	15	-	-	-	-	-	0.78	0.9	0.6	0.4	-	-	-
	C22H14O4S	373.05401	0.6	0.2	0.68	16	-	-	-	-	-	-	-	0.4	-	-	-	-

Continued on next page

Continued from previous page

	Formula	mass	H/C	O/C	AI_{mod}	DBE	t0	t0	t0	t1	t1	t1	t2	t2	t2	ctr0	ctr1	ctr2
CHS	C16H6O9S2	404.93805	0.4	0.6	0.79	14	-	-	-	-	-	-	0.9	-	0.4	-	-	-
	C22H14O4S2	405.02608	0.6	0.2	0.67	16	-	-	-	-	-	-	0.7	-	-	-	-	-
	C16H8O9S2	406.9537	0.5	0.6	0.68	13	1	0.6	-	2.3	1	0.96	2.5	0.8	1	-	-	-
	C23H14O6S	417.04384	0.6	0.3	0.68	17	-	-	-	-	-	-	-	-	-	-	-	0.9
	C17H8O9S2	418.9537	0.5	0.5	0.71	14	-	-	-	-	-	-	0.8	-	-	-	-	-
	C16H8O10S2	422.94862	0.5	0.6	0.67	13	-	-	-	1.1	-	-	0.6	-	-	-	-	-
	C18H6O9S2	428.93805	0.3	0.5	0.83	16	-	-	-	1	-	-	-	-	-	-	-	-
	C24H14O6S	429.04384	0.6	0.3	0.7	18	-	-	-	-	-	-	-	-	-	-	-	0.91
	C19H8O9S2	442.9537	0.4	0.5	0.76	16	-	-	-	-	-	-	0.9	-	-	-	-	-
	C26H10O11S	528.98711	0.4	0.4	0.79	22	0.5	-	-	-	-	-	-	-	-	-	-	-
	C47H16OS2	659.05698	0.3	0	0.84	40	10	11	14	5.3	4.5	4.77	2.7	2.6	2.5	10.9	10.6	3.7
	C48H32S2	671.18727	0.7	0	0.67	33	-	-	-	-	-	0.69	-	-	-	-	-	-
CHN	C16H12N2O	247.08769	0.8	0.1	0.7	12	-	-	-	-	-	-	-	-	-	0.49	-	-
	C16H11NO4	280.06153	0.7	0.3	0.69	12	-	-	-	-	-	-	-	-	-	0.48	-	-
	C18H12N2O3	303.07752	0.7	0.2	0.72	14	-	-	-	-	-	-	-	-	-	-	-	1.09
	C19H10N2O3	313.06187	0.5	0.2	0.81	16	-	-	-	-	-	-	-	-	-	-	-	0.85
	C19H12N2O3	315.07752	0.6	0.2	0.74	15	0.5	-	0.4	-	-	-	-	-	-	-	-	0.92
	C19H14N2O3	317.09317	0.7	0.2	0.68	14	0.7	-	-	-	-	-	-	-	-	-	-	1.25
	C21H13N3O	322.09859	0.6	0.1	0.77	17	-	-	-	-	-	-	-	0.4	-	-	-	-
	C20H12N2O3	327.07752	0.6	0.2	0.76	16	0.5	-	-	-	-	-	-	-	-	-	-	-
	C20H14N2O3	329.09317	0.7	0.2	0.7	15	-	-	-	-	-	-	-	-	-	-	-	1.1
	C22H8N4O	343.06254	0.4	0.1	0.94	21	-	-	-	-	-	-	-	0.7	1	-	-	-
	C20H13N3O4	358.08333	0.7	0.2	0.73	16	-	-	-	1.4	0.7	1.26	0.8	0.7	0.7	-	-	-
	C23H16N4O2	379.12005	0.7	0.1	0.72	18	1	-	-	-	-	-	-	-	-	-	-	1.1
	C23H17N3O3	382.11972	0.7	0.1	0.68	17	0.5	0.8	0.9	-	-	0.65	-	-	-	0.69	-	-
	C22H16N4O3	383.11497	0.7	0.1	0.7	17	0.5	-	-	-	-	-	0.7	-	-	-	-	-
	C16H6N2O10	384.99497	0.4	0.6	0.89	15	-	-	-	1.9	-	-	1.5	0.6	0.7	-	-	-
	C16H10N2O10	389.02627	0.6	0.6	0.67	13	-	-	-	1.1	0.7	-	0.8	-	-	-	-	-
	C17H8N2O10	399.01062	0.5	0.6	0.8	15	-	-	-	1.6	-	-	0.9	-	0.5	-	-	-
	C16H7N3O10	400.00587	0.4	0.6	0.88	15	1.2	0.9	0.6	-	-	-	-	-	-	0.73	1.78	-
	C16H9N3O10	402.02152	0.6	0.6	0.75	14	0.7	0.6	0.7	-	-	-	-	-	-	-	1.87	-
	C20H13N3O7	406.06808	0.7	0.4	0.7	16	-	-	-	-	-	-	-	0.5	-	-	-	-
	C17H9N3O10	414.02152	0.5	0.6	0.78	15	0.5	-	-	-	-	-	-	-	-	-	-	-
	C34H15NO2	468.103	0.4	0.1	0.81	28	-	-	-	-	-	-	-	-	-	-	1.3	-
	C24H12N2O10	487.04192	0.5	0.4	0.76	20	-	-	-	-	-	-	-	-	-	0.46	-	-
	C32H13NO5	490.0721	0.4	0.2	0.82	27	-	-	-	-	-	-	-	-	0.4	-	-	-
	C23H8N4O10	499.01677	0.4	0.4	0.93	22	-	-	-	-	-	-	-	0.5	-	-	-	-
	C23H12N2O12	507.03175	0.5	0.5	0.73	19	-	-	-	-	-	-	-	-	-	-	-	1.03
	C35H13NO5	526.0721	0.4	0.1	0.84	30	-	-	-	-	-	-	0.7	-	-	-	-	-
	C36H17NO5	542.1034	0.5	0.1	0.78	29	-	-	-	-	-	-	-	0.5	-	-	-	-
	C36H13NO6	554.06701	0.4	0.2	0.84	31	-	-	-	-	-	-	1.2	-	-	-	-	-
	C39H22N2O8	645.13034	0.6	0.2	0.73	30	-	-	-	-	-	-	-	-	-	-	2.04	-
	C29H17N3O16	662.05361	0.6	0.6	0.67	23	0.8	0.9	1.3	-	-	-	-	-	-	0.79	1.25	-
	C43H30N4O4	665.21943	0.7	0.1	0.68	31	-	-	-	4	6.3	8.41	2.6	3.5	2.2	-	-	-
	C47H29N3O7	746.19328	0.6	0.2	0.7	35	-	-	-	-	-	-	-	-	1	-	-	-
	C44H21NO16	818.07876	0.5	0.4	0.74	35	2	2.1	2.6	-	-	1.11	-	0.5	0.7	2.1	2.19	-
	C45H21N3O22	954.0544	0.5	0.5	0.74	37	-	-	-	-	-	0.73	-	0.8	-	-	-	-
	C58H23NO15	972.0995	0.4	0.3	0.8	48	1.2	1.4	1.7	-	-	-	-	-	-	1.21	-	-
CHNS	C16H11NS	248.05395	0.7	0	0.71	12	-	-	-	1.5	1.4	2.62	3.5	1	1	-	-	-
	C17H13NS	262.0696	0.8	0	0.67	12	-	-	-	-	-	0.72	0.9	0.8	0.6	-	-	-
	C16H11NO2S	280.04378	0.7	0.1	0.69	12	-	-	-	-	-	-	-	0.5	-	-	-	-
	C18H13NOS	290.06451	0.7	0.1	0.68	13	-	-	-	-	0.7	-	-	0.8	0.5	-	-	-
	C16H11NO3S	296.03869	0.7	0.2	0.68	12	-	-	-	-	-	-	-	0.7	-	-	-	-
	C18H13NO2S	306.05943	0.7	0.1	0.67	13	-	-	-	-	-	-	-	0.6	0.6	-	-	-
	C16H11NO4S	312.03361	0.7	0.3	0.67	12	-	-	-	-	-	-	-	0.5	-	-	-	-
	C18H11NO3S	320.03869	0.6	0.2	0.72	14	-	-	-	-	-	-	0.9	0.5	0.5	-	-	-
	C19H13NO3S	334.05434	0.7	0.2	0.68	14	-	-	-	-	-	-	0.6	-	-	-	-	-
	C28H13NO19S	697.97298	0.5	0.7	0.7	23	1	-	-	-	-	-	-	-	-	-	-	-
	C58H25NO13S	974.09739	0.4	0.2	0.78	47	-	-	0.8	-	-	-	-	-	-	0.67	-	-

*Supplementary Table 5: Stable carbon isotopic composition, compound class concentration and optical properties of asphalt incubation water samples. Values for biological active samples resemble means ± standard deviation of triplicates. *n.d = not determined*

Parameter	Biotic incubation			Pasteurized control		
Days	0	10	28	0	10	28
δ^{13}CDIC (‰)	-3.3 ± 0.1	-3.6 ± 0.8	-8.9 ± 0.7	-3.3	-1.2	0.2
DOC (μM)	852.8 ± 58.4	1005 ± 49	2401 ± 489	376	856	785
DOC_{SPE}(μM)	52.4 ± 3.4	278 ± 22	1236 ± 361	73	150	217
Extraction eff. (%)	6.20 ± 0.80	28.8 ± 2.2	50.9 ± 4.6	19.4	17.5	27.6
δ^{13}C DOM_{SPE} (‰)	-28.0	-28.7 ± 0.4	-28.2 ± 0.4	n.d.*	-28.6	-27.8
DOS_{SPE} (μM)	2.69 ± 0	12.5 ± 0.5	40.1 ± 4.5	4.9	9.1	17.2
DOS_{SPE} / DOC_{SPE}	0.051	0.045 ± 0.004	0.034 ± 0.006	0.067	0.06	0.07
DBC (μM)	0.83 ± 0	3.20 ± 0.11	13.3 ± 2.9	2.29	3.05	5.12
DBC/DOC (%)	0.10 ± 0.01	0.33 ± 0.01	0.55 ± 0.03	0.61	0.36	0.65
B6CA/B5CA	0.61 ± 0	0.62 ± 0.04	0.70 ± 0.12	0.36	0.39	0.38
$SUVA_{254}$ (L mg C^{-1} m^{-1})	0.3 ± 0.3	3.2 ± 0.7	4.8 ± 0.9	1.53	1.68	3.08

Supplementary Table 6: Number of molecular formulae and intensity-weighted parameters determined by FT-ICR-MS in DOM_{SPE} during the incubation. Values for biological active samples resemble means ± standard deviation of triplicates.

	Biotic incubation			Pasteurized control			Exclusive formulae	
Days	0	10	28	0	10	28	Biotic	control
Formulae	3817 ± 336	2604 ± 354	2760 ± 374	4057	2056	1681	1102	497
Mass	299.0 ± 11.3	263.7 ± 5.6	250.6 ± 5.3*	297.1	284.5	263.6*	281.7 ± 8.7	315.1
C	15.7 ± 0.6	13.8 ± 0.2	13.2 ± 0.3*§	15.6	15.4	15.6	14.1 ± 0.4	19
H	23.2 ± 1.4	18.6 ± 0.1	17.2 ± 0.4*§	22.4	22.8	23.6	15.3 ± 0.6*	29.4
O	4.2 ± 0.18	3.9 ± 0.1	3.7 ± 0.1*§	4.3	3.8	2.7*	4.3 ± 0.2*	2.6
N	0.17 ± 0.1	0.1 ± 0.02	0.04 ± 0.02*	0.12	0.07	0.02*	0.1 ± 0.03	0.11
S	0.52 ± 0.08	0.47 ± 0.02	0.47 ± 0.04*§	0.53	0.49	0.33*	0.83 ± 0.01*	0.48
P	0.04 ± 0	0.03 ± 0	0.01 ± 0	0.03	0.02	0*	0.03 ± 0.01	0.01
H/C	1.49 ± 0.03	1.36 ± 0.01	1.32 ± 0.02*§	1.45	1.49	1.52	1.11 ± 0*	1.56
O/C	0.28 ± 0	0.29 ± 0.01	0.29 ± 0§	0.29	0.26	0.18*	0.32 ± 0*	0.14
S/C	0.04 ± 0.01	0.04 ± 0	0.04 ± 0*§	0.04	0.03	0.02*	0.07 ± 0*	0.03
AI_{mod}	0.20 ± 0.01	0.28 ± 0	0.30 ± 0.01*§	0.22	0.21	0.23*	0.40 ± 0*	0.21
DBE	5.2 ± 0.1	5.6 ± 0.2	5.7 ± 0.2*§	5.5	5.1	4.8*	7.6 ± 0.1*	5.4
NOSC	-0.85 ± 0.03	-0.7 ± 0.03	-0.67 ± 0.03*§	-0.79	-0.9	-1.12*	-0.34 ± 0.01*	-1.21
NSO:C	0.33 ± 0	0.33 ± 0.01	0.33 ± 0.01§	0.33	0.29	0.20*	0.39 ± 0*	0.18

* indicates molecular parameters that are significantly different comparing 28 days to 0 days and exclusively in the biological incubation and pasteurized control detected formulae; § indicates molecular parameters that are significantly different comparing 28 days biological incubation and 28 days pasteurized control ($p < 0.001$, Wilcoxon-Whitney test).

Supplementary Table 7: Concentrations of DOC, DOS_{SPE} and DBC in the incubation bottles after 0, 10 and 28 days. The cumulative release (cum.) of each compound class was calculated according to the difference of water volume and concentration at each timepoint and normalized to the initial asphalt mass incubated.

Sample	Days	Initial asphalt mass (g)	DOC (µM)	DOS_{SPE} (µM)	DBC (µM)	Volume (ml)	Cum. DOC release (µMol)	DOC/ asphalt (µMol C/g)	Cum. DOS_{SPE} release (µMol)	DOS_{SPE} /asphalt (µMol C/g)	Cum. DBC release (µMol)	DBC/ asphalt (µMol C/g)
Bottle 1	0	3.8	825	2.69	0.83	508	419	110	1.37	0.36	0.42	0.11
Bottle 1	10		917	12.99	3.08	295	446	117	4.4	1.16	1.09	0.29
Bottle 1	28		1953	36.44	11.19	137	588	155	7.62	2	2.2	0.58
Bottle 2	0	3.74	813	2.69	0.83	518	421	113	1.39	0.37	0.43	0.12
Bottle 2	10		970	12.62	3.24	310	470	126	4.47	1.2	1.18	0.31
Bottle 2	28		2327	38.78	11.99	151	675	180	8.42	2.25	2.5	0.67
Bottle 3	0	3.74	920	2.69	0.83	501	461	123	1.35	0.36	0.42	0.11
Bottle 3	10		1015	11.98	3.29	315	491	131	4.27	1.14	1.19	0.32
Bottle 3	28		2922	45.16	16.58	143	763	204	9.02	2.41	3.09	0.83
Mean	0							115		0.36		0.11
Mean	10							125		1.17		0.31
Mean	28							180		2.22		0.69
Control	0	3.58	376	4.91	2.29	496	186	52	2.43	0.68	1.14	0.32
Control	10		856	9.1	3.05	287	324	91	3.64	1.02	1.35	0.38
Control	28		785	17.24	5.12	144	314	88	4.81	1.34	1.65	0.46

III. Manuscript 2

Effects of hydrothermal heating on porewater dissolved organic matter in Guaymas Basin sediments

Jonas Brünjes[1], Michael Seidel[2], Andreas Teske[3], Florence Schubotz[1]

[1]MARUM – Center for Marine Environmental Sciences, Bremen, Germany

[2]ICBM, University of Oldenburg, Oldenburg, Germany

[3]University of North Carolina at Chapel Hill, Chapel Hill, USA

In preparation for *Limnology & Oceanography*

Abstract

The Guaymas Basin in the Gulf of California is a young rift system where hot basaltic sill intrusions into organic-rich sediments lead to the generation of large amounts of complex petroleum compounds. The hydrothermal heating can discharge bioavailable dissolved organic matter (DOM) from the sediments into the overlying water column, thereby fueling highly active, benthic microbial communities. In our study, we investigate the effect of hydrothermal heating and the resulting presence of petroleum compounds on the porewater DOM composition. We focus on sediment samples from sites with *in situ* temperatures ranging from 4 to >106 °C that exhibited a strong petroleum smell and partially containing oil droplets. DOM composition was analyzed using a combined approach of molecular analysis by ultrahigh-resolution mass spectrometry and tensor decomposition by parallel factor analysis (PARAFAC) of the fluorescent fraction of DOM (FDOM). We observed a strong correlation of sediment temperature to both composition and quantity of DOM, driven by enhanced microbial transformation of organic matter at temperatures below ~60 °C and increasingly sulfurized DOM at high-temperature sites. DOM associated with hydrothermal heating had elevated contributions of highly unsaturated, reduced, sulfur-containing DOM and petroleum-associated PARAFAC components. A considerable DOM fraction of hydrothermal origin was present both in overlying bottom waters and in recalcitrant deep-sea DOM, suggesting hydrothermal sediments as a source of recalcitrant DOM to the water column. This study provides novel insight into the DOM composition of porewaters in hydrothermally heated sediments, which contain a recalcitrant fraction besides presumed bioavailable DOM.

III.1 Introduction

The Gulf of California is a young ocean basin actively expanding with its hydrothermal spreading center, the Guaymas Basin, located at a water depth of 2000 m (Einsele *et al.*, 1980). Oceanic dissolved organic matter (DOM) containing approximately 662 pg of dissolved organic carbon (DOC) is one of the largest pools of surface organic matter on Earth (Hansell *et al.*, 2009). Thermal degradation of DOM during hydrothermal circulation of seawater is presumed to be a sink for the most recalcitrant fractions of marine DOM via a succession of abiotic oxidation, decarboxylation and dehydration of carboxylic acids and alcohol groups eventually leading to an almost complete removal of DOM (Hawkes *et al.*, 2015b; McCollom and Seewald, 2003; Seewald, 2001). Yet, hydrothermal fluids were also proposed as a source of thermogenic, recalcitrant DOM (Dittmar and Koch, 2006; Dittmar and Paeng, 2009). In the Guaymas Basin, magmatic sill intrusions hydrothermally heat up to 540 m of overlying organic-rich sediments, resulting in the generation of hydrothermal petroleum that impregnate the sediments (Simoneit, 1985; Teske *et al.*, 2020). At localized hotspots, thermal maturation of organic matter can also generate hydrothermal petroleum in the shallow subsurface (Mara *et al.*, 2022; Ondréas *et al.*, 2018). Hydrothermal heating of surficial Guaymas Basin sediments can rapidly release large quantities of primarily labile DOM compounds to bottom waters (Lin *et al.*, 2017). The subsequent hydrothermal oil-impregnation of sediments and release of water-soluble petroleum compounds on the contrary may be a source of refractory DOM stable for millennia (Hansell, 2013), suggested by previous studies at a terrestrial oil spill site (Podgorski *et al.*, 2020) and laboratory experiments of natural oil seepage (Brünjes *et al.*, 2022).

Both marine porewaters (Chen and Bada, 1994; Gan *et al.*, 2020; Rossel *et al.*, 2020; Schmidt *et al.*, 2009; Seidel *et al.*, 2014) and hydrothermal fluids (Hawkes *et al.*, 2015b; Noowong *et al.*, 2021; Rossel *et al.*, 2015; Yang *et al.*, 2017) have previously been studied for their DOM properties using optical analysis of chromophoric DOM (CDOM), fluorescent DOM (FDOM) and more recently on the molecular level by ultrahigh-resolution mass spectrometry (Fourier-transform ion cyclotron resonance mass spectrometry, FT-ICR-MS). FT-ICR-MS resolves thousands of molecules in complex organic matter mixtures such as oil and DOM in aquatic samples (Kujawinski, 2002; Marshall and Rodgers, 2008). While an isolation of DOM such as solid-phase extraction (SPE) is necessary for molecular analysis by FT-ICR-MS, optical properties of CDOM and FDOM can be determined on bulk waters. Hydrothermal and petroleum-related DOM can have low SPE extraction yields (Brünjes *et al.*, 2022; Hansen *et al.*, 2022; Hawkes *et al.*, 2015b; Rossel *et al.*, 2015), thus investigating FDOM from bulk porewaters provides valuable additional information. Excitation-emission matrix fluorescence

spectroscopy (EEM) and subsequent tensor decomposition of underlying theoretical fluorophores by parallel factor analysis (PARAFAC) is commonly used to characterize the FDOM fraction (Murphy *et al.*, 2013).

Marine porewaters usually show an elevated concentration of DOC relative to the overlying bottom water and diffusion processes transport microbially-processed porewater DOM into bottom waters (Burdige and Komada, 2015), contributing to cycling of dissolved organic nitrogen (DON) (Abdulla *et al.*, 2018; Zhou *et al.*, 2022) and presumably stable dissolved organic sulfur (DOS) (Abdulla *et al.*, 2019; Gomez-Saez *et al.*, 2017; Pohlabeln *et al.*, 2017; Seidel *et al.*, 2014). In Guaymas Basin, advective porewater fluxes lead to highly elevated and locally varying DOC concentrations in the bottom water, ~3-50 times higher compared to the deep ocean (Lin *et al.*, 2017). Active venting sites are characterized by microbial mats and highly active benthic communities (McKay *et al.*, 2016; Teske *et al.*, 2014; Teske *et al.*, 2016) covering hot, sulfidic, methane-rich and at times oil-impregnated sediments containing a wide range of both sedimentary and dissolved aliphatic and aromatic petroleum hydrocarbons including polycondensed aromatics and polysulfides, as well as low-molecular weight organic acids and lightweight hydrocarbons (Didyk and Simoneit, 1989; Mara *et al.*, 2022; Martens, 1990; Simoneit, 1985; Song *et al.*, 2021).

A previous study by Lin *et al.* (2017) proposed, based on hot-water extraction of unaltered Guaymas Basin sediments, that hydrothermal heating can release massive amounts of labile DOM and DON on short timescales to the water column, exceeding the flux of particulate organic matter sedimentation by two orders of magnitude. Actual DOM properties of Guaymas Basin porewaters however, were not studied so far. While subfractions of DOM such as organic acids (McKay *et al.*, 2012; Teske *et al.*, 2016), alcohols (Zhuang *et al.*, 2019) and petroleum hydrocarbons (Mara *et al.*, 2022) were previously quantified in porewater, DOM properties on the molecular level remained unexplored. It is unknown what kind of DOM is present in hydrothermal porewaters, how the steep temperature gradients shape DOM characteristics, and which dissolved compounds are resistant to benthic microbial degradation and accumulate in bottom waters. In this study, we examined the DOM composition of hydrothermal porewaters and bottom waters from seven short cores originating from four different vent locations in the Southern Guaymas Basin rift zone.

By applying a combined approach of optical analysis of bulk porewater FDOM and molecular-level analysis of solid-phase (SPE) extracted DOM, we want to I) assess the composition of DOM in hydrothermal porewaters, II) investigate the effects of high temperatures on changes in the DOM composition, III) assess which fractions of hydrothermal porewater DOM reach bottom waters.

III.2 Material and Methods

Table III. 1: Metadata for sediment cores sampled for porewater. Sediments were split into 4 cm segments. Temperatures are noted as the first reading of the heat probe at 5 cm sediment depth and at the respective maximum length of each core. A map of the sampling areas is shown in Supplementary Figure 1.

Dive & Core	Sampling Area	Latitude	Longitude	Depth (m)	Length (cm)	Sediment handling	Filtration	Thermal range
4992-40	Aceto Balsamico	27.00796	111.40723	2012	48	Laboratory slicing	0.2 μM GHP	6-21°C
4992-43	Aceto Balsamico	27.00796	111.40723	2012	40	Onboard slicing	0.3 μM GF/F	6-19°C
4993-6	Mat Mound	27.00796	111.40723	2012	16	Onboard slicing	0.3 μM GF/F	10-29°C
4993-24	Mat Mound	27.0074	111.40905	2004	20	Onboard slicing	0.3 μM GF/F	19-48°C
4999-19	Reference	27.00625	111.40955	2010	18	Onboard slicing	0.3 μM GF/F	3°C
5001-41	Cathedral Hill	27.00694	111.40663	2014	21	Laboratory slicing	0.2 μM GHP	12-67°C
5001-43	Cathedral Hill	27.01143	111.40422	2013	32	Onboard slicing	0.3 μM GF/F	12-106°C

Seven short pushcores between 16 and 48 cm length were retrieved by HOV *Alvin* during ship expedition RV *Atlantis* 42-05 in November 2018 (Table 1). In addition, nine bottom water samples were taken by *Alvin's* Niskin bottles (Supplementary Table 1). Previously explored sampling areas (Teske *et al.*, 2016) were targeted in the southern Guaymas Basin in water depths of about 2000 m. Sediment and water samples were distributed to 125 mL pre-rinsed high-density polyethylene bottles in 4-cm intervals and subsequently frozen. Two cores (4992-40, 5001-41) were frozen intact in the core liner and later split into 4-cm segments right before porewater sampling in the laboratory in spring 2020. For this, frozen sediment and water samples were slowly brought to room temperature by letting them sit in a thermally insulated box overnight. Sediments were then transferred to 50 mL Falcon tubes and centrifuged for 30 minutes at 4000 rpm. Separated porewater and seawater was then filtered through pre-combusted 0.3 μm filters (GF/F, Advantec) within a filter holder (polypropylene, Advantec) using 50 mL polypropylene syringes. Porewater from cores 4992-40, 5001-41 was filtered by 0.2 μm hydrophilic polypropylene membrane filters (GHP, Acrodisc). All glassware used was combusted (450 °C, 5h) and non-combustible material was pre-cleaned by overnight-soaking in acidified (pH 2) ultrapure water and subsequent thorough rinsing with ultrapure water.

Sediment temperatures were determined with *Alvins´*s heat flow probe in 5 cm resolution. To match the *in situ* temperatures with the 4 cm sediment sampling intervals, temperatures were interpolated between each 5 cm measurement. For the sediment-water interface, a bottom water temperature of 3° C was assumed (Teske *et al.*, 2016). It is important

to note that temperatures can drastically change on small scales in the Guaymas Basin and absolute temperature values assigned to specific cores and depths may vary on short timescales (McKay *et al.*, 2016).

III.2.1 DOC Measurements

DOC concentration of acidified (pH 2, HCl, Suprapur) filtrates was determined via high temperature catalytic oxidation on a Shimadzu TOC-VCPH instrument with an analytical precision better than 5%. Accuracy was tested in each run against deep Atlantic seawater reference material provided by the consensus reference materials program (D.A. Hansell, University of Miami, Coral Gables, FL, USA), standard deviation of repetitive measurements was ± 1.6% (DOC). Extraction efficiencies were calculated by determining the concentrations of solid-phase extracted (SPE) DOC relative to DOC: for this, an aliquot of the extract was re-dissolved in ultrapure water (pH2) after evaporating the methanol solvent in an oven at 40 °C overnight. To aid re-dissolution, samples were placed in an ultrasonic bath for 15 minutes at 30 °C.

III.2.2 DOM analysis

DOM was extracted right after porewater centrifugation on the same day from acidified (pH 2, HCl, Suprapur) filtrate samples with volumes between ~25 to 80 ml by SPE using 1 g PPL sorbent cartridges (Agilent Bond Elut) and eluted with 6 mL of methanol (HPLC-grade) following Dittmar *et al.* (2008). Mean extraction efficiencies were 21 ± 14% (see supplementary discussion). To further investigate hydrophobic DOM, residual methanol in the eluted cartridges was dried overnight under the fume hood. These cartridges were then eluted again with 5 mL of dichloromethane (DCM, GC-grade). DCM was then evaporated from the extracts under nitrogen gas and dried extracts were re-dissolved in 4 mL of methanol (Supplementary discussion; Supplementary Table 3, 4). Extracts were stored in amber glass vials in the dark at -20° C.

Ultrahigh-resolution mass spectrometry was performed on a solariX XR FT-ICR-MS (Bruker Daltonik GmbH, Bremen, Germany) connected to a 15 Tesla superconducting magnet (Bruker Biospin, Wissembourg, France). DOM_{SPE} extracts were diluted to a DOC concentration of 2.5 ppm (1 ppm for the DCM fraction) in 50:50 (*v/v*) methanol/ultrapure water and directly infused by hand injection into the electrospray source (ESI, Apollo II ion source, Bruker Daltonik GmbH, Bremen, Germany) with the capillary voltage set to 4 kV in negative mode. Ions were accumulated in the hexapole for 0.2 s prior to transfer into the ICR cell. Data acquisition was done in broadband mode using 8 megaword data sets and a scanning range

of 92 – 2000 Da. The instrument was internally calibrated with a list of > 100 known $C_xH_yO_z$ molecular formulae (MF). With this calibration procedure, a mass error of < 0.1 ppm was achieved. For each mass spectrum, 200 scans were accumulated. Before each sample set, blank checks with methanol/ultrapure water 1:1 (v/v) were measured, as well as the internal NEqPIW (North Equatorial Pacific Intermediate Water) DOM_{SPE} standard to account for instrument variations (Green *et al.*, 2014). MF were assigned using ICBM ocean, following procedures in Merder *et al.* (2020). A method detection limit (MDL) of 2.7 to eliminate instrumental noise (Riedel and Dittmar, 2014) and tolerance of 0.3 ppm was chosen and molecular formulae assigned using the template $C_{1\text{-}50}H_{0\text{-}150}O_{0\text{-}50}N_{0\text{-}4}S_{0\text{-}2}P_{0\text{-}1}$ in the mass range of 100 – 1000 Da at a tolerance of 0.5 ppm. The N, S, P rule and the isotope verification were applied to exclude unlikely formulae. Known potential contaminant MF and high peaks in blank measurements were manually removed, as well as MF with a high signal/MDL ratio and high mass deviation. The dataset was filtered by removing MF with a homologous series network for CH_2, CO_2, H_2O, O of < 5 to further minimize potentially falsely assigned MF. The peak intensity of each identified MF was normalized to the sum of peak intensities in each sample and multiplied by 10.000. The molecular parameters for the aromaticity index (AI_{mod}) (Koch and Dittmar, 2016), and the ratio of nitrogen, sulfur and oxygen to carbon (NSO:C) as an indicator for DOM hydrophobicity (Liu and Kujawinski, 2015) were calculated for each detected MF. DOM_{SPE} MF diversity was calculated as the Shannon diversity using the *vegan* package (Oksanen *et al.*, 2022). The AbioS index, an indicator for abiotic sulfurization of DOM was calculated as the sum of peak intensities of 15 characteristic dissolved organic sulfur (DOS) MF reported in Gomez-Saez *et al.* (2021). MF were assigned to the following compound groups as described in Seidel *et al.* (2014): (1) polycondensed aromatics (AI_{mod} >0.66; (2) aromatics (0.5 < AI_{mod} ≤ 0.66); (3) unsaturated aliphatics (1.5 < H/C ≤ 2, O/C < 0.9, N = 0; (4) unsaturated aliphatics with nitrogen (1.5 < H/C ≤ 2, O/C < 0.9, N = 1; (5) highly unsaturated (AI_{mod} ≤ 0.5, H/C < 1.5, O/C < 0.9); (6) saturated compound (H/C ≥2 or O/C ≥ 0.9).

III.2.3 Optical measurements

Filtered water samples were stored at 4°C in the dark until analysis. Absorbance measurements of CDOM were conducted on an UV-VIS absorption spectrophotometer (UV-1280, Shimadzu) in 10 mm quartz cells directly before fluorescence measurements. Fluorescence measurements were performed using a fluorescence spectrophotometer (Agilent Cary Eclipse, USA) at room temperature in a 10 mm quartz fluorescence cell. Excitation-emission matrices (EEM) were recorded ranging from excitation 220 – 450 nm in 5 nm steps and emission 250 – 600 nm in 2 nm steps at room temperature. Samples exceeding high fluorescence intensities were diluted with ultrapure water (18 Ω) up to 10-fold. An aliquot

of DOM_{SPE} extract was transferred to an empty vial and methanol was evaporated under N2 stream. The extract was then re-dissolved in 2.5 mL of ultrapure water to reach a target-concentration of 150 μM DOC, vortexed for about 20 seconds and transferred to the quartz fluorescence cell for measurements. The fluorescence spectrum of ultrapure water was measured at the beginning and end of each measurement day and subtracted from the raw data set. Fluorescence signals were normalized to the Raman peak area of ultrapure water. Inner-filter effects were corrected using absorbance spectra. Specific absorption at 254 nm ($SUVA_{254}$) was calculated by dividing the absorption coefficient (m) at 254 nm by the DOC concentration (mg L^{-1}). CDOM slope ratios (SR) were calculated based on the slope of absorption spectra between 275 – 295 nm to 350-400 nm.

III.2.4 Statistical analysis

A seven-component PARAFAC model was calculated using the StaRdom package (Pucher *et al.*, 2019) on porewater EEMs (n = 52). Raman and Rayleigh scattering were thoroughly removed and interpolated. Samples were normalized to unit variance because of large differences in fluorescence intensities. EEMs of bottom waters were not included due to poor signal resolution and residual analysis. The final model was validated by split-half tests after splitting it into 4 subsets, recombined to 6 splits (Murphy *et al.*, 2013). To further investigate differences in original porewater and DOM_{SPE} extracts, two more 7-component models were calculated on a sample set only containing re-dissolved SPE extracts (n = 39) and a sample set combining both porewater and DOM_{SPE} EEMs (Supplementary Table 2). The loadings of PARAFAC components were reported as the relative abundance of each component to track qualitative differences in FDOM amongst samples. Results shown in this paper refer to the model calculated on the original porewater EEMs (Table 1).

A principle coordinate analysis (PCoA) was calculated on normalized intensities of DOM_{SPE} MF within a Bray-Curtis dissimilarity matrix using the vegan package (Oksanen *et al.*, 2022). Intensity-weighted averages of molecular parameters, DOM_{SPE} compound group assignments as well as centered normalized CDOM, FDOM and environmental parameters were further correlated to this matrix. Correlations between environmental and molecular parameters were assessed using Kendall´s τ, a non-parametric test (most of the resulting parameters were not normal-distributed, test for normality using a Shapiro-wilk test) which is considered robust to outliers and nonlinearity (Newson, 2002). Differences between groups of samples were assessed using a Wilcoxon test. All of the statistical analyses were performed in R v.4.2.1 (R Core Team, 2022).

III.3 Results

III.3.1 DOM in hydrothermal porewaters

III.3.1.1 Temperature and DOC profiles

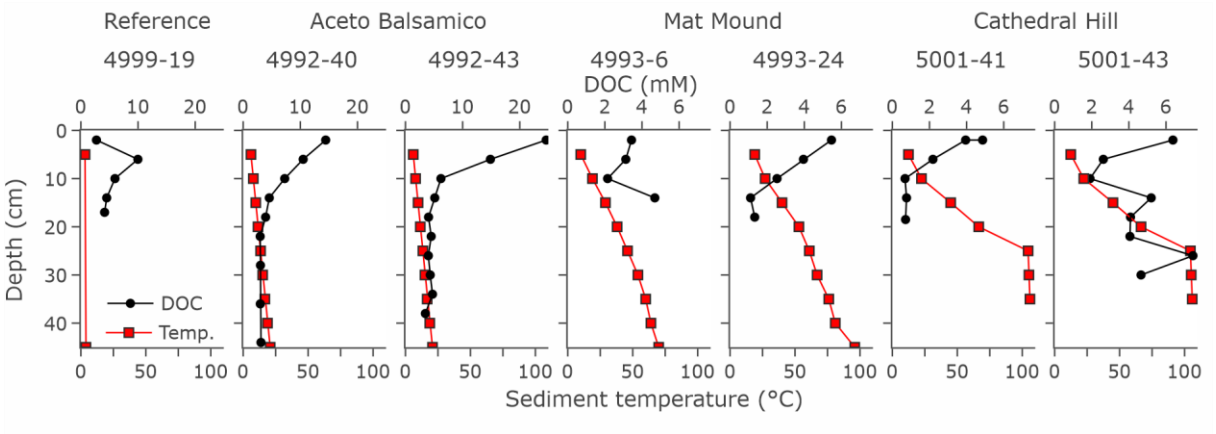

Figure III. 1: Depth profiles of porewater DOC concentrations and in situ sediment temperature (Temp.) from closest sediment heat probe for all seven pushcores investigated in this study. Note different DOC scales for Mat Mound and Cathedral Hill profiles.

Porewater DOC concentrations were highly variable within and between cores, and ranged between 1.1 - 25 mM DOC (Figure 1). The highest DOC concentrations were observed at the Aceto Balsamico site (cores 4992-40 and 4992-43), where *in situ* sediment temperatures ranged from 6 °C at 5 cm to 21 °C at 45 cm depth. Both cores were located within approximately less than 50 cm distance of each other and the sampling area was covered with thin, yellowish *Beggiatoa* mats. Here, 15 and 25 mM of DOC concentrations were measured in porewater in the 0-4 cm interval with a rapid decrease downcore to about 3 mM DOC at 40 cm sediment depth. Two cores from the Mat Mound site (cores 4993-6 and 4993-24, both cores from areas covered with orange *Beggiatoa* mats) showed elevated *in situ* sediment temperatures ranging from 10 °C to 70 °C (4993-6) and 19 °C to 96 °C (4993-24) from 5 to 45 cm. DOC concentrations were in the range of 1.1 – 5.5 mM DOC. The steepest temperature gradients were observed at the Cathedral Hill site (cores 5001-41 and 5001-43), ranging from 12 °C at 5 cm up to 106 °C at 35 cm sediment depth. Both cores were located in approximately 1 m distance of each other, and originated from an area covered with orange/bright yellow *Beggiatoa* mats. DOC concentrations in porewaters from core 5001-41 were highest below the sediment surface (4.9 mM DOC) and rapidly decreased downcore to about 0.7 mM DOC in the 16-21 cm depth interval. DOC concentrations of core 5001-43 were similarly high below the sediment surface (6.4 mM DOC) and first decreased with sediment depth and then increased again from the 12-16 cm interval on downcore. At the reference site not covered by

microbial mats, temperatures ranged from 3.2 °C at 5 cm depth to 3.9 °C at 45 cm depth. Porewater DOC concentrations rapidly increased between the surface interval from 2.7 mM DOC to 10 mM DOC in the 4-8 cm interval and then decreased downcore to 4.1 mM DOC at 16-18 cm. Extraction efficiencies were generally low and highly variable among cores and depth intervals, reaching mean efficiencies of 21 ± 14% among all cores. The lowest efficiencies were observed from Mat Mound and Cathedral Hill cores, where some samples had extraction efficiencies of < 10% (Supplementary Table 3). Bottom water had mean DOC concentrations of 903 ± 471 μM (Supplementary Table 1). Porewater DOC (τ = -0.39, p < 0.001) and DOC_{SPE} (τ = -0.49, p < 0.001) concentrations were both significantly negatively correlated with *in situ* sediment temperature (Table 3).

III.3.1.2 Optical analysis of DOM

A 7-component PARAFAC model based on porewater EEMs was calculated and components compared with the Openfluor database (Murphy *et al.*, 2014). Each PARAFAC component represents an underlying mathematical fluorophore which combined make up the EEM spectrum. In environmental samples, these PARAFAC components are not pure, isolated fluorophores but rather represent a group of dissolved compounds exhibiting similar spectral properties (Murphy *et al.*, 2013). Both C1 and C3 matched with PARAFAC components published previously related to petroleum-derived FDOM (Figure 2, Table 2). C4 and C7 matched protein-like components, whereas C2 matched microbially-derived humic-like and both C5 and C6 humic-like PARAFAC components.

Relative contributions of each PARAFAC component versus the sediment temperature are displayed in Figure 2. The relative contributions of C1 and C3 were generally lowest in the surface sediment interval for all cores and slightly increased downcore (Suppl. Fig. 4). In the hottest core of 5001-43, these two compounds made up ~65% of the total signal intensity, while only a minor contribution was observed in the reference core. Here, C4 contributed up to 50% of the total signal intensity. In the hydrothermal cores, the relative contribution of C4 was highest in the surface sediment interval (between 16 – 27%) and decreased downcore. The same trend was found for C5 and C6. The contribution of C2 and C7 was highest in the Aceto Balsamico cores. The relative abundance of C1 and C3 were significantly positively correlated with log-transformed sediment temperatures, whereas the relative abundance of C4 and C6 showed negative correlations with temperature (Figure 2, Table 3).

Because of generally low and highly varying DOM_{SPE} extraction efficiencies between cores and depth intervals, fluorescent properties or re-dissolved DOM_{SPE} extracts were analyzed to compare optical properties of bulk water DOM with DOM_{SPE}. For this, two

additional PARAFAC models were calculated, containing re-dissolved DOM_{SPE} extracts and combined model of porewater and DOM_{SPE} extracts. Both models resolved similar PARAFAC components as the original porewater model (Supplementary Table 2, Supplementary Figure 2). Relative contributions of PARAFAC components from original porewater and DOM_{SPE} extracts showed significant ($p < 0.001$) linear correlations and a theoretical 1:1 line within a 95% prediction interval. Only protein-like components C4 and C7 showed noticeable deviations, with an underrepresentation of C4 and overrepresentation of C7 for some of the reference core samples in the DOM_{SPE} extracts.

Table III. 2: Summary of excitation and emission (Ex/Em) maxima of the seven PARAFAC compounds, previously published similar PARAFAC compounds and the degree of similarity as Tuckers congruence coefficient (TCC). Factors with TTC values of ≥ 0.95 are considered similar (Lorenzo-Seva and Ten Berge, 2006)

Comp.	Ex/Em max (nm)	Synonyms	TCC Ex/Em	Description
C1	340/416	C3 in Podgorski *et al.* (2018); C4 in Brünjes *et al.* (2022)	0.98/0.96; 0.94/0.98	Aromatic petroleum resistant to biodegradation; petroleum humic-like
C2	315/384	C3 in Chen *et al.* (2018)	0.98/0.99	Microbially-derived humic-like
C3	295/360	C1 in Brünjes *et al.* (2022)	0.98/0.97	Low *m/z* PAH related
C4	280/334	C3 in Stedmon *et al.* (2011)	1.0/1.0	Protein-like (tryptophane)
C5	415/470	C6 in Zito *et al.* (2019b)	0.96/0.97	High *m/z* aromatic
C6	345/446	C6 in Podgorski *et al.* (2018)	0.95/0.95	Humic-like; highly biodegraded
C7	275/300	C4 in Amaral *et al.* (2021)	0.98/0.96	Protein-like (tyrosine); mud volcano sediments

PAH = polycyclic aromatic hydrocarbons

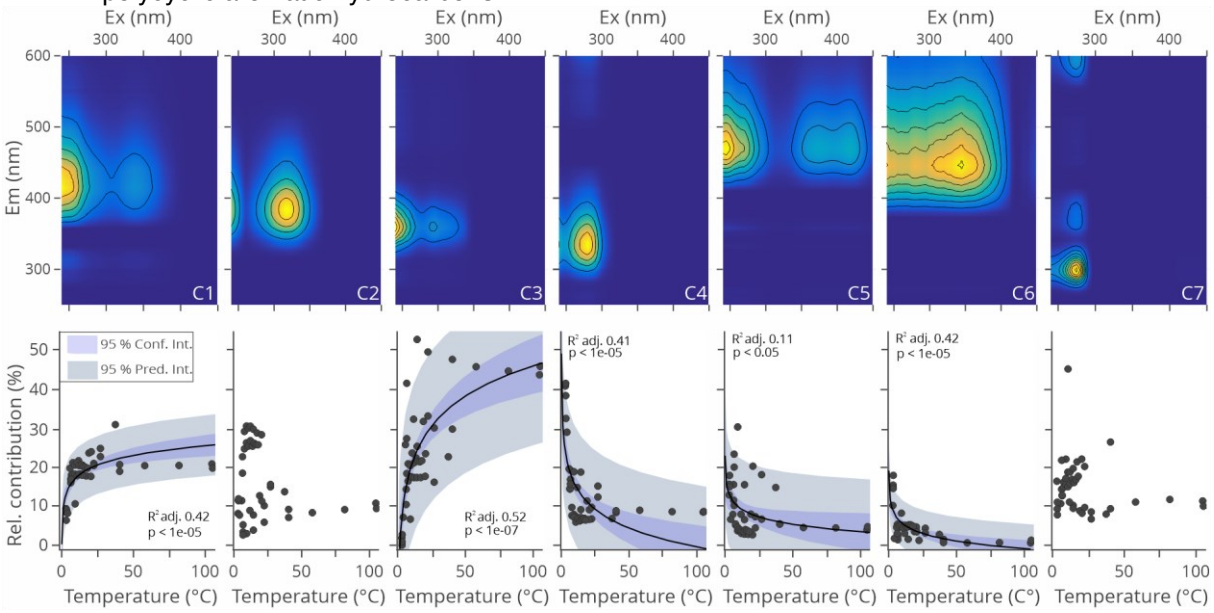

Figure III. 2: Excitation and emission maxima of a seven component PARAFAC model calculated on bulk porewater FDOM (top) and relative contribution of each respective PARAFAC component as a function of in situ sediment temperature (bottom). Plotted are linear models between the relative contribution and log-transformed in situ temperature on a non-log-transformed axis, adjusted R^2 and p-values as well as 95% confidence and prediction intervals (conf. int. and pred. int.) are shown in the plot

(n = 45). The confidence interval estimates the range of plausible values for all observed relative contributions of a respective PARAFAC component, while the prediction interval estimates the range of plausible values for an individual observation, hence showing a higher range of uncertainties.

III.3.1.3 Molecular composition of DOM

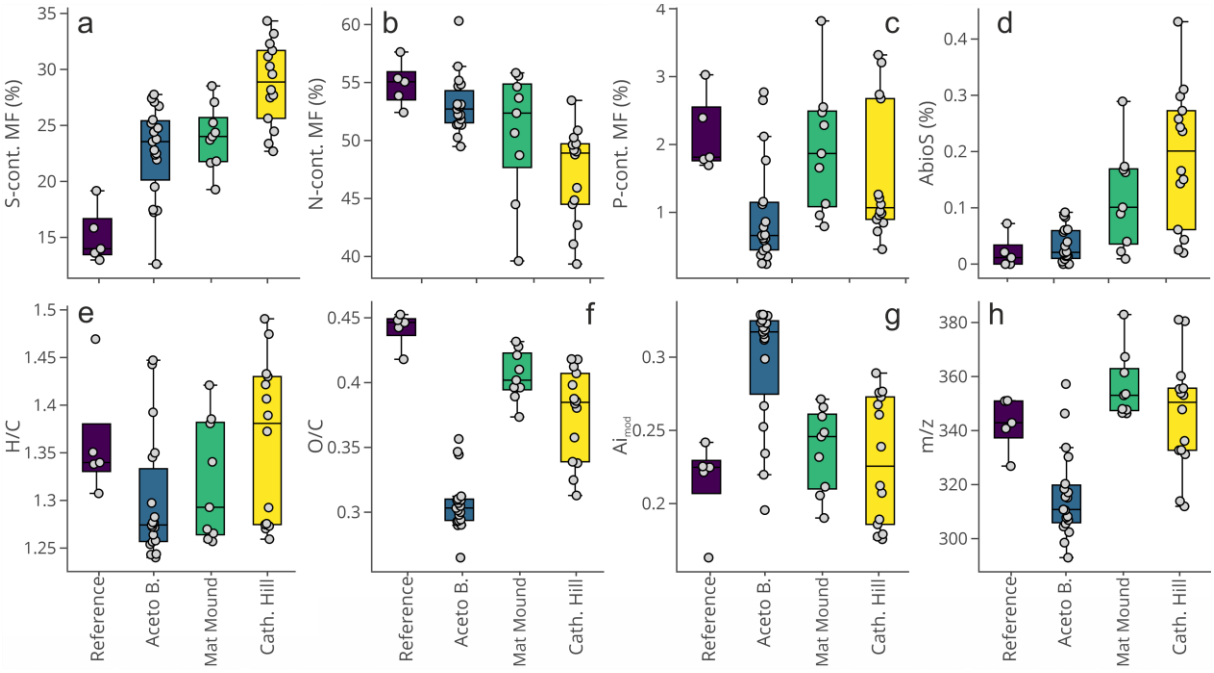

Figure III. 3: Boxplots grouped by core region showing the results of the molecular analysis of DOM_{SPE}. Plotted are the relative abundances of molecular formulae (MF) containing S (a), N (b), P (c), indicator for abiotic sulfurization (AbioS,% intensity) (d), intensity-weighted averages of H/C (e), O/C (f), modified aromaticity index (g) and molecular mass (m/z) (h). Boxplots display minimum, 25% quartile, median, 75% quartile, maximum, n = 47

DOM_{SPE} contained a large number of nitrogen and sulfur MF, on average 51.0 ± 4.6% for nitrogen and 23.9 ± 5.3% for sulfur (Figure 3). To study the relations between qualitative molecular parameters with environmental observations, a non-parametric rank-based test was applied, Kendalll´s τ. Intensity-weighted averages of nitrogen content were negatively correlated with temperature (τ = -0.49, $p < 0.001$) and sediment depth (τ = -0.57, $p < 0.001$) (Table 3; Supplementary Figure 4). Weighted averages of sulfur content and relative intensities of AbioS MF as an index for abiotic sulfurization of DOM were positively correlated with sediment temperature ($\tau = 0.38$, $p < 0.001$ and $\tau = 0.61$, $p < 0.001$). Both AbioS and weighted-average sulfur content were positively correlated (τ = 0.53, $p < 0.001$) with each other. Phosphorus was present in 1.45 ± 0.95% of MF and highly negatively correlated with sediment depth (τ = -0.65, $p < 0.001$). Intensity-weighted averages of molecular masses (*m/z*) were highly variable and in the range between 293 and 383 Da. Lowest molecular masses (mean 316 ± 16 Da), highest aromaticity (AI_{mod}) along with lowest H/C and O/C ratios were observed

at the Aceto Balsamico site. O/C ratios were lower ($p < 0.001$) at hydrothermal sites compared to the reference site ($p < 0.001$), while aromaticity was slightly higher ($p = 0.06$) but varying among individual samples of a location.

Both aromaticity and H/C were highly correlated with sediment depth ($\tau = 0.46$, $p < 0.001$, $\tau = 0.44$, $p < 0.001$ respectively). Among the assigned MF compound groups, saturated and highly unsaturated correlated with sediment temperature ($\tau = 0.33$, $p < 0.01$, $\tau = 0.55$, $p < 0.001$), while a negative correlation was observed for unsaturated aliphatic MF with nitrogen ($\tau = 0.48$, $p < 0.001$). The relative abundance of this group of MF was also highly correlated with sediment depth ($\tau = 0.54$, $p < 0.001$). It is important to note that the molecular parameters presented here are at best semi-quantitative and highly dependent on ionization efficiencies of DOM in ESI. Nonetheless, quantitative measurements of DOM fractions presented in Chapter VI generally agree with the molecular parameters.

Variety in DOM_{SPE} composition was explained to 62% by two axes in a PCoA (Figure 4). The shallow subsurface (0 – 4 cm) porewater DOM_{SPE} was relatively similar among all cores and correlated negatively on PC1 and positively on PC2. Samples from this group were enriched in N – and P-containing MF with higher H/C ratios and lower aromaticity, as well as a higher contribution of protein-like PARAFAC components C4, humic-like C5 and higher CDOM slope ratios. Reference core samples were quite similar to the surface interval samples, correlating primarily negatively with PC1. Here, the least hydrophobic DOM_{SPE} was observed as indicated by highest NSO:C ratios, as well as DOM with a low contribution of aromatics. Samples from site Aceto Balsamico were positively correlated with PC1 and most distant to all other samples. Here, particularly aromatic, reduced and hydrophobic DOM_{SPE} and aromatic CDOM were correlated with this group of samples. Samples from sites Mat Mound and Cathedral Hill were relatively similar to each other, both correlating negatively with PC2. These samples from relatively hot sites were characterized by a higher number and higher Shannon diversity of MF, an increased content of S-containing and highly unsaturated DOM_{SPE}. Hot samples further had higher contributions of petroleum-like PARAFAC components C1 and C3 and lower contents of humic-like C6, DOC and DOC_{SPE}.

Table III. 3: Kendall´s τ correlation coefficients between in situ temperature (n = 46), sediment depth, CDOM, FDOM and DOM_{SPE}molecular parameters. To ensure equal weights among cores, only porewater samples with a depth between 0 and 20 cm were considered (n = 34).

	τ temperature	τ depth (0-20 cm)
DOC	-0.39***	-0.33**
DOC_{SPE}	-0.49***	-0.2
TDN	0.1	0.1
$SUVA_{254}$	0.1	0.38**
SR	-0.1	-0.46***
C1 (%)	0.5***	0.23
C2 (%)	-0.03	0.37**
C3 (%)	0.55***	0.1
C4 (%)	-0.4***	-0.46***
C5 (%)	-0.26*	-0.39**
C6 (%)	-0.42***	0.06
C7 (%)	-0.12	-0.19
Assigned MF	0.28*	0.05
m/z (wa)	0.1	-0.04
O/C (wa)	-0.04	-0.08
H/C (wa)	-0.25*	-0.46***
N (wa)	-0.49***	-0.57***
S (wa)	0.38***	0.14
P (wa)	-0.3**	-0.65***
AI_{mod} (wa)	0.15	0.44***
NSO:C (wa)	-0.16	-0.28*
Diversity	0.34**	0.47***
AbioS	0.61***	0.31*
Saturated (% MF)	0.33**	0.09
Uns. Aliphatic (% MF)	0.04	0.24
Aliphatic with N (%MF)	-0.48***	-0.54***
H. Unsaturated (% MF)	0.55***	0.07
Aromatic (% MF)	0.05	0.18
Polycond. Arom. (% MF)	-0.11	0.13

*$p < 0.05$ = *; $p < 0.01$ = **; $p < 0.001$ = ****

wa = FT-ICR-MS intensity-weighted averages; MF = molecular formulae.

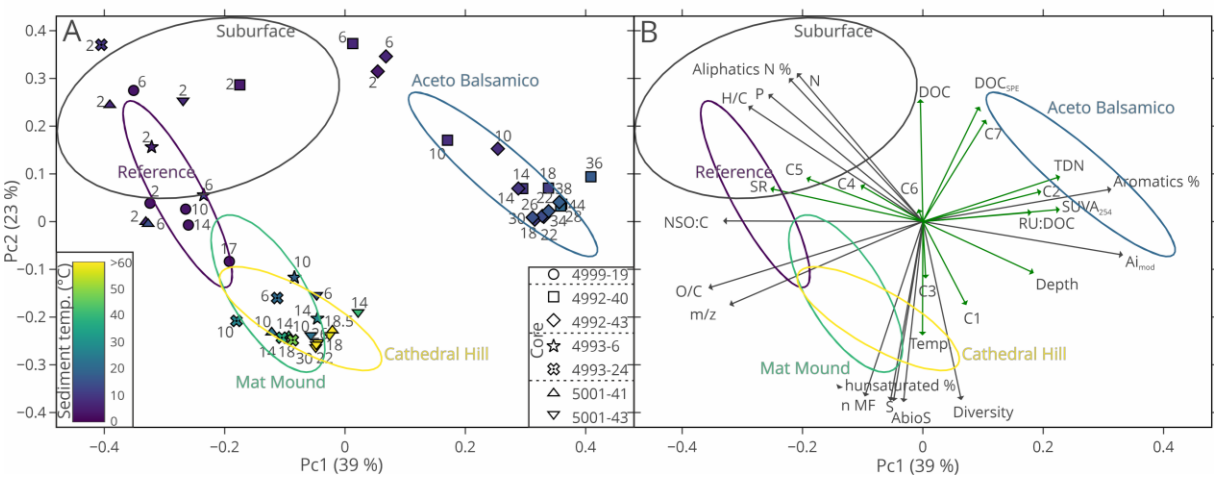

Figure III. 4: Principle coordinate analysis (PCoA) based on a Bray-Curtis dissimilarity matrix of all detected porewater DOM_{SPE} molecular formulae showing each sample color-coded by sediment temperature and annotated with sediment depth (A) and the same PCoA with hoc-fit of environmental, CDOM and FDOM parameters (green arrows) and DOM_{SPE} molecular parameters (black arrows), $p < 0.01$ (B). The ellipses correspond to samples from five different groups: Subsurface intervals (0-4 cm depth) from all cores and samples > 4 cm sediment depth from the four sites investigated (probability = 0.68). A third axis corresponded to 9.7% of sample variance and was not further considered. Temp = temperature, n MF = number of molecular formulae detected, AbioS = index for abiotic sulfurization of DOM, AI_{mod} = aromaticity index, SR = CDOM slope ratio.

III.3.2 Temperature dependency of DOM composition

To further investigate the influence of *in situ* sediment temperature on the porewater DOM composition, a linear model between log-transformed sediment temperature and DOM_{SPE} Bray-Curtis dissimilarity was calculated (Figure 5 B, plotted on a non-log-transformed axis). The hottest, presumably sterile sample (>106 °C) were compared to all other hydrothermal samples. Hot porewater DOM_{SPE} was relatively similar to DOM_{SPE} from all other samples above temperatures of approximately 40 - 60 °C. Dissimilarity increased most strongly between 3 and 25 °C, along with massively increasing concentrations of DOC_{SPE} (Figure 5 A). Notably, Bray-Curtis dissimilarity values of surface interval porewater samples to hot porewater DOM_{SPE} were between 0.54 (54%) and 0.78 (78%), or 22% to 46% similar. The same general observation was also made by calculating the Bray-Curtis dissimilarity on the relative abundances of the PARAFAC components of porewater FDOM (Figure 5 C).

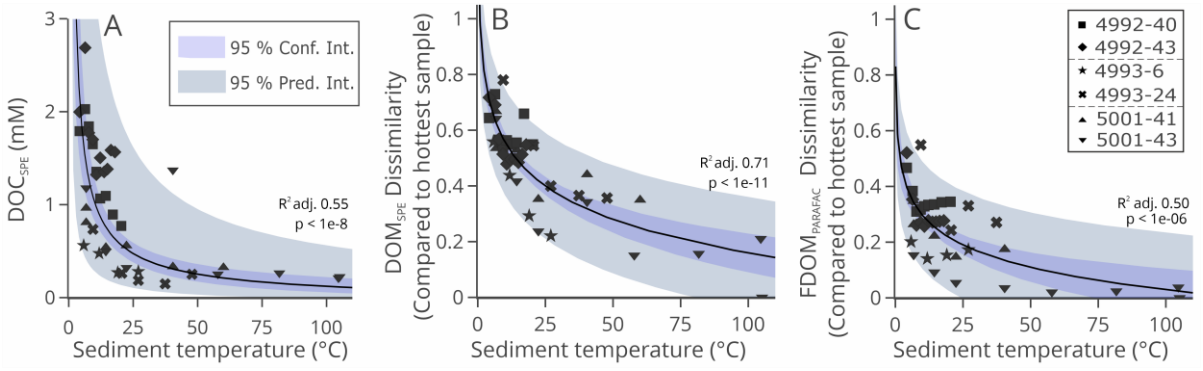

Figure III. 5: Linear models between the log-transformed in situ sediment temperature and log-transformed porewater DOC_{SPE} concentrations (n = 42) (A), Bray-Curtis dissimilarity based on DOM_{SPE} MF (n = 42) (B) and FDOM PARAFAC components (n = 40) (C) comparing the hottest sample with all other samples. Shown are adjusted R^2 and p-values as well as 95% confidence and prediction intervals (conf. int. and pred. int.) for all hydrothermal samples on non-log-transformed axes. The confidence interval estimates the range of plausible values for all observed relative contributions of a respective PARAFAC component, while the prediction interval estimates the range of plausible values for an individual observation, hence showing a higher range of uncertainties.

III.3.3 Comparison of hydrothermal porewater and bottom water DOM

In total, 14336 individual MF were assigned to peaks detected by FT-ICR-MS of DOM_{SPE} of porewater (n = 47, 13906 MF) and bottom water samples (n = 9, 8177 MF). The majority of MF were detected both in porewater and bottom water samples, only 430 MF (3%) were exclusively present in bottom water samples. Almost all MF detected in the reference core (n = 5, 8219 MF) were also found in the hydrothermal porewater samples with an exception of 199 MF (1%). Hydrothermal porewater DOM_{SPE} (n = 42) on the other hand contained 5687 unique MF (40%) that were not found in the reference core samples. To study which DOM MF are potentially discharged to the water column, we compared MF exclusively present in porewater samples (6109) and MF present in porewater & bottom water DOM (7747) (Figure 6 B & C, Table 4 Porewater). Porewater exclusive MF had significantly lower O/C and higher H/C ratios, contained more sulfur and were higher in unsaturated aliphatic and unsaturated aliphatic with nitrogen MF compared to MF that were present both in porewater and bottom water samples ($p < 0.001$). Shared MF had a high presence of highly unsaturated MF (63%) and higher NSO:C ratios ($p < 0.001$).

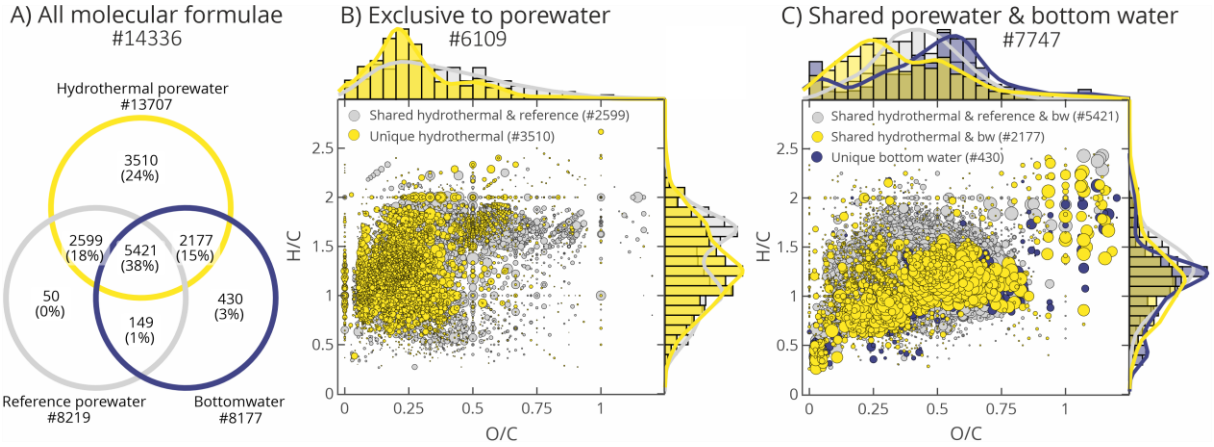

Figure III. 6: Venn diagram showing the overlap of all detected DOM_{SPE} molecular formulae in porewaters from one reference core (n = 5), six hydrothermal cores (n = 42) and bottom water samples (n = 9) above hydrothermally active sites (A), van Krevelen plot showing MF exclusively present in porewater samples but not in bottom water DOM (bw) (B) and van Krevelen plot showing MF present in both porewater and bottom water samples (C). The bubble size corresponds to the relative abundance of each MF in the respective group of samples. Van Krevelen plots further display densities and the relative abundance of MF after H/C (binsize = 0.1) and O/C (binsize = 0.05) ratios.

To distinguish between DOM present in non-hydrothermal porewater and porewater DOM associated with hydrothermal processes, MF exclusively present in hydrothermal porewater and bottom water samples, but not reference core porewater samples were further investigated: these hydrothermal DOM MF had relatively high average molecular masses (468 ± 146 Da) and a high contribution of S-containing MF (0.43 ± 0.59; 38% of MF), as well as aromatic and polycondensed aromatic MF (16.9 and 8.5%, respectively) and few unsaturated aliphatic MF, all significantly different ($p < 0.001$) to MF also present in reference core porewaters and bottom waters. Of these 2177 hydrothermal MF, 36% (791) were already present at temperatures > 100 °C showing similar distributions of H/C and O/C ratios ($p = 0.61$ and $p = 0.20$). 336 MF with high molecular mass (590 ± 109 Da) present exclusively in hydrothermal porewater and bottom water samples were also present in a North Equatorial Pacific Intermediate Water reference sample (Green *et al.*, 2014), which accounted for 10% of the MF assigned to this reference sample. These MF had a high oxygen content (O/C = 0.47 ± 0.19) and were mainly assigned to highly unsaturated DOM, although a contribution of 6% polycondensed aromatics was also present.

Table III. 4: Properties of MF found in DOM_{SPE} of porewater (n = 47) and bottom water (n = 9). Compared were molecular formulae (MF) found exclusively in porewater and not in any bottom water samples and MF found both in porewater and bottom water samples. Shown are mean values ± standard deviation and the relative abundance of MF within a compound group.

	Porewater exclusive			Shared Porewater & bottom water				
	all	shared hydrothermal & reference	Unique hydrothermal	all	shared hydrothermal & reference	Unique hydrothermal	Unique hydrothermal present at >100°C	Unique hydrothermal present in NEqPIW*
n MF	6109	2599	3510	7747	5421	2177	791	336
m/z	409 ± 148	382 ± 126	428 ± 160	421 ± 134	398 ± 122	468 ± 146	405 ± 139	590 ± 109
O/C	0.32 ± 0.21	0.39 ± 0.23	0.28 ± 0.19	0.41 ± 0.19	0.43 ± 0.17	0.37 ± 0.24	0.35 ± 0.22	0.47 ± 0.19
H/C	1.29 ± 0.41	1.3 ± 0.43	1.28 ± 0.39	1.24 ± 0.33	1.26 ± 0.3	1.18 ± 0.4	1.17 ± 0.37	1.21 ± 0.29
N	0.86 ± 1.08	1.05 ± 1.22	0.72 ± 0.94	0.9 ± 1.09	0.93 ± 1.1	0.78 ± 1.05	0.66 ± 0.92	0.54 ± 0.89
S	0.46 ± 0.62	0.34 ± 0.54	0.55 ± 0.65	0.24 ± 0.48	0.17 ± 0.4	0.43 ± 0.59	0.55 ± 0.65	0.12 ± 0.34
P	0.03 ± 0.18	0.04 ± 0.2	0.02 ± 0.16	0.03 ± 0.16	0.02 ± 0.13	0.05 ± 0.21	0.02 ± 0.13	0.05 ± 0.22
Ai_{mod}	0.29 ± 0.26	0.28 ± 0.29	0.3 ± 0.23	0.28 ± 0.22	0.26 ± 0.2	0.33 ± 0.23	0.33 ± 0.22	0.25 ± 0.18
NSO:C	0.41 ± 0.24	0.48 ± 0.27	0.35 ± 0.2	0.48 ± 0.21	0.49 ± 0.19	0.44 ± 0.26	0.42 ± 0.25	0.5 ± 0.21
Saturated (%)	1.2	0.6	1.7	0.7	0.3	1.6	1.4	0.6
Uns. Aliphatic (%)	19.2	19.0	19.3	11.1	12.7	7.8	8.2	2.1
Uns. Aliphatic N (%)	13.2	20.5	7.7	7.7	8.1	6.9	6.2	1.8
Highly Uns. (%)	44.0	35.1	50.6	63.0	65.3	56.5	58.2	83.3
Aromatic (%)	13.1	13.3	13	11.6	9.6	16.9	18.1	3.9
Polycond. Arom. (%)	8.4	10.4	7	5.1	3.6	8.5	7.0	6.0

*NEqPIW = North Equatorial Pacific Intermediate Water reference sample (Green *et al.*, 2014).

III.4 Discussion

III.4.1 *In situ* sediment temperatures as driving factor of DOM composition

Subsurface (0-4 cm) porewater DOM among all sampling locations consisted predominantly of unsaturated aliphatic, nitrogen-rich compounds similar to those found in laboratory heating experiments of Guaymas Basin sediments by Lin *et al.* (2017), indicating the transport and accumulation of heat-mobilized DOM by advective fluxes towards the sediment surface. However, such molecular signatures are also typical for microbially-released DOM, making a differentiation between heat-mobilized and microbial DOM difficult. The mixed contribution of

microbially released and heat-mobilized DOM is reflected by the PCoA clustering of all surficial porewaters (Figure 4), regardless of DOM origin from different sites and thermal regimes. Of the 8219 MF found in the reference core samples, where no contribution of heat-mobilized DOM was expected, 98% were also present in hydrothermal porewaters. This indicates that the microbial remineralization of the diatom-rich sedimentary organic matter (Calvert, 1966) is an important factor for the release of surficial, potentially bioavailable DOM at all sites independent of the prevalence of hydrothermal fluids and availability of hydrocarbons.

Below the shallow subsurface interval, DOM composition was notably influenced by location with a strong clustering of the two moderately hot Aceto Balsamico cores (6–21°C; 6-19 °C) and the four hot cores from Mat Mound (10-29°C; 19-48 °C) and Cathedral Hill (12-67 °C; 12-106 °C) (Figure 4). Despite of this, linear models of log-transformed sediment temperature as an explanatory variable also showed good correlations both for DOC_{SPE} concentrations and DOM_{SPE} composition among all hydrothermally influenced cores (Figure 5). It is possible that this DOM similarity is caused by circulating seawater containing the same marine DOM endmember in all porewater samples: in the Southern Guaymas Basin, local depressions likely enhance superficial shallow circulations at hydrothermal hotspots (Ondréas *et al.*, 2018). Experimental and field studies (Hawkes *et al.*, 2015a; Hawkes *et al.*, 2015b) have shown that most marine DOC_{SPE} and DOM MF are unstable at high temperatures and Hawkes *et al.* (2015a) inferred a removal of marine DOM above 68 °C. Although some newly formed MF at high temperatures were observed in Hawkes *et al.* (2015a), loss of DOC_{SPE} and number of DOM_{SPE} MF were generally lower at increasing temperatures. In our study, DOM_{SPE} Shannon diversity and detected number of MF were positively correlated with sediment temperature (Table 3), suggesting that the thermal cracking and mobilization of sedimentary organic matter has a far more important influence on porewater DOC_{SPE} quantity and DOM composition than possibly re-circulating marine DOM. We interpret the observed relationship between DOC_{SPE} concentrations and DOM_{SPE} composition among all hydrothermally influenced cores as the mixing of the two main source endmembers: (1) presumably sterile, hydrothermal DOM where thermally labile compounds have been abiotically removed via cracking of organic matter and (2) a combination of microbially released DOM and labile heat-mobilized DOM from deeper, hot sediments transported via advective porewater fluxing.

Microbial activity in Guaymas Basin sediments is commonly observed at *in situ* temperatures below ~60°C and a thermal limit of anaerobic oxidation of methane was observed at 75-80°C (McKay *et al.*, 2016) similar to the proposed thermal limit of subsurface microbial hydrocarbon oxidation (Head *et al.*, 2003). Microbial remineralization of organic carbon was proposed to be restricted to temperatures below 100°C at Guaymas Basin but sedimentary

cell densities of microorganisms usually drop in number very quickly below ca. 5 cm depth (McKay *et al.*, 2016; Teske *et al.*, 2009). The increased DOC_{SPE} concentrations and DOM_{SPE} dissimilarity below temperatures of ~60°C (Figure 5) can therefore be explained by increasing microbial transformation and consequently released microbial DOM from degradation of sedimentary organic matter. Notably, although samples from site Aceto Balsamico were quite distant to all other samples in the PCoA (Figure 3), they fit well into the relationship between temperature and DOM_{SPE} dissimilarity. DOM_{SPE}, CDOM and FDOM at this site consisted of reduced, aromatic, hydrophobic and relatively low intensity-weighted average of DOM_{SPE} molecular masses, indicating the molecular signal of petroleum DOM (Brünjes *et al.*, 2022; Seidel *et al.*, 2016). These results are consistent with reports of highest concentrations of petroleum hydrocarbons in moderately hot sediments and porewaters of Guaymas Basin (Mara *et al.*, 2022), and with the preference of sulfate-reducing, hydrocarbon-degrading deltaproteobacterial lineages in temperate and moderately hot sediments (Ramírez *et al.*, 2021). The higher abundance of petroleum DOM along with microbial humic-like PARAFAC component C2 primarily present in Aceto Balsamico samples, near-millimolar concentrations of acetate (Teske *et al.*, 2016) and distinct microbial communities (Ramírez *et al.*, 2021) would call for an additional source of DOM outside of the above assumed simple two-endmember mixing model. A sulfur-depleted subsurface fluid source different to other fluid sources at Guaymas Basin was proposed previously to explain the low concentrations or absence of sulfate and sulfide in sediment cores of Aceto Balsamico (Teske *et al.*, 2016). In support of such an assumption, DOM_{SPE} at Aceto Balsamico was low in sulfur-containing compounds compared to other sites (Figure 3; Supplementary Figure 4).

Despite highly variable sedimentary temperature gradients, DOC concentrations and DOM composition at the individual sites (Figure 1, Figure 3), overall DOM variance in Guaymas Basin porewaters among all studied locations can best be explained by changes in *in situ* sediment temperature: both FDOM (C1, C3, C4, C6) and DOM_{SPE} (S, AbioS, highly unsaturated MF and unsaturated aliphatic with N MF) correlated significantly ($p < 0.001$; Table 3) with temperature. Porewater DOM at high sediment temperatures consisted of mainly highly unsaturated MF and petroleum-like PARAFAC components C1 and C3 that were previously described as recalcitrant (Table 2). Noticeable is the high contribution of sulfur-containing MF in DOM_{SPE}, correlated to sediment temperature (Figure 3 a, Table 2). A high contribution of DOS compounds in porewater DOM_{SPE} of sulfidic sediments (Pohlabeln *et al.*, 2017; Schmidt *et al.*, 2009; Seidel *et al.*, 2014) and shallow hydrothermal systems (Gomez-Saez *et al.*, 2016) has been demonstrated before. Sulfur-containing petroleum hydrocarbons such as polycyclic aromatic sulfur heterocycles (PASH) are abundantly present in hydrothermal petroleum

impregnating Guaymas Basin sediments and dissolved in porewaters (Mara *et al.*, 2022; Simoneit, 1985, 1988). Moreover, sulfur-containing DOM was also enriched in laboratory incubation experiments of petroleum as part of the DOM pool (Brünjes *et al.*, 2022; Hegazi *et al.*, 2012), suggesting hydrothermal petroleum-derived DOM as a source of DOS. While a contribution of petroleum-sourced sulfur compounds is certainly the case, the strong correlation between weighted-averages of sulfur and the index for abiotic sulfurization of DOM, AbioS ($\tau = 0.53$, $p < 0.001$), suggest sulfurization as the primary process behind the high DOS contribution in sulfidic porewater samples. Abiotic sulfurization can occur in sediments, where sulfide reacts with organic matter including DOM, resulting in sulfur-enriched compounds presumably resistant to microbial degradation (Kohnen *et al.*, 1989; Pohlabeln *et al.*, 2017). Sulfide is abundant in sediments of Guaymas Basin (McKay *et al.*, 2012; Teske *et al.*, 2016) and often reaches a concentration plateau a few centimeters below the sediment surface (McKay *et al.*, 2012; Teske *et al.*, 2016). A positive correlation of intensity-weighted sulfur MF in DOM_{SPE} with sediment temperature among all samples and not sediment depth (Table 3) suggests that high *in situ* temperatures catalyze the sulfurization of DOM, similar to what has been described in laboratory experiments (Kok *et al.*, 2000; Pohlabeln *et al.*, 2017). In fact, the AbioS index reached up to 0.43% of total signal intensity in hot sediment porewaters, approximately 10 times of sulfidic porewater from cold sediments in the Black Sea (Gomez-Saez *et al.*, 2021) and 5 to 10 times of cold deep Fennoscandian Shield fracture waters (Osterholz *et al.*, 2022). We conclude that the increase in microbial activity along the temperature gradients and sulfurization reactions driven by the high sediment temperatures are likely the main factors for changes in porewater DOM composition.

III.4.2 Hydrothermal porewater DOM as potential source for oceanic DOM

Porewater DOM is generally considered a source of DOM to bottom waters, transported via diffusive fluxes along concentration gradients of DOC between sediment and water column (Burdige and Komada, 2015). At Guaymas Basin, advective fluxes accelerate this process, documented by elevated concentrations of DOC in bottom waters that were highly variable (903 ± 471 μM; Supplementary Table 1). These values are consistent with previously published literature values on bottom water DOC concentrations in the Guaymas Basin Southern rift zone (Lin *et al.*, 2017; Ziervogel and Arnosti, 2020). The majority of DOC in bottom waters, however, was not extractable by SPE (See Supplementary discussion about extraction efficiencies). DOC_{SPE} concentrations were on average 77 ± 44 μM, elevated compared to other deep-sea environments (ca. 24 μM DOC_{SPE}, assuming 60% extraction efficiency of 40 μM deep-sea

DOC (Hansell, 2013)). Non-extractable DOC at hydrothermal sites has previously been linked to the production of low molecular-weight organic acids and amino acids due to missing hydrophobic groups (Hawkes *et al.*, 2015b). Implicitly, the production of abundant organic acids in porewater (Martens, 1990; Teske *et al.*, 2016; Zhuang *et al.*, 2019) and the heat mobilization of amino acids from sedimentary organic matter (Lin *et al.*, 2017), appear to exceed benthic microbial consumption.

In our study, the subfractions of porewater FDOM and DOM_{SPE} did not show this predominance of labile compounds. Molecular Bray-Curtis dissimilarity increases from hot porewaters towards the cold sediment subsurface (Figure 5 b) while the number of detected MF and species diversity are decreasing (Table 3). These findings and a general similarity of subsurface interval hydrothermal porewater FDOM and DOM_{SPE} with non-hydrothermal reference samples (Figure 4) suggests that hydrothermal DOM is removed before reaching the sediment-water interface. Nonetheless, DOM_{SPE} at subsurface intervals was between 22 and 46% similar (Bray-Curtis) to hot (> 106° C) DOM_{SPE}, indicating the presence of a non-labile fraction on the timescale of upward fluxing of ca. 50 cm yr^{-1} (Teske *et al.*, 2016). The presence of a subfraction of hot DOM_{SPE} in subsurface porewater is in accordance with our results from the PARAFAC analysis (Figure 5 c, Supplementary Figure 4): although a higher proportion of PARAFAC components associated with microbial activity (C4, C6) was present at the subsurface interval, hydrothermal and oil-associated compounds C1 and C3 were still present contributing together between 20 to 60 percent of the total fluorescence signal.

To assess the contribution of hydrothermal DOM to bottom water DOM, we compared the presence of DOM_{SPE} MF in hydrothermal porewater samples with MF found in bottom water of Guaymas Basin (Figure 6, Table 4). Only 3% of all detected MF were exclusive to bottom waters, indicating a vast exchange of porewater with bottom waters. Considering the presence of advective fluxes, this is an expected result that has also been observed previously in diffuse porewater fluxes in arctic sediments (Rossel *et al.*, 2020). We note however, bottom waters in Rossel *et al.* (2020) were defined as water on top of a sediment core and not taken by Niskin bottles. A large number of 6109 (43%) MF on the other hand was exclusively found in porewaters and not in any of the bottom water samples (Figure 6 b, Table 4). By also comparing MF present in the reference core, MF exclusively present in hydrothermal DOM were distinguished from the molecular DOM signal in porewater that is obtained from degradation of sedimentary organic matter. MF absent in bottom water but present both at hydrothermal sites and the reference site had a high contribution of unsaturated aliphatics and nitrogen-containing aliphatics (combined 40% of MF) suggesting relatively labile DOM, and hence microbial degradation as the primary cause for their removal (D'Andrilli *et al.*, 2015;

Seidel *et al.*, 2014). Exclusively hydrothermal MF in porewaters on the other hand had distinct similarities in a van Krevelen space with undegraded petroleum DOM, for instance low O/C ratios (Brünjes *et al.*, 2022; Kleindienst *et al.*, 2015; Seidel *et al.*, 2016). Compared with non-hydrothermal porewater exclusive MF, these presumably petroleum-related MF had higher molecular masses and lower NSO:C ratios (Table 4), a measure for the polarity of dissolved petroleum MF (Liu and Kujawinski, 2015). Condensation of dissolved petroleum hydrocarbons on sediment particles or particles in the water column is commonly observed in Guaymas Basin (Kawka and Simoneit, 1994; Ondréas *et al.*, 2018). A more hydrophobic character of porewater hydrothermal MF not found in bottom water samples suggest the precipitation of petroleum-derived DOM at the sediment-water interface as a potential additional removal process besides microbial DOM degradation.

Of the 7598 MF shared between bottom waters and porewaters, 2177 were not present in any of the reference core samples and thus interpretated as hydrothermal DOM (Figure 6 c, Table 4). These 2177 hydrothermal MF had low H/C ratios and were relatively aromatic compared to MF associated with non-hydrothermal porewater (MF shared between hydrothermal and reference samples). In this subset of 2177 hydrothermal MF, only few MF assigned to presumably labile compound groups were found. Instead, highly unsaturated, aromatic and polycondensed aromatic MF were abundant, indicating more recalcitrant and possibly petroleum-derived DOM (Brünjes *et al.*, 2022). Furthermore, hydrothermal MF detected in bottom waters had a high contribution of S-containing compounds, corroborating findings in Mara *et al.* (2022) of a potential rapid migration of lightweight PASH compounds out of the sediment. These results support the hypothesis of natural petroleum seepage as a source of non-labile DOS to deep sea environments (Brünjes *et al.*, 2022).

A potential recalcitrance of unique hydrothermal MF in bottom waters is illustrated by 791 shared MF already present at >100 °C sediment temperature (Table 4), indicating both thermal stability and non-lability to microbial degradation on the timescale of porewater fluid upflow (approximately 50 cm yr^{-1} (Teske *et al.*, 2016)). Moreover, 336 of hydrothermal MF in bottom waters were also present in North Equatorial Pacific Intermediate Water, a representative for deep refractory oceanic DOM that is stable for Millenia (Green *et al.*, 2014; Hansell, 2013). This accounts for ~10% of the MF detected in the North Equatorial Pacific Intermediate Water reference sample, suggesting that hydrothermal sediments can release DOM with similar MF found in refractory deep-oceanic DOM. Hydrothermal sediments may introduce refractory DOM directly into deep-sea environments. The structural complexity and diversity of isomers of natural DOM generally increases with ongoing degradation (Zark and Dittmar, 2018). Hydrothermal petroleum generated by sedimentary organic matter in Guaymas

Basin sediments has radiocarbon ages of approximately 5000 years (Peter, 1991), similar to the age of deep-sea DOM in the Pacific Ocean (Druffel *et al.*, 2021). Thus, we expect a high structural diversity in hydrothermal porewater DOM, similar to that of deep-sea DOM and petroleum. The extend of overlap of similar structural isomers between hydrothermal porewater DOM and refractory deep-sea DOM, however, remains unknown.

Briefly, while the majority of DOC mobilized by hydrothermal heating of sediments appears to be bioavailable, an underlying fraction of non-labile, potentially refractory DOM and DOS is released to deep-sea ocean waters at the same time. Hydrothermal petroleum generation in deep-ocean spreading centers is not limited to the Guaymas Basin and has been observed in the Pescadero Basin in the Gulf of California (Paduan *et al.*, 2018), Escanaba Trough in the northeast Pacific Ocean (Kvenvolden and Simoneit, 1990), Middle Valley at the northern Juan de Fuca Ridge (Simoneit, 1994) and Rainbow Field at the Mid-Atlantic Ridge (Simoneit *et al.*, 2004). Assessing the contribution of hydrothermal petroleum DOM to deep sea element cycling should therefore be subject of future studies.

III.5 Conclusion

In this study we combined optical and molecular DOM analyses of hydrothermal porewaters. We observed significant relationships between *in situ* sediment temperature and both composition and quantity of DOM, driven by the onset of microbial carbon degradation at lower temperatures closer to the sediment surface and an increasing contribution of sulfur-containing DOM suggesting abiotic sulfurization of DOM at high sediment temperatures. Aside from previously predicted bioavailable and nitrogen-rich DOM mobilized by hydrothermal heating, an underlying fraction of highly unsaturated and particularly sulfur-rich DOM_{SPE} and petroleum-associated FDOM components was detected. Thermally stable and non-labile compounds of hydrothermal origin were present in bottom water DOM, where they contribute to pools of recalcitrant DOM and DOS. This study emphasizes the need to incorporate natural seepage into oceanic carbon and nutrient pools. A future study will focus in detail on the quantification of recalcitrant DOM and organic sulfur, nitrogen and phosphorus to assess the importance of hydrothermal sediments to deep sea element cycles.

III.6 Acknowledgement

We thank the Crew of AT42-05 and Thorsten Brinkhoff for sampling. Ina Ulber, Matthias Friebe, Melina Knoke, Christoper Klaembt and Palash Kumawat are acknowledged for help with laboratory work and analysis, Kai-Uwe Hinrichs and Thorsten Dittmar for helpful discussions and providing laboratory access. We acknowledge funding by the German Science Foundation (DFG) within the Cluster of Excellence EXC 2077 "The Ocean Floor – Earth's Uncharted Interface" (project number 390741603). Sampling in Guaymas Basin was supported by NSF Biological Oceanography (grant 1357238).

III.7 Supplementary Information

III.7.1 Supplementary Discussion

III.7.1.1 Solid phase extraction of hydrothermal and petroleum-derived DOM

In this study, molecular analysis of DOM was performed on DOM isolated by SPE using PPL resin (Dittmar *et al.*, 2008). SPE was performed after the porewater was extracted from the sediments to minimize the loss of volatile petroleum DOM and potential alteration of DOM by oxygen. Because of this, DOC concentrations could not be determined ahead of SPE extraction to evenly load cartridges with similar amounts of DOC, resulting analogue to the highly variable DOC concentrations in varying carbon-loads of 1.60 ± 1.37 mg C g^{-1} sorbent, of which 0.28 ± 0.22 mg C g^{-1} sorbent were adsorbed. For marine DOC, maximum sorption capacities of PPL were not reached at DOC load of 6 mg C g^{-1} in Dittmar *et al.* (2008) and maximum sorption capacities were recently reported as high as 137 mg C g^{-1} sorbent (11.4 mmol C) (Volikov *et al.*, 2022). All samples in our study were well below these carbon loads, hence overloading of cartridges is an unlikely explanation for the overall observed efficiencies. Carbon-based extraction efficiencies (on average 21 ± 14%) were low compared to marine DOM_{SPE}, where efficiencies of ca. 60% are commonly observed (Dittmar and Stubbins, 2014). Porewater DOM extraction efficiencies in sulfidic porewater (Seidel *et al.*, 2014) and anoxic basins (Pohlabeln *et al.*, 2017) were reported at 60 – 70%. No extraction efficiencies on heat-mobilized DOM of Guaymas Basin sediments were reported in Lin *et al.* (2017), but extraction efficiencies below 10% were previously observed in petroleum-related DOM (Brünjes *et al.*, 2022), hydrothermal DOM (Hansen *et al.*, 2022; Hawkes *et al.*, 2015b; Rossel *et al.*, 2015) and experimental hydrothermal heating of marine DOM_{SPE} (Hawkes *et al.*, 2015a).

One possible explanation for the observed low extraction yields would be irreversible adsorption of DOM onto the PPL resin, i.e. not truly dissolved hydrophobic petroleum

compounds (Wagner *et al.*, 2017) that may pass through the 0.3 μM filters, adsorb onto the PPL resin but will not be eluted in methanol. To investigate this possibility, SPE cartridges were eluted again with dichloromethane, which is sufficiently apolar to dissolve most petroleum compounds. This procedure yielded 14.7 ± 7.6% (n = 35) additional DOC_{SPE}, far more than what has been reported for marine DOM additionally eluted with acetone (Dittmar *et al.*, 2008) (Supplementary Table 3). This DCM-eluted DOM_{SPE} added on average 609 ± 438 (~13%) unique additional MF per sample and was more reduced, aromatic and hydrophobic than methanol-eluded DOM_{SPE} (Supplementary Table 4). This easy additional elution step during extraction could therefore provide a straightforward procedure to extend the analytical window of DOM_{SPE} and further characterize hydrophobic DOM fractions. However, overall extraction efficiencies were only increased marginally by this DCM elution (from 20.6 ± 10.8% to 23.3 ± 11.9% for 35 tested porewater samples).

A more likely cause for the high amount of non-extractable DOC are the abundant low molecular weight organic acids in hydrothermal DOM, which are not well retained by SPE (Hawkes *et al.*, 2015a; Hawkes *et al.*, 2015b; Rossel *et al.*, 2015). Volatile organic acids such as acetate are ubiquitously present in Guaymas Basin porewaters at near millimolar concentrations (Martens, 1990; Teske *et al.*, 2016), but rarely exceed a contribution of 10% of DOC (Zhuang *et al.*, 2019). Even by accounting for organic acids within DOC, a large fraction of DOM at Guaymas Basin remains uncharacterized on the molecular level. On the other hand, results presented from the FDOM fraction showing similar trends as DOM_{SPE} (Figure 5 b,c) were retrieved from bulk porewaters and are therefore independent of the extraction.

To assess whether DOM was lost or fractionized at such low extraction efficiencies by SPE, we analyzed EEMs of re-dissolved SPE extracts and compared them with EEMs from bulk porewater. A PARAFAC model calculated on a combined dataset of bulk porewater and re-dissolved SPE resulted in an identical (TCC > 0.95) model as bulk porewater only. DOM extraction generally preserves fluorescence spectral shapes (Murphy *et al.*, 2018), but contribution of different fluorescence fractions can vary (Wünsch *et al.*, 2018). Relative loadings of individual PARAFAC components of both datasets were well correlated close to a 1:1 line and within a 95 percent prediction interval in a linear model, with an exception of protein-like C4 (Supplementary Figure 2; Supplementary Table 2). Loadings of PARAFAC components in this spectral region of protein-like fluorescence were reportedly lower in extracts than bulk FDOM (Wünsch *et al.*, 2018) and SPE extraction results in slightly lower nitrogen content than bulk waters (Dittmar *et al.*, 2008). Murphy *et al.* (2018) observed the general preservation of fluorescence spectral shapes after SPE for sample sets from a wide range of marine and terrestrial environments. Our study expands this observation onto

hydrothermal and petroleum DOM, independent of carbon-based extraction efficiencies. In conclusion, since no major qualitative changes of FDOM after extraction even at extraction efficiencies < 10% were observed, and large amounts of non-extractable DOC_{SPE} of petroleum and hydrothermal environments were reported previously, we are confident that the results of molecular analysis presented in this study are not an artifact and that organic matter of the same analytical window as DOM_{SPE} from other environments with extraction efficiencies > 60% is being compared.

III.7.2 Supplementary Tables

Supplementary Table III. 1: Sample locating of bottom water samples taken by Alvins Niskin bottles, elevation above sediment and DOC, TDN and DOC_{SPE} concentrations.

Dive	Sampling Area	Latitude	Longitude	Distance above sediment (cm)	DOC (μM)	DOC_{SPE} (μM)	TDN (μM)
4992	Aceto Balsamico	27.0684	111.24283	300	1612	146	50
4992	Aceto Balsamico	27.0684	111.24283	300	664	137	42
4992	Aceto Balsamico	27.0684	111.24283	10	514	50	122
4992	Aceto Balsamico	27.0684	111.24283	10	1438	41	119
4993	Mat Mound	27.0074	111.24091	10-15	641	122	47
4995	Rebecca´s Roost	27.0067	111.2442	100	882	42	40
4995	Rebecca´s Roost	27.0067	111.2442	100	750	51	44
4995	Rebecca´s Roost	27.0067	111.2442	100	237	47	41
4995	Rebecca´s Roost	27.0067	111.2442	100	1393	57	42

Supplementary Table III. 2: Factor similarities of PARAFAC components comparing the three PARAFAC models calculated in this study. The degree of similarity is expressed as Tuckers congruence coefficient (TCC), factors with TTC values of ≥ 0.95 are considered similar. Highlighted are factors below 0.95. PW = Porewater, SPE = re-dissolved SPE extracts.

	Combined PW & SPE vs. PW only TCC Ex/Em	Combined PW & SPE vs. SPE only TCC Ex/Em	PW only vs. SPE only TCC Ex/Em
C1	1.0/1.0	1.0/1.0	1.0/0.98
C2	1.0/1.0	1.0/1.0	1.0/1.0
C3	0.98/1.0	1.0/0.97	0.95/0.97
C4	1.0/1.0	**0.94**/0.99	**0.93**/0.99
C5	1.0/1.0	0.99/0.98	0.99/0.96
C6	1.0/1.0	0.99/0.98	0.98/0.96
C7	0.99/1.0	0.97/1.0	0.98/1.0

Supplementary Table III. 3: Concentrations of DOC, DOC_{SPE} and DOC eluted in addition to methanol (MeOH) with dichloromethane (DCM) and calculated extraction efficiencies.

Core	Depth (cm)	DOC (μM)	DOC load SPE PPL cartridge (mg C g^{-1})	DOC_{SPE} (μM)	$DOC_{SPE-DCM}$ (μM)	Extraction efficiency (%)	Additional DCM carbon yield (%)	Overall extraction efficiency (MeOH+DCM) (%)
4992-40	6	10495	3.64	2028	89.7	19.3	4.4	20.2
4992-40	14	4570	1.48	1650	62.7	36.1	3.8	37.5
4992-40	28	3024	2.33	1094	53.2	36.2	4.9	37.9
4992-40	44	3114	2.75	771	48.7	24.8	6.3	26.3
4993-6	2	3434	1.91	561	77.4	16.3	13.8	18.6
4993-6	6	3126	1.41	476	38.4	15.2	8.1	16.4
4993-6	10	2146	0.7	269	51.3	12.6	19	14.9
4993-6	14	4690	1.48	281	85.4	6	30.4	7.8
4993-24	2	5465	3.2	735	79.6	13.4	10.8	14.9
4993-24	6	3954	0.91	262	63.9	6.6	24.4	8.2
4993-24	10	2530	0.81	185	44.8	7.3	24.2	9.1
4993-24	14	1105	0.46	148	31.7	13.4	21.4	16.3
4993-24	18	1328	0.26	251	72.2	18.9	28.7	24.4
4999-19	2	2723	1.41	529	29.1	19.4	5.5	20.5
4999-19	6	9972	3.99	1646	125	16.5	7.6	17.8
4999-19	10	5962	1.87	1101	97.5	18.5	8.9	20.1
4999-19	14	4517	1.45	805	98.1	17.8	12.2	20
4999-19	17	4144	0.43	1173	214.1	28.3	18.3	33.5
4992-43	2	24615	8.16	1997	175.5	8.1	8.8	8.8
4992-43	6	14861	3.94	2688	143.1	18.1	5.3	19.1
4992-43	10	6205	1.54	1773	178.7	28.6	10.1	31.4
4992-43	14	5124	1.19	1700	183.1	33.2	10.8	36.8
4992-43	18	4036	0.73	1323	229.8	32.8	17.4	38.5
4992-43	22	4504	0.75	1504	247.3	33.4	16.4	38.9
4992-43	26	4000	0.82	1352	252.8	33.8	18.7	40.1
4992-43	30	4334	0.78	1383	240.6	31.9	17.4	37.5
4992-43	34	4727	1.01	1586	196.1	33.6	12.4	37.7
4992-43	38	3483	0.82	1566	177.3	45	11.3	50
5001-43	2	6373	3.18	1179	167.4	18.5	14.2	21.1
5001-43	6	2623	0.99	498	129.8	19	26.1	23.9
5001-43	10	1905	0.93	322	65.4	16.9	20.3	20.3
5001-43	14	5203	1.05	1371	86.4	26.4	6.3	28
5001-43	18	4087	1.75	252	58.5	6.2	23.2	7.6
5001-43	22	4057	1.84	264	56.6	6.5	21.4	7.9
5001-43	26	7451	3.48	211	47.3	2.8	22.5	3.5
Mean ± sd	-	5254 ± 4308	1.8 ± 1.5	998 ± 668	114.2 ± 69.8	20.6 ± 10.8	14.7 ± 7.6	23.3 ± 11.9

Supplementary Table III. 4: The average number of molecular formulae and intensity-weighted molecular parameters ± standard deviation (n = 35) for DOM_{SPE} eluted with methanol and with methanol (MeOH) followed by dichloromethane (DCM). Shown are averages for the 35 tested porewater samples described in Supplementary Table 3.

	SPE-MeOH	SPE-DCM	SPE-DCM only	SPE-MeOH only
n MF	4794 ± 1445	1690 ± 979	609 ± 438	3713 ± 1505
m/z	332 ± 22	321 ± 29	373 ± 37	351 ± 23
O/C	0.36 ± 0.05	0.25 ± 0.05	0.25 ± 0.05	0.4 ± 0.04
H/C	1.31 ± 0.07	1.31 ± 0.13	1.28 ± 0.1	1.31 ± 0.04
N	0.95 ± 0.37	0.91 ± 0.56	0.66 ± 0.25	0.85 ± 0.26
S	0.19 ± 0.10	0.18 ± 0.06	0.38 ± 0.09	0.24 ± 0.11
P	0.01 ± 0.01	0.02 ± 0.02	0.04 ± 0.03	0.01 ± 0.01
Ai_{mod}	0.26 ± 0.05	0.31 ± 0.09	0.33 ± 0.06	0.25 ± 0.02
NSO:C	0.44 ± 0.07	0.32 ± 0.08	0.31 ± 0.05	0.47 ± 0.05
DBE	7.3 ± 0.4	7.7 ± 0.9	8.9 ± 1.3	7.4 ± 0.5

III.7.3 Supplementary Figures

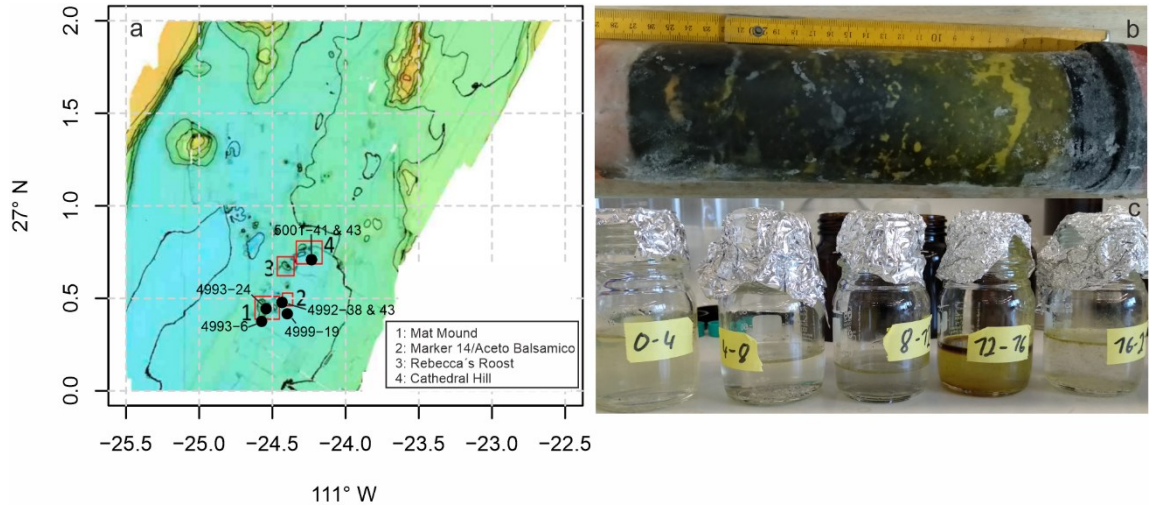

Supplementary Figure III. 1: Bathymetric map showing the vent areas sampled during cruise AT 42-05 (a). Picture of frozen oil-soaked sediment core 5001-41 (b) and petroleum-containing porewaters extracted by centrifugation from this core before filtration.

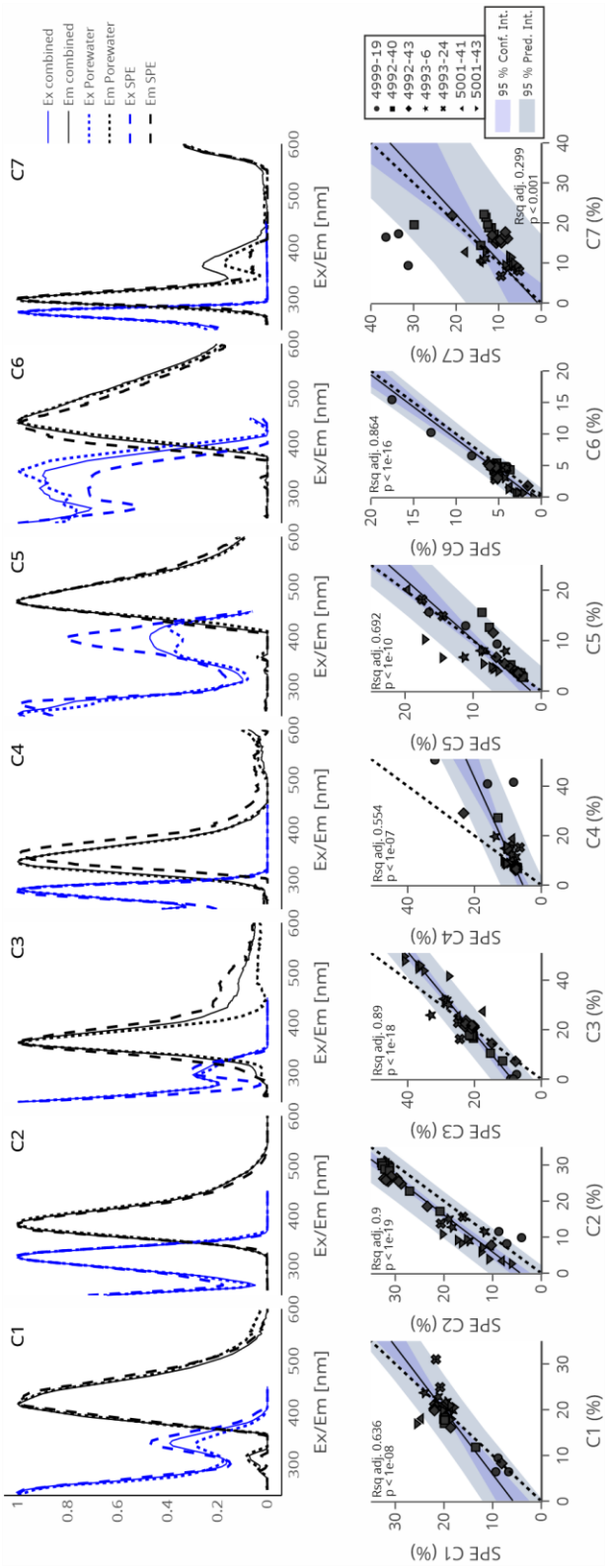

Supplementary Figure III. 2: Excitation and Emission maxima of loadings of all seven PARAFAC components calculated in the three different models. SPE = re-dissolved SPE extracts, combined = combined dataset of porewater and re-dissolved extracts (A). Linear correlations of relative loadings of PARAFAC components of bulk porewater on the x-axis and re-dissolved extracts on the y-axis.

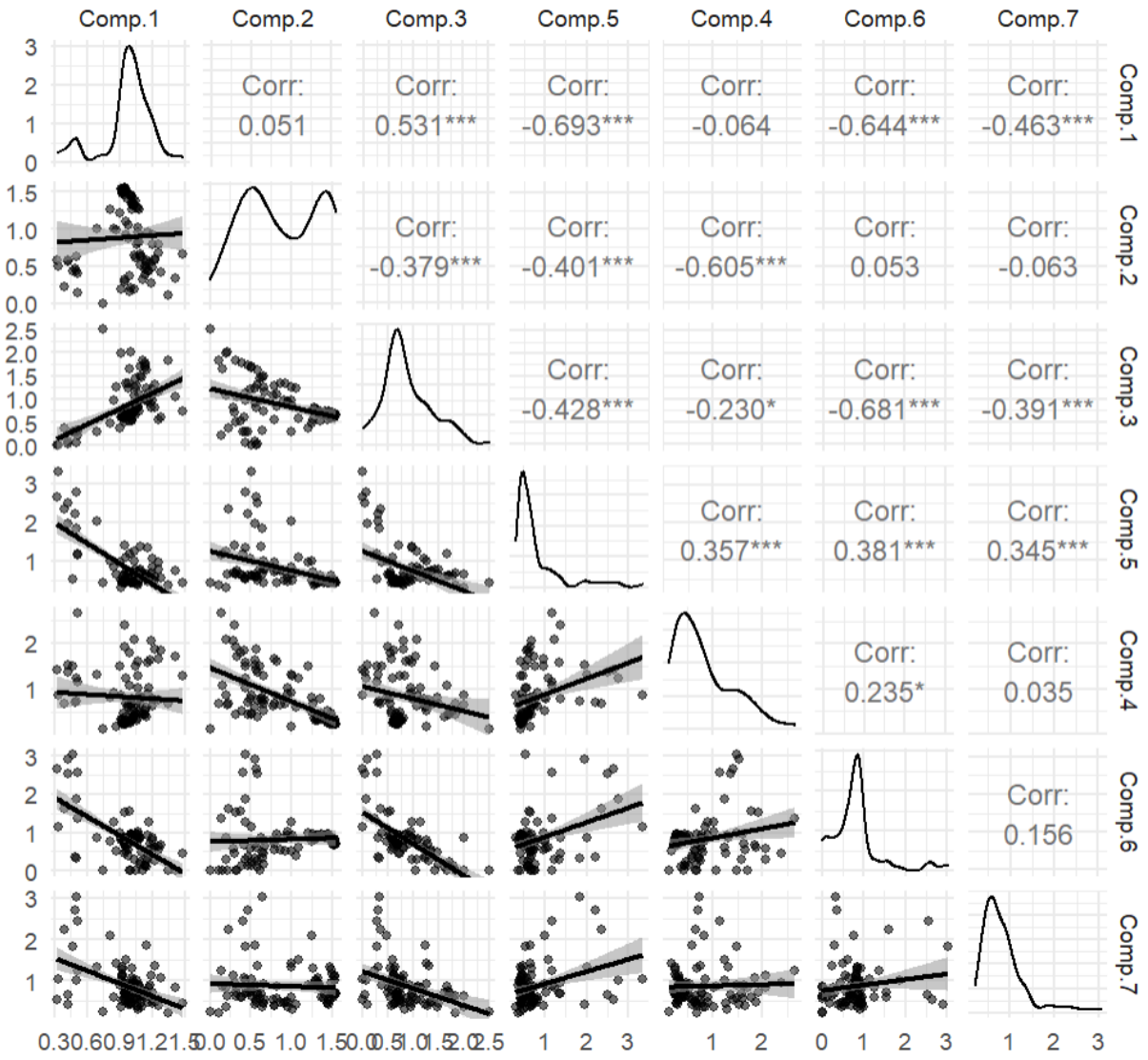

Supplementary Figure III. 3: Correlation of all seven PARAFAC components of the bulk porewater model. Perfect correlations would violate the assumption of variability of the PARAFAC algorithm (Murphy et al., 2013).

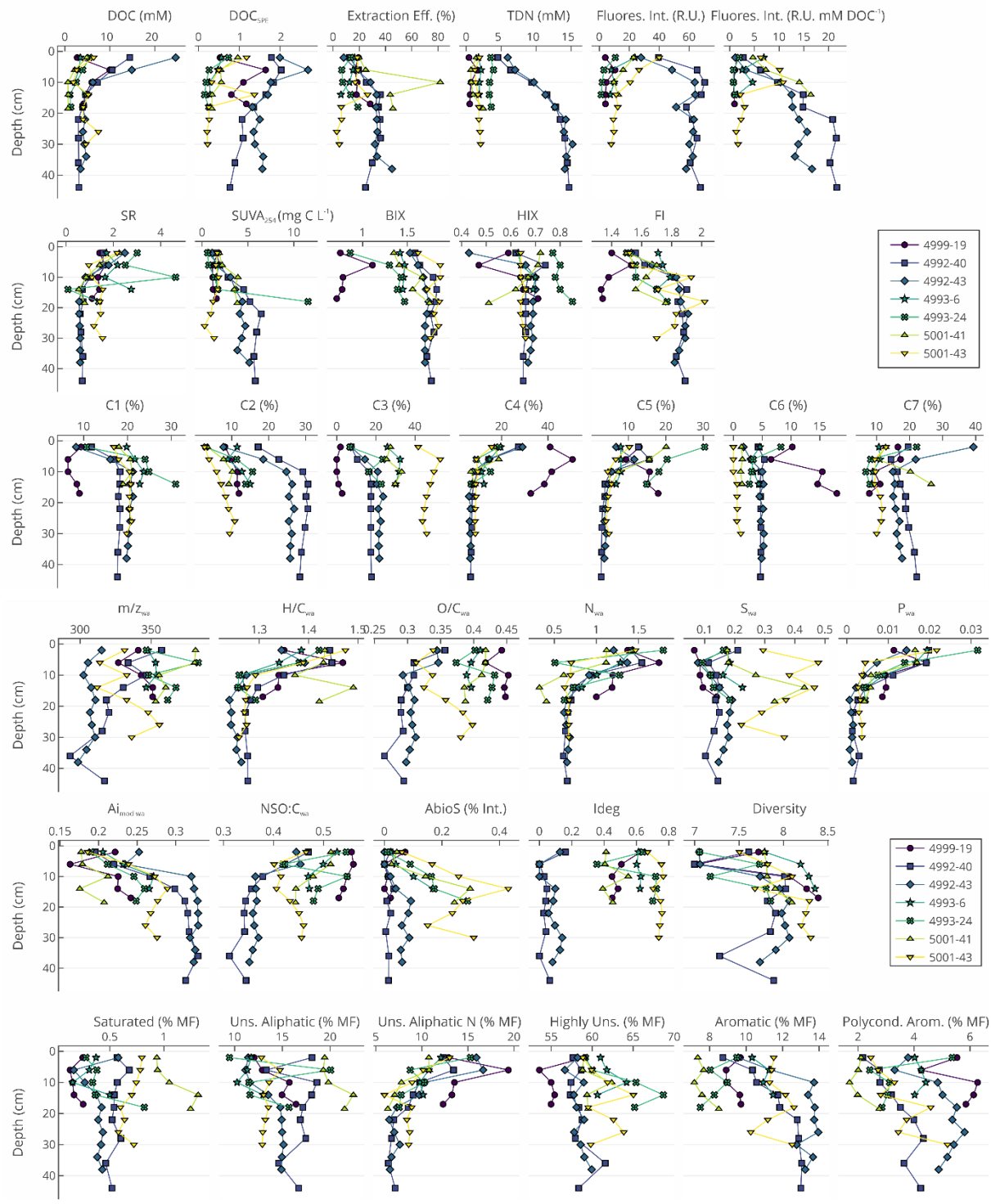

Supplementary Figure III. 4: Depth profiles of bulk porewater parameters, CDOM and FDOM, relative contribution of PARAFAC components, intensity-weighted averages of DOM$_{SPE}$ molecular parameters and relative assignment to compound groups.

IV. Manuscript 3

Hydrothermal sediments are a potential source of recalcitrant dissolved black carbon and dissolved organic sulfur in the Guaymas Basin

Jonas Brünjes[†],Michael Seidel[‡], Andreas Teske[#], Kai-Uwe Hinrichs[†] and Florence Schubotz[†]

[†]MARUM Center for Marine Environmental Sciences, University of Bremen, Bremen, 28359, Germany

[‡]Institute for Chemistry and Biology of the Marine Environment (ICBM), Carl von Ossietzky University of Oldenburg, 26129, Oldenburg, Germany

[#] University of North Carolina at Chapel Hill, Chapel Hill, USA

In preparation for *Geophysical Research Letters*

Abstract

The Guaymas Basin (GB) in the Gulf of California is a young rift system where hot basaltic sill intrusions into unconsolidated organic-rich sediments generate large amounts of complex petroleum compounds and hydrothermal circulation releases dissolved organic matter (DOM) into the overlying water column. Polycondensed aromatic compounds such as dissolved black carbon (DBC) in marine DOM are thought to be mainly derived from incomplete combustion of terrestrial organic matter on land. DBC accumulates in the oceanic carbon reservoir over thousands of years and is thus considered to be recalcitrant. Recent research suggested additional marine DBC sources, for instance, petrogenic carbon. We investigated whether hydrothermally heated sediments with *in situ* temperatures ranging from 4 to >106 °C release DOM that can contribute to the recalcitrant oceanic DOM pool. By analyzing both porewater and the hot-water extractable fraction of the same sediments, our study provides a comprehensive quantitative approach in assessing the elemental fluxes of DOM from these hydrothermal systems. Our results show highly elevated porewater concentrations of DBC and potentially recalcitrant dissolved organic sulfur, suggesting the release of both DOM fractions in hydrothermal sediments. DBC in porewaters and hot-water extracts originated from two distinct sources: hydrothermal petroleum and re-dissolved presumably terrestrial-derived, pre-aged DBC. However, concentrations of DBC were not elevated in bottom waters, likely caused by a dilution or precipitation of hydrothermal petroleum-derived DBC in colder bottom waters. We further assessed quantities of DBC and dissolved organic nitrogen, sulfur and phosphorus that could be discharged into the water column in case of basin-wide hydrothermal heating. Our results indicate that hydrothermal alteration of sediments can be sources of recalcitrant dissolved organic sulfur and DBC to deep sea environments. Hydrothermal alteration of sediments could be an explanation for observed old DBC in deep ocean waters.

IV.1 Introduction

In the Guaymas Basin in the Gulf of California, hydrothermal petroleum permeates sediments in 2000 m water depth. Magmatic sill intrusions hydrothermally heat up to 540 m of overlying organic-rich sediments, generating a wide range of particularly sulfur-rich and aromatic petroleum hydrocarbons via thermal maturation of sedimentary organic matter (Didyk and Simoneit, 1990; Mara *et al.*, 2022; Simoneit, 1985, 1988; Teske *et al.*, 2020). Hydrothermal petroleum compounds such as polycondensed aromatic hydrocarbons (PAH) and polycondensed aromatic heterocycles (PASH) are not only present in the oil phase adsorbed to sediment particles but also dissolved in porewaters (Didyk and Simoneit, 1989; Mara *et al.*, 2022; Simoneit, 1985). Elevated *in situ* sediment temperatures, hydrothermal fluids up to 315 °C, high partial pressure at 2000 m water depth and abundant dissolved gases enhance the solubility of hydrocarbons in Guaymas Basin sediment porewaters (Didyk and Simoneit, 1990; Liu and Kujawinski, 2015; Price, 1976; Simoneit, 1985; Von Damm *et al.*, 1985).

Hydrothermally mobilized water-soluble hydrocarbons may join the pool of oceanic dissolved organic matter (DOM), which contains 662 Pg of dissolved organic carbon (DOC) (Hansell *et al.*, 2009). A fraction of the deep-oceanic DOM consists of about 12 Pg ultra-refractory DOC with a radiocarbon age of more than 20,000 years (Coppola and Druffel, 2016; Dittmar and Paeng, 2009). This fraction contains dissolved black carbon (DBC) which has proposed core structures of fused rings with carboxylic functional groups, comparable to compounds detected in petroleum asphaltenes (Dittmar and Paeng, 2009; Ruiz-Morales and Mullins, 2007). In this study, we want to investigate whether hydrothermal petroleum can be a source of oceanic DBC.

The sulfidic, hydrothermal sediments of Guaymas Basin contain porewater with highly variable and elevated DOC concentrations between 0.7 mM and more than 100 mM (Mara *et al.*, 2022; Ramírez *et al.*, 2021); Chapter III. The major fraction of hydrothermal porewater DOM is assumed to consist of labile compounds with high contributions of low molecular-weight organic acids and labile nitrogen-containing compounds (Lin *et al.*, 2017; Martens, 1990; Zhuang *et al.*, 2019); Chapter III. Marine porewater often contains elevated DOC concentrations compared to the overlying bottom water and diffusive transport is considered a source of microbially-processed porewater DOM to the adjacent water column (Burdige and Komada, 2015). Porewater diffusion and outwelling can, for example, contribute dissolved organic nitrogen (DON) (Abdulla *et al.*, 2018; Zhou *et al.*, 2022), dissolved organic phosphorus (DOP) (Worsfold *et al.*, 2008) and potentially recalcitrant dissolved organic sulfur (DOS) to the water column (Abdulla *et al.*, 2019; Pohlabeln *et al.*, 2017; Seidel *et al.*, 2014). In Guaymas

Basin sediments and hydrothermal systems in general, porewater can additionally be transported via advective porewater fluxes that lead to highly elevated and locally varying DOC concentrations in the bottom water, which are three to 50 times higher than deep ocean concentrations (Lin *et al.*, 2017); Chapter III. Based on hot-water extractions of Guaymas Basin sediments, Lin *et al.* (2017) reported that hydrothermal heating can release large amounts of primarily bio-available DOM compounds to the bottom water. Yet we observed potentially recalcitrant DOM compounds in porewaters and bottom waters such as sulfur-enriched and polycondensed aromatic molecular formulae, possibly representing petroleum-derived DBC (Chapter III).

While DBC is assumed to be mainly produced by the incomplete combustion of terrestrial organic matter on land, recent studies have pointed out mismatches between carbon isotopic composition and radiocarbon ages of known terrestrial DBC sources and marine DBC, suggesting additional non-pyrogenic, including petroleum and petrogenic DBC sources (Coppola and Druffel, 2016; Coppola *et al.*, 2022; Wagner *et al.*, 2018; Wagner *et al.*, 2019). Particulate terrestrial black carbon that is several thousands of radiocarbon years older than marine organic matter found in abyssal deep-sea sediments (Coppola *et al.*, 2014; Masiello and Druffel, 1998; Middelburg *et al.*, 1999). It was previously hypothesized that resuspension of these sediments may be a source of pre-aged, re-dissolved DBC to the deep ocean (Wagner *et al.*, 2018). However, this would re-introduce DBC with a terrestrial carbon isotopic signature, but deep-sea DBC contains a marine isotopic signature (Wagner *et al.*, 2019). Both hydrothermal vents and petroleum seepages were proposed to be sources of marine DBC (Brünjes *et al.*, 2022; Dittmar and Koch, 2006; Dittmar and Paeng, 2009). However, laboratory experiments and environmental hydrothermal vent samples could not confirm them as a DBC source but rather suggested hydrothermal cycling as an efficient sink for recalcitrant marine DOM via thermal degradation at temperatures exceeding 200°C (Hawkes *et al.*, 2015a; Hawkes *et al.*, 2015b). Laboratory incubation experiments in our previous study revealed natural petroleum seepages as potential DBC sources (Brünjes *et al.*, 2022). Although enhanced DBC concentrations were observed in groundwater after an oil spill on land (Podgorski *et al.*, 2020), petroleum as a DBC source in marine environmental samples has not yet been confirmed. In our previous study (Brünjes *et al.*, 2022), we also suggested that petroleum seepages are potential sources of potentially recalcitrant DOS. DOS is a petagram inventory of oceanic DOM, mainly originated from phytoplankton-derived biomolecules in the surface ocean (Ksionzek *et al.*, 2016). Approximately 8% of marine DOS is not generated by phytoplankton but hypothesized to originate from abiotically sulfurized DOM in sulfidic sediments (Phillips *et al.*, 2022; Pohlabeln *et al.*, 2017). Building on our previous results from

molecular DOM analysis of samples from the Guaymas Basin (Chapter III) we want to test, if hydrothermal, sulfidic, petroleum-impregnated sediments contribute DOS to natural deep-sea environments.

In this study, we quantify different DOM fractions in hydrothermal porewaters and overlying bottom waters: ultra-refractory DBC and recalcitrant DOS as well as potentially bio-available DON and DOP. To assess the potential release of these DOM fractions into natural environments, we simulate hydrothermal hot-water mobilization of sedimentary organic matter using hot-water Soxhlet extractions of the same sediments used to gain porewater samples. Using this comprehensive approach, we want to evaluate the importance and contribution of hydrothermal alteration of sediments on deep-sea DOM pools. We hypothesize that hydrothermal heating of subsurface Guaymas Basin sediments mobilizes recalcitrant DBC and DOS as well as potentially bio-available DOP and DON to deep-sea environments.

IV.2 Materials and Methods

IV.2.1 Sample origin

Seven push cores between 16 and 48 cm length were retrieved by HOV *Alvin* during ship expedition *RV* Atlantis 42-05 in November 2018. In addition, nine bottom water samples were using *Alvin's* Niskin bottles. Previously explored sampling areas were targeted in the southern Guaymas Basin in water depths of about 2000 m. Porewater was extracted from previously frozen sediments by centrifugation in a 4-cm resolution described in detail in Chapter III. Detailed sample locations and a bathymetric map are available therein.

IV.2.2 Sediment analysis

Approximately 0.5 g of freeze-dried sediment was decalcified using HCl, weighted in tin capsules and analyzed with continuous-flow elemental analyzer–isotope ratio mass spectrometer for the content and isotopic compositions of total organic carbon (TOC) and total nitrogen (TN). We used a ThermoFinnigan Flash EA 2000 connected to a Delta V Plus isotope ratio mass spectrometer (IRMS). Each sample was measured twice and the mean of those two measurements is reported here as $\delta^{13}C$ (VPDB) and $\delta^{15}N$. The internal precision was ± 0.1 ‰ for $\delta^{13}C$ and $\delta^{15}N$.

IV.2.3 Soxhlet extraction

Soxhlet extractions were carried out following Schmidt *et al.* (2014). An aliquot of 20 - 30g of dry-centrifuged (30 min at 4000 rpm) sediment was transferred into combusted glass fiber thimbles (30 x 100 mm, Whatman). 200 mL of ultrapure water (18 Ω) and boiling chips (PTFE, Roth) were added to the round-bottom flask. Soxhlet extraction units were combusted and units were extracted with ultrapure water for 24h to remove potential contaminants before each extraction cycle. The system was flushed with nitrogen gas and closed with a gas balloon. Sediments were extracted for 48h in the dark at temperatures of approximately 80 °C (Schmidt *et al.*, 2014). This approach did not simulate *in situ* conditions where both sediment temperatures (3 to 106°C) and fluid migration times (approximately 50 cm yr^{-1} (Teske *et al.*, 2016)) differ from this setup. Instead, Soxhlet extractions provide a hypothetical approximation of the maximum amount of hot-water soluble organic matter that could be mobilized by hot-water discharge events. After extraction, the water extracts were cooled to room temperature, filtered through 0.3 μm pre-combusted filters (GF/F) within a filter holder (polypropylene, Advantec) using 50 mL polypropylene syringes. All glassware used was combusted (450 °C, 5h) and non-combustible material was pre-cleaned by overnight-soaking in acidified (HCl p.a., pH 2) ultrapure water and subsequent thorough rinsing with ultrapure water. The percentage of water-extractable organic carbon (DOC_{we}, weight-percent) was calculated based on the amount of organic carbon provided with the sediments in the thimbles and the quantity of DOC in 200 mL of water used for the extraction.

IV.2.4 DOM Quantification

DOM was extracted on the same day after porewater centrifugation and Soxhlet extraction from acidified (pH 2, HCl, Suprapur) and filtered samples by solid phase extraction (SPE) using 1 g PPL sorbent cartridges (Agilent Bond Elut) and eluted with 6 mL of methanol (HPLC-grade) after desalination with ultrapure water (pH 2, HCl, Suprapur) following previously published protocols (Dittmar *et al.*, 2008). To further investigate hydrophobic DOM, residual methanol in the extracted PPL cartridges was dried overnight under the fume hood. These cartridges were eluted with 5 mL of dichloromethane (DCM, GC-grade). DCM was then evaporated from the extracts under nitrogen gas and dried extracts were re-dissolved in methanol. All extracts were stored in amber glass vials in the dark at -20° C.

DOC and total dissolved nitrogen (TDN) concentrations of acidified (pH 2, HCl, Suprapur) and filtered water samples were determined by high temperature catalytic oxidation on a Shimadzu TOC-VCPH instrument. DOC and dissolved organic nitrogen (DON) concentrations in SPE extracts (DOC_{SPE}, DON_{SPE}) concentrations were determined by

evaporating an aliquot of the methanolic extracts at 40°C overnight and re-dissolving them in ultrapure water (pH 2) using an ultrasonic bath for 15 minutes at 30 °C. Accuracy and trueness of the DOC and TDN analyses were tested in each run against deep Atlantic seawater reference material provided by the consensus reference materials program (D.A. Hansell, University of Miami, Coral Gables, FL, USA), standard deviations of repetitive measurements were ± 4.3% (DOC) ± 2.1% DON. Extraction efficiencies were calculated by determining the concentrations of DOC_{SPE} relative to DOC. Extraction efficiencies of Soxhlet extracts were on average 27 ± 8% (n = 32), and they were higher than the respective porewater samples (23 ± 14%, n = 47, Chapter III) and previously reported values of 19 ± 7% in Schmidt *et al.* (2014).

Organic sulfur and organic phosphorus concentrations of DOM_{SPE} (DOS_{SPE} and DOP_{SPE}) were determined using an inductively coupled plasma mass spectrometer (ICP-MS, Neptune Plus, ThermoScientific). DOM_{SPE} extract aliquots were evaporated under a nitrogen stream and re-dissolved in 2% nitric acid (Suprapur). Detection limits were 0.025 mg L^{-1} (DOP) and 0.05 mg L^{-1} (DOS), standard deviations of repetitive measurements were ± 2.9% (DOP) and ± 5.2% (DOS).

DBC concentrations were determined by oxidizing a dried aliquot of SPE extract with concentrated nitric acid (Suprapur) to benzenepolycarboxylic acid (BPCA) and subsequent separation and quantification by liquid chromatography and diode-array detection (Waters Acquity UPLC) following Dittmar (2008). BPCAs were identified according to retention time and absorbance spectra (220–380 nm). Individual BPCA concentrations were then converted to the sum of DBC concentration using benzenepenta- and benzenehexacarboxylic acids (B5CA and B6CA), according to Stubbins *et al.* (2015). Standard deviations of repetitive measurements were ± 4.8% (B5CA) and ± 0.9% (B6CA).

IV.2.5 DOM molecular analysis

Ultrahigh-resolution mass spectrometry was performed on a solariX XR FT-ICR-MS (Bruker Daltonik GmbH, Bremen, Germany) connected to a 15 Tesla superconducting magnet (Bruker Biospin, Wissembourg, France), as reported previously in Chapter III. In short, DOM_{SPE} extracts diluted to a DOC concentration of 2.5 ppm in 50:50 (v/v) methanol/ultrapure water were directly infused by hand injection into the electrospray source (ESI, Apollo II ion source, Bruker Daltonik GmbH, Bremen, Germany) at a scanning range of 92-2000 Da. 200 scans were accumulated for each mass spectrum at a mass error of < 0.1 ppm. Molecular formulae were assigned in the mass range of 100 – 1000 Da at a tolerance of 0.5 ppm using the server-based tool ICBM-OCEAN (Merder *et al.*, 2020). A method detection limit (MDL) of 2.7 and tolerance of 0.3 ppm was chosen to eliminate instrumental noise based on Riedel and Dittmar

(2014). Recalibration was applied with an elemental composition of $C_{1-50}H_{2-80}O_{2-15}N_0$. The range of the chemically possible molecular formulae of the elements were set to $C_{1-50}H_{2-175}O_{0-50}N_{0-4}S_{0-2}P_{0-1}$. The N, S, P rule and the isotope verification were applied to exclude unlikely formulae. The homologous series network was applied for CH_2, CO_2, H_2O, and O.

We calculated the aromaticity index (AI_{mod}) (Koch and Dittmar, 2006, 2016) for each molecular formula, as well as the ratio of NSO to C (NSO:C) as an indicator for hydrophobicity of petroleum-derived DOM (Liu and Kujawinski, 2015). Molecular formulae were assigned to the compound group of polycyclic aromatics if AI_{mod} >0.66), including condensed DBC if C ≥ 15. This DOM group was further divided into polycyclic aromatics containing sulfur (dissolved black sulfur, DBS) (AI_{mod} > 0.66 & C ≥ 15 & S > 0, (Hertkorn *et al.*, 2016)) and containing nitrogen (dissolved black nitrogen, DBN) (AI_{mod} > 0.66 & C ≥ 15 N > 0) (Wagner *et al.*, 2015).

IV.3 Results and Discussion

IV.3.1 DBC and DBS highly elevated in hydrothermal porewater

In this study, we analyzed the DOM composition from the southern hydrothermal spreading center in the Guaymas Basin in about 2000 m water depth of bottom waters and porewaters in seven sediment cores from four locations of varying hydrothermal heat flows (Table 1). DBC was quantified using B5CA and B6CA chemical markers which indicate the presence of polycondensed aromatics with at least 5fused rings, presumed to be of thermogenic origin (Kappenberg *et al.*, 2016; Ziolkowski *et al.*, 2011). Detailed descriptions of DOC and sedimentary heat flow profiles were presented previously (Chapter III). Bottom water samples had on average DBC concentrations of 0.57 ± 0.12 μM (Table 1, Supplementary Table 2) which is within the range of published DBC concentrations in deep pacific waters (~0.25-0.6 μM) (Wagner *et al.*, 2019; Yamashita *et al.*, 2022; Ziolkowski and Druffel, 2010) . Porewater DBC concentrations in sediment cores with high temperature gradients from sites Mat Mound (both between 10 and 48 °C) and Cathedral Hill (both between 12 and 106 °C) were between 2.4 – 16.7 μM (Figure 1). Compared to these hot cores, highly elevated DBC concentrations were observed in moderately warm cores from site Aceto Balsamico (6 to 21°C), with concentrations between 9.5 and 71.7 μM DBC, increasing with sediment depth. Noticeable is the concentration of DBC in the reference core, showing values between 5.3 and 13.7 μM, slightly elevated compared to the hot sites. The presence of particulate BC in deep sea sediments has been shown before (Coppola *et al.*, 2014; Masiello and Druffel, 1998; Middelburg *et al.*, 1999), but studies on porewater DBC are still scarce. Seidel *et al.* (2014) reported porewater DBC

concentrations of 8.8 to 305 μM in a sulfidic tidal creek in the North Sea Wadden Sea with terrestrial and anthropogenic DBC sources. DBC contents are usually being compared by the ratio of DBC:DOC (%), which was between 0.13 and 0.23% at the reference site, 0.06 and 0.51% at the hot sites, and again elevated between 0.06 and 1.62% at the Aceto Balsamico site (Figure 5, Supplementary Figure1). Typically, 2% DBC:DOC are observed in deep oceanic waters (Dittmar and Paeng, 2009) and porewater DBC:DOC ratios in the sulfidic tidal creek sediments in Seidel *et al.* (2014) were as high as 6.6 – 13.6%. However, a direct comparison is difficult, because Guaymas Basin porewater DOC contains a large fraction of labile DOC that is not present in deep waters or rivers. Nevertheless, porewater DBC concentrations were elevated by a factor of ~5 and up to 120 compared to Guaymas Basin bottom waters and typical deep sea DBC concentrations.

Table IV. 1: Geochemical parameters determined in Guaymas Basin porewater and bottom waters above hydrothermally active sites. Concentrations of DOC and DOCSPE were previously reported in Chapter III.

	Bottom water	Reference site	Aceto Balsamico		Mat Mound		Cathedral Hill	
Sample ID		4999-19	4992-40	4992-43	4993-6	4993-24	5001-41	5001-43
Depth (cm)		0-19	0-48	0-40	0-16	0-20	0-21	0-32
Thermal range (°C)	3	3	6-21	6-19	10-29	19-48	12-67	12-105
n	9	5	9	10	4	5	6	8
DOC (mM)	0.9 ± 0.5	5.5 ± 2.8	5.9 ± 4.1	7.6 ± 6.8	3.3 ± 1.0	2.9 ± 1.8	2.2 ± 1.8	4.5 ± 1.8
DOC_{SPE} (mM)	0.08 ± 0.04	1.1 ± 0.4	1.4 ± 0.5	1.7 ± 0.4	0.4 ± 0.1	0.3 ± 0.2	0.6 ± 0.3	0.5 ± 0.5
DON_{SPE} (μM)	4.7 ± 4.9	124 ± 59	58 ± 67	142 ± 76	44 ± 21	34 ± 40	n.d.	38 ± 46
DOS_{SPE} (μM)	n.d§.	11.6 ± 6.0	10.5 ± 4.5	27 ± 7.8	10.5 ± 1.4	n.d.	8.6 ± 3.7	14.4 ± 10.4
DOP_{SPE} (μM)	n.d.	1.6 ± 1.0	1.1 ± 0.7	1.5 ± 1.5	0.4 ± 0.3	n.d.	1.1 ± 1.0	0.3 ± 0.4
DBC (μM)	0.57* ± 0.12	10.4 ± 3.8	18.3 ± 3.9	49.3 ± 14.3	6.7 ± 4.0	9.3 ± 7.2	3.3 ± 0.3	5.3 ± 2.3
DBC:DOC (%)	0.09 ± 0.05	0.19 ± 0.04	0.45 ± 0.24	1.00 ± 0.49	0.20 ± 0.13	0.29 ± 0.21	0.27 ± 0.19	0.14 ± 0.09
$DBC:DOC_{SPE}$ (%)	1.0 ± 0.5	1.1 ± 0.2	1.5 ± 0.7	3.1 ± 1.1	1.7 ± 0.7	3.8 ± 3.7	0.7 ± 0.3	1.3 ± 0.5
B6CA/ B5CA	0.28 ± 0.03	0.62 ± 0.08	0.21 ± 0.02	0.23 ± 0.01	0.35 ± 0.09	0.24 ± 0.04	0.35 ± 0.08	0.28 ± 0.01

§ n.d. = not determined

*Deep pacific water published DBC concentrations: (~0.25-0.5 μM in Yamashita *et al.* (2022), ~0.6 μM in Wagner *et al.* (2019), 0.33 μM (ultra-filtrated DBC) in Ziolkowski and Druffel (2010))

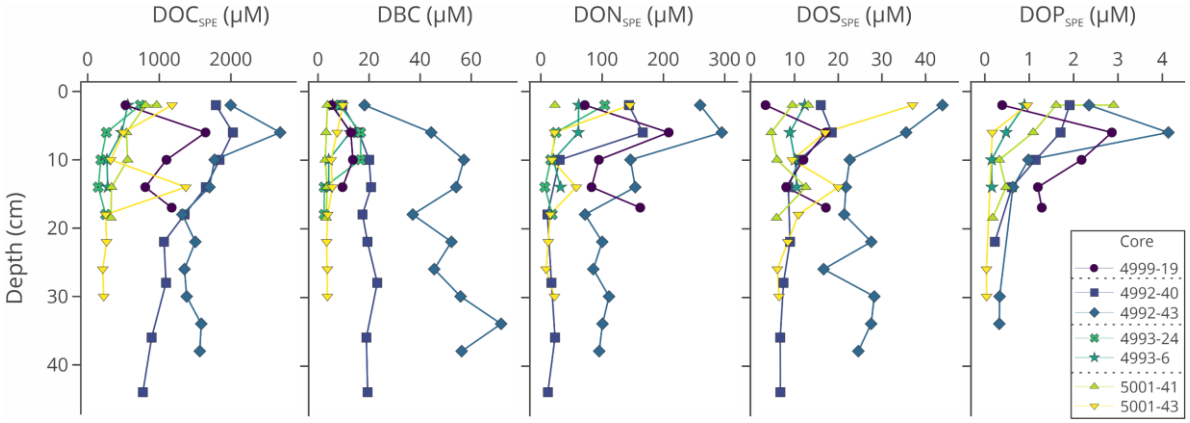

Figure IV. 1: Porewater concentrations of DOC$_{SPE}$, DBC, DON$_{SPE}$, DOS$_{SPE}$ and DOP$_{SPE}$ vs. sediment depth. Porewater was sampled in 4-cm intervals. DOC$_{SPE}$ profiles were previously reported in Chapter III and shown again here as a reference. Core 4999-19 (purple) represents the reference core without signs of hydrothermal alteration.

Porewater concentrations of DON$_{SPE}$, DOS$_{SPE}$ and DOP$_{SPE}$ were determined (Figure 1, Table 1). Porewater DON$_{SPE}$ concentrations varied between 7-295 µM, showing higher concentrations towards the sediment subsurface and generally decreasing concentrations with sediment depth and *in situ* temperature. A decrease of DON concentrations with depth is unusual for anoxic porewaters (Abdulla *et al.*, 2018; Burdige and Komada, 2015) but expected given the prevalence of advective porewater fluxes in Guaymas Basin and similar to observed profiles of DOC (Chapter III). In general, DON can be both considered bioavailable containing compound groups such as peptides and amino acids and recalcitrant as deaminated peptides that accumulate in anoxic sediment porewaters (Abdulla *et al.*, 2018). Total organic nitrogen concentrations in Guaymas Basin porewaters were recently reported and reached >8000 µM in hydrothermal porewater at the Aceto Balsamico and Cathedral Hill sites (Mara *et al.*, 2022; Ramírez *et al.*, 2021). At the same time, total DON concentrations in porewater from the reference site were much lower, between 180 and 240 µM N (Mara *et al.*, 2022). DON$_{SPE}$ in porewater samples in our study on the other hand were in the same range comparing reference and hydrothermal sites, suggesting that the highly elevated total DON concentrations (without SPE) in hydrothermal porewaters reported by Mara *et al.* (2022) and (Ramírez *et al.*, 2021) are predominantly composed of compounds that are not retained by the PPL during SPE. Hydrothermal alteration of sedimentary organic matter produces free amino acids (Lin *et al.*, 2017) which contain nitrogen and are not well retained by the PPL resin (Hawkes *et al.*, 2015b). DON$_{SPE}$ may therefore provide a more concise picture about the hydrothermal porewater DON pool by excluding the highly labile free amino acids originating from hydrothermal alteration; instead consisting of organic nitrogen compounds released during the microbial transformation of sedimentary organic matter that are less labile to subsequent degradation.

DOP_{SPE} profiles generally resembled trends observed for DON_{SPE} with high concentrations of DOP_{SPE} in shallow subsurface porewater samples (between 0.39 and 2.90 μM) decreasing with depth and increasing *in situ* temperatures, where concentrations of 0.04 μM, similar to deep ocean DOP concentrations (without SPE) (Karl and Björkman, 2015; Liang *et al.*, 2022), were observed (Figure 1, Table 1). DOP cycling in sediments is a scarcely studied topic that was examined previously in lake sediments (Kurek *et al.*, 2020; Ni *et al.*, 2022) and tidal flat sediments (Yamaguchi *et al.*, 2015) while deep sea sediment data are still rare. Similar to DON, DOP consists of both labile and recalcitrant compounds primarily derived from marine phytoplankton (Karl and Björkman, 2015; Ni *et al.*, 2022; Worsfold *et al.*, 2008). We interpret DON and DOP concentration profiles in the context of our study largely as a sign of biodegradation of sedimentary organic matter originating from the highly productive surface waters in the Guaymas Basin: ratios of DON_{SPE}:DOC_{SPE} and DOP_{SPE}:DOC_{SPE} decreased with increasing sediment depth in hydrothermal samples (Supplementary Figure 1), likely reflecting the rapid decline in microbial activity within a few centimeters below the sediment surface generally observed in Guaymas Basin sediments (McKay *et al.*, 2016; Teske *et al.*, 2016). Moreover, we consider incorporation of petroleum-derived DOM to not add significant amounts of DON and DOP, because petroleum is generally considered to not contain phosphorus and only small amounts of nitrogen (0.73-0.77 weight-percent were previously detected in hydrothermal petroleum from the Guaymas Basin (Didyk and Simoneit, 1989; Didyk and Simoneit, 1990).

Porewater DOS_{SPE} concentrations were highly variable between sampling sites, ranging between 3.4 and 43.9 μM as well as DOS_{SPE}:DOC_{SPE} ratios between 0.6 and 3.1% (shallow subsurface) and up to 4.3% in samples from the hot Cathedral Hill site (Figure 1, Supplementary Figure 1). These concentrations and ratios are among the highest reported values in literature so far, exceeding DOS_{SPE} concentrations and ratios reported from sulfidic Crimea porewater (5.9 μM, 2.7% DOS_{SPE}:DOC_{SPE}) (Gomez-Saez *et al.*, 2021) and saltmarsh porewater (10 μM DOS_{SPE}, 1.4% DOS_{SPE}:DOC_{SPE}) (Gomez-Saez *et al.*, 2017), and are on par with concentrations in sulfidic tidal flat sediments (32.3 μM DOS_{SPE}, 3.7% DOS_{SPE}:DOC_{SPE}) (Pohlabeln *et al.*, 2017). In a previous study, Didyk and Simoneit (1990) reported Guaymas Basin hydrothermal petroleum sulfur-content to be 1.30 weight-percent, and sulfur-containing petroleum hydrocarbons such as condensed thiophenes were identified both in petroleum-soaked sediments and porewaters at the same sampling sites as in our study (Mara *et al.* (2022). The abundant porewater DOS_{SPE} could be in part related to the release by sulfur-containing petroleum hydrocarbons.

The highest concentrations of DOS_{SPE} were observed at the Aceto Balsamico site, where Mara *et al.* (2022) also reported the highest concentrations of dissolved petroleum hydrocarbons in porewaters and molecular analysis indicated a highly reduced DOM pool which was likely derived from water-soluble petroleum compounds (Chapter III). However, ratios of S:C ratios in hydrothermal Guaymas Basin oil (S:C = 0.59% atomic ratio; 82.29 weight-percent C, 1.30 weigh-percent S) (Didyk and Simoneit, 1990) were much lower than observed porewater DOS_{SPE}:DOC_{SPE} ratios at the Aceto Balsamico and other sites (1.9 ± 1.1%; Figure 4). Our higher DOS_{SPE}:DOC_{SPE} ratios would therefore require a highly selective enrichment of sulfur-containing petroleum compounds in the DOM. Water-soluble sulfur-containing petroleum hydrocarbons such as condensed thiophenes are generally considered to be bio-refractory (Kropp and Fedorak, 1998) and a selective enrichment of sulfur-compounds was previously observed in incubation with petroleum-derived DOM suggesting their recalcitrant character (Brünjes *et al.*, 2022; Hegazi *et al.*, 2012; Liu and Kujawinski, 2015). However, we consider it unlikely that the observed porewater DOS_{SPE}:DOC_{SPE} ratios of up to 4.3% can solely be explained by petroleum incorporation and subsequent enrichment of recalcitrant petroleum-derived DOS. Instead, we suggest that the major fraction of DOS is probably derived from the abiotic incorporation of sulfide into DOM (sulfurization (Pohlabeln *et al.*, 2017)), which is likely accelerated by the high *in situ* temperatures or potential buildup of polysulfides (Teske *et al.*, 2016). We previously found a strong sulfur-enrichment of DOM molecular formulae and proposed this to be the result of abiotic DOS formation based on molecular analysis of DOM by ultrahigh-resolution mass spectrometry in Guaymas Basin porewaters (Chapter III). Porewater in sulfidic environments is generally enriched in DOS suggesting its recalcitrant character (Abdulla *et al.*, 2019; Gomez-Saez *et al.*, 2021; Gomez-Saez *et al.*, 2017; Pohlabeln *et al.*, 2017; Schmidt *et al.*, 2009; Seidel *et al.*, 2014).

IV.3.2 Incorporation of hot-water soluble DBC and DOS into sedimentary organic matter

IV.3.2.1 Assessment of hydrothermal alteration state of sediment by hot-water extractable DOC

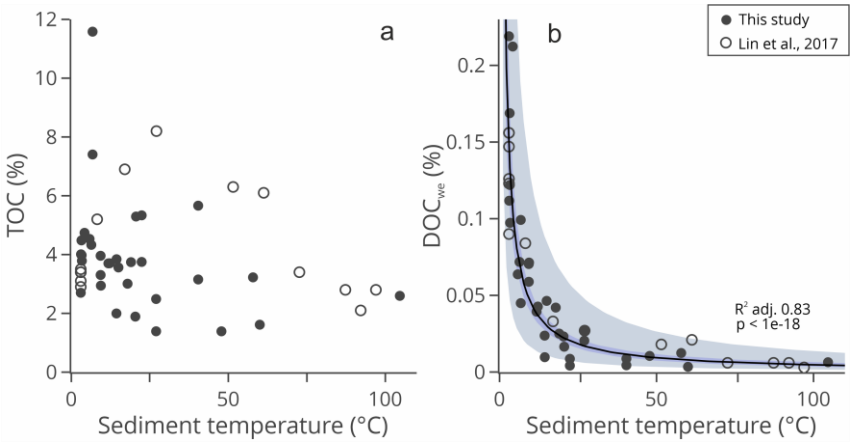

Figure IV. 2: The total organic carbon (TOC) content (weight%) (a) and the water-extractable DOC content (DOC_{we} weight%) (b) versus in situ sediment temperature. Open circles represent data reported by Lin et al. (2017); (Lin et al., 2020). Sediment temperatures of different heat probes published in Lin et al. (2017) were averaged and interpolated between each measurement interval to match our sediment sampling resolution. Shown in (b) is a linear model of log-transformed DOC_{we} and log-transformed sediment temperature on non-log-transformed axes. Blue areas represent 95% confidence intervals, grey areas 95% prediction intervals. The correlation is also considered significant using only data presented in this study (adjusted $R^2 = 0.77$, $p < 1e\text{-}10$).

The hydrothermal activity in the Guaymas Basin sediments drives advective porewater fluxes and porewater discharge into the water column, releasing large amounts of porewater DOC as demonstrated by highly elevated DOC concentrations in the bottom water (Lin *et al.* (2017); Chapter III). By applying hot-water (Soxhlet) extractions of the same sediments analyzed for porewater DOM composition, we simulated hot-water discharge events and assessed the potential release of DBC, DON, DOS and DOP to the water column. Extracted sediments had a wide range of TOC contents, between 1.4 and 11.6 weight-%, while the hydrothermally unaltered reference core had TOC contents of 4.0 ± 0.3% (Figure 2a, Supplementary Table 1). Water-extractable organic matter was as high as 0.21 weight-% (2.1 mg C g^{-1} sediment) for surficial sediments and decreased by a factor of 62 with higher *in situ* sediment temperatures to values as low as 0.003% (Figure 2b). While no significant linear correlation between the sedimentary TOC content and *in situ* sediment temperatures was observed, the sedimentary content of DOC_{we} correlated well on a double logarithmic axis with sediment temperatures (Figure 2). A similar relationship has previously been observed in a study by Zhu *et al.* (2015) for water-extracts of black shales, where the amount of DOC_{we} showed a good correlation with

the thermal maturity of the shale. Since hydrothermal heating in the Guaymas Basin generates petroleum from thermal cracking of sedimentary organic matter (Simoneit, 1985), an analogy with black shales is reasonable. We therefore interpret the amount of DOC_{we} as a proxy for hydrothermal alteration that may be more accurate than the *in situ* sediment temperature alone which can be highly variable in space and time in the Guaymas Basin (Teske *et al.*, 2016). For instance, lowest DOC_{we} values were observed in core 5001-41 from the Hot Cathedral Hill site at *in situ* sediment temperatures of approximately 60 °C compared to the deepest and hottest samples of approximately 106 °C at the neighboring core 5001-43, which probably reflects the thermal history of each site.

IV.3.2.2 Hydrothermal alteration can increase sedimentary hot-water soluble DBC and DOS

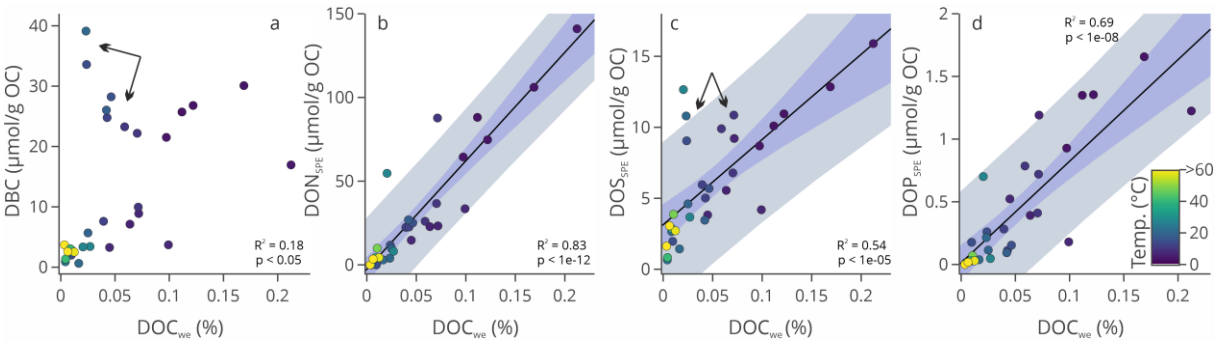

Figure IV. 3 The amount of hot-water extractable DBC (a), DON_{SPE} (b), DOS_{SPE} (c), DOP_{SPE} (d) as a function of DOC_{we}. Linear models (n = 31) were calculated for each parameter and shown are 95% confidence intervals (blue) and 95% prediction intervals (grey). Although a linear model between DBC and TOC_{we} in (a) was considered significant ($p < 0.05$), a regression is not shown because of a poor fit and highlighted outlier. The color scale denotes in situ sediment temperatures of extracted sediments. Highlighted in (a) and (c) are a subgroup of samples from the Aceto Balsamico region showing high amounts of water-extractable DBC and DOS_{SPE} at low sedimentary contents of water-extractable organic carbon (OC).

The amounts of hot-water extractable DBC, DON_{SPE}, DOS_{SPE} and DOP_{SPE} were correlated with the alteration state of the respective sediments, i.e., DOC_{we} (Figure 3). Unaltered surficial sediments and sediments from the reference core released ~20-30 µmol DBC g^{-1} OC, ~100 µMol DON_{SPE} g^{-1} OC, ~13 µMol DOS_{SPE} g^{-1} OC and 1.3 µMol DOP_{SPE} g^{-1} OC after 48 hours of Soxhlet extraction. Highly altered sediment samples (< 0.02% DOC_{we}) with high *in situ* temperatures released between 0.6 and 3.7 µMol DBC g^{-1} OC, 3.4 and 9.9 µMol DON_{SPE} g^{-1} OC, 0.7 and 3.9 µMol DOS_{SPE} g^{-1} OC and 0.01 and 0.18 µMol DON_{SPE} g^{-1} OC. Noticeable deviations from linear correlation were observed for water-extractable DBC and DOS_{SPE}, whereas linear regressions of extractable DON_{SPE} and DOP_{SPE} were close to the coordinate origin. A subset of samples had high amounts of extractable DBC and DOS_{SPE} (highlighted in Figure 3). A moderate hydrothermal alteration and hence previous release of

sedimentary organic matter, however, was suggested by several factors: *in situ* temperatures of 12 - 20 °C, the amount of DOC_{we} 5 to 10 times lower than in non-altered surficial sediments and both water-extractable DON_{SPE} and DOP_{SPE} released in accordance to the general linear trend. This clearly demonstrates that hydrothermal alteration does not only mobilize sedimentary organic matter, but can also increase the contents of water-soluble thermogenic DBC and DOS_{SPE} over non-altered sediments that may later be mobilized by hot water discharge events. It is noteworthy that the amount of water-extractable DBC from moderately altered and from surficial sediments were in the same range as DBC derived from charred plant-derived organic matter (Wagner *et al.*, 2017).

The quantity of water-extractable organic matter at highly altered sites was minor compared to the potential release of unaltered or moderately altered sediments, likely because almost all original and hydrothermally impregnated DOC_{we} had been discharged previously. Nevertheless, water-extractable fluids were enriched in DBC and DOS_{SPE} relative to their DOC contents (0.25-2.1% and 2.5-7.3%, respectively) and they showed similar DON_{SPE}:DOC_{SPE} and only slightly lower DOP_{SPE}:DOC_{SPE} ratios compared to the reference site (Figure 5, Supplementary Figure 1).

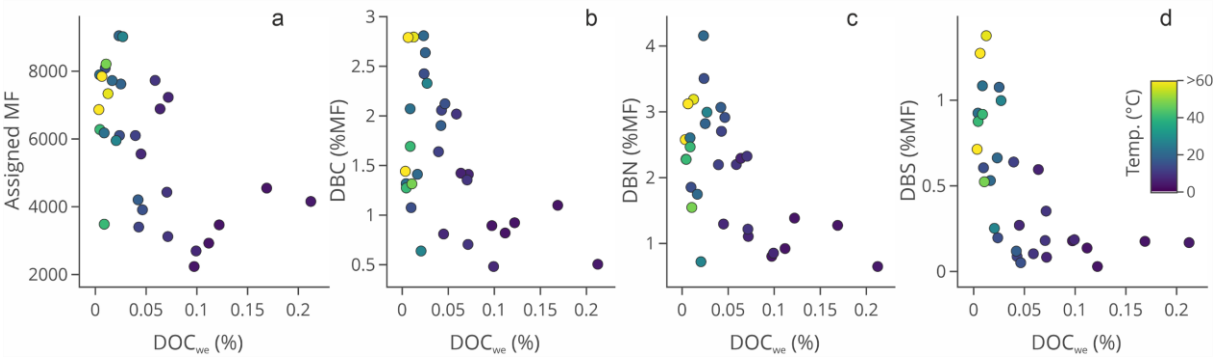

Figure IV. 4: Total number of assigned molecular formulae (MF) from FT-ICR-MS (a), the relative abundance of polycyclic aromatic molecular formulae (AI_{mod} > 0.66; C ≥ 15) without heteroatoms (CHO; DBC) (b), containing nitrogen (CHN; dissolved black nitrogen; DBN) (c), containing sulfur (CHS; dissolved black sulfur; DBS) (d) as a function of hot-water extractable sedimentary organic carbon (DOC_{we}). The color scale represents in situ sediment temperatures of the extracted sediments.

Moreover, the molecular analysis of water-extractable DOM by FT-ICR-MS revealed that hydrothermally altered samples contained an increasing relative abundance of polycyclic aromatic molecular formulae, including DBC without heteroatoms, as well as DBC containing nitrogen (DBN) (Wagner *et al.*, 2015), and containing sulfur (DBS) (Hertkorn *et al.*, 2016) (Figure 4). While DBC molecular formulae made up approximately 2.5% of all detected molecular formulae, DBN was ~3-4%, and DBS was ~1% of all molecular formulae in hydrothermally altered samples. DBN and DBS fractions are not included in the quantitative BPCA chemical tracer approach to quantify DBC, indicating that the real concentrations of

polycondensed aromatic compounds are underestimated. To date, environmental implications of DBS and DBN are unknown, although their sources were previously associated with biomass burning and spilled diesel fuel (Roebuck *et al.*, 2018; Wagner *et al.*, 2015). DBS and DBN were also detected in asphalt-derived DOM in Brünjes *et al.* (2022), demonstrating water-soluble petroleum compounds are sources of DBS and DBN to the environment.

IV.3.2.3 Comparison of porewater with hot-water extractable DOM

The general trends of the water-extractable DOM composition resembled those of the porewater, both by quantitatively determined ratios (Figure 5, Supplementary Figure 2 a-d) and by molecular characterization of DOM_{SPE} using FT-ICR-MS (Supplementary Figure 2 e-l). However, water-extractable DOM was significantly more aromatic (AI_{mod} and DBC:DOC) ($p < 0.01$, Wilcoxon test), contained more sulfur (DOS_{SPE}:DOC_{SPE} and intensity-weighted averages of S/C) and was more hydrophobic (intensity-weighted averages of NSO:C) (Supplementary Figure 2, Figure 5). Particularly intensity-weighted averages of O/C ratios were lower ($p < 0.001$, Wilcoxon test) in Soxhlet extracts than in respective porewaters. These findings contrast with a previous case of Soxhlet extraction of sedimentary organic matter, where higher O/C ratios, a higher abundance of nitrogen-containing molecular formulae and generally more diverse DOM compared to porewater samples were observed (Schmidt *et al.*, 2014). We explain this apparent contradiction with the *in situ* hot water advective porewater fluxes in our samples: These hot water fluxes already mobilize and transport parts of the water-extractable DOM pool *in situ*, leaving behind more hydrophobic water-extractable DOM in the particulate phase that was released in our Soxhlet experiment. At the same time, hydrothermally mobilized compounds will be part of the *in situ* porewater DOM pool.

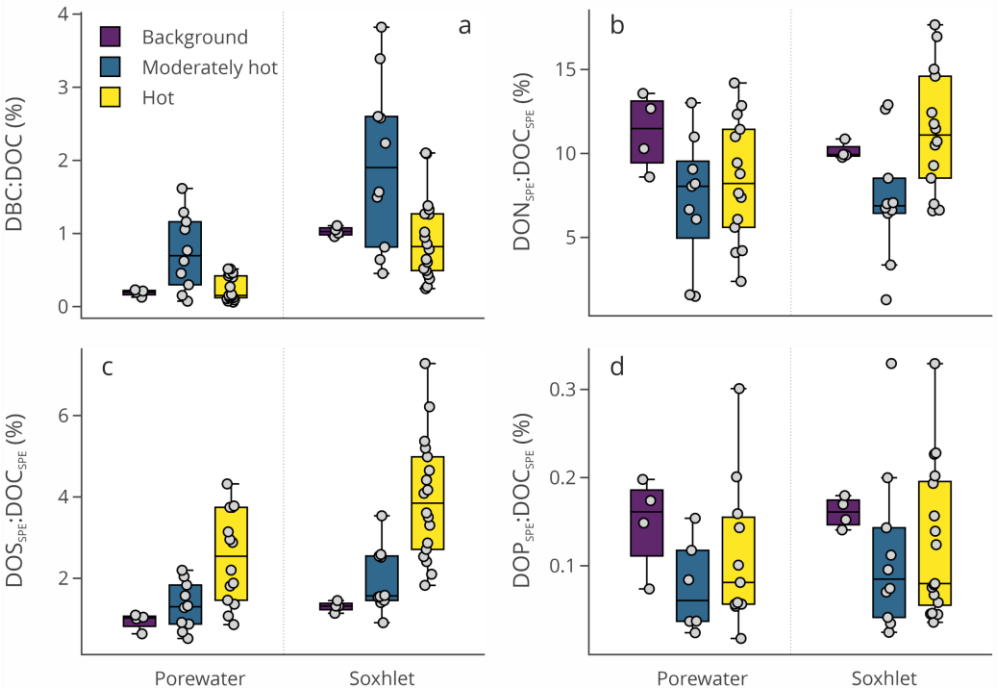

Figure IV. 5: Boxplots comparing porewater and Soxhlet-extracted sediments in ratios of DBC:DOC (a), DON_{SPE}:DOC_{SPE} (b), DOS_{SPE}:DOC_{SPE} (c), DOP_{SPE}:DO_{CSPE} (d). Ratios are given as mol%, i.e. how many mols of DBC/S/N/P per 100 mols of C. The samples are grouped into the reference core without signs of hydrothermal alteration, moderately hot cores (n = 2) from the Aceto Balsamico site (6–21°C; 6-19 °C) and hot cores (n = 4) from the Mat Mound (10-29°C; 19-48 °C) and Cathedral Hill (12-67 °C; 12-106 °C) sites. Shown are only samples that were analyzed both for their porewater DOM and hot-water soluble DOM composition (32 samples).

This assumption of a previous *in situ* hydrothermal mobilization of sedimentary organic matter and subsequent accumulation within the porewater DOM pool is supported by the fact that the number of detected molecular formulae in Soxhlet samples (5725 ± 2073) was not significantly elevated compared to respective porewater samples (4780 ± 1472) ($p > 0.05$, Wilcoxon test). Moreover, of the 16659 molecular formulae detected in both porewater and Soxhlet extracts, 84% (14056) were present in both fractions and only 9% (1555) were exclusively detected in the hot-water extracts. The unique (exclusive) water-extractable molecular formulae had lower O/C and H/C ratios compared to porewater DOM, indicating more reduced and more aromatic DOM (Supplementary Figure 3a). To determine hydrophobic compounds in water-extractable DOM, PPL cartridges used to extract DOM_{SPE} samples were eluted again with DCM, which extends the analytical window of DOM_{SPE} towards hydrophobic DOM (Chapter III). We saw a clear negative correlation between the amount of water-extractable DOC and additional carbon yield by DCM elution, which was linear on a double-log axis (Supplementary Figure 3b): for highly altered sediment samples, up to 60% of SPE-DOC (equivalent to 14% of total DOC) was additionally recovered by subsequent elution with the less polar DCM solvent, whereas samples not affected by hydrothermalism had additional

yields of < 2%. This indicates that highly altered samples contain a hydrophobic fraction as part of the water-extractable DOM that is likely to precipitate under *in situ* conditions. Nonetheless, the quantified DBC, DON, DOS, and DOP concentrations reported in this study are derived from the more polar methanol-eluted PPL fraction and hence likely represent DOM that is dissolved under *in situ* conditions.

IV.3.3 Petroleum and terrestrial-derived DBC in porewaters and water-extractable DOC

DBC is assumed to be primarily derived from incomplete combustion of biomass on land, but hydrothermal vents and petroleum were previously proposed as potential marine DBC sources (Brünjes *et al.*, 2022; Coppola *et al.*, 2022; Dittmar and Koch, 2006; Dittmar and Paeng, 2009). In Guaymas Basin sediments, a contribution of all three potential sources seems plausible. The isotopic composition of sedimentary TOC did not indicate major input of terrestrial-derived sedimentary organic matter, as shown by $\delta^{13}C$ TOC values of -20.8 ± 1.3 ‰ typical for marine organic matter (Silverman and Epstein, 1958) (Supplementary Table 1). A fraction of the TOC in deep-sea sediments can contain pre-aged particulate black carbon, and a combination of adsorbed and precipitated particulate black carbon from the water column was suggested as their source (Coppola *et al.*, 2014). Porewater DOM from the reference core in our study contained DBC (Figure 1, Table 1). Here, a high condensation status was indicated by B6CA:B5CA ratios, where B6 and B5CA represent converted 5- and 6-ring DBC, respectively (Dittmar and Paeng, 2009). The B6CA:B5CA ratios of 0.62 ± 0.08 in porewater samples from the reference site were elevated compared to typical deep ocean ratios of ~0.3 (Dittmar and Paeng, 2009) and more similar to terrestrial-derived particulate black carbon in abyssal deep-sea sediments (~0.9) (Coppola *et al.*, 2014), and riverine DBC (~0.4) in large rivers (Stubbins *et al.*, 2015). We hypothesize that the highly condensed DBC in DOM of the reference core samples represents precipitated or adsorbed terrestrial black carbon from the water column which was re-dissolved in porewater, possibly by enhanced solubility due to higher DOC concentrations compared to the water column (i.e., (Boehm and Quinn, 1973; Brünjes *et al.*, 2022; Wagner *et al.*, 2017).

Elevated DBC concentrations and the amount of hot-water extractable DOM compared to the reference core samples were observed for sample from site Aceto Balsamico (Figure 1, Figure 4). It is possible that the elevated DBC concentrations are derived from previously buried terrestrial black carbon in the sediments. Buried sedimentary DBC could be mobilized by hydrothermal heating of deeper sediments and subsequently transported within advective porewater fluxes, accumulating in both dissolved in porewaters and adsorbed onto sediment particles. However, a distinct source of DBC is suggested by lower B6CA:B5CA ratios in

porewater samples and the respective DOC_{we} fractions of hydrothermal samples compared to reference samples (Figure 6) as well as the increasing contribution of DBC, DBN and DBS molecular formulae in hydrothermally altered samples (Figure 4). While a hypothesized production of DBC during hydrothermal circulation (Dittmar and Koch, 2006; Dittmar and Paeng, 2009) could not be verified in environmental samples and laboratory heating experiments with marine DOM (Hawkes *et al.*, 2015a; Hawkes *et al.*, 2015b), hot hydrothermal fluids can generate hydrothermal petroleum with a high content of polycondensed aromatic hydrocarbons by altering sedimentary organic matter (Simoneit, 1988). Thus, we attribute the elevated presence of DBC in porewater samples in our study to the formation of water-soluble hydrothermal petroleum, similar to laboratory findings of asphalt-derived DBC (Brünjes *et al.*, 2022). Our study confirms that natural petroleum seepage can release water-soluble compounds that probably become a part of the ultra-refractory oceanic DOM pool upon discharge into the water column.

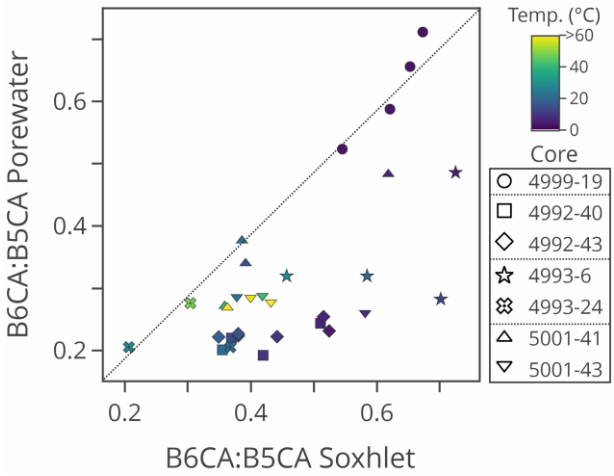

Figure IV. 6: The ratio of B6CA:B5CA (BPCA-converted 6-ring over 5-ring DBC) for hot-water extractable (Soxhlet) DOM and the respective actual porewater B6CA:B5CA ratio, color-coded by in situ sediment temperature. Core 4999-19 represents a reference core without signs of hydrothermal alteration. The dotted line shows a 1:1 line between B6CA:B5CA ratios of Soxhlet-extracted and porewater DBC.

IV.3.4 Importance of hydrothermal sediments for deep sea elemental cycles

Both porewater DOM analysis (Figure 1) and hot-water-extractions (Figure 3) of hydrothermal sediments suggest that hydrothermal alteration of sediments are an additional source of DBC to natural environments and possibly deep ocean waters. However, we did not observe elevated concentrations of DBC in bottom water samples (Table 1). There can be several reasons for this. For example, the discharged hydrothermal DBC is rapidly diluted with the low-

DBC deep sea bottom water DOC pool and/or discharged porewater DBC may precipitate in the water column. The latter has been observed for lightweight hydrocarbons condensing on particles in the hydrothermal plume due to lower solubilities for petroleum hydrocarbons in the water column (Kawka and Simoneit, 1994; Ondréas *et al.*, 2018). While hydrothermally altered samples had an increasing contribution of hydrophobic water-extractable DOM with increasing alteration status (Supplementary Figure 2l; 3b), porewater DBC from all hydrothermal samples had a similar condensation degree compared to bottom water DBC (B6CA:B5CA = 0.27 ± 0.07 and 0.28 ± 0.03, respectively; Table 1) which could indicate that hydrothermal petroleum DBC remains dissolved in bottom waters. This result suggests that dilution is a more likely explanation for non-elevated DBC concentrations in bottom waters, similar to ashes from a wildfire event that leached DBC in laboratory experiments but DBC in environmental water samples was diluted (Wagner *et al.*, 2021). Yet, we observed enriched bottom water DOC concentrations likely derived from advective porewater fluxes, arguing for a precipitation of DBC instead. As a result, an assessment of the impact of hydrothermal petroleum-derived DBC to ocean waters is unclear and would need to be addressed in future studies for example by using *in situ* flux chambers. However, hydrothermal alteration of sediments could be a constant, minor source of petroleum-derived DBC to ocean waters with a marine ^{13}C signature in the Guaymas Basin and likely other locations of hydrothermal petroleum generation such as the Pescadero Basin in the Gulf of California (Paduan *et al.*, 2018), Escanaba Trough in the northeast Pacific Ocean (Kvenvolden and Simoneit, 1990), Middle Valley at the northern Juan de Fuca Ridge (Simoneit, 1994) and Rainbow Field at the Mid-Atlantic Ridge (Simoneit *et al.*, 2004).

The largest yields of water-extractable DBC were observed from hydrothermally unaffected background sediment samples, likely representing terrestrial-derived DBC (Figure 3). Therefore, the release of hydrothermal petroleum-DBC appears to be minor in comparison to the hydrothermal remobilization of previously sedimented terrestrial black carbon. Regardless, both sources would contribute pre-aged DBC to the deep ocean, where it could be distributed over large distances since the major removal mechanism for DBC, photooxidation, does not apply (Stubbins *et al.*, 2010). Petroleum in Guaymas Basin has ^{14}C-ages of 4240-5705 years (Peter *et al.*, 1991), while particulate black carbon in deep-sea sediments was found to be 6200 ± 2200 ^{14}C years older than non-black carbon TOC (Coppola *et al.*, 2014). Considering that both terrestrial and petroleum-derived DBC would contribute pre-aged carbon, assessing the compound-specific stable carbon isotopic composition of DBC could clarify the contribution of terrestrial-derived versus hydrothermal petroleum-derived DBC but is beyond the scope of this study.

By applying batch and Soxhlet extractions of Guaymas Basin sediments, Lin *et al.* (2017) estimated a maximum DOC efflux of 27 Gg C yr^{-1} assuming the rapid heating of unaltered sediments within an area of 4950 km² of active sill intrusion. A close fit of amounts of water-extractable organic matter of our with data presented in Lin *et al.* (2017) suggest that approximately 1% of released DOC consists of DBC. Consequently, Guaymas Basin sediments could release 0.27 Gg DBC yr^{-1} due to re-dissolution of terrestrial DBC alone plus a still unknown but likely smaller amount of petroleum-derived (hydrothermal) DBC. Furthermore, ratios of solid-phase extracted DON:DOC, DOS:DOC and DOP:DOC allow an estimate of the quantities of potential release of these compound groups. We observed average atomic ratios of 10.1 ± 0.5% DON_{SPE}, 1.3 ± 0.1 DOS_{SPE} and 0.16 ± 0.02% DOP_{SPE} per mol of DOC_{SPE} for the reference core samples. By multiplying the estimated maximum DOC efflux of $27*10^9$ g C yr^{-1} with the average extraction efficiencies of 32.4 ± 3.9% for these samples, we estimate an annual release of 64–$82*10^7$ mol DOC_{SPE} (7.7-$9.8*10^9$ g C), 61-$87*10^6$ mol DON_{SPE} (85.4-$122*10^7$ g N), 7.7- $11.5*10^6$ mol DOS_{SPE} (246-$368*10^6$ g S) and 0.9- $1.5*10^6$ mol DOP_{SPE} (27.9-$46.5*10^6$ g P) plus non-extractable DOM such as low molecular-weight organic acids and amino acids (Hawkes *et al.*, 2015b). As stated in the discussion by Lin *et al.* (2017), these values re-present the maximum efflux in case of ongoing basin-wide spreading and magma intrusions. Our study provides insights into ratios of released DOM fractions in such a case and demonstrates that also ultra-refractory DBC and potentially recalcitrant DOS will be released to ocean waters.

IV.4 Conclusions

This study presents a comprehensive approach of studying elemental fluxes in hydrothermal porewater from the Guaymas Basin. Porewater from hydrothermally moderately altered samples contained elevated amounts of DBC and DOS compared to a non-altered reference core. By applying hot-water extractions of the same sediments, hot-water discharge events were simulated and a potential release of DOM to the water column was evaluated. The amount of water-extractable DOM represented a good indicator for hydrothermal alteration state of the sediment. We provided evidence that hydrothermal alteration of sedimentary organic matter can increase porewater concentrations of DBC and DOS, and amplify the amount of water-extractable DBC and DOS relative to a core from a non-hydrothermal reference site. At the same time, these DOM compound classes were likely previously discharged into the water column or thermally altered in the sediments. Regardless, concentrations of DBC were not elevated in bottom waters which indicates a rapid dilution with low-DBC seawater; in consequence, the contribution of hydrothermal petroleum DBC to the

marine DOM pool is likely minor. Nonetheless, considerable amounts of DBC were also water-extractable from sediments of the non-hydrothermal reference site, likely relict terrestrial DBC sedimented from the water column. By applying the DOM elemental ratios observed in our study of hot-water extractable DBC, DON, DOS and DOP relative to DOC, we were able to assess quantities of these compound classes that could be discharged into the water column in case of basin-wide hydrothermal heating from non-altered sediments. Our data suggest a contribution of hydrothermal petroleum derived- and remobilized terrestrial (pre-aged) DBC to the deep oceanic carbon cycle, however, the total fluxes still need to be constrained better. Assessing the stable-carbon isotopic composition of DBC in these environments is a promising approach that should be addressed in future studies.

IV.5 Acknowledgement

We thank the Crew of AT42-05 and Thorsten Brinkhoff for sampling, Jenny Wendt, Xavier Prieto-Mollar, Christopher Klaembt (Marum) and Ina Ulber, Matthias Friebe, Eleonore Gründken, Melina Knoke, Jana Günther, Heike Simon (ICBM) for help with laboratory work and sample measurements. We acknowledge funding by the German Science Foundation (DFG) within the Cluster of Excellence EXC 2077 “The Ocean Floor – Earth’s Uncharted Interface” (project number 390741603). Sampling in Guaymas Basin was supported by NSF Biological Oceanography (grant 1357238).

IV.6 Supplementary Information

IV.6.1 Supplementary Tables

Supplementary Table IV. 1: Sediment properties of Soxhlet-extracted sediments and interpolated in situ sediment temperatures.

Core	Depth (cm)	Temperature (°C)	TOC (%)	OC_{we} (%)	TN (%)	C/N	$\delta^{13}C$	$\delta^{15}N$
5001-41	2	7	7.4	0.045	0.6	15	-21.2	4.1
5001-41	6	14	3.8	0.010	0.2	21	-20.9	4.9
5001-41	10	22	5.3	0.004	0.2	40	-20.2	6.2
5001-41	14	40	5.7	0.004	0.1	53	-20.2	5.4
5001-41	18.5	60	1.6	0.003	0.0	60	-19.9	2.4
4992-40	6	6	4.3	0.072	0.5	10	-22.5	5.5
4992-40	14	9	3.3	0.059	0.4	11	-21.2	5.7
4992-40	28	14	2.0	0.024	0.1	16	-20.0	
4992-40	44	20	1.9	0.023	0.1	16	-19.8	
4993-6	2	6	4.5	0.064	0.4	13	-20.2	5.7
4993-6	6	12	3.7	0.039	0.4	12	-20.0	6.0
4993-6	10	19	3.7	0.025	0.3	15	-20.0	5.5
4993-6	14	27	2.5	0.027	0.2	15	-20.5	
4993-24	2	9	2.9	0.071	0.2	14	-24.2	
4993-24	6	21	5.3	0.017	0.6	10	-21.9	6.0
4993-24	10	27	1.4	0.020	0.1	18	-24.6	
4993-24	18	48	1.4	0.010	0.1	20	-22.5	
4999-19	2	3.1	4.0	0.112	0.5	10	-19.5	6.7
4999-19	6	3.2	4.5	0.169	0.5	10	-19.8	5.6
4999-19	10	3.3	4.0	0.122	0.5	10	-19.8	5.9
4999-19	14	3.4	3.8	0.097	0.4	10	-19.3	6.3
4992-43	2	4	4.7	0.212	0.6	9	-21.6	5.3
4992-43	14	9	4.0	0.070	0.4	13	-19.6	5.9
4992-43	22	12	3.7	0.043	0.3	15	-19.5	
4992-43	30	15	3.6	0.046	0.3	14	-19.6	
4992-43	38	18	3.0	0.042	0.2	14	-19.5	
5001-43	2	7	11.6	0.099	0.6	23	-21.1	5.2
5001-43	10	22	3.7	0.009	0.2	20	-21.2	5.4
5001-43	14	40	3.2	0.009	0.2	17	-21.1	5.4
5001-43	18	58	3.2	0.012	0.2	16	-21.3	5.2
5001-43	26	105	2.6	0.006	0.2	16	-21.1	5.2

Supplementary Table IV. 2: Geochemical parameters determined in bottom water samples.

Dive	cm above seafloor	DOC (μM)	TDN (μM)	DOC_{SPE} (μM)	DON_{SPE} (μM)	DBC (μM)	DBC:DOC (%)	B6CA/B5CA
4993-24	10-15	641	47	122	2.42	0.69	0.11	0.35
4992-43	300	1612	50	146	2.71	0.44	0.03	0.27
4992-43	300	664	42	137	5.98	0.62	0.09	0.26
4992-43	10	514	122	50	1.01	0.54	0.11	0.29
4992-43	10	1438	119	41	4.19	0.59	0.04	0.27
4995	10	882	40	42	0.7	0.77	0.09	0.26
4995	10	750	44	51	0.94	0.62	0.08	0.23
4995	10	237	41	47	1.39	0.46	0.2	0.27
4995	10	1393	42	57	2.71	0.42	0.03	0.31
mean ± sd		903 ± 471	61 ± 34	77 ± 44	2.45 ± 1.74	0.57 ± 0.12	0.09 ± 0.05	0.28 ± 0.03

IV.6.2 Supplementary Figures

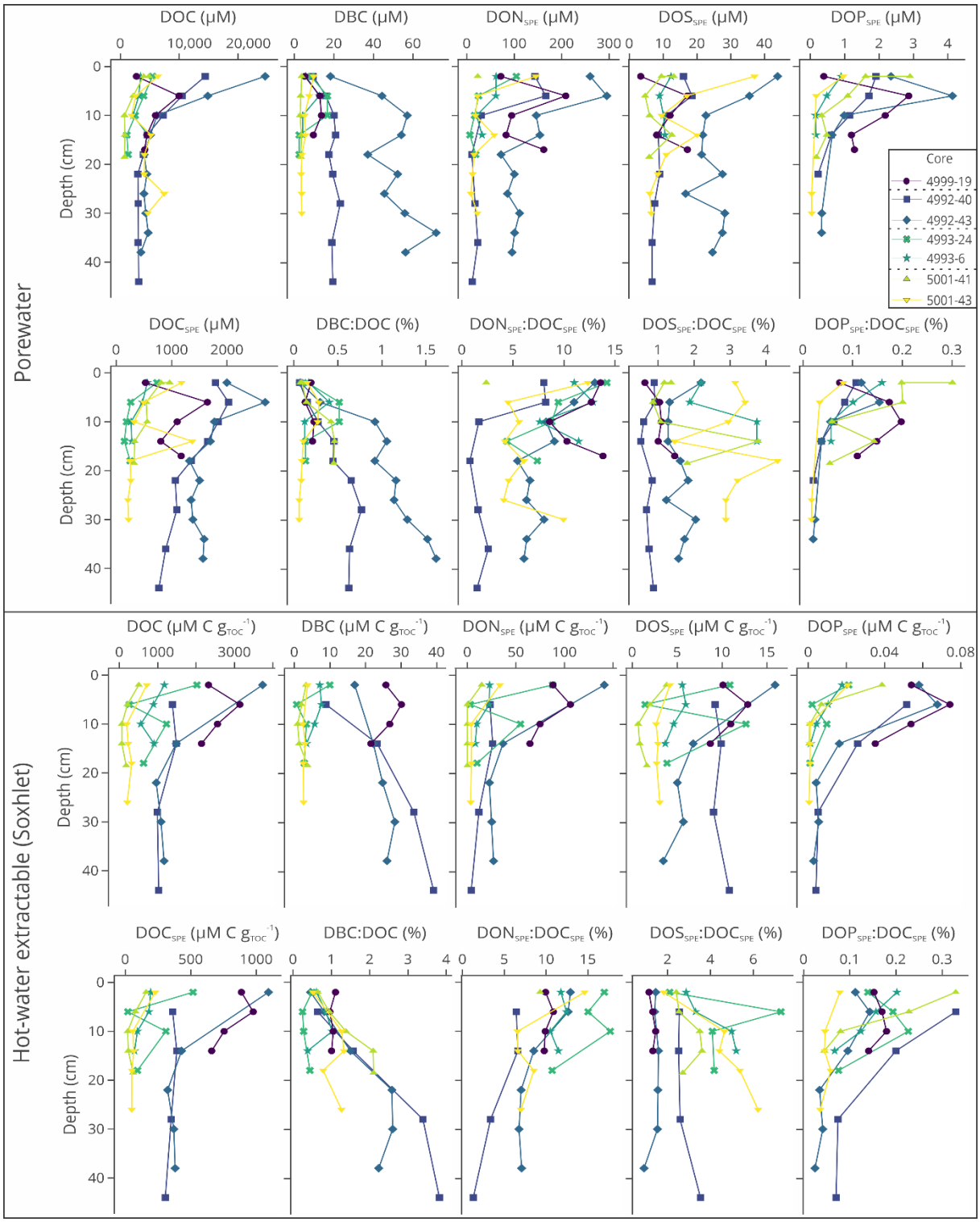

Supplementary Figure IV. 1: Top: Porewater depth profiles of DOC, DBC, DON_{SPE}, DOS_{SPE} and DOP_{SPE}, as well as DOC_{SPE} concentrations and the molar ratio (%) of DBC:DOC and DON_{SPE}:DOC_{SPE}, DOS_{SPE}:DOC_{SPE} and DOP_{SPE}:DOC_{SPE}. Bottom: Quantities of Soxhlet-extracted DOC, DBC, DON_{SPE}, DOS_{SPE}, DOP_{SPE}, DOC_{SPE} per gram of sedimentary organic carbon, as well as the molar ratio (%) of DBC:DOC and DON_{SPE}:DOC_{SPE}, DOS_{SPE}:DOC_{SPE} and DOP_{SPE}:DOC_{SPE}.

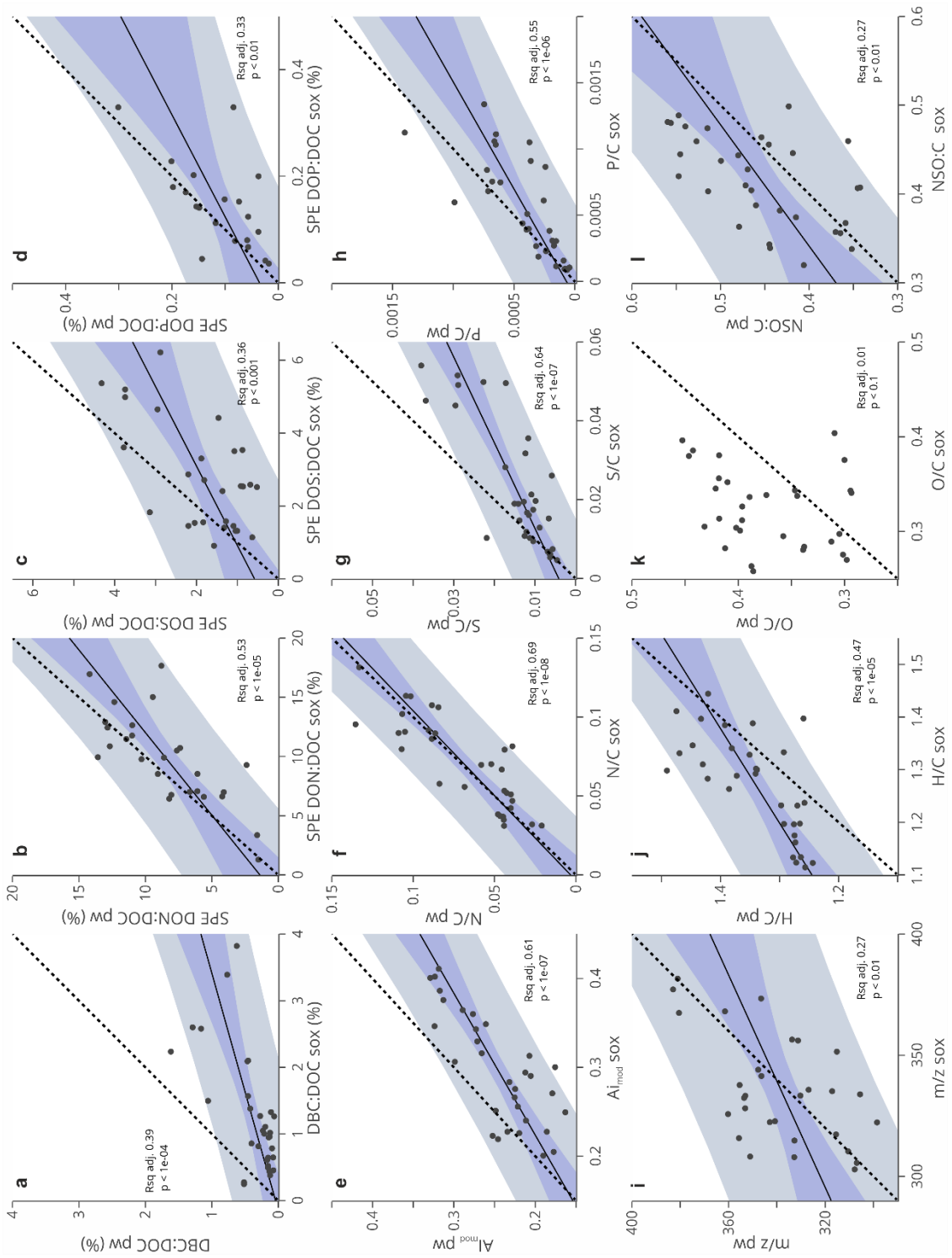

Supplementary Figure IV. 2: Linear correlations of quantitatively determined ratios (a-d) and molecular parameters of DOM$_{SPE}$ (e-l) between Soxhlet-extracted DOM (sox) and the respective actual porewater (pw). Regressions lines (black), 95% confidence intervals (blue) and 95% prediction intervals (grey) were displayed when p < 0.05. The dotted line represents a 1:1 line between porewater and Soxhlet-extracted parameters.

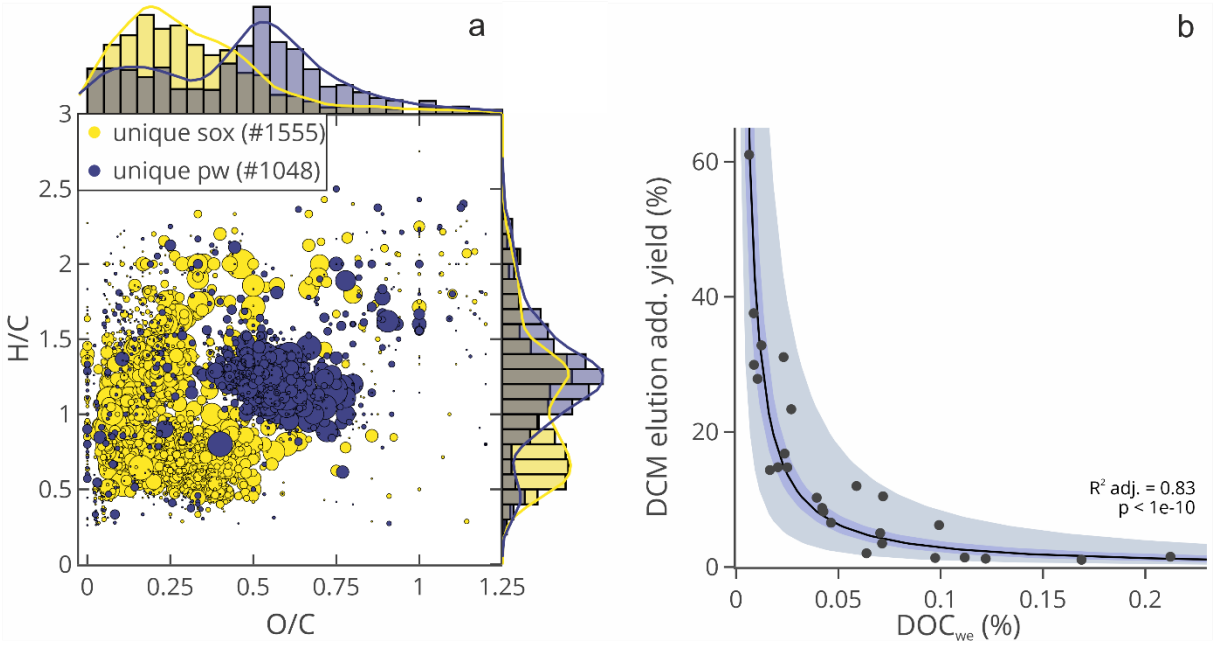

Supplementary Figure IV. 3: a) Van Krevelen plot showing molecular formulae exclusively present in Soxhlet extracts (sox) and exclusively present in respective porewater samples (pw). The 1555 molecular formulae in Soxhlet extracts represent 9% of all molecular formulae (16659), exclusive porewater molecular formulae 6%. The bubble size corresponds to the relative abundance of each MF in the respective group of samples. Van Krevelen plots further display densities and the relative abundance of MF after H/C (binsize = 0.1) and O/C (binsize = 0.05) ratios. Exclusive porewater molecular formulae are in a similar region of the Van Krevelen plot as carboxyl-rich alicyclic molecules (CRAM, (Hertkorn et al., 2006)) that are a major component of refractory oceanic DOM but were shown previously as thermally instable (Hawkes et al., 2015a). b) Linear correlation between log-converted water-extractable DOC (DOC_{we}, weigth-%) and the additional carbon yield by eluting the SPE PPL cartridges again with dichloromethane. Shown are a regression line (black), 95% confidence intervals (blue) and 95% prediction intervals (grey).

V. Concluding remarks

V.1 Conclusions

This thesis investigated molecular transformations of DOM in natural petroleum seepages and assessed the potential release of petroleum-compounds to oceanic deep-sea DOM. Two locations with active petroleum seepage were studied: the Chapopote asphalt volcano in the Southern Gulf of Mexico and hydrothermal, petroleum-impregnated sediments of Guaymas Basin in the Gulf of California.

By conducting laboratory incubation experiments using Chapopote asphalt in artificial seawater, the potential release of water-soluble petroleum compounds was examined on a qualitative and quantitative basis. Compositional changes in DOM were assessed using a combined approach of ultra-high-resolution mass spectrometric analysis and fluorescence spectroscopy coupled with PARAFAC analysis. Results showed a fast microbial transformation of labile petroleum DOM, whereas sulfur-rich aromatic compounds were resistant to biodegradation and accumulated throughout the experimental time. A quantitative chemical tracer approach confirmed the release of DBC and non-labile DOS by these natural seep samples, potentially impacting deep-sea cycling of both compound classes.

To extent these laboratory observations onto the deep-sea environment, porewaters and bottom waters of the oil-laden hydrothermal sediments of the Guaymas Basin were analyzed. Both ultra-high resolution mass spectrometry and PARAFAC analysis indicated the presence of large amounts of presumably labile DOM compounds at the sediment-water interface. In addition, an underlying fraction of refractory compounds was also present in these porewaters, which were particularly enriched in DOS. Molecular signals of hydrothermal, petroleum-associated and sulfur-rich DOM at > 106°C hot porewaters were found in bottom waters at Guaymas Basin and may be part of refractory deep pacific DOM, corroborating the results from the asphalt laboratory incubation study. By quantifying different DOM fractions in these porewaters, high concentrations of DBC and DOS were confirmed, exceeding concentrations of DBC in non-altered porewaters by a factor of up to ~5. DBC and DOS in porewaters were associated with hydrothermal petroleum impregnation and sulfurization of DOM, whereas DON and DOP generally reflected microbial degradation of sedimentary organic matter.

Finally, the potential release of DOM by hydrothermal alteration was assessed by simulating hot-water discharge events of the oil-impregnated sediments. The amount of water-extractable DOM represented a good indicator for hydrothermal alteration state of the

sediment. Results showed that hydrothermal alteration of sedimentary organic matter can amplify the amount of water-extractable DBC and DOS relative to sediments sample from a non-hydrothermal reference site. Regardless, concentrations of DBC were not elevated in bottom waters, possibly due to a rapid dilution by low-DBC seawater; in consequence, the contribution of hydrothermal petroleum DBC to the marine DOM pool may be minor. Nonetheless, sediments of the non-hydrothermal reference site also had considerable amounts of water-extractable DBC, likely representing relict terrestrial DBC sedimented from the water column. By applying the DOM elemental ratios observed in hot-water extractable DBC, DON, DOS and DOP relative to DOC, the quantities of these compound classes that could be discharged into the water column in case of basin-wide hydrothermal heating were assessed.

In conclusion, natural petroleum seepage and hydrothermal alteration of sediments could be an explanation for observed old radiocarbon ages in refractory deep-sea DOM by releasing radiocarbon-depleted organic matter. This thesis demonstrated that water-soluble petroleum is a constant source of DOM to natural environments, and provided important constraints on evaluating cycles of refractory DOM in the deep sea.

V.2 Outlook

This thesis provided evidence that natural petroleum seepages can release water-soluble petroleum compounds that are stable on timescales of millennia. However, the actual fluxes of petroleum-derived DOM are speculative. Petroleum is, next to DOM, one of the most complex mixtures of organic matter on our planet, hence naturally seeping oil has different compositions across the ocean. It is unknown if the release of DBC and other water-soluble petroleum compounds by different source oils is in a similar range as the asphaltene-rich heavy-oil from Chapopote. Future experiments should therefore target petroleum of different origins and, if possible, mimic conditions that are similar to the natural deep-sea environment, e.g., cold temperatures, low ambient DOC concentrations and high ambient pressure.

In the Guaymas Basin, DBC was released from petroleum and/or hydrothermal alteration of non-petroleum-impregnated sediments, representing petroleum-derived and presumably re-dissolved DBC of terrestrial origin. The contributions of both respective sources to porewater and bottom water DBC could be resolved by compound specific stable carbon isotopic analysis of DBC. *In situ* incubations may provide a possibility to assess quantities of DOM transported by advective porewater fluxes out of the sediments and estimate whether hydrothermal sediments provide a constant, significant source of DBC and DOS to bottom waters and ultimately to the deep ocean.

Molecular analysis by FT-ICR-MS has shown that microbial degradation oxidizes petroleum-derived DOM, resulting in compounds in a similar location on the van Krevelen plot as refractory marine DOM. Several thousands of molecular formulae associated with petroleum and its degradation intermediates were identified in this thesis, possibly representing tens of thousands of individual structural isomers (Zark *et al.*, 2017). The actual persistence of oxidized intermediates of petroleum degradation remains unknown, though recent research suggests that polar intermediates of PAH degradation could be further degraded by diverse microbial communities present in the seawater (Liu *et al.*, 2020).

Finally, in order to better constrain fluxes of petroleum-derived DOM to the natural environment, quantities of discharged oil by natural seepage need to be assessed in greater detail. The most recent estimation on global discharge by natural petroleum seepage was published two decades ago (Kvenvolden and Cooper, 2003). However, the available methodology of quantifying oil slicks on the sea surface will likely continue to underestimate the contribution by less buoyant discharged petroleum in deep sea environments. More work on the seafloor at natural seepage sites is required to constrain the contribution of natural petroleum seepage to deep-sea DOM cycling.

VI. Author contribution

Chapter II: Natural asphalt seeps are potential sources for recalcitrant dissolved organic sulfur and dissolved black carbon

Jonas Brünjes, Michael Seidel, Thorsten Dittmar, Jutta Niggemann, Florence Schubotz

Published in *Environmental Science & Technology* (2022), Vol 56, pages 9092-9102, doi: 10.1021/acs.est.2c01123

Florence Schubotz, Michael Seidel and I designed the study. Florence Schubotz collected the samples in 2006 and 2015. The 4-week incubation experiment was part of a former master thesis, where FT-ICR-MS data was generated. During this PhD, I re-processed all measurements by FT-ICR-MS and re-measured and processed CDOM and FDOM data and re-modeled the PARAFAC model. I performed laboratory work for determining DBC and DOS concentrations and the isotopic composition of DOM, analyzed data and performed statistical analysis with input from Florence Schubotz and Michael Seidel. I performed the calculations on global release of DOS and DBC and ^{14}C modeling of oceanic DBC. I wrote the first draft, which was revised by Florence Schubotz and Michael Seidel and then finalized with inputs from Thorsten Dittmar and Jutta Niggemann.

Chapter III: Effects of hydrothermal heating on porewater dissolved organic matter in Guaymas Basin sediments

Jonas Brünjes, Michael Seidel, Andreas Teske, Florence Schubotz

In preparation for *Limnology and Oceanography*

Florence Schubotz, Michael Seidel and I designed the research. I performed the laboratory work and analyzed samples collected in 2018 by Thorsten Brinkhoff. Measurements by FT-ICR-MS were carried out by Michael Seidel and me. I performed data processing, statistical analysis, PARAFAC modeling, prepared figures and defined the story-line of this paper with inputs from Florence Schubotz and Michael Seidel. I performed the additional elution of DOM by dichloromethane and compared fluorescent DOM of the extracts with bulk waters to assess potential reasons for low extraction efficiencies. I wrote the manuscript, which was revised by Florence Schubotz, Michael Seidel and finalized with inputs from Andreas Teske.

Chapter IV: Hydrothermal sediments are a potential source of recalcitrant dissolved black carbon and dissolved organic sulfur in the Guaymas Basin

Jonas Brünjes, Michael Seidel, Andreas Teske, Kai-Uwe Hinrichs, Florence Schubotz

In preparation for *Geophysical Research Letters*

Florence Schubotz, Michael Seidel and I designed the research with significant input regarding the hot-water extractions by Kai-Uwe Hinrichs. I performed the laboratory work and analyzed samples collected in 2018 by Thorsten Brinkhoff. Measurements by FT-ICR-MS were carried out by Michael Seidel and me. I performed data processing, statistical analysis, prepared figures and defined the story-line of this paper with inputs from Florence Schubotz and Michael Seidel. Initial results were discussed with Florence Schubotz and Michael Seidel. I wrote the manuscript, which was first revised by Florence Schubotz and Michael Seidel and finalized with inputs from Andreas Teske.

VII. References

Abdulla H. A., Burdige D. J. and Komada T. (2018) Accumulation of deaminated peptides in anoxic sediments of Santa Barbara Basin. *Geochimica et Cosmochimica Acta* **223**, 245-258.

Abdulla H. A., Burdige D. J. and Komada T. (2019) Abiotic Formation of Dissolved Organic Sulfur in Anoxic Sediments of Santa Barbara Basin. *Organic Geochemistry* **139**, 103879.

Alvin Framegrabber (2023) http://4dgeo.whoi.edu/alvin Last accessed: 12.01.2023.

Amaral V., Romera-Castillo C. and Forja J. (2021) Submarine mud volcanoes as a source of chromophoric dissolved organic matter to the deep waters of the Gulf of Cádiz. *Scientific Reports* **11**, 3200.

Amon R. M. and Benner R. (1996) Bacterial utilization of different size classes of dissolved organic matter. *Limnology and Oceanography* **41**, 41-51.

Bekins B., Brennan J., Tillitt D., Cozzarelli I., Illig J. and Martinovic-Weigelt D. (2020) Biological Effects of Hydrocarbon Degradation Intermediates: Is the Total Petroleum Hydrocarbon Analytical Method Adequate for Risk Assessment? *Environmental Science & Technology* **54,** 11396-11404.

Beyer J., Trannum H. C., Bakke T., Hodson P. V. and Collier T. K. (2016) Environmental effects of the Deepwater Horizon oil spill: A review. *Marine Pollution Bulletin* **110**, 28-51.

Bianchi T. S., Osburn C., Shields M. R., Yvon-Lewis S., Young J., Guo L. and Zhou Z. (2014) Deepwater Horizon Oil in Gulf of Mexico Waters after 2 Years: Transformation into the Dissolved Organic Matter Pool. *Environmental Science & Technology* **48**, 9288-9297.

Boehm P. D. and Quinn J. G. (1973) Solubilization of hydrocarbons by the dissolved organic matter in sea water. *Geochimica et Cosmochimica Acta* **37**, 2459-2477.

Bohrmann G., Spiess V. and participants a. c. (2008) *Report and preliminary results of R/V Meteor Cruise M67/2a and 2b, Balboa - Tampico - Bridgetown,*. University Bremen, Bremen.

Bro R. (1997) PARAFAC. Tutorial and applications. *Chemometrics and intelligent laboratory systems* **38**, 149-171.

Brünjes J., Seidel M., Dittmar T., Niggemann J. and Schubotz F. (2022) Natural Asphalt Seeps Are Potential Sources for Recalcitrant Oceanic Dissolved Organic Sulfur and Dissolved Black Carbon. *Environmental Science & Technology* **56**, 9092-9102.

Brussaard C. P. D., Peperzak L., Beggah S., Wick L. Y., Wuerz B., Weber J., Samuel Arey J., van der Burg B., Jonas A., Huisman J. and van der Meer J. R. (2016) Immediate ecotoxicological effects of short-lived oil spills on marine biota. *Nature Communications* **7**, 11206.

Burdige D. J. and Komada T. (2015) Chapter 12 - Sediment Pore Waters. In *Biogeochemistry of Marine Dissolved Organic Matter (Second Edition)* (eds. D. A. Hansell and C. A. Carlson). Academic Press, Boston. pp. 535-577.

Calvert S. E. (1966) Origin of Diatom-Rich, Varved Sediments from the Gulf of California. *The Journal of Geology* **74**, 546-565.

Chanton J. P., Jaggi A., Radović J. R., Rosenheim B. E., Walker B. D., Larter S. R., Rogers K., Bosman S. and Oldenburg T. B. (2020) Mapping Isotopic and Dissolved Organic Matter Baselines in Waters and Sediments of the Gulf of Mexico. In *Scenarios and Responses to Future Deep Oil Spills*. Springer. pp. 160-181.

Chen B., Huang W., Ma S., Feng M., Liu C., Gu X. and Chen K. (2018) Characterization of Chromophoric Dissolved Organic Matter in the Littoral Zones of Eutrophic Lakes Taihu and Hongze during the Algal Bloom Season. *Water* **10**, 861.

Chen R. F. and Bada J. L. (1994) The fluorescence of dissolved organic matter in porewaters of marine sediments. *Marine chemistry* **45**, 31-42.

Coble P. (1996) Characterization of Marine and Terrestrial DOM in Seawater Using Excitation–Emission Matrix Spectroscopy. *Marine Chemistry* **51**, 325-346.

Comisarow M. B. and Marshall A. G. (1974) Fourier transform ion cyclotron resonance spectroscopy. *Chemical Physics Letters* **25**, 282-283.

Coppola A. I. and Druffel E. R. M. (2016) Cycling of black carbon in the ocean. *Geophysical Research Letters* **43**, 4477-4482.

Coppola A. I., Ziolkowski L. A., Masiello C. A. and Druffel E. R. M. (2014) Aged black carbon in marine sediments and sinking particles. *Geophysical Research Letters* **41**, 2427-2433.

Coppola A. I., Wagner S., Lennartz S. T., Seidel M., Ward N. D., Dittmar T., Santín C. and Jones M. W. (2022) The black carbon cycle and its role in the Earth system. *Nature Reviews Earth & Environment* 10.1038/s43017-022-00316-6.

Coppola A. I., Seidel M., Ward N. D., Viviroli D., Nascimento G. S., Haghipour N., Revels B. N., Abiven S., Jones M. W. and Richey J. E. (2019) Marked isotopic variability within and between the Amazon River and marine dissolved black carbon pools. *Nature communications* **10**, 1-8.

Corilo Y. E., Podgorski D. C., McKenna A. M., Lemkau K. L., Reddy C. M., Marshall A. G. and Rodgers R. P. (2013) Oil Spill Source Identification by Principal Component Analysis of Electrospray Ionization Fourier Transform Ion Cyclotron Resonance Mass Spectra. *Analytical Chemistry* **85**, 9064-9069.

D'Andrilli J., Cooper W. T., Foreman C. M. and Marshall A. G. (2015) An ultrahigh-resolution mass spectrometry index to estimate natural organic matter lability. *Rapid Communications in Mass Spectrometry* **29**, 2385-2401.

D'souza N., Subramaniam A., Juhl A. R., Hafez M., Chekalyuk A., Phan S., Yan B., MacDonald I., Weber S. and Montoya J. (2016) Elevated surface chlorophyll associated with natural oil seeps in the Gulf of Mexico. *Nature Geoscience* **9**, 215.

Das N. and Chandran P. (2011) Microbial Degradation of Petroleum Hydrocarbon Contaminants: An Overview. *Biotechnology Research International* **2011**.

Degens E. T. (1969) Biogeochemistry of Stable Carbon Isotopes. In *Organic Geochemistry: Methods and Results* (eds. G. Eglinton and M. T. J. Murphy). Springer Berlin Heidelberg, Berlin, Heidelberg. pp. 304-329.

Derrien M., Shin K.-H. and Hur J. (2019) Biodegradation-induced signatures in sediment pore water dissolved organic matter: Implications from artificial sediments composed of two contrasting sources. *Science of The Total Environment* **694**, 133714.

Didyk B. M. and Simoneit B. R. (1989) Hydrothermal oil of Guaymas Basin and implications for petroleum formation mechanisms. *Nature* **342**, 65.

Didyk B. M. and Simoneit B. R. T. (1990) Petroleum characteristics of the oil in a Guaymas Basin hydrothermal chimney. *Applied Geochemistry* **5**, 29-40.

Dittmar T. (2008) The molecular level determination of black carbon in marine dissolved organic matter. *Organic Geochemistry* **39**, 396-407.

Dittmar T. (2015) Chapter 7 - Reasons Behind the Long-Term Stability of Dissolved Organic Matter. In *Biogeochemistry of Marine Dissolved Organic Matter (Second Edition)* (eds. D. A. Hansell and C. A. Carlson). Academic Press, Boston. pp. 369-388.

Dittmar T. and Koch B. P. (2006) Thermogenic organic matter dissolved in the abyssal ocean. *Marine Chemistry* **102**, 208-217.

Dittmar T. and Paeng J. (2009) A heat-induced molecular signature in marine dissolved organic matter. *Nature Geoscience* **2**, 175.

Dittmar T. and Stubbins A. (2014) 12.6 - Dissolved Organic Matter in Aquatic Systems A2 - Holland, Heinrich D. In *Treatise on Geochemistry (Second Edition)* (ed. K. K. Turekian). Elsevier, Oxford. pp. 125-156.

Dittmar T., Koch B., Hertkorn N. and Kattner G. (2008) A simple and efficient method for the solid-phase extraction of dissolved organic matter (SPE-DOM) from seawater. *Limnology and Oceanography: Methods* **6**, 230-235.

Dittmar T., Stubbins A., Ito T. and Jones D. C. (2017) Comment on “Dissolved organic sulfur in the ocean: Biogeochemistry of a petagram inventory”. *Science* **356**, 813-813.

Dittmar T., Lennartz S. T., Buck-Wiese H., Hansell D. A., Santinelli C., Vanni C., Blasius B. and Hehemann J.-H. (2021) Enigmatic persistence of dissolved organic matter in the ocean. *Nature Reviews Earth & Environment* **2**, 570-583.

Dong Y., Liu Y., Hu C., MacDonald I. R. and Lu Y. (2022) Chronic oiling in global oceans. *Science* **376**, 1300-1304.

Dvorski S. E. M., Gonsior M., Hertkorn N., Uhl J., Müller H., Griebler C. and Schmitt-Kopplin P. (2016) Geochemistry of Dissolved Organic Matter in a Spatially Highly Resolved Groundwater Petroleum Hydrocarbon Plume Cross-Section. *Environmental Science & Technology* **50**, 5536-5546.

Einsele G., Gieskes J. M., Curray J., Moore D. M., Aguayo E., Aubry M.-P., Fornari D., Guerrero J., Kastner M., Kelts K., Lyle M., Matoba Y., Molina-Cruz A., Niemitz J., Rueda J., Saunders A., Schrader H., Simoneit B. and Vacquier V. (1980) Intrusion of basaltic sills into highly porous sediments, and resulting hydrothermal activity. *Nature* **283**, 441-445.

Flerus R., Lechtenfeld O., Koch B. P., McCallister S., Schmitt-Kopplin P., Benner R., Kaiser K. and Kattner G. (2012) A molecular perspective on the ageing of marine dissolved organic matter. *Biogeosciences* **9**, 1935-1955.

Fujikura K., Yamanaka T., Sumida P. Y. G., Bernardino A. F., Pereira O. S., Kanehara T., Nagano Y., Nakayama C. R., Nobrega M., Pellizari V. H., Shigeno S., Yoshida T., Zhang J. and Kitazato H. (2017) Discovery of asphalt seeps in the deep Southwest Atlantic off Brazil. *Deep Sea Research Part II: Topical Studies in Oceanography* **146**, 35-44.

Gan S., Schmidt F., Heuer V. B., Goldhammer T., Witt M. and Hinrichs K.-U. (2020) Impacts of redox conditions on dissolved organic matter (DOM) quality in marine sediments off the River Rhône, Western Mediterranean Sea. *Geochimica et Cosmochimica Acta* **276**, 151-169.

Goldberg E. D. (1985) Black carbon in the environment: properties and distribution.

Gomez-Saez G., Dittmar T., Holtappels M., Pohlabeln A., Schnetger B. and Niggemann J. (2021) Sulfurization of dissolved organic matter in the anoxic water column of the Black Sea. *Science Advances* **7**, eabf6199.

Gomez-Saez G. V., Pohlabeln A. M., Stubbins A., Marsay C. M. and Dittmar T. (2017) Photochemical alteration of dissolved organic sulfur from sulfidic porewater. *Environmental science & technology* **51**, 14144-14154.

Gomez-Saez G. V., Niggemann J., Dittmar T., Pohlabeln A. M., Lang S. Q., Noowong A., Pichler T., Wörmer L. and Bühring S. I. (2016) Molecular evidence for abiotic sulfurization of dissolved organic matter in marine shallow hydrothermal systems. *Geochimica et Cosmochimica Acta* **190**, 35-52.

Goranov A. I., Schaller M. F., Long J. A., Podgorski D. C. and Wagner S. (2021) Characterization of Asphaltenes and Petroleum Using Benzenepolycarboxylic Acids (BPCAs) and Compound-Specific Stable Carbon Isotopes. *Energy & Fuels* **35**, 18135-18145.

Green N. W., Perdue E. M., Aiken G. R., Butler K. D., Chen H., Dittmar T., Niggemann J. and Stubbins A. (2014) An intercomparison of three methods for the large-scale isolation of oceanic dissolved organic matter. *Marine Chemistry* **161**, 14-19.

Gros J., Socolofsky S. A., Dissanayake A. L., Jun I., Zhao L., Boufadel M. C., Reddy C. M. and Arey J. S. (2017) Petroleum dynamics in the sea and influence of subsea dispersant injection during Deepwater Horizon. *Proceedings of the National Academy of Sciences* **114**, 10065-10070.

Hansell D. A. (2013) Recalcitrant dissolved organic carbon fractions. *Annual review of marine science* **5**, 421-445.

Hansell D. A., Carlson C. A., Repeta D. J. and Schlitzer R. (2009) Dissolved organic matter in the ocean: A controversy stimulates new insights. *Oceanography* **22**, 202-211.

Hansen C., Kleint C., Böhnke-Brandt S., Klose L., Adam-Beyer N., Sass K., Zitoun R., Sander S., Indenbirken D., Dittmar T., Koschinsky A. and Perner M. (2022) Impact of high Fe-concentrations on microbial community structure and dissolved organics in hydrothermal plumes: an experimental study. *Scientific Reports* **12**.

Harriman B. H., Zito P., Podgorski D. C., Tarr M. A. and Suflita J. M. (2017) Impact of photooxidation and biodegradation on the fate of oil spilled during the Deepwater Horizon Incident: Advanced stages of weathering. *Environmental science & technology* **51**, 7412-7421.

Hawkes J., Hansen C., Goldhammer T., Bach W. and Dittmar T. (2015a) Molecular alteration of marine dissolved organic matter under experimental hydrothermal conditions. *Geochimica et Cosmochimica Acta* **175**.

Hawkes J. A., Rossel P. E., Stubbins A., Butterfield D., Connelly D. P., Achterberg E. P., Koschinsky A., Chavagnac V., Hansen C. T., Bach W. and Dittmar T. (2015b) Efficient removal of recalcitrant deep-ocean dissolved organic matter during hydrothermal circulation. *Nature Geoscience* **8**, 856-860.

Head I. M., Jones D. M. and Larter S. R. (2003) Biological activity in the deep subsurface and the origin of heavy oil. *Nature* **426**, 344-352.

Hedges J. (1988) Polymerization of humic substances in natural environments. *Humic substances and their role in the environment*, 605-625.

Hedges J. I., Hu F. S., Devol A. H., Hartnett H. E., Tsamakis E. and Keil R. G. (1999) Sedimentary organic matter preservation; a test for selective degradation under oxic conditions. *American Journal of Science* **299**, 529-555.

Hegazi A. H., Fathalla E. M., Panda S. K., Schrader W. and Andersson J. T. (2012) High-molecular weight sulfur-containing aromatics refractory to weathering as determined by Fourier transform ion cyclotron resonance mass spectrometry. *Chemosphere* **89**, 205-212.

Helms J. R., Stubbins A., Ritchie J. D., Minor E. C., Kieber D. J. and Mopper K. (2008) Absorption spectral slopes and slope ratios as indicators of molecular weight, source, and photobleaching of chromophoric dissolved organic matter. *Limnology and Oceanography* **53**, 955-969.

Hertkorn N., Harir M., Cawley K. M., Schmitt-Kopplin P. and Jaffé R. (2016) Molecular characterization of dissolved organic matter from subtropical wetlands: a comparative study through the analysis of optical properties, NMR and FTICR/MS. *Biogeosciences* **13**, 2257-2277.

Hertkorn N., Benner R., Frommberger M., Schmitt-Kopplin P., Witt M., Kaiser K., Kettrup A. and Hedges J. I. (2006) Characterization of a major refractory component of marine dissolved organic matter. *Geochimica et Cosmochimica Acta* **70**, 2990-3010.

Hertkorn N., Ruecker C., Meringer M., Gugisch R., Frommberger M., Perdue E. M., Witt M. and Schmitt-Kopplin P. (2007) High-precision frequency measurements: indispensable tools at the core of the molecular-level analysis of complex systems. *Anal Bioanal Chem* **389**, 1311-1327.

Huguet A., Vacher L., Relexans S., Saubusse S., Froidefond J. M. and Parlanti E. (2009) Properties of fluorescent dissolved organic matter in the Gironde Estuary. *Organic Geochemistry* **40**, 706-719.

Incardona J. P., Gardner L. D., Linbo T. L., Brown T. L., Esbaugh A. J., Mager E. M., Stieglitz J. D., French B. L., Labenia J. S., Laetz C. A., Tagal M., Sloan C. A., Elizur A., Benetti D. D., Grosell M., Block B. A. and Scholz N. L. (2014) Deepwater Horizon crude oil impacts the developing hearts of large predatory pelagic fish. *Proceedings of the National Academy of Sciences* **111**, E1510-E1518.

Islam A., Ahmed A., Hur M., Thorn K. and Kim S. (2016) Molecular-level evidence provided by ultrahigh resolution mass spectrometry for oil-derived DOC in groundwater at Bemidji, Minnesota. *Journal of hazardous materials* **320**, 123-132.

ITRC (2023) TPH Risk Evaluation at Petroleum-Contaminated Sites. https://tphrisk-1.itrcweb.org/ Last accessed: 11.01.2023.

Jaffé R., Ding Y., Niggemann J., Vähätalo A. V., Stubbins A., Spencer R. G., Campbell J. and Dittmar T. (2013) Global charcoal mobilization from soils via dissolution and riverine transport to the oceans. *Science* **340**, 345-347.

Jannasch H. W., Nelson D. C. and Wirsen C. O. (1989) Massive natural occurrence of unusually large bacteria (Beggiatoa sp.) at a hydrothermal deep-sea vent site. *Nature* **342**, 834-836.

Jiao N., Herndl G. J., Hansell D. A., Benner R., Kattner G., Wilhelm S. W., Kirchman D. L., Weinbauer M. G., Luo T., Chen F. and Azam F. (2010) Microbial production of recalcitrant dissolved organic matter: long-term carbon storage in the global ocean. *Nat Rev Microbiol* **8**, 593-599.

Jones D. O. B., Walls A., Clare M., Fiske M. S., Weiland R. J., O'Brien R. and Touzel D. F. (2014) Asphalt mounds and associated biota on the Angolan margin. *Deep Sea Research Part I: Oceanographic Research Papers* **94**, 124-136.

Kappenberg A., Bläsing M., Lehndorff E. and Amelung W. (2016) Black carbon assessment using benzene polycarboxylic acids: Limitations for organic-rich matrices. *Organic Geochemistry* **94**, 47-51.

Karl D. M. and Björkman K. M. (2015) Dynamics of dissolved organic phosphorus. In *Biogeochemistry of marine dissolved organic matter*. Elsevier. pp. 233-334.

Kawka O. E. and Simoneit B. R. T. (1994) Hydrothermal pyrolysis of organic matter in Guaymas Basin: I. Comparison of hydrocarbon distributions in subsurface sediments and seabed petroleums. *Organic Geochemistry* **22**, 947-978.

Kim S., Kramer R. W. and Hatcher P. G. (2003) Graphical method for analysis of ultrahigh-resolution broadband mass spectra of natural organic matter, the van Krevelen diagram. *Analytical Chemistry* **75**, 5336-5344.

Kleindienst S., Seidel M., Ziervogel K., Grim S., Loftis K., Harrison S., Malkin S. Y., Perkins M. J., Field J., Sogin M. L., Dittmar T., Passow U., Medeiros P. M. and Joye S. B. (2015) Chemical dispersants can suppress the activity of natural oil-degrading microorganisms. *Proceedings of the National Academy of Sciences* **112**, 14900-14905.

Koch B. P. and Dittmar T. (2006) From mass to structure: an aromaticity index for high-resolution mass data of natural organic matter. *Rapid Communications in Mass Spectrometry* **20**, 926-932.

Koch B. P. and Dittmar T. (2016) From mass to structure: an aromaticity index for high-resolution mass data of natural organic matter. *Rapid Communications in Mass Spectrometry* **30**, 250-250.

Kohnen M. E. L., Damsté J. S. S., ten Haven H. L. and de Leeuw J. W. (1989) Early incorporation of polysulphides in sedimentary organic matter. *Nature* **341**, 640-641.

Kok M. D., Schouten S. and Sinninghe Damsté J. S. (2000) Formation of insoluble, nonhydrolyzable, sulfur-rich macromolecules via incorporation of inorganic sulfur species into algal carbohydrates. *Geochimica et Cosmochimica Acta* **64**, 2689-2699.

Korak J. A., Dotson A. D., Summers R. S. and Rosario-Ortiz F. L. (2014) Critical analysis of commonly used fluorescence metrics to characterize dissolved organic matter. *Water Research* **49**, 327-338.

Korsten H. (1997) Characterization of hydrocarbon systems by DBE concept. *AIChE Journal* **43**, 1559-1568.

Kropp K. G. and Fedorak P. M. (1998) A review of the occurrence, toxicity,and biodegradation of condensed thiophenes found in petroleum. *Canadian Journal of Microbiology* **44**, 605-622.

Ksionzek K. B., Lechtenfeld O. J., McCallister S. L., Schmitt-Kopplin P., Geuer J. K., Geibert W. and Koch B. P. (2016) Dissolved organic sulfur in the ocean: Biogeochemistry of a petagram inventory. *Science* **354**, 456-459.

Kujawinski E. (2002) Electrospray Ionization Fourier Transform Ion Cyclotron Resonance Mass Spectrometry (ESI FT-ICR MS): Characterization of Complex Environmental Mixtures. *Environmental Forensics* **3**, 207-216.

Kujawinski E. B. (2011) The impact of microbial metabolism on marine dissolved organic matter. *Ann Rev Mar Sci* **3**, 567-599.

Kurek M. R., Harir M., Shukle J. T., Schroth A. W., Schmitt-Kopplin P. and Druschel G. K. (2020) Chemical fractionation of organic matter and organic phosphorus extractions from freshwater lake sediment. *Analytica Chimica Acta* **1130**, 29-38.

Kvenvolden K. A. and Simoneit B. R. (1990) Hydrothermally Derived Petroleum: Examples from Guaymas Basin, Gulf of California, and Escanaba Trough, Northeast Pacific Ocean (1). *AAPG Bulletin* **74**, 223-237.

Kvenvolden K. A. and Cooper C. K. (2003) Natural seepage of crude oil into the marine environment. *Geo-Marine Letters* **23**, 140-146.

Laane R. and Koole L. (1982) The relation between fluorescence and dissolved organic carbon in the Ems-Dollart estuary and the western Wadden Sea. *Netherlands Journal of Sea Research* **15**, 217-227.

LaRowe D. E. and Van Cappellen P. (2011) Degradation of natural organic matter: A thermodynamic analysis. *Geochimica et Cosmochimica Acta* **75**, 2030-2042.

Lawaetz A. J. and Stedmon C. A. (2009) Fluorescence Intensity Calibration Using the Raman Scatter Peak of Water. *Applied Spectroscopy* **63**, 936-940.

Lemkau K. L., McKenna A. M., Podgorski D. C., Rodgers R. P. and Reddy C. M. (2014) Molecular evidence of heavy-oil weathering following the M/V Cosco Busan spill: insights from Fourier transform ion cyclotron resonance mass spectrometry. *Environmental science & technology* **48**, 3760-3767.

Lennartz S. T. and Dittmar T. (2022) Controls on turnover of marine dissolved organic matter—testing the null hypothesis of purely concentration-driven uptake: Comment on Shen and Benner, “Molecular properties are a primary control on the microbial utilization of dissolved organic matter in the ocean”. *Limnology and Oceanography* **67**, 673-679.

Liang Z., McCabe K., Fawcett S. E., Forrer H. J., Hashihama F., Jeandel C., Marconi D., Planquette H., Saito M. A., Sohm J. A., Thomas R. K., Letscher R. T. and Knapp A. N. (2022) A global ocean dissolved organic phosphorus concentration database (DOPv2021). *Scientific Data* **9**, 772.

Lin Y.-S., Koch B., Feseker T., Ziervogel K., Goldhammer T., Schmidt F., Witt M., Kellermann M., Zabel M., Teske A. and Hinrichs K.-U. (2017) Near-surface Heating of Young Rift Sediment Causes Mass Production and Discharge of Reactive Dissolved Organic Matter. *Scientific Reports* **7**, 44864.

Lin Y.-S., Koch B. P., Feseker T., Ziervogel K., Goldhammer T., Schmidt F., Witt M., Kellermann M. Y., Zabel M., Teske A. P. and Hinrichs K.-U. (2020) Sedimentary dissolved organic matter of the Guaymas Basin. PANGAEA.

Liu W., Liao Y., Shi Q., Hsu C. S., Jiang B. and Peng P. a. (2018) Origin of polar organic sulfur compounds in immature crude oils revealed by ESI FT-ICR MS. *Organic Geochemistry* **121**, 36-47.

Liu Y. and Kujawinski E. B. (2015) Chemical Composition and Potential Environmental Impacts of Water-Soluble Polar Crude Oil Components Inferred from ESI FT-ICR MS. *PLOS ONE* **10**, e0136376.

Liu Y., White H. K., Simister R. L., Waite D., Lyons S. L. and Kujawinski E. B. (2020) Probing the chemical transformation of seawater-soluble crude oil components during microbial oxidation. *ACS Earth and Space Chemistry* **4**, 690-701.

Lizarralde D., Soule S. A., Seewald J. S. and Proskurowski G. (2011) Carbon release by off-axis magmatism in a young sedimented spreading centre. *Nature Geoscience* **4**, 50-54.

Longnecker K., Oswald L., Kido Soule M. C., Cutter G. A. and Kujawinski E. B. (2020) Organic sulfur: A spatially variable and understudied component of marine organic matter. *Limnology and Oceanography Letters* **5**, 305-312.

Lonsdale P. and Becker K. (1985) Hydrothermal plumes, hot springs, and conductive heat flow in the Southern Trough of Guaymas Basin. *Earth and Planetary Science Letters* **73**, 211-225.

Lorenzo-Seva U. and Ten Berge J. M. (2006) Tucker's congruence coefficient as a meaningful index of factor similarity. *Methodology* **2**, 57-64.

Lübcke-von Varel U., Machala M., Ciganek M., Neca J., Pencikova K., Palkova L., Vondracek J., Löffler I., Streck G., Reifferscheid G., Flückiger-Isler S., Weiss J. M., Lamoree M. and Brack W. (2011) Polar Compounds Dominate in Vitro Effects of Sediment Extracts. *Environmental Science & Technology* **45**, 2384-2390.

MacDonald I., Bohrmann G., Escobar E., Abegg F., Blanchon P., Blinova V., Brückmann W., Drews M., Eisenhauer A., Han X., Heeschen K., Meier F., Mortera C., Naehr T., Orcutt B., Bernard B., Brooks J. and de Faragó M. (2004) Asphalt Volcanism and Chemosynthetic Life in the Campeche Knolls, Gulf of Mexico. *Science* **304**, 999-1002.

MacDonald I. R., Garcia-Pineda O., Beet A., Daneshgar Asl S., Feng L., Graettinger G., French-McCay D., Holmes J., Hu C., Huffer F., Leifer I., Muller-Karger F., Solow A., Silva M. and Swayze G. (2015) Natural and unnatural oil slicks in the Gulf of Mexico. *Journal of Geophysical Research: Oceans* **120**, 8364-8380.

Macgregor D. S. (1993) Relationships between seepage, tectonics and subsurface petroleum reserves. *Marine and Petroleum Geology* **10**, 606-619.

Mara P., Nelson R. K., Reddy C. M., Teske A. and Edgcomb V. P. (2022) Sterane and hopane biomarkers capture microbial transformations of complex hydrocarbons in young hydrothermal Guaymas Basin sediments. *Communications Earth & Environment* **3**, 250.

Marcon Y., Sahling H., MacDonald I. R., Wintersteller P., dos Santos Ferreira C. and Bohrmann G. (2018) Slow Volcanoes. The Intriguing Similarities Between Marine Asphalt and Basalt Lavas. *Oceanography* **31**, 194-205.

Marshall A. G. and Rodgers R. P. (2008) Petroleomics: Chemistry of the underworld. *Proceedings of the National Academy of Sciences* **105**, 18090-18095.

Martens C. S. (1990) Generation of short chain acid anions in hydrothermally altered sediments of the Guaymas Basin, Gulf of California. *Applied Geochemistry* **5**, 71-76.

Masiello C. and Druffel E. (1998) Black carbon in deep-sea sediments. *Science* **280**, 1911-1913.

Mayer L. M. (1994) Relationships between mineral surfaces and organic carbon concentrations in soils and sediments. *Chemical Geology* **114**, 347-363.

McCollom T. M. and Seewald J. S. (2003) Experimental study of the hydrothermal reactivity of organic acids and acid anions: II. Acetic acid, acetate, and valeric acid. *Geochimica et Cosmochimica Acta* **67**, 3645-3664.

McKay L., Klokman V. W., Mendlovitz H. P., LaRowe D. E., Hoer D. R., Albert D., Amend J. P. and Teske A. (2016) Thermal and geochemical influences on microbial biogeography in the hydrothermal sediments of G uaymas B asin, G ulf of C alifornia. *Environmental microbiology reports* **8**, 150-161.

McKay L. J., MacGregor B. J., Biddle J. F., Albert D. B., Mendlovitz H. P., Hoer D. R., Lipp J. S., Lloyd K. G. and Teske A. P. (2012) Spatial heterogeneity and underlying geochemistry of phylogenetically diverse orange and white Beggiatoa mats in Guaymas Basin hydrothermal sediments. *Deep Sea Research Part I: Oceanographic Research Papers* **67**, 21-31.

McKenna A. M., Nelson R. K., Reddy C. M., Savory J. J., Kaiser N. K., Fitzsimmons J. E., Marshall A. G. and Rodgers R. P. (2013) Expansion of the Analytical Window for Oil Spill Characterization by Ultrahigh Resolution Mass Spectrometry: Beyond Gas Chromatography. *Environmental Science & Technology* **47**, 7530-7539.

McKnight D. M., Boyer E. W., Westerhoff P. K., Doran P. T., Kulbe T. and Andersen D. T. (2001) Spectrofluorometric characterization of dissolved organic matter for indication of precursor organic material and aromaticity. *Limnology and Oceanography* **46**, 38-48.

Meckenstock R. U., von Netzer F., Stumpp C., Lueders T., Himmelberg A. M., Hertkorn N., Schmitt-Kopplin P., Harir M., Hosein R., Haque S. and Schulze-Makuch D. (2014) Water droplets in oil are microhabitats for microbial life. *Science* **345**, 673-676.

Melbye A. G., Brakstad O. G., Hokstad J. N., Gregersen I. K., Hansen B. H., Booth A. M., Rowland S. J. and Tollefsen K. E. (2009) Chemical and toxicological characterization of an unresolved complex mixture-rich biodegraded crude oil. *Environmental Toxicology and Chemistry: An International Journal* **28**, 1815-1824.

Merder J., Freund J. A., Feudel U., Hansen C. T., Hawkes J. A., Jacob B., Klaproth K., Niggemann J., Noriega-Ortega B. E., Osterholz H., Rossel P. E., Seidel M., Singer G., Stubbins A., Waska H. and Dittmar T. (2020) ICBM-OCEAN: Processing ultrahigh-resolution mass spectrometry data of complex molecular mixtures. *Analytical Chemistry* **92**, 6832-6838.

Middelburg J. J., Nieuwenhuize J. and van Breugel P. (1999) Black carbon in marine sediments. *Marine Chemistry* **65**, 245-252.

Mitschke N. (2022) NMR spectroscopy of dissolved organic matter: a review. *Environmental Chemistry Letters* 10.1007/s10311-022-01528-4, 1-35.

Murphy K. R., Stedmon C. A., Graeber D. and Bro R. (2013) Fluorescence spectroscopy and multi-way techniques. PARAFAC. *Analytical Methods* **5**, 6557-6566.

Murphy K. R., Stedmon C. A., Wenig P. and Bro R. (2014) OpenFluor– an online spectral library of auto-fluorescence by organic compounds in the environment. *Analytical Methods* **6**, 658-661.

Murphy K. R., Timko S. A., Gonsior M., Powers L. C., Wünsch U. J. and Stedmon C. A. (2018) Photochemistry Illuminates Ubiquitous Organic Matter Fluorescence Spectra. *Environmental Science & Technology* **52**, 11243-11250.

Naehr T. H., Birgel D., Bohrmann G., MacDonald I. R. and Kasten S. (2009) Biogeochemical controls on authigenic carbonate formation at the Chapopote “asphalt volcano”, Bay of Campeche. *Chemical Geology* **266**, 390-402.

Newson R. (2002) Parameters behind “Nonparametric” Statistics: Kendall's tau, Somers’ D and Median Differences. *The Stata Journal* **2**, 45-64.

Ni Z., Huang D., Xiao M., Liu X. and Wang S. (2022) Molecular weight driving bioavailability and intrinsic degradation mechanisms of dissolved organic phosphorus in lake sediment. *Water Research* **210**, 117951.

Noowong A., Gomez-Saez G. V., Hansen C. T., Schwarz-Schampera U., Koschinsky A. and Dittmar T. (2021) Imprint of Kairei and Pelagia deep-sea hydrothermal systems (Indian Ocean) on marine dissolved organic matter. *Organic Geochemistry* **152**, 104141.

Noriega-Ortega B. E., Wienhausen G., Mentges A., Dittmar T., Simon M. and Niggemann J. (2019) Does the Chemodiversity of Bacterial Exometabolomes Sustain the Chemodiversity of Marine Dissolved Organic Matter? *Frontiers in Microbiology* **10**.

NRC (2003) *National Research Council. Oil in the sea III: inputs, fates, and effects*. National Academies Press (US).

Ohno T. (2002) Fluorescence inner-filtering correction for determining the humification index of dissolved organic matter. *Environmental science & technology* **36**, 742-746.

Oksanen, Simpson G and Blanchet F K. R., Legendre P, Minchin P, O'Hara R, Solymos P, Stevens M, Szoecs E, Wagner H, Barbour M, Bedward M, Bolker B, Borcard D, Carvalho G, Chirico M, De Caceres M, Durand S, Evangelista H, FitzJohn R, Friendly M, Furneaux B, Hannigan G, Hill M, Lahti L, McGlinn D, Ouellette M, Ribeiro Cunha E, Smith T, Stier A, Ter Braak C, Weedon J (2022) vegan: Community Ecology Package.

Ondréas H., Scalabrin C., Fouquet Y. and Godfroy A. (2018) Recent high-resolution mapping of Guaymas hydrothermal fields (Southern Trough). *BSGF - Earth Sci. Bull.* **189**, 6.

Osterholz H., Dittmar T. and Niggemann J. (2014) Molecular evidence for rapid dissolved organic matter turnover in Arctic fjords. *Marine Chemistry* **160**, 1-10.

Osterholz H., Kirchman D. L., Niggemann J. and Dittmar T. (2016) Environmental Drivers of Dissolved Organic Matter Molecular Composition in the Delaware Estuary. *Frontiers in Earth Science* **4**.

Osterholz H., Turner S., Alakangas L. J., Tullborg E.-L., Dittmar T., Kalinowski B. E. and Dopson M. (2022) Terrigenous dissolved organic matter persists in the energy-limited deep groundwaters of the Fennoscandian Shield. *Nature Communications* **13**, 4837.

Otte J. M., Blackwell N., Soos V., Rughöft S., Maisch M., Kappler A., Kleindienst S. and Schmidt C. (2018) Sterilization impacts on marine sediment---Are we able to inactivate microorganisms in environmental samples? *FEMS Microbiology Ecology* **94**.

Paduan J. B., Zierenberg R. A., Clague D. A., Spelz R. M., Caress D. W., Troni G., Thomas H., Glessner J., Lilley M. D., Lorenson T., Lupton J., Neumann F., Santa Rosa-del Rio M. A. and Wheat C. G. (2018) Discovery of Hydrothermal Vent Fields on Alarcón Rise and in Southern Pescadero Basin, Gulf of California. *Geochemistry, Geophysics, Geosystems* **19**, 4788-4819.

Pante E. and Simon-Bouhet B. (2013) marmap: A Package for Importing, Plotting and Analyzing Bathymetric and Topographic Data in R. *PLOS ONE* **8**, e73051.

Parlanti E., Wörz K., Geoffroy L. and Lamotte M. (2000) Dissolved organic matter fluorescence spectroscopy as a tool to estimate biological activity in a coastal zone submitted to anthropogenic inputs. *Organic geochemistry* **31**, 1765-1781.

Passow U. (2016) Formation of rapidly-sinking, oil-associated marine snow. *Deep Sea Research Part II: Topical Studies in Oceanography* **129**, 232-240.

Passow U. and Stout S. A. (2020) Character and sedimentation of “lingering” Macondo oil to the deep-sea after the Deepwater Horizon oil spill. *Marine Chemistry* **218**, 103733.

Peter J., Peltonen P., Scott S., Simoneit B. and Kawka O. (1991) 14C ages of hydrothermal petroleum and carbonate in Guaymas Basin, Gulf of California: implications for oil generation, expulsion, and migration. *Geology* **19**, 253-256.

Peters K. E., Walters C. C. and Moldowan J. M. (2007) *The Biomarker Guide. Biomarkers and Isotopes in Petroleum Systems and Earth History*.

Peterson C. H., Rice S. D., Short J. W., Esler D., Bodkin J. L., Ballachey B. E. and Irons D. B. (2003) Long-Term Ecosystem Response to the Exxon Valdez Oil Spill. *Science* **302**, 2082-2086.

Phillips A. A., White M. E., Seidel M., Wu F., Pavia F. F., Kemeny P. C., Ma A. C., Aluwihare L. I., Dittmar T. and Sessions A. L. (2022) Novel sulfur isotope analyses constrain sulfurized porewater fluxes as a minor component of marine dissolved organic matter. *Proceedings of the National Academy of Sciences* **119**, e2209152119.

Podgorski D. C., Zito P., McGuire J. T., Martinovic-Weigelt D., Cozzarelli I. M., Bekins B. A. and Spencer R. G. M. (2018) Examining Natural Attenuation and Acute Toxicity of Petroleum-Derived Dissolved Organic Matter with Optical Spectroscopy. *Environmental Science & Technology* **52**, 6157-6166.

Podgorski D. C., Zito P., Kellerman A. M., Bekins B. A., Cozzarelli I. M., Smith D. F., Cao X., Schmidt-Rohr K., Wagner S., Stubbins A. and Spencer R. G. M. (2020) Hydrocarbons to Carboxyl-Rich Alicyclic Molecules: A Continuum Model to Describe Biodegradation of Petroleum-Derived Dissolved Organic Matter in Contaminated Groundwater Plumes. *Journal of Hazardous Materials* **402**, 123998.

Pohlabeln A. M. and Dittmar T. (2015) Novel insights into the molecular structure of non-volatile marine dissolved organic sulfur. *Marine Chemistry* **168**, 86-94.

Pohlabeln A. M., Gomez-Saez G. V., Noriega-Ortega B. E. and Dittmar T. (2017) Experimental evidence for abiotic sulfurization of marine dissolved organic matter. *Frontiers in Marine Science* **4**, 364.

Pohlman J. W., Bauer J. E., Waite W. F., Osburn C. L. and Chapman N. R. (2010) Methane hydrate-bearing seeps as a source of aged dissolved organic carbon to the oceans. *Nature Geoscience* **4**, 37.

Price L. C. (1976) Aqueous solubility of petroleum as applied to its origin and primary migration. *AAPG bulletin* **60**, 213-244.

Pucher M., Wünsch U., Weigelhofer G., Murphy K., Hein T. and Graeber D. (2019) staRdom: Versatile Software for Analyzing Spectroscopic Data of Dissolved Organic Matter in R. *Water* **11**, 2366.

R Core Team (2022) R: A language and environment for statistical computing. R Foundation for Statistical Computing, Vienna, Austria.

Ramírez G., Mara P., Sehein T., Wegener G., Chambers C., Joye S., Peterson R., Philippe A., Burgaud G., Edgcomb V. and Teske A. (2021) Environmental factors shaping bacterial, archaeal and fungal community structure in hydrothermal sediments of Guaymas Basin, Gulf of California. *PLOS ONE* **16**, e0256321.

Retelletti Brogi S., Kim J.-H., Ryu J.-S., Jin Y. K., Lee Y. K. and Hur J. (2019) Exploring sediment porewater dissolved organic matter (DOM) in a mud volcano: Clues of a thermogenic DOM source from fluorescence spectroscopy. *Marine Chemistry* **211**, 15-24.

Riedel T. and Dittmar T. (2014) A Method Detection Limit for the Analysis of Natural Organic Matter via Fourier Transform Ion Cyclotron Resonance Mass Spectrometry. *Analytical Chemistry* **86**, 8376-8382.

Roebuck J. A., Seidel M., Dittmar T. and Jaffé R. (2018) Land Use Controls on the Spatial Variability of Dissolved Black Carbon in a Subtropical Watershed. *Environmental Science & Technology* **52**, 8104-8114.

Rossel P., Bienhold C., Hehemann L., Dittmar T. and Boetius A. (2020) Molecular Composition of Dissolved Organic Matter in Sediment Porewater of the Arctic Deep-Sea Observatory HAUSGARTEN (Fram Strait). *Frontiers in Marine Science* **7**, 428.

Rossel P. E., Stubbins A., Hach P. F. and Dittmar T. (2015) Bioavailability and molecular composition of dissolved organic matter from a diffuse hydrothermal system. *Marine Chemistry* **177**, 257-266.

Ruiz-Morales Y. and Mullins O. C. (2007) Polycyclic aromatic hydrocarbons of asphaltenes analyzed by molecular orbital calculations with optical spectroscopy. *Energy & fuels* **21**, 256-265.

Sahling H. and Bohrmann G. (2016) Seafloor images of ROV profile GeoB19340-1, dive359, In: Sahling, G; Bohrmann, Gerhard (2016): Seafloor images along 14 ROV profiles during METEOR cruise M114/2. PANGAEA, https://doi.org/10.1594/PANGAEA.863824. PANGAEA.

Sahling H., Ahrlich F., Bohrmann G., Borowski C., Breitzke M., Buchheister S., Büttner H., Ferreira, , C. G.-C., A., , Geprägs P. and Groeneveld J.-D., Hsu, C.-W., Jiménez- Guadarrama, E., Klar, S., Klaucke, I., Klüber, S., Leymann, T., Loher, M., Mai, H.-A., Mau, S., MacDonald, I., Marcon, Y., Meinecke, G., Melcher, A.-C., Morales-Dominguez, E., Raeke, A., Rehage, R., Renken, J., Reuter, M., Rohleder, C., Römer, M., Rubin-Blum, M., Schade, T., Schubotz, F., Seiter, C., Smrzka, D., Spiesecke, U., Torres, M., Vittori, V., Von Neuhoff, S., von Wahl, T., Wegener, G., Wiebe, M., Wintersteller, P., Zarrouk, M., Zwicker, J. (2017) *R/V METEOR Cruise Report M114, Natural hydrocarbon seepage in the southern Gulf of Mexico, Kingston – Kingston, 12 February – 28 March 2015*. University of Bremen, Bremen.

Sahling H., Borowski C., Escobar-Briones E., Gaytán-Caballero A., Hsu C. W., Loher M., MacDonald I., Marcon Y., Pape T., Römer M., Rubin-Blum M., Schubotz F., Smrzka D., Wegener G. and Bohrmann G. (2016) Massive asphalt deposits, oil seepage, and gas venting support abundant chemosynthetic communities at the Campeche Knolls, southern Gulf of Mexico. *Biogeosciences* **13**, 4491-4512.

Šantl-Temkiv T., Finster K., Dittmar T., Hansen B. M., Thyrhaug R., Nielsen N. W. and Karlson U. G. (2013) Hailstones: A Window into the Microbial and Chemical Inventory of a Storm Cloud. *PLOS ONE* **8**, e53550.

Schmidt F., Koch B. P., Witt M. and Hinrichs K.-U. (2014) Extending the analytical window for water-soluble organic matter in sediments by aqueous Soxhlet extraction. *Geochimica et Cosmochimica Acta* **141**, 83-96.

Schmidt F., Elvert M., Koch B. P., Witt M. and Hinrichs K.-U. (2009) Molecular characterization of dissolved organic matter in pore water of continental shelf sediments. *Geochimica et Cosmochimica Acta* **73**, 3337-3358.

Schmidt M. W. I., Torn M. S., Abiven S., Dittmar T., Guggenberger G., Janssens I. A., Kleber M., Kögel-Knabner I., Lehmann J., Manning D. A. C., Nannipieri P., Rasse D. P., Weiner S. and Trumbore S. E. (2011) Persistence of soil organic matter as an ecosystem property. *Nature* **478**, 49-56.

Schubotz F., Lipp J. S., Elvert M., Kasten S., Mollar X. P., Zabel M., Bohrmann G. and Hinrichs K.-U. (2011) Petroleum degradation and associated microbial signatures at the Chapopote asphalt volcano, Southern Gulf of Mexico. *Geochimica et Cosmochimica Acta* **75**, 4377-4398.

Schuler B., Meyer G., Peña D., Mullins O. C. and Gross L. (2015) Unraveling the Molecular Structures of Asphaltenes by Atomic Force Microscopy. *Journal of the American Chemical Society* **137**, 9870-9876.

Seewald J. S. (2001) Aqueous geochemistry of low molecular weight hydrocarbons at elevated temperatures and pressures: constraints from mineral buffered laboratory experiments. *Geochimica et Cosmochimica Acta* **65**, 1641-1664.

Seidel M., Vemulapalli S. P. B., Mathieu D. and Dittmar T. (2022) Marine Dissolved Organic Matter Shares Thousands of Molecular Formulae Yet Differs Structurally across Major Water Masses. *Environmental Science & Technology* **56**, 3758-3769.

Seidel M., Kleindienst S., Dittmar T., Joye S. B. and Medeiros P. M. (2016) Biodegradation of crude oil and dispersants in deep seawater from the Gulf of Mexico: Insights from ultra-high resolution mass spectrometry. *Deep Sea Research Part II: Topical Studies in Oceanography* **129**, 108-118.

Seidel M., Beck M., Riedel T., Waska H., Suryaputra I. G., Schnetger B., Niggemann J., Simon M. and Dittmar T. (2014) Biogeochemistry of dissolved organic matter in an anoxic intertidal creek bank. *Geochimica et cosmochimica acta* **140**, 418-434.

Seidel M., Yager P. L., Ward N. D., Carpenter E. J., Gomes H. R., Krusche A. V., Richey J. E., Dittmar T. and Medeiros P. M. (2015) Molecular-level changes of dissolved organic matter along the Amazon River-to-ocean continuum. *Marine Chemistry* **177**, 218-231.

Shen Y. and Benner R. (2020) Molecular properties are a primary control on the microbial utilization of dissolved organic matter in the ocean. *Limnology and Oceanography* **65**, 1061-1071.

Silverman S. R. and Epstein S. (1958) Carbon Isotopic Compositions of Petroleums and Other Sedimentary Organic Materials1. *AAPG Bulletin* **42**, 998-1012.

Simoneit B. R. (1985) Hydrothermal petroleum: genesis, migration, and deposition in Guaymas Basin, Gulf of California. *Canadian Journal of Earth Sciences* **22**, 1919-1929.

Simoneit B. R. (1988) Petroleum generation in submarine hydrothermal systems; an update. *The Canadian Mineralogist* **26**, 827-840.

Simoneit B. R. (1994) Lipid/bitumen maturation by hydrothermal activity in sediments of Middle Valley, Leg 139.

Simoneit B. R., Kawka O. and Brault M. (1988) Origin of gases and condensates in the Guaymas Basin hydrothermal system (Gulf of California). *Chemical Geology* **71**, 169-182.

Simoneit B. R., Lein A. Y., Peresypkin V. and Osipov G. (2004) Composition and origin of hydrothermal petroleum and associated lipids in the sulfide deposits of the Rainbow field (Mid-Atlantic Ridge at 36 N). *Geochimica et Cosmochimica Acta* **68**, 2275-2294.

Sipler R. E. and Bronk D. A. (2015) Chapter 4 - Dynamics of Dissolved Organic Nitrogen. In *Biogeochemistry of Marine Dissolved Organic Matter (Second Edition)* (eds. D. A. Hansell and C. A. Carlson). Academic Press, Boston. pp. 127-232.

Siron R., Rontani J. F. and Giusti G. (1987) Chemical characterization of a water soluble fraction (WSF) of crude oil. *Toxicological & Environmental Chemistry* **15**, 223-229.

Sleighter R. L. and Hatcher P. G. (2008) Molecular characterization of dissolved organic matter (DOM) along a river to ocean transect of the lower Chesapeake Bay by ultrahigh resolution electrospray ionization Fourier transform ion cyclotron resonance mass spectrometry. *Marine Chemistry* **110**, 140-152.

Smit N. (2016) Geochemical characterization of asphalt deposits in the Campeche Bay (southern Gulf of Mexico), Master Thesis. M.Sc Marine Geocience University of Bremen.

Song M., Schubotz F., Kellermann M. Y., Hansen C. T., Bach W., Teske A. P. and Hinrichs K.-U. (2021) Formation of ethane and propane via abiotic reductive conversion of acetic acid in hydrothermal sediments. *Proceedings of the National Academy of Sciences* **118**, e2005219118.

Stedmon C. A., Markager S. and Bro R. (2003) Tracing dissolved organic matter in aquatic environments using a new approach to fluorescence spectroscopy. *Marine Chemistry* **82**, 239-254.

Stedmon C. A., Thomas D. N., Papadimitriou S., Granskog M. A. and Dieckmann G. S. (2011) Using fluorescence to characterize dissolved organic matter in Antarctic sea ice brines. *Journal of Geophysical Research: Biogeosciences* **116**.

Stubbins A., Niggemann J. and Dittmar T. (2012) Photo-lability of deep ocean dissolved black carbon. *Biogeosciences* **9**, 1661-1670.

Stubbins A., Spencer R. G. M., Mann P. J., Holmes R. M., McClelland J. W., Niggemann J. and Dittmar T. (2015) Utilizing colored dissolved organic matter to derive dissolved black carbon export by arctic rivers. *Frontiers in Earth Science* **3**.

Stubbins A., Spencer R. G., Chen H., Hatcher P. G., Mopper K., Hernes P. J., Mwamba V. L., Mangangu A. M., Wabakanghanzi J. N. and Six J. (2010) Illuminated darkness: Molecular signatures of Congo River dissolved organic matter and its photochemical alteration as revealed by ultrahigh precision mass spectrometry. *Limnology and Oceanography* **55**, 1467-1477.

Suresh G. (2015) Offshore oil seepage visible from space: A Synthetic Aperture Radar (SAR) based automatic detection, mapping and quantification system. Staats-und Universitätsbibliothek Bremen.

Tanaka S., Oba K., Fukushima M., Nakayasu K. and Hasebe K. (1997) Water solubility enhancement of pyrene in the presence of humic substances. *Analytica Chimica Acta* **337**, 351-357.

Teske A. (2018) Hydrocarbon-Degrading Microbial Communities in Natural Oil Seeps. In *Microbial Communities Utilizing Hydrocarbons and Lipids: Members, Metagenomics and Ecophysiology* (ed. T. J. McGenity). Springer International Publishing, Cham. pp. 1-31.

Teske A., Callaghan A. V. and LaRowe D. E. (2014) Biosphere frontiers of subsurface life in the sedimented hydrothermal system of Guaymas Basin. *Frontiers in microbiology* **5**, 362.

Teske A., Edgcomb V., Rivers A. R., Thompson J. R., de Vera Gomez A., Molyneaux S. J. and Wirsen C. O. (2009) A molecular and physiological survey of a diverse collection of hydrothermal vent Thermococcus and Pyrococcus isolates. *Extremophiles* **13**, 905-915.

Teske A., Hinrichs K.-U., Edgcomb V., Gomez A. d. V., Kysela D., Sylva S. P., Sogin M. L. and Jannasch H. W. (2002) Microbial Diversity of Hydrothermal Sediments in the Guaymas Basin: Evidence for Anaerobic Methanotrophic Communities. *Applied and Environmental Microbiology* **68**, 1994-2007.

Teske A., de Beer D., McKay L. J., Tivey M. K., Biddle J. F., Hoer D., Lloyd K. G., Lever M. A., Røy H., Albert D. B., Mendlovitz H. P. and MacGregor B. J. (2016) The Guaymas Basin Hiking Guide to Hydrothermal Mounds, Chimneys, and Microbial Mats: Complex Seafloor Expressions of Subsurface Hydrothermal Circulation. *Frontiers in Microbiology* **7**.

Teske A. P., Lizarralde D. and Höfig T. W. (2020) International Ocean Discovery Program Expedition 385 Preliminary Report.

Tomco P., Duddleston K., Driskill A., Hatton J., Grond K., Wrenn T., Tarr M., Podgorski D. and Zito P. (2021) Dissolved organic matter production from herder application and in-situ burning of crude oil at high latitudes: Bioavailable molecular composition patterns and microbial community diversity effects. *Journal of Hazardous Materials* **424**, 127598.

Valentine D. L., Reddy C. M., Farwell C., Hill T. M., Pizarro O., Yoerger D. R., Camilli R., Nelson R. K., Peacock E. E., Bagby S. C., Clarke B. A., Roman C. N. and Soloway M. (2010) Asphalt volcanoes as a potential source of methane to late Pleistocene coastal waters. *Nature Geoscience* **3**, 345.

Volikov A. B., Sobolev N. A., Khreptugova A. N. and Perminova I. V. (2022) Static and dynamic sorption of DOM on Bond Elute PPL and Bondesil PPL sorbents: physical-chemical characteristics. *Separation Science and Technology* **58**, 642-653.

Von Damm K. v., Edmond J. t., Measures C. and Grant B. (1985) Chemistry of submarine hydrothermal solutions at Guaymas Basin, Gulf of California. *Geochimica et Cosmochimica Acta* **49**, 2221-2237.

Wagner S., Dittmar T. and Jaffé R. (2015) Molecular characterization of dissolved black nitrogen via electrospray ionization Fourier transform ion cyclotron resonance mass spectrometry. *Organic Geochemistry* **79**, 21-30.

Wagner S., Ding Y. and Jaffé R. (2017) A New Perspective on the Apparent Solubility of Dissolved Black Carbon. *Frontiers in Earth Science* **5**.

Wagner S., Jaffé R. and Stubbins A. (2018) Dissolved black carbon in aquatic ecosystems. *Limnology and Oceanography Letters* **3**, 168-185.

Wagner S., Harvey E., Baetge N., McNair H., Arrington E. and Stubbins A. (2021) Investigating atmospheric inputs of dissolved black carbon to the Santa Barbara Channel during the Thomas Fire (California, USA). *Journal of Geophysical Research: Biogeosciences* 10.1029/2021JG006442.

Wagner S., Brandes J., Spencer R. G. M., Ma K., Rosengard S. Z., Moura J. M. S. and Stubbins A. (2019) Isotopic composition of oceanic dissolved black carbon reveals non-riverine source. *Nature Communications* **10**.

Walker S. A., Amon R. M., Stedmon C., Duan S. and Louchouarn P. (2009) The use of PARAFAC modeling to trace terrestrial dissolved organic matter and fingerprint water masses in coastal Canadian Arctic surface waters. *Journal of Geophysical Research: Biogeosciences* **114**.

Wang X.-C., Chen R. F., Whelan J. and Eglinton L. (2001) Contribution of “Old” carbon from natural marine hydrocarbon seeps to sedimentary and dissolved organic carbon pools in the Gulf of Mexico. *Geophysical Research Letters* **28**, 3313-3316.

Wang X., Xu C., Druffel E. M., Xue Y. and Qi Y. (2016) Two black carbon pools transported by the Changjiang and Huanghe Rivers in China. *Global Biogeochemical Cycles* **30**, 1778-1790.

Wegener G., Knittel K., Bohrmann G. and Schubotz F. (2020) Benthic Deep-Sea Life Associated with Asphaltic Hydrocarbon Emissions in the Southern Gulf of Mexico. In *Marine Hydrocarbon Seeps: Microbiology and Biogeochemistry of a Global Marine Habitat* (eds. A. Teske and V. Carvalho). Springer International Publishing, Cham. pp. 101-123.

Weiland R. J., Adams G. P., McDonald R. D., Rooney T. C. and Wills L. M. Geological and biological relationships in the Puma appraisal area: From salt diapirism to chemosynthetic communities. *Offshore Technology Conference*. Offshore Technology Conference.

Weishaar J. L., Aiken G. R., Bergamaschi B. A., Fram M. S., Fujii R. and Mopper K. (2003) Evaluation of Specific Ultraviolet Absorbance as an Indicator of the Chemical Composition and Reactivity of Dissolved Organic Carbon. *Environmental Science & Technology* **37**, 4702-4708.

Widdel F. and Bak F. (1992) Gram-negative mesophilic sulfate-reducing bacteria. In *The prokaryotes*. Springer. pp. 3352-3378.

Wintersteller P. (2019) Gridded bathymetry from multibeam echosounder EM122 data of METEOR cruise M114 (Southern Gulf of Mexico). PANGAEA.

Worsfold P. J., Monbet P., Tappin A. D., Fitzsimons M. F., Stiles D. A. and McKelvie I. D. (2008) Characterisation and quantification of organic phosphorus and organic nitrogen components in aquatic systems: A Review. *Analytica Chimica Acta* **624**, 37-58.

Wünsch U. J. and Murphy K. (2020) A simple method to isolate fluorescence spectra from small dissolved organic matter datasets. *Water Research* **190**, 116730.

Wünsch U. J., Murphy K. R. and Stedmon C. A. (2017) The One-Sample PARAFAC Approach Reveals Molecular Size Distributions of Fluorescent Components in Dissolved Organic Matter. *Environmental Science & Technology* **51**, 11900-11908.

Wünsch U. J., Geuer J. K., Lechtenfeld O. J., Koch B. P., Murphy K. R. and Stedmon C. A. (2018) Quantifying the impact of solid-phase extraction on chromophoric dissolved organic matter composition. *Marine Chemistry* **207**, 33-41.

Yamaguchi A., Umezawa Y., Wada M. and Sayama M. (2015) Potential contribution of microalgal intracellular phosphorus to phosphorus distribution in tidal flat sediments during winter. *Plankton and Benthos Research* **10**, 1-10.

Yamashita Y., Nakane M., Mori Y., Nishioka J. and Ogawa H. (2022) Fate of dissolved black carbon in the deep Pacific Ocean. *Nature Communications* **13**, 307.

Yang L., Zhuang W.-E., Chen C.-T. A., Wang B.-J. and Kuo F.-W. (2017) Unveiling the transformation and bioavailability of dissolved organic matter in contrasting hydrothermal vents using fluorescence EEM-PARAFAC. *Water Research* **111**, 195-203.

Zark M. and Dittmar T. (2018) Universal molecular structures in natural dissolved organic matter. *Nature Communications* **9**, 3178.

Zark M., Christoffers J. and Dittmar T. (2017) Molecular properties of deep-sea dissolved organic matter are predictable by the central limit theorem: Evidence from tandem FT-ICR-MS. *Marine Chemistry* **191**, 9-15.

Zhang Y., Siskin M., Gray M. R., Walters C. C. and Rodgers R. P. (2020) Mechanisms of Asphaltene Aggregation: Puzzles and a New Hypothesis. *Energy & Fuels* 10.1021/acs.energyfuels.0c01564.

Zhou Y., Zhao C., He C., Li P., Wang Y., Pang Y., Shi Q. and He D. (2022) Characterization of dissolved organic matter processing between surface sediment porewater and overlying bottom water in the Yangtze River Estuary. *Water Research* **215**, 118260.

Zhou Z., Guo L., Shiller A. M., Lohrenz S. E., Asper V. L. and Osburn C. L. (2013) Characterization of oil components from the Deepwater Horizon oil spill in the Gulf of Mexico using fluorescence EEM and PARAFAC techniques. *Marine Chemistry* **148**, 10-21.

Zhu Y., Vieth-Hillebrand A., Wilke F. D. H. and Horsfield B. (2015) Characterization of water-soluble organic compounds released from black shales and coals. *International Journal of Coal Geology* **150-151**, 265-275.

Zhuang G.-C., Montgomery A., Samarkin V. A., Song M., Liu J., Schubotz F., Teske A., Hinrichs K.-U. and Joye S. B. (2019) Generation and Utilization of Volatile Fatty Acids and Alcohols in Hydrothermally Altered Sediments in the Guaymas Basin, Gulf of California. *Geophysical Research Letters* **46**, 2637-2646.

Ziegelgruber K. L., Zeng T., Arnold W. A. and Chin Y.-P. (2013) Sources and composition of sediment pore-water dissolved organic matter in prairie pothole lakes. *Limnology and Oceanography* **58**, 1136-1146.

Ziervogel K. and Arnosti C. (2020) Substantial Carbohydrate Hydrolase Activities in the Water Column of the Guaymas Basin (Gulf of California). *Frontiers in Marine Science* **6**, 815.

Ziolkowski L. A. and Druffel E. R. M. (2010) Aged black carbon identified in marine dissolved organic carbon. *Geophysical Research Letters* **37**.

Ziolkowski L. A., Chamberlin A., Greaves J. and Druffel E. R. (2011) Quantification of black carbon in marine systems using the benzene polycarboxylic acid method: a mechanistic and yield study. *Limnology and Oceanography: Methods* **9**, 140-140.

Zito P., Ghannam R., Bekins B. A. and Podgorski D. C. (2019a) Examining the Extraction Efficiency of Petroleum-Derived Dissolved Organic Matter in Contaminated Groundwater Plumes. *Groundwater Monitoring & Remediation* **39**, 25-31.

Zito P., Podgorski D. C., Bartges T., Guillemette F., Roebuck J. A., Spencer R. G. M., Rodgers R. P. and Tarr M. A. (2020) Sunlight-Induced Molecular Progression of Oil into Oxidized Oil Soluble Species, Interfacial Material, and Dissolved Organic Matter. *Energy & Fuels* **34**, 4721-4726.

Zito P., Podgorski D. C., Johnson J., Chen H., Rodgers R. P., Guillemette F., Kellerman A. M., Spencer R. G. M. and Tarr M. A. (2019b) Molecular-Level Composition and Acute Toxicity of Photosolubilized Petrogenic Carbon. *Environmental Science & Technology* **53**, 8235-8243.

Versicherung an Eides Statt / *Affirmation in lieu of an oath*

gem. § 5 Abs. 5 der Promotionsordnung vom 18.06.2018 /
according to § 5 (5) of the Doctoral Degree Rules and Regulations of 18 June, 2018

Ich / I,

_____

(Vorname / First *Name*, Name / *Name*, Anschrift / *Address*, ggf. Matr.-Nr. / *student ID no., if applicable)*

versichere an Eides Statt durch meine Unterschrift, dass ich die vorliegende Dissertation selbständig und ohne fremde Hilfe angefertigt und alle Stellen, die ich wörtlich dem Sinne nach aus Veröffentlichungen entnommen habe, als solche kenntlich gemacht habe, mich auch keiner anderen als der angegebenen Literatur oder sonstiger Hilfsmittel bedient habe und die zu Prüfungszwecken beigelegte elektronische Version (PDF) der Dissertation mit der abgegebenen gedruckten Version identisch ist. / *With my signature I affirm in lieu of an oath that I prepared the submitteddissertation independently and without illicit assistance from third parties, that I appropriately referenced any text or content from other sources, that I used only literature and resources listed in the dissertation, and that the electronic (PDF) and printed versions of the dissertation are identical.*

Ich versichere an Eides Statt, dass ich die vorgenannten Angaben nach bestem Wissen und Gewissen gemacht habe und dass die Angaben der Wahrheit entsprechen und ich nichts verschwiegen habe*. / I affirm in lieu of an oath that the information provided herein to the best of my knowledge is true and complete.*

Die Strafbarkeit einer falschen eidesstattlichen Versicherung ist mir bekannt, namentlich die Strafandrohung gemäß § 156 StGB bis zu drei Jahren Freiheitsstrafe oder Geldstrafe bei vorsätzlicher Begehung der Tat bzw. gemäß § 161 Abs. 1 StGB bis zu einem Jahr Freiheitsstrafe oder Geldstrafe bei fahrlässiger Begehung. / *I am aware that a false affidavit is a criminal offence which is punishable by law in accordance with § 156 of the German Criminal Code (StGB) with up to three years imprisonment or a fine in case of intention, or in accordance with § 161 (1) of the German Criminal Code with up to one year imprisonment or a fine in case of negligence.*

_____ _____

Ort / *Place*, Datum / *Date* Unterschrift / *Signature*